# WAVELETS AND MULTILEVEL ANALYSIS TO DETERMINE SPATIAL DEPENDENCIES OF SEASONAL INFLUENZA, WEATHER AND POLLUTION ASSOCIATION ACROSS CHILE 2010-2016

by

**Christian Rodrigo Garcia Calavaro**

Medico Cirujano, Universidad de Chile, Chile, 2005

Magister en Salud Publica, Universidad de Chile, Chile, 2014

Submitted to the Graduate Faculty of

the Department of Epidemiology

Graduate School of Public Health in partial fulfillment

of the requirements for the degree of

Doctor of Public Health

University of Pittsburgh

2019

UNIVERSITY OF PITTSBURGH

GRADUATE SCHOOL OF PUBLIC HEALTH

This dissertation was presented

by

**Christian Rodrigo Garcia Calavaro**

It was defended on

February 8th, 2019

and approved by

**Dissertation Advisor:**

Lee H. Harrison, MD
Professor of Medicine, Epidemiology and Infectious Diseases and Microbiology
School of Medicine and Graduate School of Public Health
University of Pittsburgh

Committee members:

Wilbert Van Panhuis, MD, PhD
Assistant Professor of Epidemiology
Graduate School of Public Health
University of Pittsburgh

Maria M. Brooks, PhD
Professor of Epidemiology
Graduate School of Public Health
University of Pittsburgh

Christina F. Mair, PhD
Assistant Professor of Behavioral and Community Health Sciences
Graduate School of Public Health
University of Pittsburgh

Lee H. Harrison, MD

# WAVELETS AND MULTILEVEL ANALYSIS TO DETERMINE SPATIAL DEPENDENCIES OF SEASONAL INFLUENZA, WEATHER AND POLLUTION ASSOCIATION ACROSS CHILE 2010-2016

Christian Rodrigo Garcia Calavaro, DrPH

University of Pittsburgh, 2019

## ABSTRACT

Influenza virus causes high burden of disease, especially in older adults and young children. The dynamics of influenza are not completely understood. Weather, population movement, and virus survival interact in complex fashion to produce annual epidemics. Chile is a country with a large range of latitudes with a public healthcare sector that covers 74% of the population. Influenza surveillance, pollution and weather data are periodically reported and publicly available. In our work we aimed to determine the spatial dependencies of influenza and the association between weather, pollution and influenza cases across Chile. For our purposes we used data from the Ministry of Health, national air pollution surveillance, national meteorological service between 2010 and 2016. We used cross-wavelet analysis to determine the timing relation between influenza-like surveillance and laboratory surveillance system. Also, we used wavelet transform and phase difference to determine the relationship between latitude and epidemic timing and to determine the presence of local waves of influenza between health networks. Finally, we used a zero-inflated negative binomial multilevel model to determine the association between influenza cases, weather and pollution across hospitals.

Influenza-like illness had no difference in timing compared to laboratory-confirmed influenza A. A north to south pattern of influenza epidemic was found, especially in the central zone of the country where most of the population lives. Population size and latitude were associated to start and peak day of annual epidemics of seasonal influenza. Local outgoing and incoming travelling waves of influenza were found in 11 and 10 health networks, respectively. Local waves were located principally in the center and in the south of the country and were associated to population size. Finally, influenza cases were negatively associated with maximum temperature, minimum temperature and had a positive association with the concentration of particulate matter <2.5 μm (PM2.5).

**Public Health Significance:** Our findings can help decision-makers to prepare influenza season, prioritize areas for early vaccination campaigns, establish standards for pollution, and set a baseline to compare the impact of policies to reduce particulate matter.

## TABLE OF CONTENTS

## LIST OF TABLES

## LIST OF FIGURES

# PREFACE

This dissertation theme arose from practical observations of seasonal influenza epidemics and from the experience acquired by the author and the Ministry of Health of Chile after the 2009 H1N1 pandemic. The first cases of the pandemic were diagnosed in the south of the country, despite active surveillance of all plane passengers that arrived from Mexico and other countries with reported cases. Evidently first cases were undetected, but questions arose: how does influenza travels through the country? Are there patterns, climate and pollution factors that could influence the epidemic? Chowell found a south to north pattern of hospitalized patients with H1N1 in the second semester of 2009. Does seasonal influenza present a similar pattern? These questions are principally driven by the need of preventing, controlling and reducing the impact of influenza. The highest impact of influenza is among the most vulnerable populations in Chile, including the elderly and children. We hope that this research can contribute to the understanding of influenza patterns and contribute to reduce the burden in the most vulnerable population.

This dissertation is divided in five chapters: An introduction to the topic followed by three individual but related manuscripts, and a discussion. The first chapter is an introduction to influenza virus focused on virus characteristics and on what it's known about influenza dynamics. Also includes a description about Chilean healthcare system, influenza and pollution surveillance systems. To orient the reader, we included a general explanation about wavelets, the

main method used in this document, which might be unfamiliar to most public health professionals.

Chapter two includes an analysis of influenza-like illness surveillance to laboratory confirmed surveillance in hospitals from Chile, to determine which virus had the most similar timing to influenza-like illness as a validation method to use influenza-like illness as an influenza proxy. The third chapter shows the spatial dependencies and latitudinal patterns of influenzas-like illness across healthcare networks and determine the presence of local travelling waves of influenza. The fourth chapter aims to determine the association between influenza, weather and pollution variables across different hospitals across Chile. Finally, in Chapter 5 we included three subsections to conclude, highlight public health significance of the findings, and propose future directions for applied research on this topic.

## ACKNOWLEDGMENTS

To my family Pia, Franco, Mercedes and Teresa, who supported this endeavor and generously left their family and friends in Chile, followed me to the United States and gave me the strength to fulfill this challenge.

To my parents Eduardo and Carla, brothers Andres and Sebastian, my in laws Guido, Maria Pia, Guido and Gianinna for their unconditional support, time and love.

To my Pittsburgh family Cristobal, Militza, Diego, Maria Gracia, Gabriel, Abelino, Nicole and Agustin who helped overcome difficulties in this faraway land and turned it into our home.

To all our family members and friends who visited us: Sergio, Alejandra, Josefa, Carolina, Daniel, Agustin, Javier, Federico, Rosario, Francesca, Pamela, Pepa, Michelle, Domenico, Maria Teresa, Manny, David, Cara, Mia, Emily, Ava, Daniela, Bret, Loreto, Cristobal, Rafael, Emilio, Barbara, Ruben, Loreto, Leonardo, Claudio, Pilar, Cristobal, Marcel, Hugo and specially to Fernanda for your time, love and for supporting us as a family.

To our Pittsburgh friends: Maria, Pablo, Francisco, Ignacio, Soledad, Jose, Gabriela, Amalia, Erika, Gabriel, Braulio, Carito, Isabela, Laura, Soledad, Alex, Mia, Trini, Sebastian, Max, Borja, Varuna, David, Martha, Claudia, Ron, Miguel, Danna, Emma, Virginia, Javier, Martin, Benja, Vivian, Lester, Diego, Mathew (Mateo), Rob, Martha, Osvaldo, Julita, Lucia, Marion, Ignacio, Giulia, Filippo, Davide, Antonio, Alessandro, Vane, Daniel, Leti, Astrid,

Ignacio, Jenny, Devon, Miss Alyssa, Miss Leslie, Miss Lizzie, Ms. Lori, Ms. Hills, Ms. Jen, Beatriz, Patty, Yohali, Hannah, Tenley, Hemant, Mohammed, Abby, and Leonardo, for your help, for your kindness, for the laughter, and the good times we had in the city of bridges. We will miss you all.

To my advisor Lee Harrison, committee members Maria Brooks, Christina Mair and especially to Wilbert Van Panhuis, my gratitude for your advice, generosity and the opportunity to open my mind to new and exciting knowledge.

To the Ministry of Health and especially to Dr. Lorna Luco and Dr. Pedro Crocco, for their support and advise.

To our neighborhood, Squirrel Hill and especially to the Jewish Community Center and the members of the Tree of Life synagogue, victims of intolerance and of the stupidity of this era, we are stronger than hate.

To the city of Pittsburgh, simple, friendly and lovely city that I will always call home.

This work was funded by the CONICYT PFCHA/BECAS CHILE 2014 Folio 79090016

# 1.0 INTRODUCTION

## 1.1 INFLUENZA VIRUS

Influenza virus is part the Orthomyxoviridae family that includes the genera of influenza A, B, C and thogotovirus. Influenza viruses are composed of negative-sense RNA segment and a lipid envelope that provides resistance to environmental conditions (1, 2). Influenza A and B cause disease in humans; are responsible for an important burden of disease world-wide, affecting 5-10% of the world's population including 250,000-500,000 deaths annually (3). In the Americas 40,880-160,270 deaths occur every year associated with influenza infection and in the United States it causes 31.4 million outpatients visits, 334,000 hospitalizations and 41,000 deaths with an estimated cost of U$87.1 billion (4, 5). Even though all populations are at risk of influenza infection, persons of 65 years and more, and children under 5 are the most severely affected (6-8). Moreover, influenza is the second most commonly identified pathogen in children with acute lower respiratory infections globally (9).

The high burden of disease caused by influenza is in part attributable to the ability of the virus to elude host immunity and cause annual epidemics. The main mechanism to evade immunity is attributed to changes in the two types of surface glycoproteins: Haemaglutinin and neuraminidase. Haemaglutinin allows binding and infection of epithelial lung cells while N allows the release of new virus particles from infected cells (10). Influenza B has a single version of H and N. On the other hand, influenza A has 15 different haemaglutinin types (H1-H15) and 9

types of neuraminidase (N1-N9) (2). Haemaglutinin and neuraminidase can suffer two types of surface glycoprotein modifications. The first, antigenic shift, is present only in influenza A. In antigenic shift, successive single point mutations in the H or N genes occur as part of the continuous evolution process that triggers annual epidemics. The second, antigenic drift, is present in both influenza A and B. Antigenic drift is a more extreme mutation that results in completely new H or new H and N, normally as a result of the transmission of animal influenza to humans. The consequence is an immunologically different virus from those present in the past years capable of generating new pandemics (2, 11). Antibodies that target H and N decrease the probabilities of infection and severe disease but confer limited or no protection against other types (12-14). The evasion of immunity and the mechanism of transmission from person-to-person through sneezing, coughing or fomites, gives influenza the ability to produce local and global epidemics.

## 1.2 INFLUENZA DYNAMICS

The dynamics of influenza at global and local scales are not fully understood, but can be addressed using demographic, geo-climatic and national census data to improve accuracy of models and advance towards the precision that meteorological models have nowadays (15). In temperate climates, there is annual seasonality in winter months, but this issue remains a mystery in tropical areas (16, 17). Tamerius et al studied the evidence of different mechanisms associated with influenza seasonality reviewing epidemiologic, animal and laboratory model studies (17). They used a framework with three primary mediators that include: contact rate, virus survival and host immunity. They found some association mediated by human contact rates; including a

relationship between influenza and temperatures in temperate regions, rainfall in tropical locations, school schedule and travel patterns (11, 18, 19). Virus survival in the environment is a basic condition for the spread of influenza. Temperature, humidity (relative and absolute) and ultraviolet radiation showed association with virus survival and could explain in part influenza spread and seasonality (1, 20-22). Finally, photoperiod, humidity, temperature, nutritional factors, as well as the presence of other circulating viruses might affect population immunity and therefore influenza rates (17, 23-29). Even though these associations appear to play an important role in seasonality of influenza, it is hard to avoid collinearity of variables and confounding factors. The most accepted hypothesis to understand influenza seasonality is that absolute humidity may be negatively associated with seasonal epidemics (17).

The observed periodicity of influenza is caused by complex interactions of factors. To understand these phenomena, diverse levels of analysis and convergence of fields will be needed, including environmental science, biology, sociology, meteorology, medical science and epidemiology (11). The main challenge to influenza dynamic research is to obtain reliable data from surveillance systems with the necessary resolution to understand local patterns and with international standards to compare and analyze global patterns. Chile has followed the World Health Organization recommendations and implemented a strong influenza surveillance systems for decades. Information from the Chilean surveillance system can help understand the dynamics of influenza.

## 1.3 HEALTHCARE, INFLUENZA AND POLLUTION SURVEILLANCE IN CHILE

Chile is a high-income country located in south America with a GDP per capita of U$ 15,346 in 2017 (30). It has the largest latitude range in the southern hemisphere (36 degrees from 17S to 53S), with 10 types of climate categories ranging from desertic to artic (31). Healthcare provision is organized in 29 Public Health Networks that include primary healthcare and hospital services. Healthcare networks are organized geographically and are funded via taxes and by the public healthcare insurance (National Health Fund: FONASA). FONASA covers 74.4% of the 17 million population and the rest are covered by private or army health insurance (32). Influenza surveillance was enhanced after the 2009 pandemic with year-round surveillance of influenza-like illness (ILI) in emergency departments (ED), laboratory in sentinel providers and surveillance of severe respiratory disease hospitalizations (33). Hospitals record and report to the Ministry of Health daily ED diagnosis. ED and laboratory surveillance showed that in Chile influenza usually starts in fall and peaks in winter (34, 35).

A series of weather and pollution stations across the country are part of the Meteorological Services, the national systems of air quality (SINCA) and the Ministry of Agriculture (36-38). Since different measures of air pollution depend on local characteristics, like local industry development and the type of heating fuel used, there is variation of the air pollutants measured (37). Particulate matter <10 μg and <2.5 μg are measured as well as gases like sulfur dioxide ($SO_2$) and ozone ($O_3$). All 4 pollutants are associated to health risks, increased respiratory symptoms and hospital visits (39, 40). Data of influenza surveillance, weather and pollution are publicly available and can be obtained from the respective institutional web sites.

## 1.4 WAVELETS

In science we manipulate and represent information based on different geographical coordinate systems. For example, we use latitude, longitude and altitude to determine a point in the earth's surface. For complex information, as signals such as influenza time series, a different system must be used. Fourier demonstrated that a periodic signal can be decomposed into simple waves, each one with a constant frequency multiple of a fixed frequency (41). This decomposition can be used to rebuild the original signal. Nowadays this method is used to compress information in computers like music into MP3. The compression consists in separating the signal, e.g. the range of wavelength audible by humans in music, from noise or recorded sounds that human cannot perceive. Then we can hear music using a fraction of the space (megabites) with a sound quality like the original. Wavelets are a refinement of the Fourier function. A wavelet is a mathematical function that divides a signal into different components that accounts for the presence of abrupt changes in time and frequency (Non-periodic signal). Then, signals can be studied using a resolution that matches a specific component or scale. We are in contact with these methods daily, given that is an essential part of the image compression format JPG (42). The main advantage of wavelets over Fourier is that wavelets represent functions that have breaks and peaks. Furthermore, wavelets can deconstruct and separate the signal from noise more precisely when signals are non-periodic or non-stationary.

Wavelets are used in different areas of science, for example in physics to study crystal defects, in meteorology to study non-stationary phenomena like El Niño and in astronomy to detect gravitational waves from the fusion of two neutron stars (43-45). Wavelets have also been used in health science to study different infectious diseases such as, dengue, pertussis, measles, and influenza (46-54). The incorporation of methods from other fields to public health can help to a better understanding of patterns that are otherwise difficult to detect with classic methods.

## 1.5 AIMS

The purpose of this investigation is to understand the spatial relation of influenza between different regions in Chile and the association with weather and pollution.

### 1.5.1 Specific Aims

**Aim 1: Determine if influenza like illness in emergency departments is a reliable measure of laboratory confirmed influenza timing**

Hypotheses:

a) There is seasonality of lab confirmed influenza and ILI compared to randomly generated time series (White noise).

b) There is a predominant annual seasonality across hospitals for confirmed influenza and for ILI.

c) Seasonality of lab confirmed influenza and ILI presents synchrony within each hospital.

d) There is no difference in timing between ILI and laboratory confirmed influenza.

**Aim 2: Determine the seasonality of influenza in Chile, their similarities and spatiotemporal relations**

Hypotheses:

a) ILI presents an annual seasonality compared to randomly generated time series (White noise).

b) The annual epidemic start and peak of seasonal influenza in health networks is associated to latitude

c) The presence of incoming and outgoing traveling waves of influenza in health networks is associated to population

**Aim 3: Determine the association of weather, air pollution and cases of seasonal influenza epidemic**

Hypothesis:

a) Influenza cases are associated to temperature and air pollution.

## 2.0 INFLUENZA-LIKE ILLNESS AND LABORATORY SURVEILLANCE TIMING: A CROSS-WAVELET ANALYSIS IN 25 CHILEAN HOSPITALS

Christian Garcia, MD MPH[1,2]; Lee H. Harrison, MD[1,3]; Maria M. Brooks PhD[1]; Christina F. Mair, MPH PhD[4]; Wilbert van Panhuis, MD PhD[1]

1.Department of Epidemiology, University of Pittsburgh Graduate School of Public Health

2.Division of Disease Prevention and Control, Ministry of Health, Chile

3.Infectious Diseases Epidemiology Research Unit, University of Pittsburgh

4.Department of Behavioral and Community Health Sciences, University of Pittsburgh Graduate School of Public Health

## 2.1 ABSTRACT

**Background:** Influenza is associated to a high burden of mortality and morbidity in Chile and elsewhere. Studies about influenza activity from influenza-like illness (ILI) surveillance are focused on the sensitivity and the specificity of case definition. The estimation of influenza timing from ILI should consider the cocirculation of other pathogens that could increase ILI symptoms in the population to avoid over-attribution of ILI to influenza.

**Objective:** Determine if ILI in emergency rooms is a reliable measure of laboratory confirmed influenza timing

**Method:** We used weekly ILI and laboratory surveillance of Respiratory Syncytial Virus (RSV), Adenovirus (ADV), Parainfluenza (PARA), Influenza A (INFA), Influenza B (INFB), and Metapneumovirus (META) from 25 Chilean hospitals. To test synchrony between ILI and viruses we performed cross-wavelet analysis, extracted the predominant seasonality, and compared the timing component of the signals (phase). Finally, to test the hypothesis that there was no difference in timing between ILI and laboratory-confirmed influenza virus, we compared the average phase differences between ILI and each laboratory-confirmed virus.

**Results:** We found no timing difference between ILI and influenza A. In contrast, the rest of the viruses showed significant differences in timing.

**Conclusion:** ILI is a reliable measure of influenza A timing in Chile.

## 2.2 INTRODUCTION

Influenza is associated with a high burden of morbidity and mortality, in Chile and elsewhere (4, 55-59). Surveillance of influenza is an important tool to prepare health systems for annual epidemics, determination of vaccine content, and preparedness for eventual pandemics (60). Influenza surveillance, as recommended by the World Health Organization (WHO), has been implemented by several countries around the world (61). The standard promoted by the WHO is a combination of clinical and virologic surveillance by sentinel providers (62). Clinical surveillance is based on Influenza-like illness (ILI) used as a proxy of influenza A and influenza B to describe temporal trends between and within seasons. ILI surveillance accuracy to describe influenza activity increases when combined with laboratory surveillance, which is thought to deliver more precise information about influenza virus activity (63-65). Even though, laboratory surveillance has been implemented to complement clinical surveillance, it tends to be restricted to a small number of providers and smaller number of patients tested due to financial and time constrains (66).

Studies about influenza activity from ILI surveillance are mainly focused on the sensitivity and specificity of case definition for ILI compared to laboratory-confirmed influenza (67-70). For the purpose of studying influenza epidemic timing within a country, it is of more interest to examine whether increase in ILI consultation rates are more closely associated with increases of laboratory-confirmed influenza virus compared to other viruses. Viruses like influenza A, influenza B, respiratory syncytial virus, parainfluenza, metapneumovirus, and adenovirus (AD) are regarded as potential causes of ILI. Most of these pathogens are not monitored with the consequent poor positive predictive values of ILI of laboratory confirmed influenza (66, 71, 72). The estimation of influenza from ILI rates should consider the

cocirculation of other pathogens that could increase ILI symptoms in the population to avoid over-attribution of ILI to influenza. The same principle applies to determining seasonal epidemic timing when using ILI surveillance. Hence, in this study our aim is to determine the timing association between ILI and 7 different laboratory confirmed viruses and to determine if ILI is a reliable measure of influenza, using data from 25 Chilean hospitals from 2011 to 2016.Methods

To determine if ILI reflects laboratory confirmed influenza timing, we obtained official governmental data. To test the hypothesis that there is a seasonality of lab confirmed influenza and ILI compared to randomly generated time series we performed a wavelet analysis. Then, to determine a predominant annual seasonality within each hospital for confirmed influenza and ILI we performed cross-wavelet analysis and extracted the predominant seasonality. Then, to test time series synchrony of ILI and each virus within each hospital we extracted and compared the timing component of the signals (phase). Finally, to test the hypothesis that there was no difference in timing between ILI and laboratory-confirmed influenza virus across hospitals, we compared the average phase differences of ILI and each laboratory-confirmed virus across hospitals.

### 2.2.1 Data sources

We obtained weekly cases of laboratory confirmed viruses reported from hospitals to the national reference laboratory, as part of the laboratory surveillance of respiratory viruses (35). Reports were available from 2011 to 2016 and included the total number of samples tested for respiratory viruses, number of cases of respiratory syncytial virus, adenovirus, parainfluenza, influenza A, influenza B, and metapneumovirus. For ILI, we used weekly cases between 2011 and 2016 from emergency departments (ED) of public hospitals reported by the Chilean Ministry of Health (73).

We included only hospitals with data for both ILI and laboratory surveillance for the period 2011-2016.

We used hospital location, census data, and population coverage from official governmental institutions to estimate the population that access each hospital. These data sources included the Ministry of Health, National Public Insurance (FONASA), National Institute of Statistics (INE) and the National Repository of Geospatial Information (32, 74, 75). To calculate rates, we estimated the population that access each hospital using the gridded population data from World Pop (76).

### 2.2.2 Data preparation

Access to hospital EDs decrease with distance (77-79). Consequently, we used a 5 kilometers radius to estimate the population that is covered by each hospital. First, we obtained population data for 2010 and 2015 from Worldpop. We obtained the estimated population numbers per 100x100m grid square from Worldpop and adjusted it by census data for each municipality and year (31, 76). Second, we used a linear interpolation to impute the population for years 2011, 2012, 2013, 2014 and 2016. Third, we applied the proportions of the population with public insurance for each municipality and year to the corresponding parts of the radius covered by each hospital (32). Finally, we calculated weekly rates of ILI using the estimated population and the weekly rate of laboratory confirmed viruses adjusted by the total number of samples as shown in the equation:

$$r_{v,w,h} = \frac{\left(\frac{l_{v,w,h}}{N_{w,h}}\right)}{t_{w,h}} \; x \; 100{,}000$$

Where r is the adjusted rate of virus v on week w for hospital h. The number of positive samples for each virus v is represented by l, N is the population that access each hospital and t is the total number of samples.

We assumed missing data were missing at random (MAR) conditional on the observed data and imputed ILI and laboratory-confirmed time series using time series imputation with Kalman Smoothing (80, 81). We calculated the total influenza cases (influenza AB) as the sum of the imputed data of influenza A plus influenza B. For the imputation of metapneumovirus we used a simple moving average as an alternative method for imputing metapneumovirus cases due to non-convergence of Kalman Smoothing model secondary to the high number of zeros.

### 2.2.3 Statistical analysis

#### 2.2.3.1 Wavelet transformation

We used wavelet analysis to determine the best periodicity (e.g. seasonality) and compare timing of ILI in the ED and laboratory confirmed viruses: respiratory syncytial virus, adenovirus, parainfluenza, metapneumovirus, influenza A, influenza A, and influenza AB in each hospital. Wavelet transform is a well-suited method to determine seasonality for non-stationary time series. Likewise, wavelet transform is a good approach to determine the seasonality of a periodic time series without assuming a specific seasonality (82). Wavelet analysis has been used before to study different infectious diseases such as, dengue, pertussis, measles, and influenza (46-53). Wavelet transform can be understood as the cross-correlation of ILI rates time series with a group of wavelets of diverse “widths” or “scales” at different time points (82). The Morlet wavelet has been used before to study infectious disease incidence rates (46, 47, 54).

For each scale s and time interval δt, the continuous wavelet transform of a time series xk is defined as (83):

**Equation 2.1**

$$Wn(s) = \sum_{k=0}^{N-1} xk\,\psi * \frac{(k-n)\delta t}{s}$$

Where ψ* represents the complex conjugate of the Morlet wavelet function. N represents the time index, ranging from zero to the total number of time points and s are the scales.

To quantify the relationships between two time series the wavelet cross-spectrum and the wavelet coherence can be computed (84). An advantage of these 'wavelet-based' methods is that they can vary in time and detect transitory associations between time-series(84). Cross-wavelets and wavelet coherency allow to analyze scale dependencies between two signals (84).

We used Morlet wavelet coherence and Morlet cross-wavelet transformations to determine the association between ILI in the ED and each laboratory confirmed virus. Coherence is a direct measure of the correlation between the spectra of two time-series (85). Wavelet coherence is a representation of how two signals are correlated, hence, the interpretation is similar to a correlation coefficient and a measure of the degree of association of the two series (86).

Cross-wavelet transformation is used to reconstruct two time series simultaneously to determine the seasonality at any time t and determine the local relative timing between them (47, 83, 84). Cross wavelet provides an appropriate tool for comparing the frequency of two time series and for drawing conclusions about the synchrony at certain periods and a given time range (86). Given two time series X and Y with wavelet transforms WnX(s) and WnY(s), the cross-wavelet spectrum is defined as (83):

**Equation 2.2**

$$WnXY(s) = WnX(s)WnY*(s)$$

Where WnY*(s) is the complex conjugate of Wn Y(s).

The cross-wavelet spectrum is a complex function, defined as |WnXY(s)|, and can be interpreted as the cross-wavelet power (83). Cross-wavelet power can be used as a measure of the cross-correlation of two series in the time-frequency (or time-scale) domain (86). Cross-wavelet power spectrum and its significance was calculated for all ILI/virus pairs and hospitals (82, 83).The complex argument of a cross-wavelet transform, arg(Wxy ), represents the local relative timing (phase) between two time series xn and yn in a time frequency space (87). The local relative phase is represented in the cross-wavelet power spectrum as local arrows, where the angle represents the local timing difference between both signals. The time series xn leads for angles 0∘-90∘ and xy for angles 270∘-360∘, when both signals are synchronized (in-phase). On the other hand, both signals differ in timing (are out-of-phase) when the arrows range between 90∘ - 270∘.

For all transformations we used the same parameters. We used a non-dimensional frequency ω0 = 6, that has shown a good performance, good resolution and has been used previously for infectious disease (53, 83). We used periodicity step size δj of 1 on a linear scale that represents a weekly resolution and periods (scales) from 14 to 144 weeks. Statistical significance was tested by comparing the wave signal against randomly generated time series (i.e. white noise) with a significance level of 0.05 (84).

The cross-wavelet spectrum considers a zone that is affected by the edge effects related to the size of the periods. Consequently, the data not affected by edge effects, the cone of influence (COI), can be interpreted with more confidence (87). As a sensitivity analysis, we tested our analysis restricting our data for significant time points from the cross-wavelet transformation,

restricting to the COI, and restricting data to the combination of both significant time point included in COI. We obtained the same results compared to the complete data.

We selected separately the best seasonality for the cross-wavelet transformations of each ILI/Virus time series pair, per hospital. We defined the best seasonality as the range of periods within the 95th percentile of average power across all time points. Therefore, each hospital had its own seasonality for every pair of ILI/virus. To determine the periods with higher power, we computed the average cross-wavelet power for each period over all time points n from the cross-wavelet spectrum. We computed the average power according to the work of Torrence (83):

**Equation 2.3**

$$\overline{WXY^2}(s) = \frac{1}{N}\sum_{n=0}^{N}|WnXY(s)|^2$$

Where, N represents the number of observations, WnXY the cross-wavelet spectrum, and s are the scales.

Then, we filtered the cross-wavelet transforms for each hospital and ILI/virus pair using the range of best periods, excluding sub-annual cycles of periods <40 weeks. We reconstructed the epidemic cycles using a filter defined by Torrence and Campo (83):

**Equation 2.4**

$$x_n' = \frac{\delta t\sqrt{\delta t}}{C_\delta \psi_0}\sum_{j=j1}^{j2}\frac{\Re\{W_n(sj)\}}{\sqrt{sj}}$$

Where δt, the periodicity step size, was 1 and Cδ, the reconstruction factor, was 0.776 empirically derived for the non-dimensional frequency ω0 = 6 (83). Values from j1 and j2 were the lower and upper limits of the range of periods that included the 95th percentile of power.

Since the Morlet wavelet is a complex function with a real and an imaginary part, this allows us to separate the amplitude (magnitude of the difference between extreme values) and the phase of a signal as the timing of a signal within a specific period, regardless of the amplitude (82). The real part enables the extraction of phases as an indicator of epidemic timing. We extracted phases for each hospital ILI/Virus pair as described previously by Torrence (47, 82, 83):

**Equation 2.5**

$$\phi_n(s) = tan^{-1}\left(\frac{\Im\{W_n^{XY}(s)\}}{\Re\{W_n^{XY}(s)\}}\right)$$

Where ϕn(s) is the phase for a scale s, ℑ{WnXY(s)) is the imaginary part, and ℜ{WnXY(s)), the real part.

Phases are continuous and are presented as phase angles in radians from -π, the starting point, to +π before resetting and starting a new cycle (84). We extracted the phase angles using a band of periods within the 95th percentile of average power as described previously and calculated the difference between both ILI and lab-confirmed virus. A negative phase difference represented an earlier ILI peak compared to lab-confirmed virus and vice versa. We used a t-test to test the hypothesis that there was no difference in timing between ILI and each laboratory confirmed virus across hospitals (average phase difference was = 0). To determine the virus that reflected most closely ILI timing, we compared the distributions of phase differences between viruses. Finally, we compared wavelet coherency distribution for each filtered time series of ILI-virus across hospitals. We used R and the R package Waveletcomp for data transformation and analysis (88, 89).

## 2.3 RESULTS

### 2.3.1 Hospitals Selected

A total of 25 hospitals were selected from all the 15 regions of the country (Figure 2.1). Three hospitals had zero metapneumovirus cases in the period, and therefore were excluded (hospitals 06-100, 06-103 and 19-100).

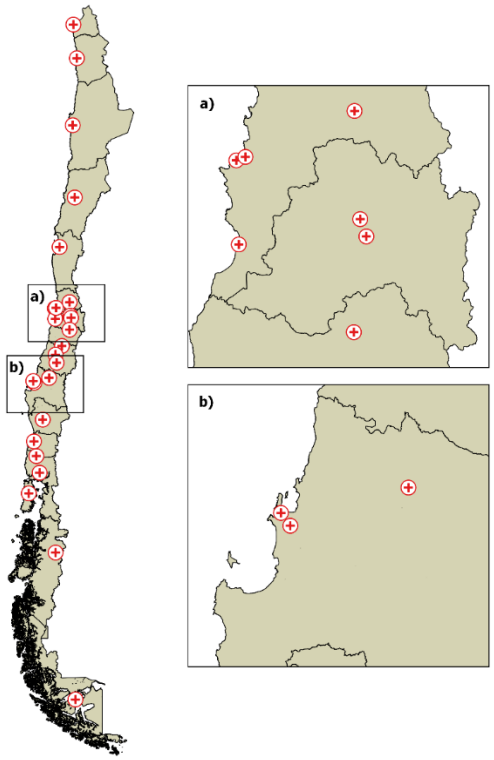


**Figure 2.1. 25 Hospitals included (+ sign) with laboratory surveillance and influenza-like illness surveillance, Chile 2011-2016**

### 2.3.2 Cross-Wavelet

The cross-wavelet power spectrum showed a consistent annual seasonality for all viruses across hospitals. Annual seasonality was presented in the cross-wavelet power spectrum as red/yellow zones within the black contour in the range of periods between 40 and 70 that covered more than 4 years (208 weeks) in the time axis. An example, for hospital 10-100 from the center of the country, is shown in **Figure 2.2**, the rest of the hospitals' cross-wavelet power spectrums are available in Appendix A.

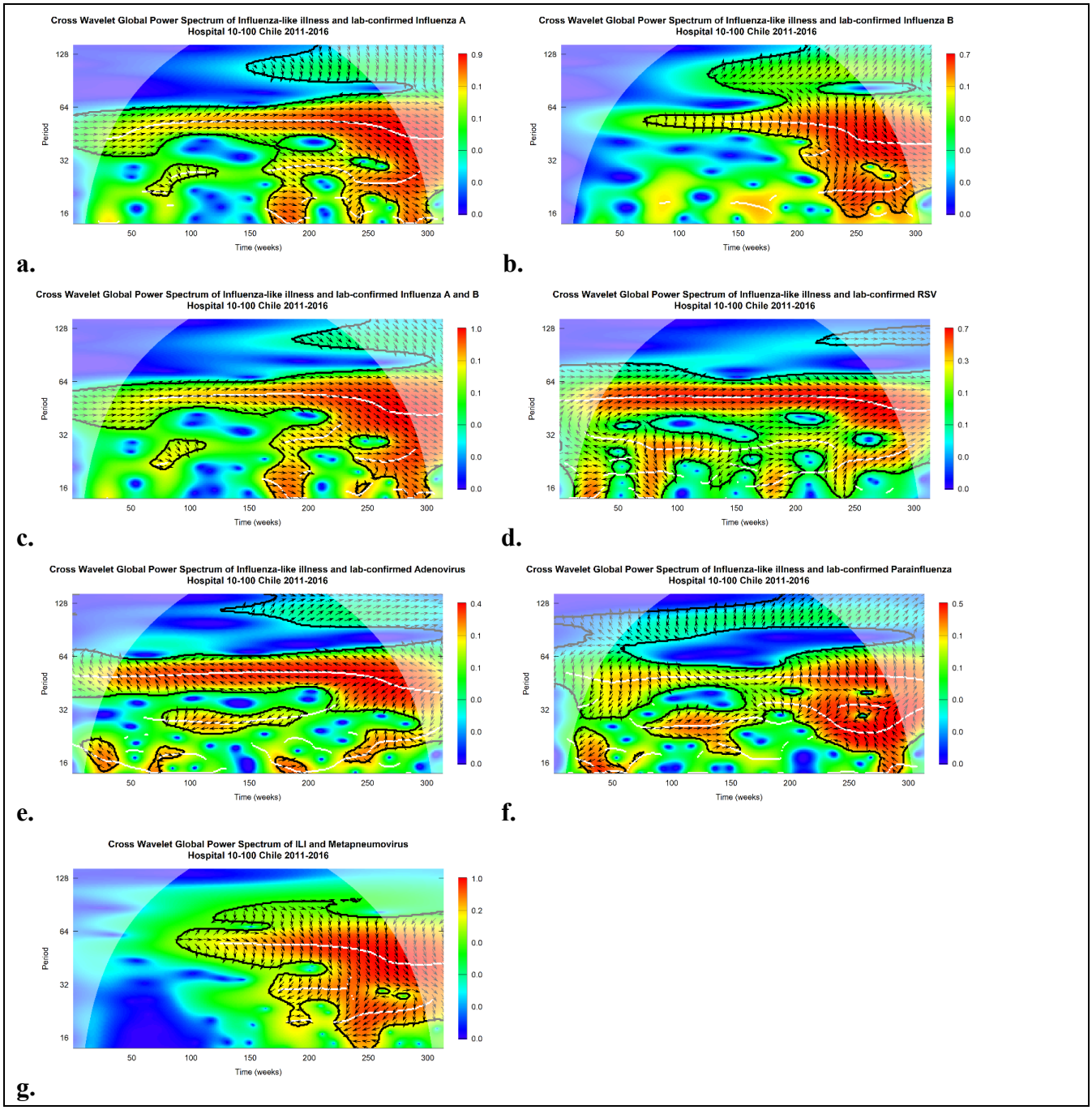


**Figure 2.2. Cross-Wavelet Power Spectrum for ILI and Lab-confirmed Viruses in Hospital 10-100, Chile 2011-2016**

Cross Wavelet Power Spectrum for ILI and **a.** influenza A, **b.** influenza B, **c.** influenza A and B, **d.** respiratory sincicial virus, **e.** adenovirus, **f.** parainfluenza, and **g.** metapneumovirus. Colors represent cross wavelet power representing the correlation between both time series and a wavelet with a seasonality equivalent to the period (y axis) in a given week (x axis) . Black lines mark significant power with a 95% confidence level compared to white noise, white line the ridge of power values and shaded area demark the zone affected by edge effect delimiting the cone of inflluence inside. Whithe line correspond to the power ridge. Arrows show the relative timing difference (phase difference ) between both signals. Arrows pointing right represent synchronicity between both signals (in-phase), on the contrary, an arrow to the left represents asynchronic time series (out of

phase). An arrow pointing up represents ILI leading and an arrow down represents the corresponding virus leading timing over ILI.

Most hospitals had annual seasonal patterns for at least 4 years. For influenza A, influenza AB, respiratory syncytial virus and Adenovirus 92% of the hospitals displayed an annual seasonal pattern for ≥4 years. For influenza B, had 88% of the hospitals displayed an annual pattern for more than 4 years, 73% of hospitals for metapneumovirus and 60% for parainfluenza (Table 2.1 and Table 2.2). Few hospitals (n=4) had a sub-annual or multiannual predominant seasonality for influenza B, parainfluenza, adenovirus and metapneumovirus.

**Table 2.1. Number of hospitals and type of seasonality in the Cross-wavelet power spectrum in 25 hospitals, Chile 2011-2016**

| | Influenza A n(%) | Influenza B n(%) | Influenza A and B n(%) | RSV n(%) | Parainfluenza n(%) | Adenovirus n(%) | Metapneumovirus n(%) |
|---|---|---|---|---|---|---|---|
| **Sub-annual Seasonality (< 40weeks)** | | | | | | | |
| Duration of seasonality | | | | | | | |
| *≥4 years* | | | | | | | |
| *<4 years* | | | | | 1 (0.04) | | |
| **Annual Seasonality (40 - 70 weeks)** | | | | | | | |
| Duration of seasonality | | | | | | | |
| *≥4 years* | 24 (0.96) | 14 (0.56) | 24 (0.96) | 24 (0.96) | 21 (0.84) | | 15 (0.68) |
| *<4 years* | 1 (0.04) | 10 (0.4) | 1 (0.04) | 1 (0.04) | 2 (0.08) | 3 (0.12) | 6 (0.27) |
| **Multiannual Seasonality (>70 weeks)** | | | | | | | |
| Duration of seasonality | | | | | | | |
| *≥4 years* | | | | | 1 (0.04) | | |
| *<4 years* | | 1 (0.04) | | | | 1 (0.04) | 1 (0.04) |
| **TOTAL** | 25 (1) | 25 (1) | 25 (1) | 25 (1) | 26 (1) | 25 (1) | 22 (1) |

### 2.3.3 Coherence

All viruses had a high coherence compared to ILI that ranged from 0.84 to 1 ( ). The highest modes were observed for respiratory syncytial virus, influenza A and influenza AB with 0.99, 0.98, and 0.98 respectively.

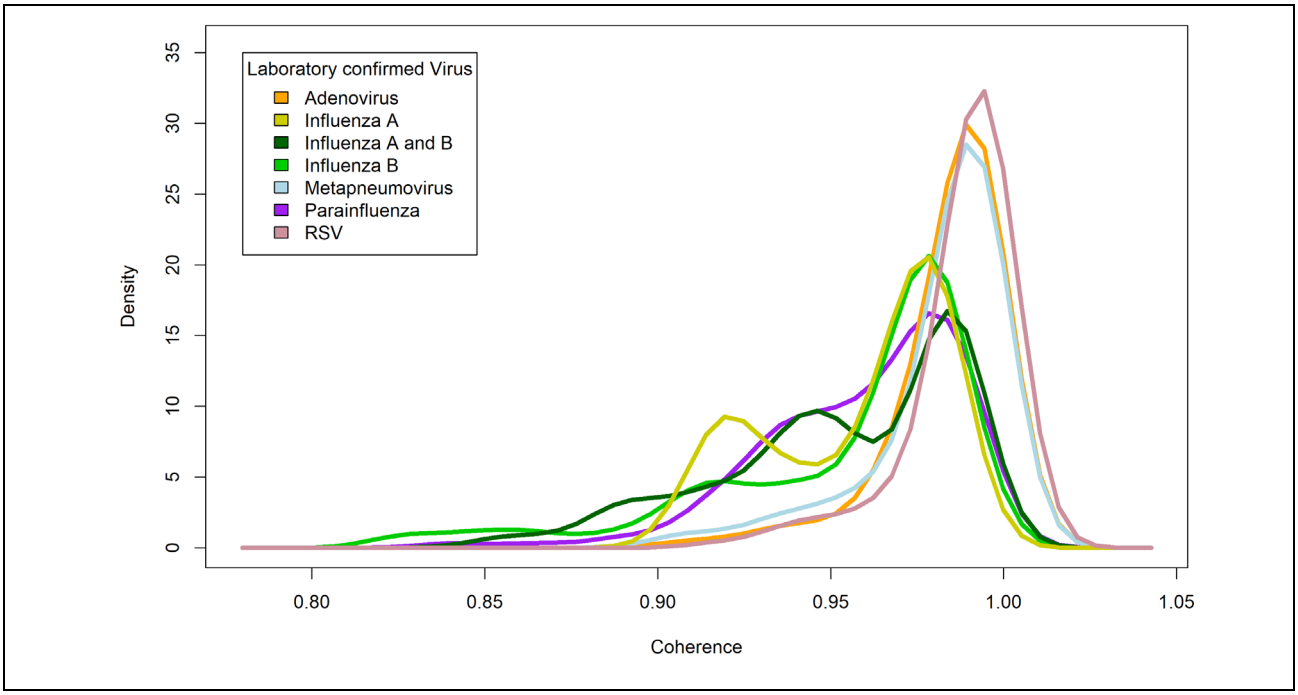


**Figure 2.3. Coherence distribution across hospitals of ILI and Lab-confirmed viruses, Chile 2011-2016**

Distribution of coherence between ILI and Lab-confirmed viruses across hospitals. Coherence is a measure of correlation between two signals. All viruses' time series have a high correlation with ILI.

### 2.3.4 Best Seasonality

The average power showed a similar seasonal pattern across hospitals for all ILI/Virus pairs. The pattern is represented by the vertically aligned red zones in Figure 2.4 column B. The 95th percentile of power, the best seasonality, for each hospital showed a range of similar periods close to an annual seasonality (52 weeks). In general, the best seasonality ranged between 40 - 56 weeks for influenza A and influenza AB, 42-58 for AD, 42-57 for parainfluenza, 43-98 for influenza B, 48–57 for respiratory syncytial virus, and 46-105 weeks for metapneumovirus (Figure 2.4 column C). Twenty-five (25) hospitals had best seasonality >40 weeks for respiratory syncytial virus, 24 for influenza A and influenza AB, 21 for influenza B and metapneumovirus, 20 for adenovirus and 17 for parainfluenza.

| A | B | C |
|---|---|---|
| Influenza A | 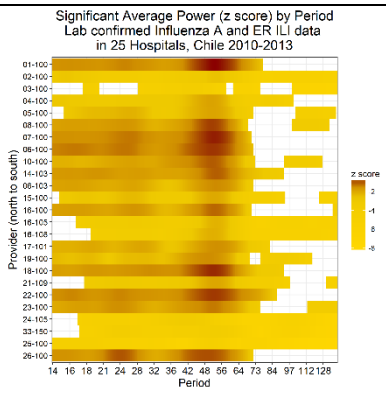 | 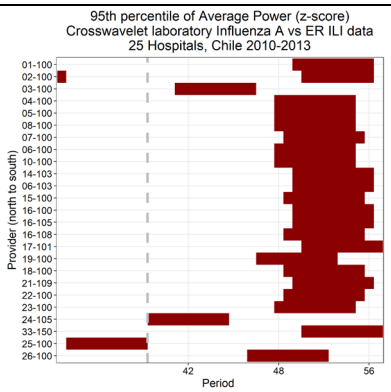 |
| Influenza B | 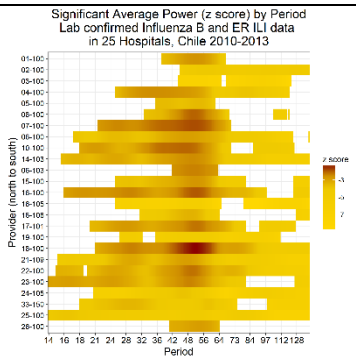 | 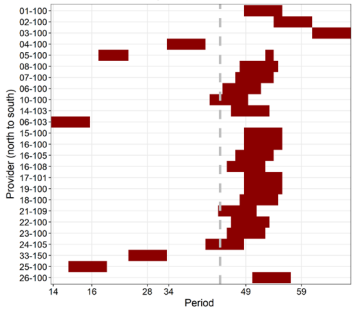 |
| Influenza A and B | 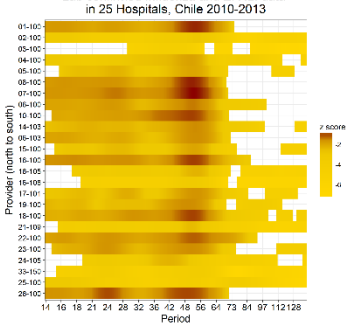 | 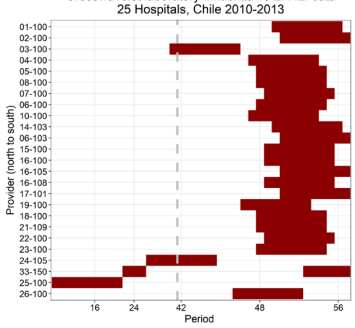 |
| RSV | 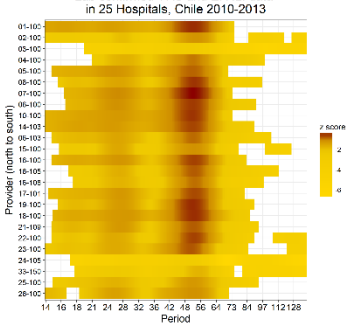 | 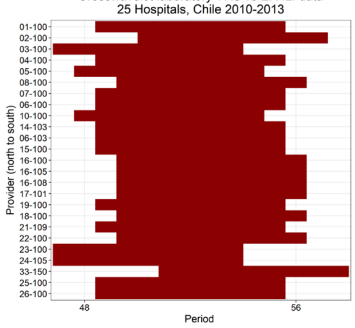 |

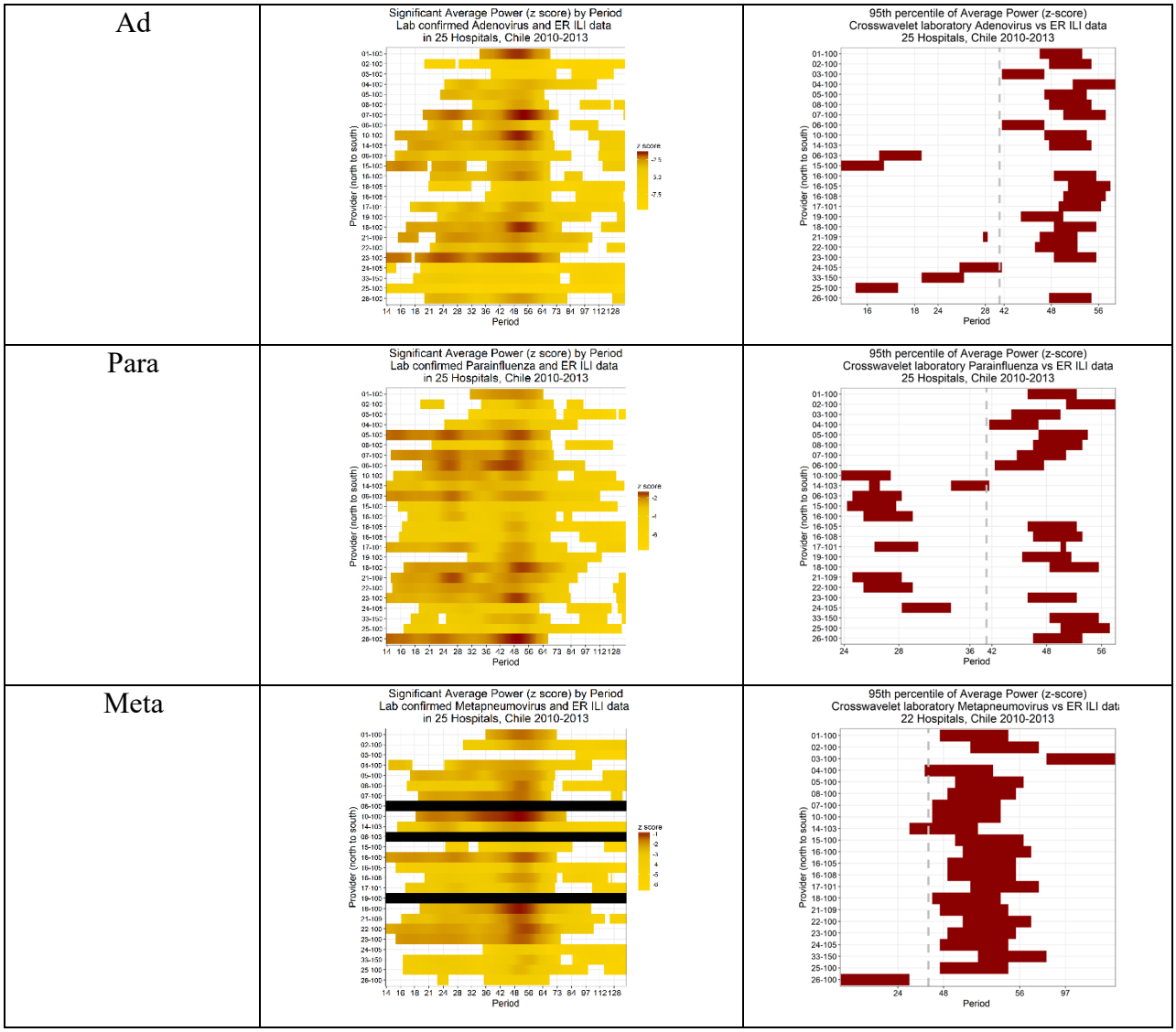


**Figure 2.4. Significant average power and best seasonality of ILI and lab-confirmed virus for hospitals, Chile 2011-2016**

Column A) Lab confirmed virus compared to ILI B) Cross wavelet average power per period for hospitals. Colors represent average cross wavelet power representing the correlation between both time series and a wavelet with a seasonality equivalent to the period (x axis) for each hospital ordered by latitude (y axis). Only significant average power with a 95% confidence compared to white noise are colored. Power was transformed to z-score for comparison. Missing data due to non-reported metapneumovirus in black. Column C) 95th percentile of average cross wavelet power for each hospital. Range of periods for each hospitals are presented in red. Dashed grey dashed line denote the lower limit of annual cycles of 40 weeks.

In general, ILI and most viruses time series were synchronized (in-phase) with the laboratory confirmed viruses. Influenza AB and respiratory syncytial virus were in-phase in all hospitals, influenza A and metapneumovirus were in phase for all hospitals except one and two

hospitals respectively. Influenza B and parainfluenza had similar number of in-phase and out-of phase hospitals (Table 2.2). Adenovirus had more hospitals with time series out-of-phase vs ILI. Figure 2.5 and Figure 2.6 shows examples of in-phase and out-of-phase time series. In the hospital 10-100, influenza A and ILI had similar rate (Figure 2.5 top), wavelet transform (Figure 2.5 middle) and phases timing (Figure 2.5 bottom). Instead, Figure 2.6 shows out-of-phase time series of adenovirus and ILI in hospital 10-100. The rest of the rate time series, wavelet transformed rates and phase for each virus/ILI pair per hospital are available in Appendix B.

**Table 2.2. Number of hospitals and phase synchrony of ILI and Laboratory-confirmed viruses in 25 hospitals, Chile 2011-2016**

| Virus | In-phase n(%) | Out-of-Phase n(%) | TOTAL |
|---|---|---|---|
| Influenza A | 23 (0.96) | 1 (0.04) | 24 |
| Influenza B | 10 (0.48) | 11 (0.52) | 21 |
| Influenza A and B | 24 (1.00) | 0 (0.00) | 24 |
| RSV | 25 (1.00) | 0 (0.00) | 25 |
| Parainfluenza | 10 (0.59) | 7 (0.41) | 17 |
| Adenovirus | 3 (0.15) | 17 (0.85) | 20 |
| Metapneumovirus | 19 (0.90) | 2 (0.10) | 21 |
| TOTAL | 114 | 38 | 152 |

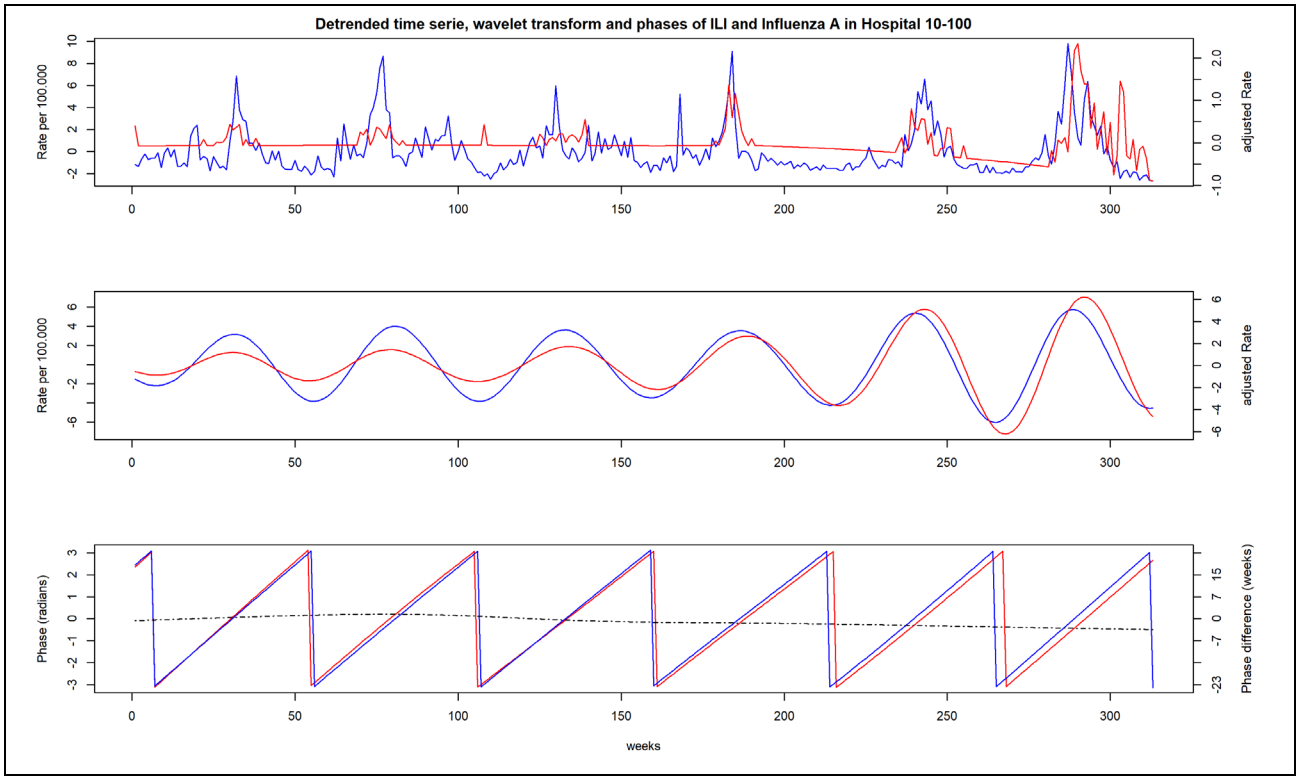


**Figure 2.5. Detrended rate time series, wavelet transformed rates and phases of ILI and influenza A in hospital 10-100, Chile 2011-2016**

Example of influenza-like illness and lab-confirmed influenza A time series comparison in Hospital 10-100 from Santiago, the capital city. Blue: ILI, Red: Influenza A. Top: Detrended time series rates ILI and detrended adjusted rates of Influenza A. Middle: Wavelet transformed rates with the best seasonality filter of periods between 48 – 54 (see Figure 2.4 Line 1, column C). Bottom: Phase angles and phase angles difference (dashed black line) between ILI and Influenza A. The cycles or seasons for each time series, starts at -3.14-degree radians, lower point in the middle graph, then the increase up to 0 degree correspond to the rates peak, then follows the descending rates represented by positive increase of phase angles up to 3.14 radians, then the cycle reset and start all over again. Here, phases are synchronized in timing with signals that are in-phase.

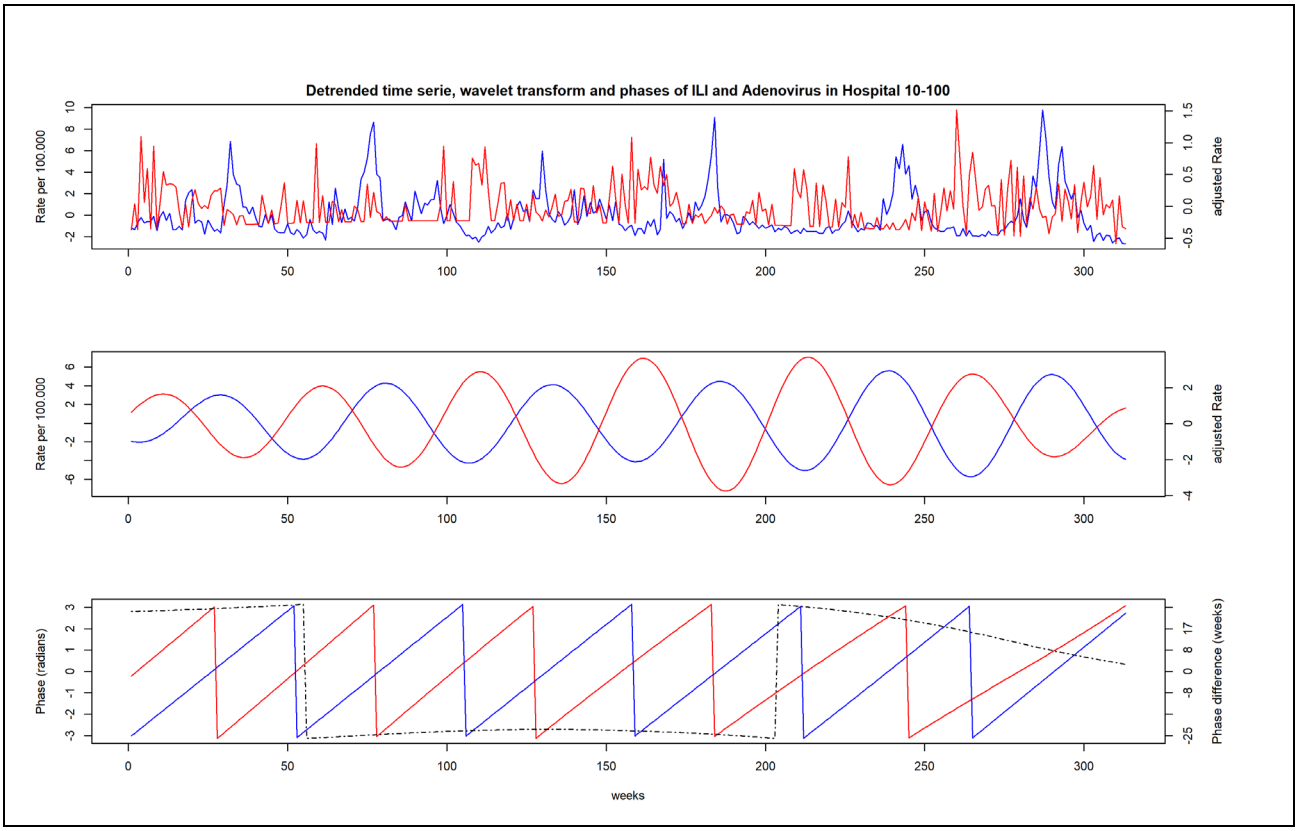


**Figure 2.6. Detrended rate time series, wavelet transformed rates and phases of ILI and Adenovirus in Hospital 10-100, Chile 2011-2016**

Example of Influenza-like illness and lab-confirmed adenovirus time series comparison in Hospital 10-100 from Santiago, the capital city. Blue: ILI, Red: Influenza A. Top: Detrended time series rates ILI and detrended adjusted rates of adenovirus. Middle: Wavelet transformed rates with the best seasonality filter of periods between 46 – 54 weeks (see Line 5, column C). Bottom: Phase angles and phase angles difference (dashed black line) between ILI and adenovirus. The cycles or seasons for each time series, starts at -3.14-degree radians, lower point in the middle graph, then the increase up to 0 degree correspond to the rates peak, then follows the descending rates represented by positive increase of phase angles up to 3.14 radians, then the cycle reset and start all over again. Here, phases differ in timing with signals that are out-of-phase.

### 2.3.5 Phase difference

Phase difference represents the relative timing between ILI and lab-confirmed viruses, where a negative value represents ILI preceding lab-confirmed viruses. We found that phase differences were normally distributed for the different viruses across hospitals. We found that metapneumovirus, influenza B, influenza AB and respiratory syncytial virus had, on average,

significantly different timing compared to ILI across hospitals. metapneumovirus, influenza B, influenza AB were delayed 8, 2.5 and 11 weeks compared to ILI respectively. Instead, respiratory syncytial virus preceded ILI by 2.5 weeks. On the other hand, non-significant differences were found for influenza A and parainfluenza that were delayed 0.21 (1.5 days) and 0.65 (4.55 days) weeks respectively compared to ILI, and adenovirus that led ILI by 0.37 (2.6 days) weeks (Figure 2.7). From these three viruses, parainfluenza and adenovirus presented wide distributions without a clear predominant phase difference. In contrast, influenza A had a phase difference that peaked close to zero (Figure 2.8).

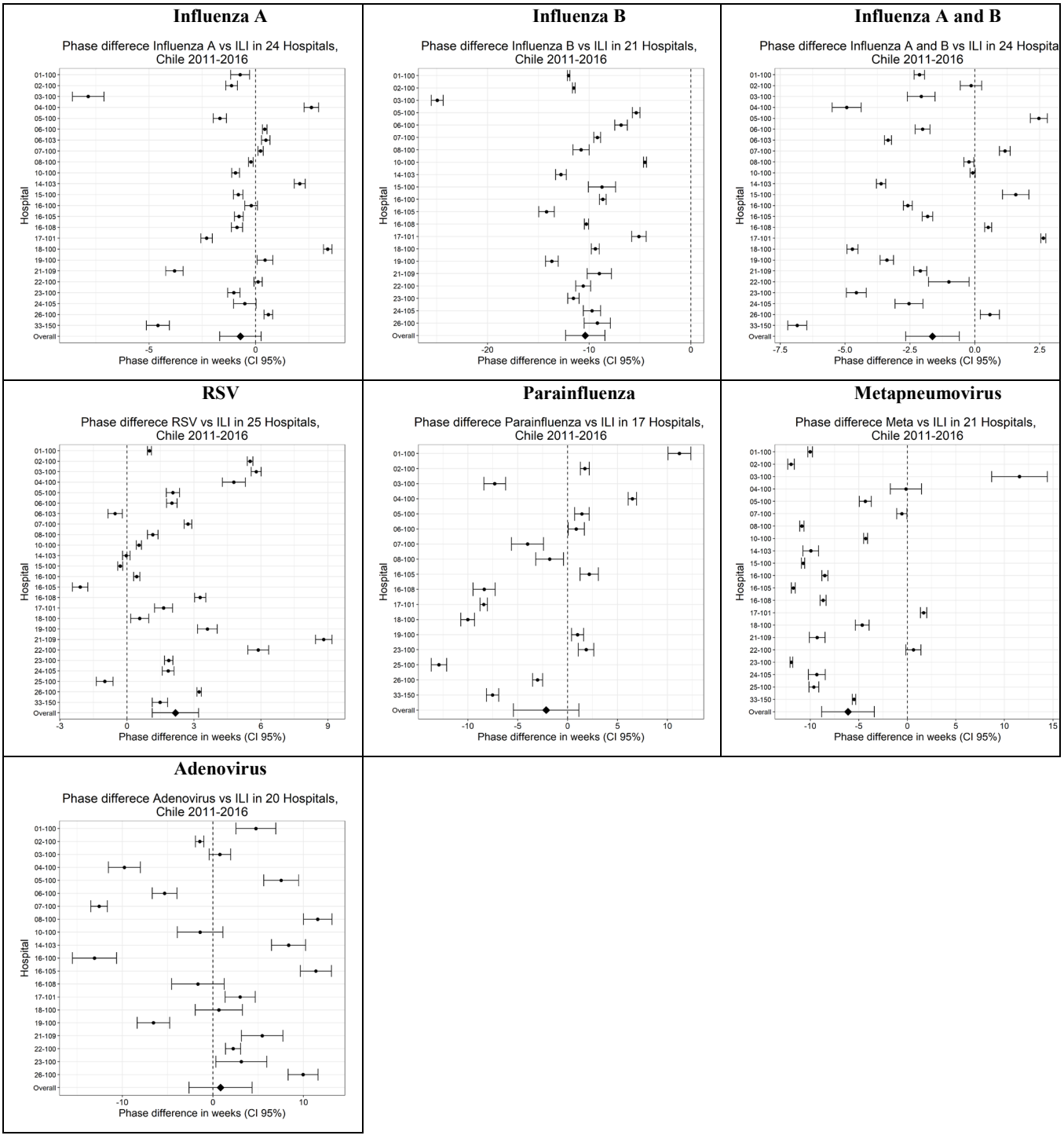


**Figure 2.7. Phase difference distribution across hospital between ILI and lab-confirmed viruses, Chile 2011-2016**

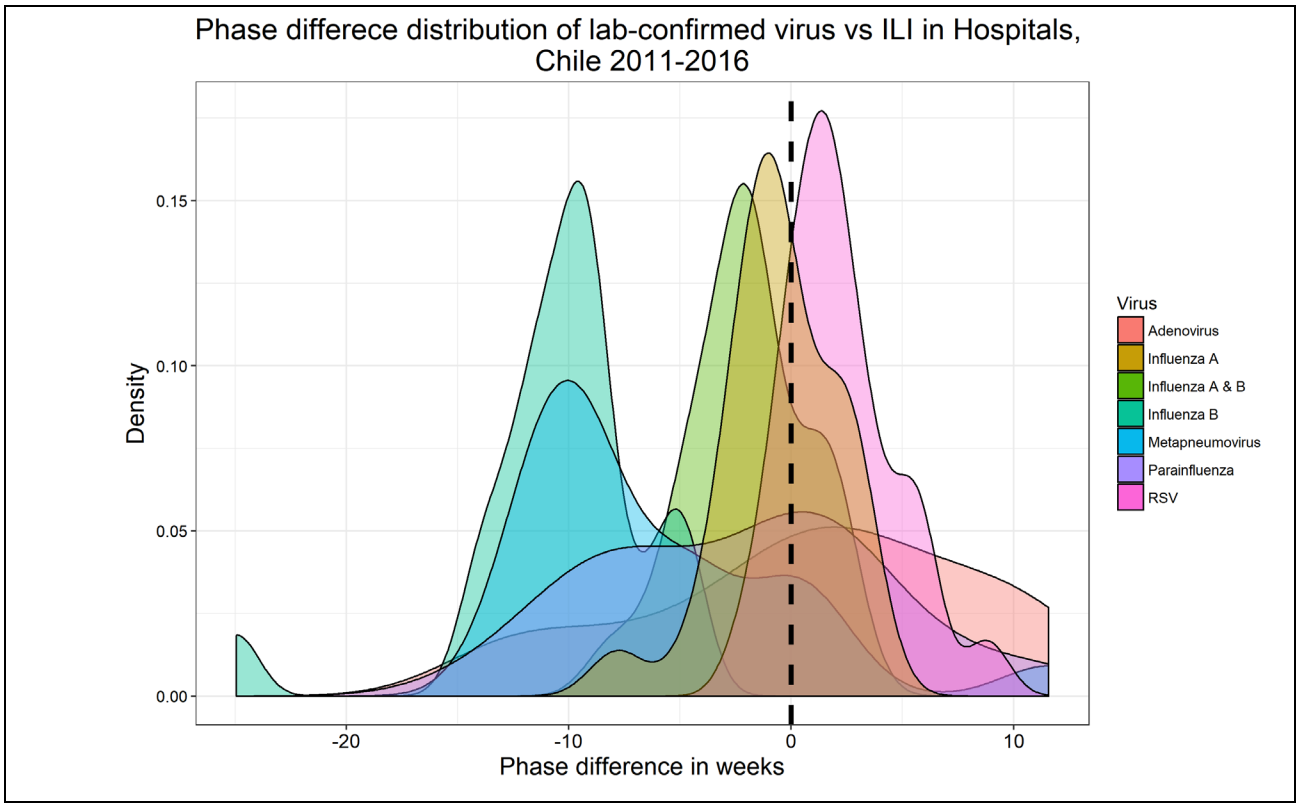


**Figure 2.8. Distribution of phase angle difference between ILI and lab-confirmed viruses, Chile 2011-2016**

Distribution of phase angle difference with ILI by Lab-confirmed viruses. Dashed line represents no difference in timing between ILI and the corresponding virus.

## 2.4 DISCUSSION

Most studies compare ILI and influenza or other viruses using one pair of time series of a region, city or country (11, 58, 65, 90-94). In this study, we evaluated 25 hospitals from various zones of the country to assess the relation between ILI and 6 different laboratory confirmed viruses and the sum of influenza A and influenza B. Rather than assuming an annual seasonality a priori, we used individual hospital seasonality for each ILI/virus pair.

We found that ILI timing was most closely related to influenza A compared to other viruses in the laboratory surveillance system. There was no difference in weekly timing between influenza A and ILI across all hospitals, with a clear predominant phase difference close to zero. Influenza A was most closely related in timing to ILI with a clear peak in the phase difference distribution. Even though neither adenovirus nor parainfluenza demonstrated a difference in timing compared to ILI, both had wide phase differences distributions that made it difficult to determine a consistent time difference and limits the interpretation of ILI as a consistent measure of these viruses. In other words, ILI in a given week, appears to represent influenza A with respect to timing. ILI has been described as a good measure of influenza (62, 72, 95). In Hong Kong, ILI rates in primary care showed a similar seasonal pattern to influenza virus activity (94). Similarly, to our study, Yang used a range of periods between 48 – 56 weeks and found no phase difference between ILI and influenza. Here, ILI preceded by 1.6 weeks (-2.5 to 4.3) in general outpatient clinics and by 4.1 weeks (-0.3 – 6.0) in general practitioners (94). Further, ILI has been found to be reliable for predicting influenza epidemics as ILI data was correlated with laboratory data in temperate regions (96).

In is not surprising that we found that most viruses were closely synchronized (in-phase) with ILI, given that all the viruses are part of ILI syndrome. Curiously, we found that respiratory syncytial virus preceded ILI. It is possible that this is because respiratory syncytial virus affects mostly children, and we did not analyze data by age group. Despite the lack of age categories, we used hospitals that covered children and adults in their emergency departments. Bias may still be present given that is difficult to samples children and samples might be drawn from children with severe infection. Influenza B and metapneumovirus showed a late peak compared to ILI. Influenza peak coincided with the experience of temperate areas and reports from the Chilean Ministry of Health (33, 92). The earlier peak of influenza A compared to ILI can explain the

differences of influenza B and influenza AB to influenza A. Further, differences between timing of influenza A and influenza B to ILI timing emphasizes the importance of measuring different strains of influenza in the surveillance system.

This study has some limitations. Data were obtained from ED and surveillance registers and did not relate each ILI case to a case sampled. We assumed that all laboratory tested cases were registered as ILI cases. We were unable to include age group in the analysis. To control by population and intensity of sampling through the year, we used laboratory rates and adjusted them by the total number samples (positives and negatives) given the increased probability of finding a positive sample as the number of samples increase. This may decrease the possibility of finding associations between time series that are known to have an implicit seasonality. Regardless, we found good coherence (correlation) of ILI and all viruses studied. It would be important in further studies to include age to determine timing differences between different age groups and have a better understanding of respiratory virus dynamics.

## 2.5 CONCLUSION

ILI in EDs preceded most viruses measured in the Chilean laboratory surveillance system. Influenza A had a consistent timing difference across hospitals. It is likely that ILI reflects the weekly circulation of influenza A. ILI is a good measure of influenza A timing compared to other viruses from the laboratory surveillance system and can be used to determine influenza A timing in Chile.

# 3.0 NORTH TO SOUTH GRADIENT AND LOCAL WAVES OF INFLUENZA IN CHILE: A TIME-SERIES ANALYSIS USING WAVELETS

Christian Garcia, MD MPH[1,2]; Lee H. Harrison, MD[1,3]; Christina F. Mair, MPH PhD[4]; Maria M. Brooks PhD[1]; Wilbert van Panhuis, MD PhD[1]

1. Department of Epidemiology, University of Pittsburgh Graduate School of Public Health
2. Division of Disease Prevention and Control, Ministry of Health, Chile.
3. Infectious Diseases Epidemiology Research Unit, University of Pittsburgh
4. Department of Behavioral and Community Health Sciences, University of Pittsburgh Graduate School of Public Health

## 3.1 ABSTRACT

**Background:** Influenza cause a high burden disease worldwide. Influenza seasonality is caused by complex interactions of weather factors, virus mutations, population crowding, and human travel. Even though annual surveillance reports of influenza show an annual seasonality in Chile, no studies have estimated the seasonality and latitudinal patterns of seasonal influenza within the country.

**Objective:** We aim to evaluate influenza timing across Chile and the presence of travelling patterns through different territories as local waves of influenza.

**Method:** We conducted an ecological study of the 29 public health networks from Chile. We obtained ILI surveillance data and estimated the seasonality across health networks using wavelet analysis. Then, we assessed the relationship between the start, the peak of ILI epidemic, and latitude using a linear and piecewise regressions. Finally, we estimated the presence of incoming and outgoing travelling waves (timing vs distance) between networks and the relation to population using linear and logistic regression respectively.

**Results:** We found a north to south latitudinal gradient of influenza and travelling waves that were present principally in the center of the country and associated to larger population size.

**Conclusion:** Our findings suggest that larger population located in the center of the country drives seasonal influenza epidemics in Chile.

## 3.2 INTRODUCTION

Influenza persists as an important cause of disease worldwide. Annual influenza epidemics affects 5-10% of the world population causing 250,000-500,000 deaths every year (16). Influenza seasonality is caused by complex interactions of factors including virus mutations, temperature, humidity, rainfall, population crowding and human travel (1, 11, 18, 19). In temperate areas influenza peaks in winter months. On the other hand, in tropical and subtropical areas influenza is present year-round with peaks related to the rainy season (16, 17).

The antigenic drift of influenza virus causes mutations in surface proteins that generate new viruses that elude immunity and can lead to global epidemics (2). Identification of influenza seasonality is crucial for implementation of effective control strategies worldwide and in different countries (18, 97). Moreover, countries can tailor control strategies to their national and local patterns (90).

Influenza timing has been studied in different regions of the world. The virus travels from reservoirs in tropical areas to temperate areas (90, 92, 98-100). Similarly, influenza frequently moves from high to low populated areas associated with human movement (18, 101, 102). Local climates and social characteristics can generate specific patterns of influenza. Most evidence of influenza timing comes from the northern hemisphere, from developed countries, and from Asia. There are few studies from South America, and seasonal influenza timing has not been studied in Chile.

Several studies of influenza timing have used laboratory surveillance, mortality data and symptomatic surveillance of influenza-like illness (ILI). ILI is a useful measure to characterize influenza epidemics (91, 103-106). Even though, ILI surveillance has a high sensitivity and low specificity, it is a useful measure to describe influenza season and identify influenza population

patterns (94, 107). National surveillance is common throughout the world, but patterns within countries need large subnational and local datasets to estimate influenza dynamics. There is a need for information from the local level with the highest data resolution possible to inform prevention measures such as vaccination campaigns and provider preparedness.

In this study we evaluate influenza timing across Chile and the presence of travelling patterns through different territories as local waves of influenza. Chile is the country with the largest latitude range in the southern hemisphere (36 degrees from 17S to 53S), with 10 types of climate categories ranging from desertic to artic (31). Healthcare provision is organized in 29 Public Health Networks that include primary healthcare and hospital services. The Public Healthcare Insurance (National Health Fund: FONASA) covers 74.4% of the 17 million population (32). Influenza surveillance was enhanced after the 2009 pandemic with year-round surveillance of influenza-like illness (ILI) in emergency departments (ED), laboratory surveillance by sentinel providers and surveillance of severe respiratory disease hospitalizations (33). Hospitals record and report to the ministry of health daily ED diagnosis. ED and laboratory surveillance showed that in Chile influenza usually starts in fall (April-May) and peaks in winter (July-August)(34, 35). Chowell et al. found a south to north pattern of hospitalizations for H1N1 pandemic strain in 2009 (95). Burger confirmed this pattern using mathematical simulation of the same data and found that Santiago, the capital, was a hub that spread the epidemic rapidly to the rest of the country (108).

A better understanding of seasonal influenza in Chile can help implement timely vaccination campaigns and allocate resources to control seasonal influenza. Further, knowledge about seasonality of influenza could help to identify unusual patterns associated with new strains. Additionally, local waves information can show the spatial relation between seasonal patterns in different zones of the country. These relations can help to prioritize zones with earlier start times

with earlier vaccination campaigns. On the other hand, zones with similar timing of influenza will need to implement prevention campaigns at the same time to protect the population. Finally, factors that increase the odds of incoming or outgoing travelling waves of influenza would inform actions to prepare and respond to the annual epidemics.

Even though annual surveillance reports of influenza show an annual seasonality, no studies have estimated the seasonality of seasonal influenza in Chile. The geographic characteristics, health system organization and influenza surveillance system make Chile a suitable country to study, the yet unknown, influenza patterns between locations. Hence, we aimed to estimate the seasonality and spatial dependencies of influenza across Chile using ILI reported in ED.

## 3.3 METHODS

### 3.3.1 Design

We conducted an ecological study to assess the seasonality of influenza in Chile and the relationship with local influenza patterns. We first collected time-series data from daily ED visits and calculated health network-specific rates of ILI. Second, to test the hypothesis that there is an annual seasonality of ILI, we estimated the seasonality of ILI across health networks using wavelet analysis. Then, to test the hypothesis that annual epidemic start and peak are associated to latitude, we extracted the annual start and peak dates within each health network and assessed the relationship between the start and peak of ILI and latitude using a linear and piecewise regression. Finally, to test the hypothesis that there are local travelling waves associated to population, we

estimated the relation between timing versus distance represented as incoming and outgoing travelling waves for each health network using linear regression and the relation to population using a logistic regression model.

### 3.3.2 Data sources

We obtained daily ILI cases between 2010 and 2016 from EDs of large- and medium- size public hospitals, collected by the Chilean Ministry of Health. We used hospital location, census data and population coverage from official governmental institutions to estimate the population that access each hospital. These data sources included the Ministry of Health, National Public Insurance (FONASA), National Institute of Statistics (INE) and the National Repository of Geospatial Information (32, 74, 75). To calculate rates, we estimated population that access each hospital using the gridded population data from World Pop (76).

We excluded small (community) hospitals and hospitals with no ED. Large and medium size hospitals that reported <75% of the 6-year period were also excluded (<1920 days). Hospitals that presented ≥5% missing data in groups of 20 consecutive days were also excluded to reduce imputation errors. We assumed the time-series missing data was missing at random (MAR) conditional on observed data. We used the same imputation method mentioned previously in subsection 2.2.2.

### 3.3.3 Data preparation

Access to ER in hospitals decrease with distance (77-79). Consequently, to calculate the population covered by each hospital, we used the same method mentioned in subsection 2.2.2. To

determine seasonality across Health Networks, we calculated ILI rate by network by merging daily ILI reports data and population from all hospitals within each health network. We used a mid-point location from hospitals within each network to determine the health network's latitude.

### 3.3.4 Data transformation

We used wavelet analysis to determine the best periodicity (namely seasonality) of influenza across the country. We used wavelet transform as explained in subsection 2.2.3.1 and in Equation 2.1. Differing from what we used in chapter 2, we did not use cross-wavelet to transform simultaneously two signals, rather we applied wavelet transformation to one time series at a time.

We conducted wavelet transformations for periods (scales) from 14 to 144 weeks. Statistical significance was tested by comparing the wave signal against randomly generated time series (i.e. white noise) with a difference considered to be statistically significant at the level of 0.05 (84). The local wavelet power spectrum was used to visualize the cross-correlation between rates and each group of wavelets, namely the power, and its significance (Figure 3.3) (82, 83).

To determine the best seasonality (periods with higher power), we computed the average power of wavelet transforms for each period over all time points, n, from the local wavelet power spectrum. We computed the average power separately for the country, for each Health Network, and for each hospital, according to the work of Torrence (83):

**Equation 3.1**

$$\bar{W}^2(s) = \frac{1}{N}\sum_{n=0}^{N}|Wn(s)|^2$$

Where, N represents the number of observations.

We defined the best seasonality of influenza as the range of periods within the 95th percentile of average power across periods. The best seasonality for the whole country, across health networks and across hospitals showed the same range of periods.

### 3.3.5 Association between epidemic timing and latitude in Health Networks.

To determine the association of influenza timing and latitude we filtered the wavelet transform using the range corresponding to the best seasonality for each Health Network. We used the same filter mentioned in subsection 2.2.3.1 and Equation 2.4.

We determined the start and peak date of annual ILI epidemic for each Health Network. We defined start date as the date when the reconstructed cycles reached half point between the lowest point and the peak of the signal for each year. Then, we calculated the peak day as the date of the highest point of the signal for each year. Finally, we calculated the median start and median peak date for each Health Network.

We used separated linear models to assess the relationship of latitude as a predictor of the start and peak of the epidemic across Health Networks. For both outcomes, we created univariate, piecewise and multivariate linear models. For the piecewise models, we separated the country into 3 zones: north, center and south with latitude range of <31, 31-40 and >41, respectively. For multivariate models, we included the independent variables latitude and population as continuous variables, airport nearby as a binary variable, and year as dummy variables with 2013 as the reference year. Predominant strain was excluded due to linear dependencies with years 2011 and 2014. We forced years, as a dummy variable, into the models to adjust for epidemic year. We selected the best multivariate model using the best subset method (109). For each outcome, we

compared all possible models for each number of variables using regression sum of squares method. The best model was selected using BIC and Mallow's Cp (109, 110).

### 3.3.6 Local traveling waves of influenza

Morlet wavelet is complex with a real and an imaginary part. The real part of the Morlet wavelet enables the extraction of phases as indicator of epidemic timing. Also has the advantage of separating the amplitude (magnitude of the difference between extreme values) and the phase of a signal as the timing of a signal within a specific period, regardless of the amplitude (82). We used the same filter mentioned in subsection 2.2.3.1 and used Equation 3.2 to extract phase angles as a measure of timing. We extracted the phase angles using a band of periods within the 95th percentile of average power as described previously (2.2.3.1).

We calculated the median difference of phase angles (timing) for the complete period for all possible pairs of Health Networks and tested the association to distance.

We created two distinct linear models for each of the 29 Health Network to all others, one for positive phase differences and the second for negative phase difference that correspond to outgoing and incoming travelling waves respectively. The sign of the phase difference represented the relative timing of the health services such that a negative difference indicated a delayed timing of influenza and vice versa. The linear regression models we used were:

**Equation 3.2**

$$\theta_{p,q} = \begin{Bmatrix} C - \beta_p d_{p,q} & for\ \theta < 0,\ incoming\ waves \\ C + \beta_p d_{p,q} & for\ \theta > 0,\ outgoing\ waves \end{Bmatrix}$$

Where θp,q is the lag between Health Networks p and q, and dp,q is the distance in kilometers between Health Networks. The distance sign was inverted for negative lag times for a more

intuitive display of incoming waves. We considered a local traveling wave as a significant linear association between phase difference and distance using a corrected Bonferroni significance level of 0.0017.

In order to define what is a "local" distance, we used a second-degree local polynomial regression model (loess) of spearman's correlation between pairs of Health Networks phase angle time series to distance with parameter $\alpha = 0.75$. Then, local was defined as the distance between 0 kilometers and the kilometers with the smallest correlation after an initial linear segment of the loess model. All pairs of Health Networks within this distance limit were included for each of the 29 linear models for traveling waves. The significance level used in these models was adjusted using Bonferroni methods in order to account for the multiple comparisons.

Finally, we created separate logistic regression for incoming and outgoing waves to determine the association between the presence of travelling waves and population adjusted by latitude for each of the 29 Health Networks. We used the receiver operating characteristic (ROC) curve and the area under the curve (AUC) to evaluate model discrimination (111).

We used R environment for analysis, R package Leaps for model selection and R package WaveletComp for data transformation and extraction of phases (86, 88, 89, 110).

## 3.4 RESULTS

### 3.4.1 Hospitals included

We included 71 of the 78 large and medium size hospitals in Chile in our analyses. Four large and 3 medium size hospitals were excluded. Of the 4 large hospitals excluded, 3 were from Santiago,

the capital of the country, and one was from Valparaiso, the second most populated city. All 3 medium size hospitals excluded were from small cities from the center, south, and extreme south of the country. Six pairs of hospitals from Santiago were combined. Four out of the six combined pairs corresponded to the merging of a pediatric and adult hospital from the north, east, south-east, and south Health Networks in the city. The additional two pairs of combined hospitals were located in the center and southern networks (see Appendix). The 65 hospitals included in the analysis covered the 15 regions of the country, all the 29 public Health Networks, and included cases from both adults and children (Figure 3.1).

A total of 242,982 ILI cases were reported from January 2010 to December 2016. Sixty five percent of the days reported by all hospitals had zero cases, and 34% (959,792) had ≥1 cases reported. There were 1861 (1.04%) days with missing data that were imputed. Missing data from hospitals ranged from 0 to 5% of the period.

ILI rates presented a cyclic pattern in all hospitals. Vertical linear patterns in the raster plot showed an annual seasonality of ILI. Timing had high synchrony and a high rate across hospitals in 2010 with a more spread pattern was present in the following years (Figure 3.1).

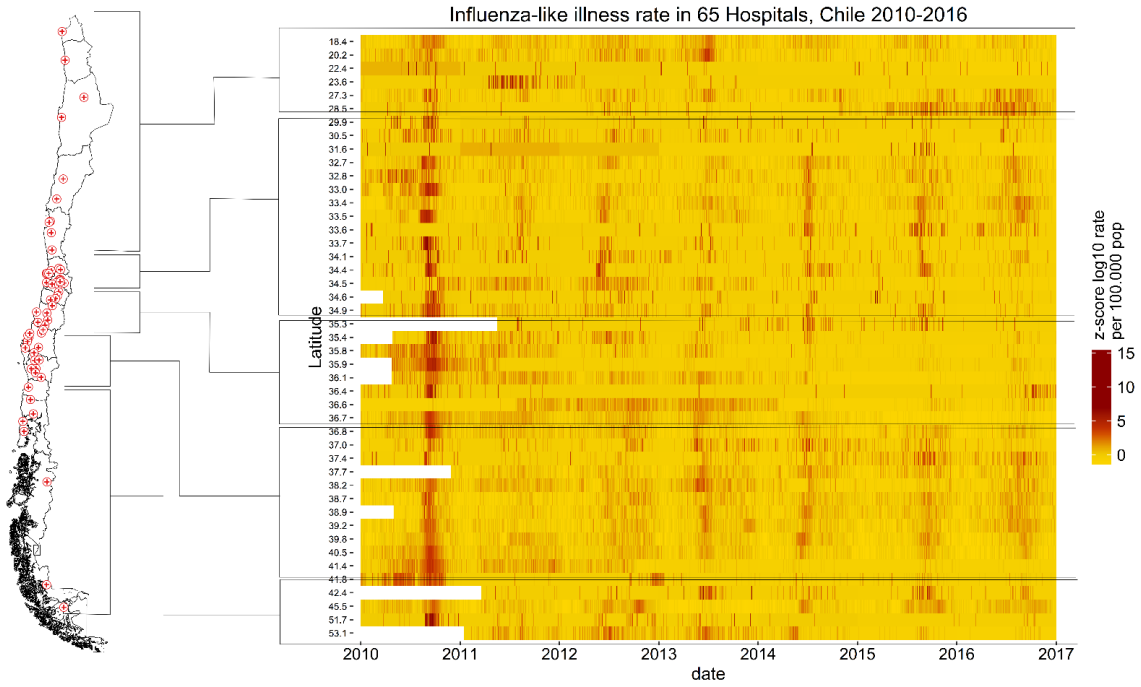


**Figure 3.1. Hospitals' location and ILI rates, Chile 2010-2016**

### 3.4.2 Predominant annual seasonality

We reconstructed national ILI rates and found a predominant annual seasonality. The annual pattern of ILI was present in the original time series and in the wavelet-reconstructed data (Figure 3.2). The local wavelet power spectrum showed that an annual seasonality was present within a band of periods from 40 to 64 and the highest average power corresponded to a period of 50 weeks (Figure 3.3 and Figure 3.4 respectively).

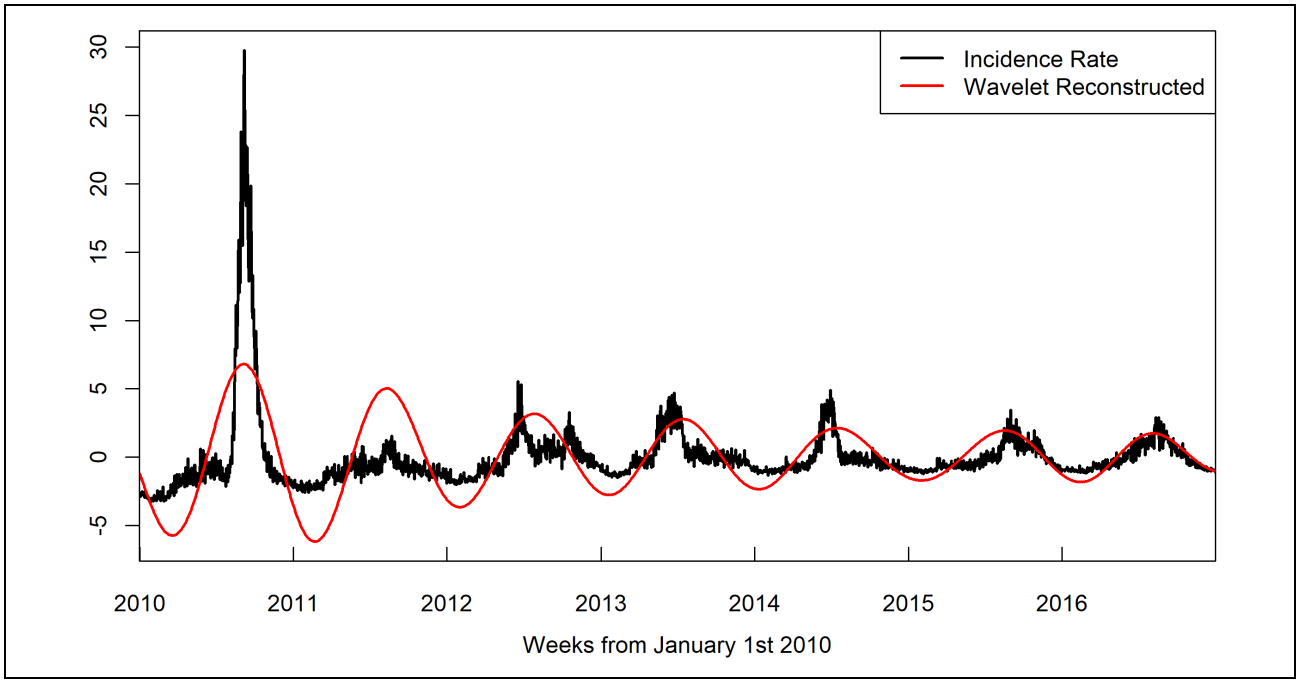


**Figure 3.2. Detrended ILI incidence rate and wavelet reconstruction (period = 46-53 weeks), Chile 2010-2016**

Detrended ILI incidence rate time series and wavelet reconstructed time series (red). Wavelet reconstruction used periods between 46-53 weeks.

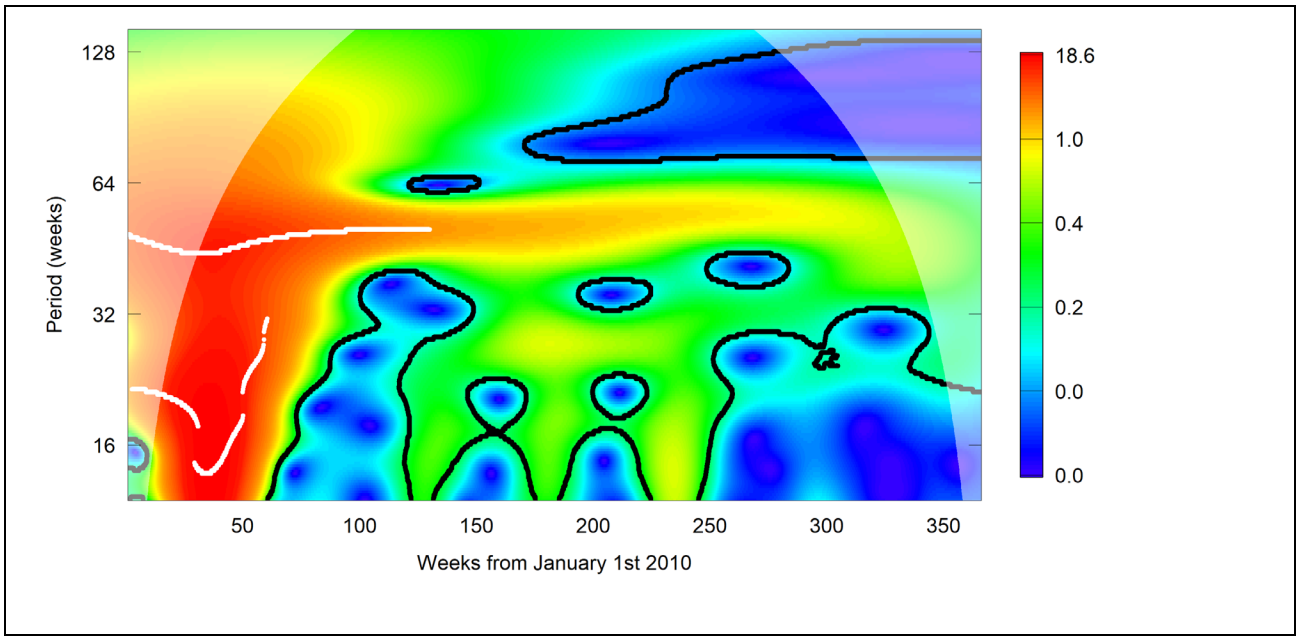


**Figure 3.3. Local Wavelet Power Spectrum of ILI rates, Chile 2010-2016**

Local power for periods and time in weeks. Significant power against white noise inside black contour. Ridge in white. A significant and high power was present through the complete time series for periods between 40 and 60.

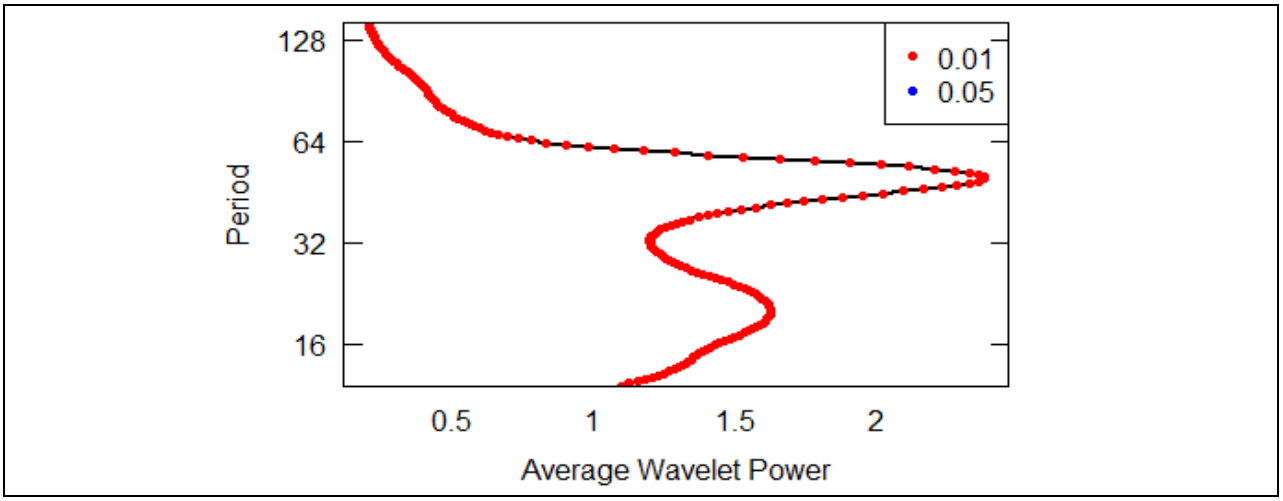


**Figure 3.4. Average power of wavelet transformation per period, Chile 2010-2016**
Average power for periods, representing the average of local power shown in Figure 3.3 with significance levels <0.01 (red) and <0.05 (blue).

For each hospital, we calculated the 95th percentile of the power and found that the best seasonality was between 46 and 53 weeks. Health Network and the country showed the same annual period range for the best seasonality pattern (Appendix D). Ergo, we used an annual periodicity from 46 to 53 weeks to filter the Morlet wavelet of Health Networks and to obtain the transformed time series with the best seasonality.

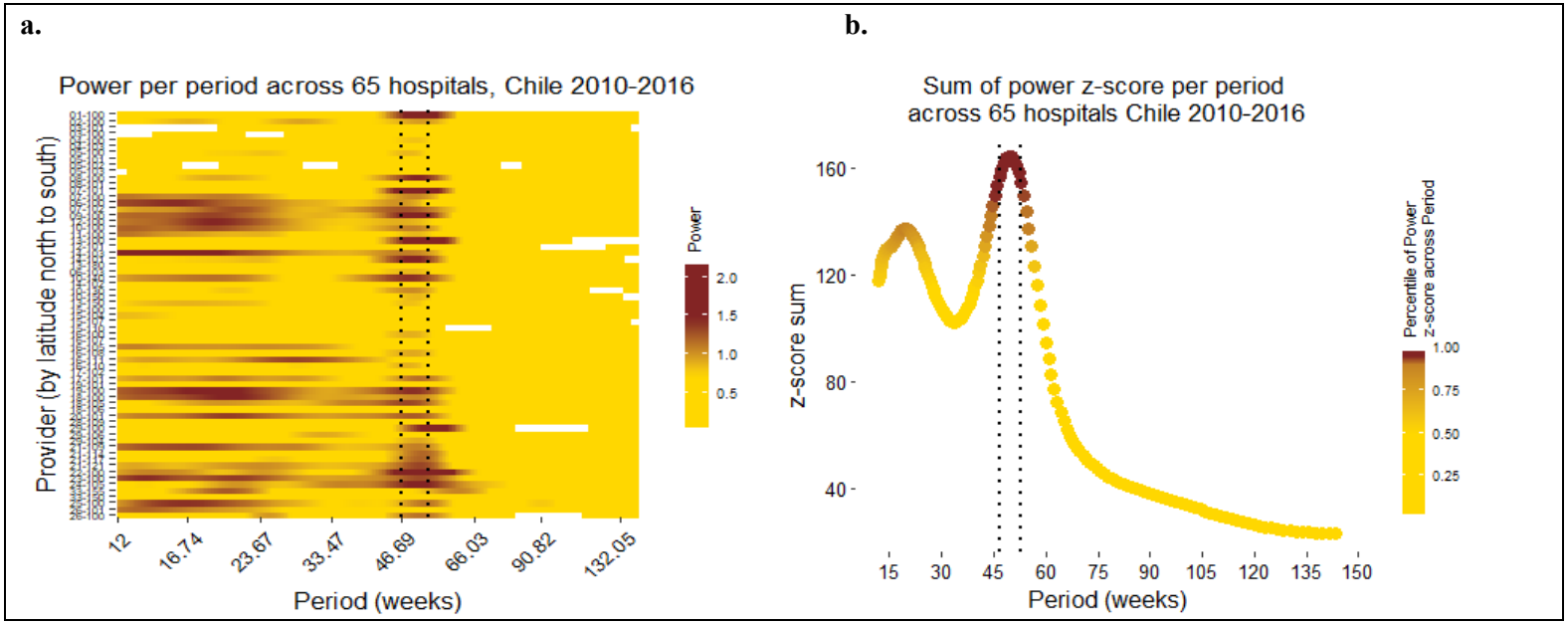


**Figure 3.5. Average power per period in individual hospitals and 95th percentile of power z-score across period and hospitals, Chile 2010-2016**

**a.** Power per each of the 65 hospitals across all periods. Dark red is higher power, namely better fit of the data to the period. Yellow represents low power and fit to the period. White spaces denote non-significant power. Dotted lines represent the 95$^{th}$ percentile of power across hospitals, same as in b.

**b.** Cumulative power z-score to calculate the periods with best fit across hospitals. Power for each hospital were normalized. Data was log transform, subtracted the mean and divided by the standard deviation. Then the sum of z-score for each period was plotted with the 95$^{th}$ percentile (dotted lines in both a and b).

### 3.4.3 Start and peak day of seasonal influenza in Health Networks

The median start of the epidemic for all Health Networks and years was May 11 that coincided with the autumn season (Day 131 of each year; IQR 117, 152). The median peak day was August 4th that coincide with the winter season (Day 217 of each year; IQR 200, 237). The median duration from start to peak of the epidemic for all hospitals and years was 84 days (IQR 82, 88), equivalent 12 weeks or 3 months.

Despite the presence of some variability of start and peak day between and within Health Networks, there was consistency across the country with respect to the timing of the start and the peak of ILI. The duration of the epidemic, difference between the start and the peak, appeared constant across Health Networks and latitudes (Figure 3.6).

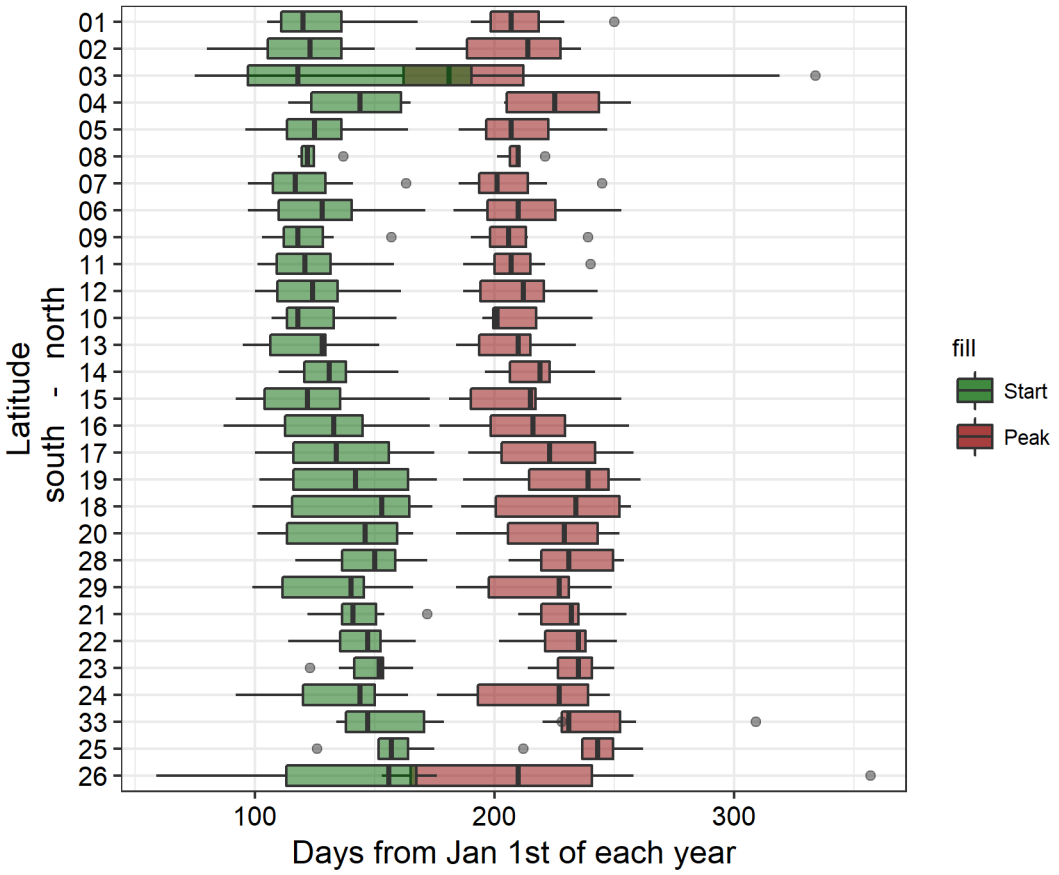


**Figure 3.6. Start and Peak of ILI in emergency room by Health Service and Latitude, Chile 2010-2016**

The start of the annual ILI epidemic tended to start earlier between 2010 and 2013, and after 2013 ILI epidemic was delayed each year compared to the previous year. No clear relation was found between the peak of the epidemic and predominant strain in the country for each year (Figure 3.7).

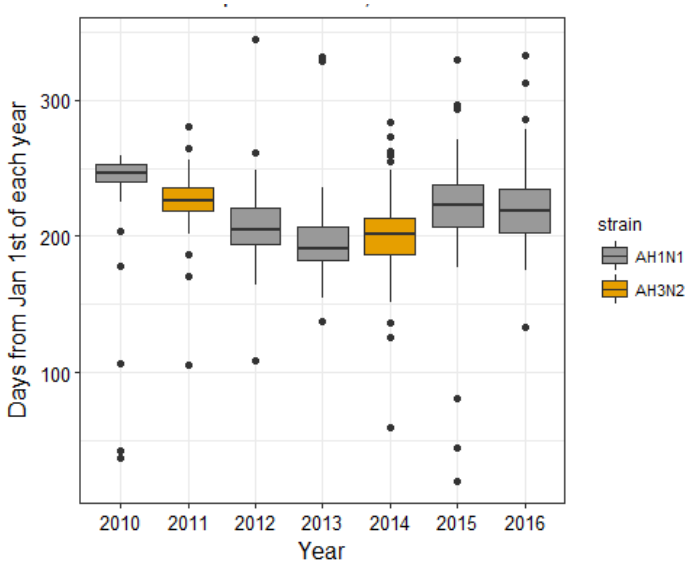


**Figure 3.7. Start of influenza season and predominant strain per year in 65 hospitals, Chile 2010-2016**

### 3.4.4 Population and a North to south pattern associated to early annual epidemics

The univariate regressions results showed a positive association between population size and earlier start and peak time of influenza. A north to south pattern was evident. The increase of latitude from north to south was associated to a delayed start and peak of influenza Figure 3.8a and Figure 3.9a). The observed north to south patterns were dominated by the central zone of the country where the association between latitude and timing of influenza was significant. In contrast, no association between latitude and timing of influenza was present in the north and south extremes of the country (Figure 3.8b and Figure 3.9b). Influenza season varies every year, consequently, years, analyzed as a categorical variable, had a significant association with start and peak day. Similarly, each year had a predominant strain in the country. Accordingly, strains H3N2 had earlier peak day and shorter start-peak time compared to influenza AH1N1. The

presence of an airport in the territory of the Health Network had no association to any outcome of influenza timing (Table 3.1).

**Table 3.1. Univariate regressions for start day, peak day and days from start to peak**

**Table 1a. Univariate Regressions predictors estimates ILI start day**

| | β | Std.Error | p-value | Adjusted $R^2$ |
|---|---|---|---|---|
| Latitude | 0.996 | 0.334 | 0.00321 | 0.038 |
| Year (continuous) | -3.331 | 1.135 | 0.0037 | 0.036 |
| Population (10,000) | -0.322 | 0.116 | 0.0060 | 0.032 |
| Year | | | | 0.171 |
| 2010 | 50.000 | 7.880 | 0.0000 | |
| 2011 | 30.793 | 7.880 | 0.0001 | |
| 2012 | 13.069 | 7.880 | 0.099 | |
| 2013 | - | - | | |
| 2014 | 14.828 | 7.880 | 0.061 | |
| 2015 | 23.517 | 7.880 | 0.0032 | |
| 2016 | 23.172 | 7.880 | 0.0037 | |
| Strain | | | | -0.0048 |
| AH1N1 | - | - | - | |
| AH3N2 | 0.859 | 5.133 | 0.867 | |
| Airport | | | | 0.003 |
| No | - | - | - | |
| Yes | 6.374 | 4.992 | 0.203 | |

**Table 1b. Univariate Regressions predictors estimates ILI peak day**

| | β | Std.Error | p-value | Adjusted $R^2$ |
|---|---|---|---|---|
| Latitude | 0.844 | 0.277 | 0.003 | 0.040 |
| Year (continuous) | -3.172 | 0.935 | 0.001 | 0.050 |
| Population (10,000) | -0.215 | 0.09661 | 0.027 | 0.019 |
| Year | | | | 0.348 |
| 2010 | 47.966 | 5.796 | 0.0000 | |
| 2011 | 28.862 | 5.796 | 0.0000 | |
| 2012 | 11.862 | 5.796 | 0.042 | |
| 2013 | - | - | - | |
| 2014 | -1.103 | 5.796 | 0.849 | |
| 2015 | 31.586 | 5.796 | 0.000 | |
| 2016 | 20.862 | 5.796 | 0.0004 | |
| Strain | | | | 0.015 |
| AH1N1 | - | - | - | |
| AH3N2 | -8.576 | 4.212 | 0.043 | |
| Airport | | | | -0.004 |
| No | - | - | - | |
| Yes | 1.844 | 4.153 | 0.658 | |

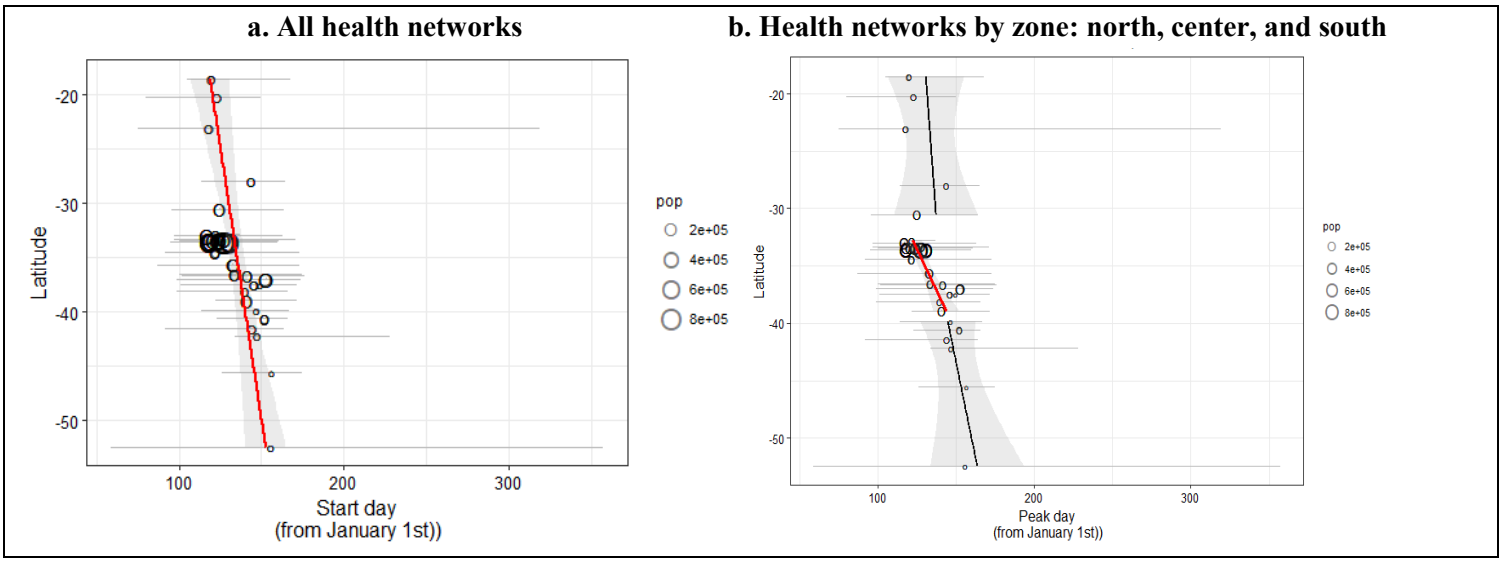


**Figure 3.8. Start of ILI vs Latitude, 29 Health Networks in Chile, 2010-2016**

**a.** Colored line represents red: p-value < 0.05, black: p-value > 0.05. Vertical grey zones denote 95% CI, horizontal grey: range of start days for de period for each health network. Black circles size: population size. Black circle position: median start day. Linear model: β = 0.99, p-value = 0.003, R2 = 0.04.

**b.** Colors and circles same as in a. North zone linear regression (top): β = 0.5, p-value = 0.75, R2 = 0.003. Center zone linear regression (middle): β = 3.49, p-value < 0.01, R2 = 0.09. Southern zone linear regression (bottom): β = 1.49, p-value = 0.33, R2 = 0.02

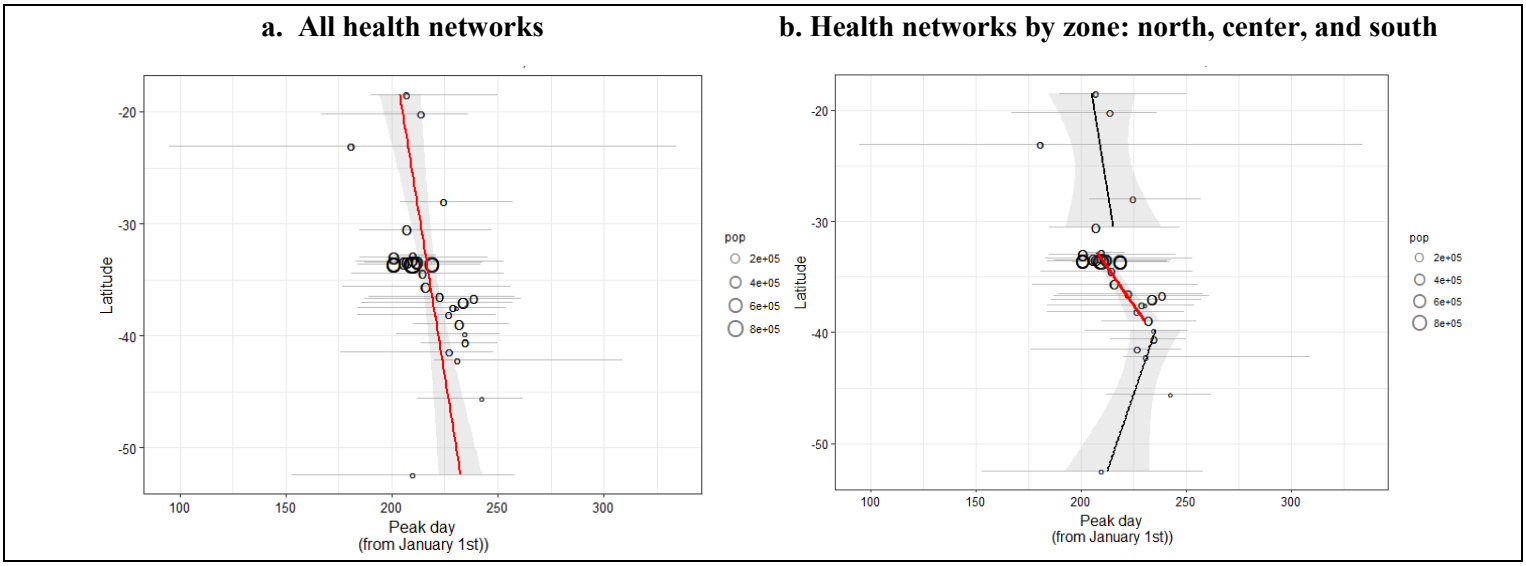


**Figure 3.9. Peak of ILI vs Latitude, 29 Health Networks in Chile, 2010-2016**

**a.** Colored line represents red: p-value < 0.05, black: p-value > 0.05. Vertical grey zones denote 95% CI, horizontal grey: range of start days for de period for each health network. Black circles size: population. Black circle position: median peak day. Linear model: β = 0.8, p-value = 0.002, R2 = 0.04

**b.** Colors same as in a. North zone linear regression (top): β = 0.8, p-value = 0.554, R2 = 0.01. Center zone linear regression (middle): β = 3.65, p-value < 0.01, R2 = 0.11. Southern zone linear regression (bottom): β = -1.8, p-value = 0.08, R2 = 0.05

We found that the best multivariate model for the start day outcome included 9 variables: latitude, population, presence of airport and years. A negative association was found for start day and population size (β = -0. 3, CI 95% -0. 5 - -0. 1, P<0.01). Health networks with an airport was associated with an estimated delay of 9.5 days for the start of an ILI epidemic (CI 95%, 0.848-18.190, p<0.05). A north to south pattern was also found such that a one degree increase in latitude was associated with nearly a one day delay in ILI (north to south, β = 0.903, CI 95% 0.315-01.491, P<0.01) (Equation 3.3, Table 3.2a and Table 3.3).

**Equation 3.3**

$$S_d = 170.9 + 0.9(Lat) - 0.31(Pop_{10,000}) + 9.5(\text{Airport}) + 49.7\,(Y_{2010}) + 30.5(Y_{2011}) + 12.9\,(Y_{2012}) + 14.8(Y_{2014}) + 23.5(Y_{2015}) + 23.3(Y_{2016})$$

Where Sd = Start day from January 1st from each year; Lat = South Latitude; Airport = Indicator variable for presence of airport; Y = Indicator variable for the year noted in the subscript. For the ILI peak the best multivariate model included 8 variables: latitude, population and years. A north to south pattern was found for latitude (β = 0.780, CI 95% 0.346-1.215, P<0.01)) and a negative association with population size (β = -0.00002, CI 95% -0.00003 - -0.000001, P<0.05) (Equation 3.4, Table 3.2b and Table 3.3 ).

**Equation 3.4**

$$P_d = 173.43 + 0.78(Lat) - 0.16(Pop_{10,000}) + 47.8\,(Y_{2010}) + 28.7\,(Y_{2011}) + 11.8\,(Y_{2012}) - 1.09\,(Y_{2014}) + 31.59\,(Y_{2015}) + 20.94\,(Y_{2016})$$

Where Pd = Peak day from January 1st from each year; Lat = South Latitude; Y = Indicator variable for the year noted in the subscript.

**Table 3.2. Multivariate regression model selection for ILI start day and peak day, using best subset method**

Table 2a. Start day models

| Model‡ | # of Variables | Variables used* | $R^2$ | Adjusted $R^2$ | Cp | BIC |
|---|---|---|---|---|---|---|
| A | 7 | year, latitude | 0.24 | 0.21 | 16.0 | -13.0 |
| B | 8 | year, latitude, population | 0.26 | 0.23 | 12.0 | -14.0 |
| C† | 9 | year, latitude, population, airport | 0.28 | 0.25 | 9.0 | -14.0 |

Table 2b. Peak day models

| Model‡ | # of Variables | Variables used* | $R^2$ | Adjusted $R^2$ | Cp | BIC |
|---|---|---|---|---|---|---|
| A | 7 | year, latitude | 0.41 | 0.39 | 11.0 | -65 |
| B† | 8 | year, latitude, population | 0.43 | 0.40 | 8.4 | -65 |
| C | 9 | year, latitude, population, airport | 0.43 | 0.40 | 9.0 | -61 |

‡ Best model for all possible models with the given numbers of variables using RSS

*Year was considered as 6 dummy variables and was forced in. Strain was excluded given the high correlation with year.

† Selected model

**Table 3.3. Selected Multivariate Models for ILI start day and peak day**

| | β | 95% CI | p-value | Adjusted $R^2$ |
|---|---|---|---|---|
| Outcome: Start Day | | | 0.000 | 0.2471 |
| Latitude | 0.9027 | 0.3147 , 1.4907 | 0.0028 | |
| Population (10,000) | -0.31250 | -0.51956 , -0.10539 | 0.0033 | |
| Airport | | | | |
| Yes | 9.519 | 0.8479 , 18.190 | 0.03266 | |
| Year | | | | |
| 2010 | 49.71 | 34.892 , 64.518 | 0.00000 | |
| 2011 | 30.5 | 15.687 , 45.313 | 0.00007 | |
| 2012 | 12.96 | -1.850 , 27.773 | 0.08597 | |
| 2013 | - | - | - | |
| 2014 | 14.86 | 0.0508 , 29.674 | 0.049 | |
| 2015 | 23.52 | 8.7108 , 38.334 | 0.002 | |
| 2016 | 23.31 | 8.4998 , 38.123 | 0.002 | |
| | β | 95% CI | p-value | Adjusted $R^2$ |
| Outcome: Peak Day | | | 0.0000 | 0.4016 |
| Latitude | 0.7801 | 0.3455 , 1.2145 | 0.00050 | |
| Population (10,000) | -0.16640 | -0.316 , -0.016 | 0.03013 | |
| Year | | | | |
| 2010 | 47.81 | 36.861 , 58.756 | 0.000000 | |
| 2011 | 28.71 | 17.758 , 39.653 | 0.000001 | |
| 2012 | 11.8 | 0.8581 , 22.751 | 0.034690 | |
| 2013 | - | - | - | |
| 2014 | -1.085 | -12.03 , 9.8615 | 0.845200 | |
| 2015 | 31.59 | 20.642 , 42.535 | 0.000000 | |
| 2016 | 20.94 | 9.9897 , 31.882 | 0.000215 | |

### 3.4.5 Local Travelling waves

We used a second-degree local polynomial regression model (LOESS) to determine the upper distance limit for the local travelling waves' models. We found a descending Spearman's correlation of phase angles up to 1250 km that disappeared for larger distances (Figure 3.10b). Consequently, we included health networks closer than 1250 km in each model of local travelling waves. We found a similar descending pattern of correlation versus distance for the wavelet reconstructed time series. On the contrary, the original rate time series showed low correlation and a pattern that increased of up to 400 km followed by descending curve from 400 to 1250 km. Despite the differences of the patterns and average correlation for the three models, all three presented a change in the pattern at a distance close to 1250 km (Figure 3.10a).

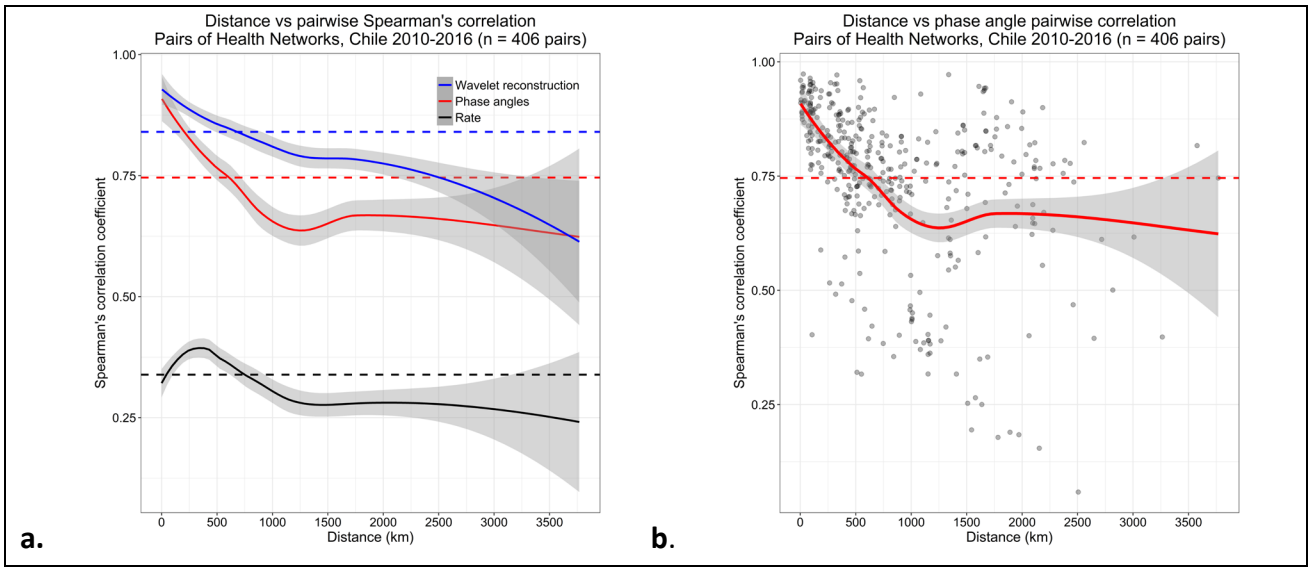


**Figure 3.10. Distance vs pairwise Spearman's correlation of ILI rate, phase angles and wavelet reconstruction. Health Networks, Chile 2010-2016**
**a.** Spearman's correlation versus distance between pairs of Health Networks. Wavelet reconstructed time series (blue), phase angle time series (red), rates (black). Dashed lines represent the average correlation. The 3 models used a loess model with $\alpha = 0.75$ and 95% CI (grey). Different correlations and patterns showed a change at the distance of 1250 km that we used as the upper distance limit to define local wave.
**b.** Same as a. showing the phase angle time series model.

There were 11 health networks with outgoing travelling waves (Bonferroni corrected p-value < 0.0017) located at the center of the country. There were 10 health networks that presented incoming waves with the corrected p-value < 0.0017 (Figure 3.11).

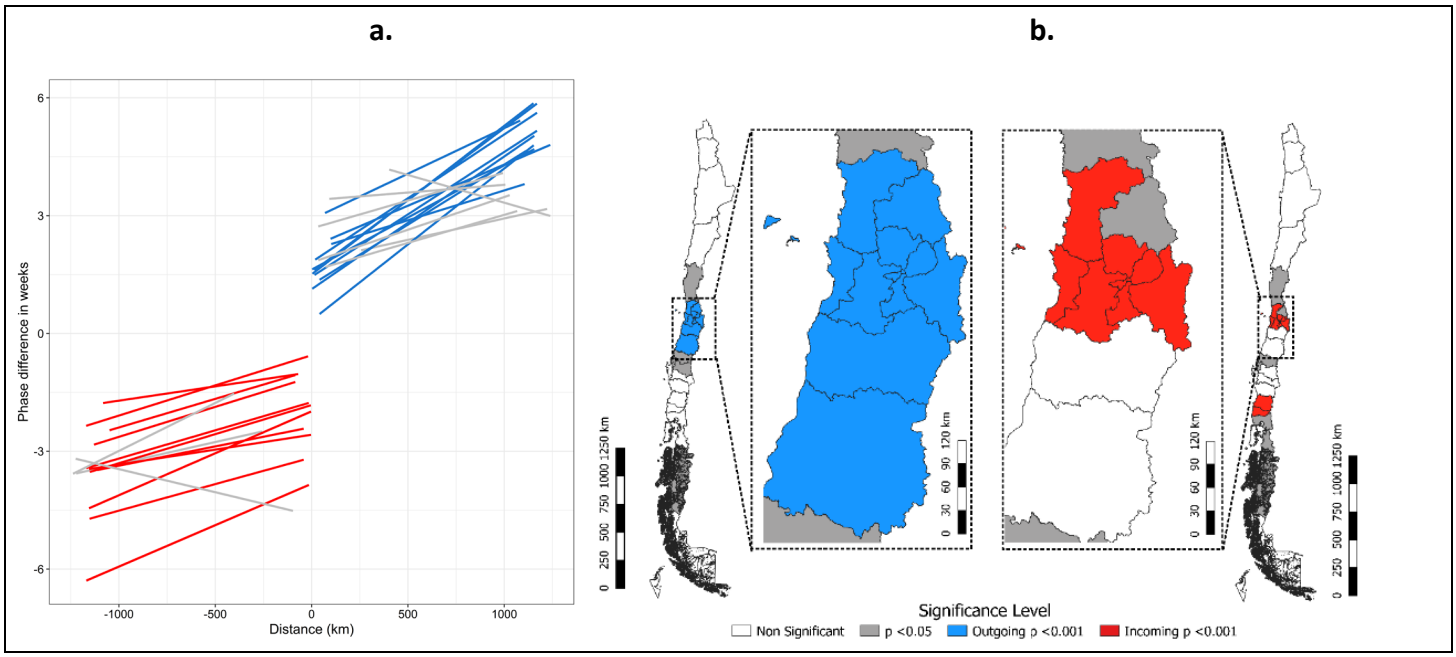


**Figure 3.11. Travelling waves of influenza in Health Networks. Chile 2010-2016**
**a.** Phase difference in weeks vs distance (km) for Health Networks with incoming (red) and outgoing (blue) waves. In grey linear models with a significance level of 0.05. In red and blue, linear models with a Bonferroni corrected significance level < 0.001.
**b.** Geographic location of Health Networks with significant travelling waves. Incoming and outgoing waves are clustered in the center of the country. Colors same as in **a.**

The prescence of outgoing and incoming waves in Health Networks were associated with population size, adjusting by latitude. For every 10,000 people a Health Network has a 23% greater odds of presenting local outgoing waves (OR = 1.23, CI 95% 1.05, 1.44, p = 0.001) and 18% higher odds of presenting incoming waves of influenza (OR = 1.18, CI 95% 1.03, 1.34, p = 0.01) (Table 3.4). Both logistic models had good discrimination with AUC of 0.914 (CI 95% 0.8, 1.0 ) for outgoing waves and 0.884 (CI 95% 0.729, 1.0 ) for incoming waves.

**Table 3.4. Logistic models for outgoing and incoming influenza waves in Health Networks. Chile 2010-2016**

| Model | 10,000 Population OR (CI 95%) | Latitude (South) OR (CI 95%) | AUC (95% IC) |
|---|---|---|---|
| Outgoing Waves | 1.23 (1.05,1.44) | 0.95 (0.78,1.15) | 0.914 (0.800, 1.00) |
| Incoming Waves | 1.18 (1.03,1.34) | 1.08 (0.86,1.36) | 0.884 (0.729, 1.00) |

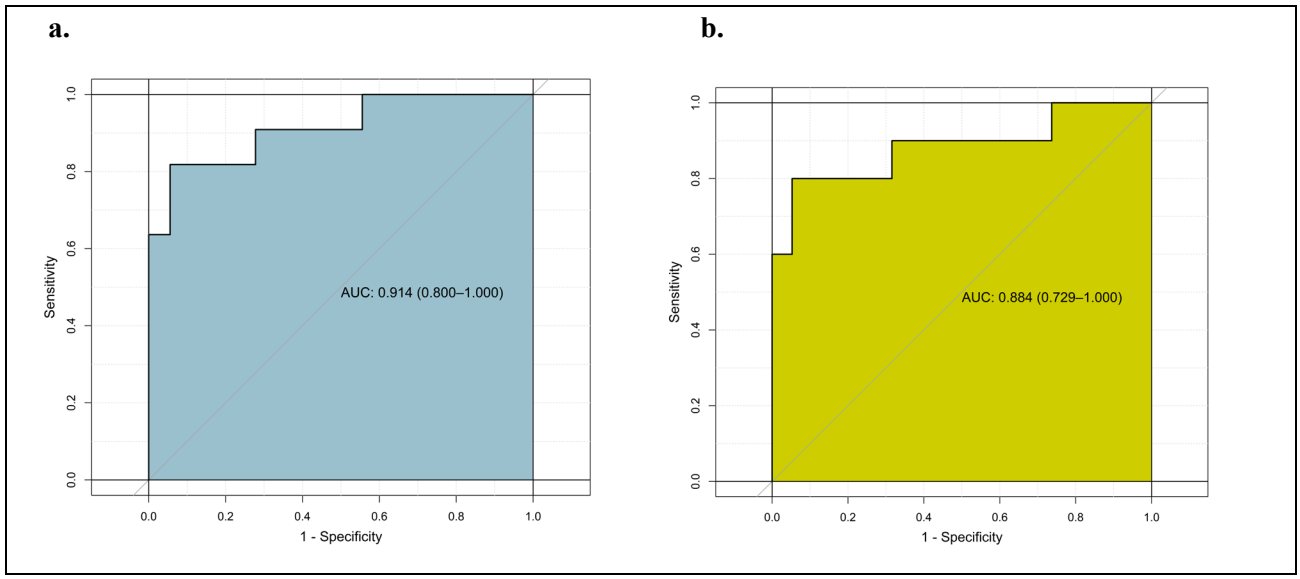


**Figure 3.12. ROC curves of logistic models for incoming and outgoing influenza waves in Health Networks. Chile 2010-2016**
**a.** ROC curve and AUC for logistic model of outgoing influenza waves.
**b.** Same as **a.** for incoming influenza waves.

## 3.5 DISCUSSION

We found a predominant annual seasonality of influenza in Chile with a periodicity of 50 weeks (95% CI 43, 53). This period coincides with the annual seasonality of influenza reported for other temperate territories and the reports from influenza surveillance from the Chilean Ministry of

Health (34). To our knowledge, this is the first study that confirms a cycle of seasonal influenza in Chile using multiple years.

There was a north to south latitudinal gradient for the start and peak of influenza across the country. Most of that gradient was related to the central zone between latitudes 31 and 40 south. The central zone is the area of the country where most of the population lives. Chowell found a south to north hospitalization gradient for H1N1 2009 pandemic (95). The difference with our findings can be explained by the annual variability of influenza epidemics due to weather, population immunity, human movement (112). We did not include 2009 in our analysis, but we found a south-north latitudinal gradient in 2015 (Appendix). In 2009 and 2015, the first cases were reported in southern cities with large populations that lead that year's epidemic. Even though, Health Networks with large populations from the center of the country have higher chances of presenting the first cases of influenza, southern zones with relatively large populations can lead an epidemic.

Population was also a factor associated with the start and peak of influenza as described previously (18, 90, 101, 102). The patterns found were mostly influenced by the center zone of the country where the capital Santiago, the most populated city, is located. Similarly, Burger et al. found that Santiago was a hub that spread influenza rapidly to the rest of the country (108). These findings are supported by the results from the local travelling waves. Population was associated with the presence of local incoming and outgoing waves. Further, Health Networks with significant local outgoing waves were in the center of the country. The Health Networks with incoming travelling waves were largely located at the center of the country and two of them in the south zone of the country. Our findings suggest that the larger population located in the center of the country drives seasonal influenza epidemics. Health Networks with larger population from the

central zone spread to neighboring Networks with the form of outgoing travelling waves to Network acting as receivers (incoming waves) in the same zone and in the south of the country.

This study has some limitations. First, we use secondary data from reports from ED visits. These were diagnosis of ILI based on clinical judgement and have no necessary laboratory confirmation. Second, we assumed that all hospitals had the same population structure as we did not include population age structure of Health Networks in the analysis. Control by age group might give a more detailed information on influenza transmission and could be an interesting challenge for future work. Third, we did not include ED data from private insurance companies, private hospitals or private practices since they were not available. Nevertheless, the public insurance covers 74% of the population in Chile. Finally, we assumed a constant proportion of emergency consultation to other providers. Private hospitals, private practices and public primary healthcare centers could attract patients with public insurance especially in seasons of high demand. We assessed this limitation partially by estimating the population with public insurance that lives in a 5km radius that are more likely to visit the hospital ED rather than other providers (public or private). One of the strengths of our study was that we included data of hospitals from a wide range of latitudes from a single healthcare system. Also, the centralized reporting system and national guidelines increase data quality. ILI surveillance operates year-round in all hospitals resulting in more reliable data of seasonality of influenza. We did not assume an annual seasonality, on the contrary, we estimated the best seasonality before fitting our models. Finally, we selected the best models for the start and peak of influenza by comparing the fit of all the possible models for the variables measured.

## 3.6 CONCLUSSION

This is the first study to estimate seasonal influenza seasonality in Chile and its patterns across latitudes. New strains should be considered when different patterns are detected. Likewise, if a new strain is detected early, patterns could differ from the ones found here.

Our findings can help decision-makers to prepare influenza season, to prioritize zones for early vaccination campaigns, prepare hospital beds reallocation for annual influenza epidemics and allocate resources according to patterns of influenza. Zones with larger population and in the center of the country would need earlier actions that could reduce influenza spread and its impact across the country.

# 4.0 ASSOCIATION OF WEATHER, POLLUTION AND DAILY INFLUENZA CASES IN EMERGENCY ROOMS, A MULTILEVEL ANALYSIS OF CHILEAN HOSPITALS

Christian Garcia, MD MPH[1,2]; Maria Brooks PhD[1]; Wilbert van Panhuis MD PhD[1],
Christina Mair, MPH PhD[4]; Lee H. Harrison, MD[1,3]

1.Department of Epidemiology, University of Pittsburgh Graduate School of Public Health
2.Division of Disease Prevention and Control, Ministry of Health, Chile.
3.Infectious Diseases Epidemiology Research Unit, University of Pittsburgh
4.Department of Behavioral and Community Health Sciences, University of Pittsburgh Graduate School of Public Health

## 4.1 ABSTRACT

**Background:** Influenza affects 5-10% of the world's population including 250,000-500,000 deaths annually. In the Americas 40,880-160,270 deaths occur every year associated with influenza infection. Weather factors and air pollution are associated to influenza transmission, morbidity and hospital visits. Understanding the patterns of influenza and the factors associated can benefit public health.

**Objective:** In this study we aimed to determine the association between daily influenza cases and daily temperature, relative humidity, precipitation, PM10, PM2.5, SO2 and O3 across Chile.

**Method:** We obtained data from daily influenza-like illness in emergency rooms, data from weather and pollution stations. We constructed a multilevel zero-inflated negative binomial as the weather model to test the hypothesis that influenza cases were associated to low temperature. Finally, to test the hypothesis that influenza cases are associated to air pollution we included pollution measures to the weather model to determine the association between influenza and pollution.

**Results:** Lower minimum and maximum temperature were associated to fewer influenza cases and a small positive association was found between influenza and PM2.5.

**Conclusion:** Our findings can help to understand the complex relation between influenza, weather and pollution. The results could also help design vaccination campaigns, stablish pollution standards and to calculate health effects of policies to reduce particulate matter.

## 4.2 INTRODUCION

Influenza affects 5-10% of the world's population including 250,000-500,000 deaths annually (16). In the Americas, 40,880-160,270 deaths occur every year associated with influenza infection (4, 113). Understanding the patterns of influenza and associated factors can bring concrete benefits to public health, as it may help reduce the burden of seasonal influenza and improve preparedness for pandemics (19). The dynamics of influenza at the global and local scales are not fully understood, but can be addressed using demographic, geo-climatic and national census data to improve accuracy of the models and advance results towards the precision that meteorological models have nowadays (15).

Climatic factors are associated with influenza transmission. Temperature and humidity are associated with increased spread of influenza by affecting virus survival (1, 20-22, 92, 114-116). Further, lower temperature in temperate areas and rainfall in tropical regions were associated with a rise of influenza cases mediated by an increase of human contact rates (11, 17-19, 92, 117). Immunologic response to influenza can prevent contagion, but population immunity is affected by climatic factors like humidity, temperature, and photoperiod (17, 23-29). The mix of factors that drive influenza spread are complex. The associations between factors appear to play an important role in seasonality of influenza but it is hard to avoid collinearity of variables and confounding factors. The most accepted hypothesis to understand influenza seasonality is that absolute humidity may be negatively associated with seasonal influenza epidemics (1, 17, 20, 21, 92, 116, 118, 119). Beyond weather factors, air pollution can play a role on influenza transmission.

There is a close association between air pollution and different diseases (120-126). Particulate matter (PM) is a mix of materials that include dust, dirt, soot, smoke, and liquid droplets released into the air. The inhaled particles, that are limited $\leq$10μm (PM10) include two

size of particles <2.5μm (PM2.5) and > 2.5μm. PM10 are known to increase respiratory admissions to hospitals(127, 128). Likewise, PM2.5, fine particles resulting from combustion, penetrates deep into the lungs to the bloodstream, and are associated with respiratory disease, cardiovascular disease, and mortality (121-123, 125, 129-134). Air pollution increases risk of upper respiratory infections and influenza-like illness (ILI) even after controlling for the weather conditions (39, 40). Droplets that contain influenza are attached to PM that provides "condensation nuclei" increasing virus survival and potentially increasing transmission (135-140). Similarly, industrial activity and motor vehicle emissions like sulfur dioxide (SO2) and ozone (O3) are related to acute inflammation of the pulmonary epithelium (128). Both gases can reduce the first defensive barrier against viruses in the respiratory epithelium, produce local inflammation and increase the risk of influenza infection. SO2 and O3 cause respiratory symptoms and increased hospital respiratory admissions (128, 141-143). Countries can enhance influenza surveillance including weather and pollution data to increase model accuracy to face seasonal influenza (15).

In this study, we studied the influenza with weather and pollution across Chile. Chile is the country with the largest latitude range in the southern hemisphere (36 degrees from 17S to 53S), with 10 types of climate categories ranging from desertic to artic (31). The Chilean public healthcare provision system is organized into 29 Public Health Networks that covers 74.4% of the 17 million population (32). Influenza surveillance was enhanced after the 2009 pandemic, with year-round surveillance of influenza-like illness (ILI) in emergency departments (ER), laboratory in sentinel providers and surveillance of severe respiratory disease hospitalizations (33). A series of weather and pollution stations across the country are part of the Meteorological Services, the national systems of air quality (SINCA) and the Ministry of Agriculture. We used data from the meteorological services, SINCA, and from the Climatic Explorer data repository from the Center

for Climate and Resilience Research that consolidates weather data from different official sources (36-38). Since different measures of air pollution depend on local characteristics, like local industry development and the type of heating fuel used locally, there are variations of the air pollutants in some locations (37). The data we obtained, covers the principal cities of the country with daily measures and is available online from the 3 sources mentioned (36-38). As a temperate country, influenza has annual epidemics that peaks in winter season. Lower temperatures were associated to the peak of H1N1 pandemic in 2009 (95). Also, Bertoglia found a positive association of temperature and ILI between 2012 and 2014 in the Metropolitan Region where the capital Santiago is located (144). In the same study, ILI cases showed a small association to PM2.5. The country-wide association between weather measures, PM, gas pollutants, and seasonal influenza is still unknown.

## 4.3 METHODS

In this ecological study we determined the association between daily influenza cases and daily temperature, relative humidity, precipitation, PM10, PM2.5, SO2 and O3 across Chile. We first collected time-series data from daily ED, data from weather, and from air pollution stations. Second, we constructed and compared different models for weather variables. Third, to test the hypothesis that influenza cases are associated to temperature we used a multilevel zero-inflated negative binomial as the weather model. Finally, to test the hypothesis that influenza cases are associated to air pollution we included pollution measures to the weather model.

### 4.3.1 Data source

We obtained daily ILI cases from the influenza surveillance system reported by public hospitals to the Ministry of Health of Chile from 2010 to 2016. Daily rates were calculated for each hospital using an estimated population covered by each provider population for World Pop, FONASA and Census as described in subsection 0. We obtained weather and pollution data from Meteorological Services, SINCA and CR2 (33, 36, 38). We paired each hospital to the closest station within a radius of 10 km. Some stations were used for more than one hospital.

### 4.3.2 Data preparation

#### 4.3.2.1 Influenza data

Influenza-like illness is highly correlated to laboratory confirmed influenza and a good proxy of influenza circulation in the population (16, 72, 94, 95). We defined our outcome as ILI from emergency departments from large and middle size hospitals that reported daily cases to the Ministry of Health. We calculated hospital population using a radius of 5km to estimate population that access each emergency room as described previously in subsection 2.2.2. Daily rate was calculated using daily ILI and the population estimated for each hospital and year.

#### 4.3.2.2 Weather data

We included data for precipitation, temperature, relative humidity, PM2.5, PM10, SO2 and O3 of stations that had ≥ 600 days with reported for the period 2010-2016 (≥ 25%). We calculated daily precipitation as the cumulative precipitation milliliters (mm) registered for days with ≥6 hours reported. Relative humidity was reported as the average daily relative humidity. Daily minimum

(Tmin) and maximum (Tmax) temperatures were recorded by the official sources (36-38). The weather and pollution variables were measured in conventional units. Relative Humidity was measured as average daily percentage of water vapor in air over the maximum expected adjusted by temperature. PM10 and PM2.5 were measured as daily average in microgram per squared meters (μg/m3). Both gases, SO2 and O3 were measured as daily average in part per billion per volume (ppbv). Median temperature was excluded due to multiple correlation, evaluated with the variance inflation factor (VIF). Lagged variables (up to 14 days) of weather and pollution variables were excluded given non-significant difference in the cross-correlation between weather, pollution, and ILI when comparing lagged and non-lagged values

### 4.3.3 Data imputation

We assumed ILI time-series, weather and pollution missing data was missing at random (MAR) conditional on observed data. For ILI data, different imputation methods were tested and selected the best imputation method as described previously in subsection 2.2.2 (80, 81). We imputed weather and pollution data using the average of non-missing values from the same day and month from other years.

### 4.3.4 Statistical analysis

In epidemiology, count data are frequently analyzed using a Poisson model. One limitation of the Poisson model is that assumes that the mean and variance of the dependent variable are equal (145). A problem with this approach arise when the response variable is over-dispersed, when variance is greater than the mean (146). If overdispersion is present, standard errors might be

underestimated, hence a significant association may appear when is in fact non-significant (145). Negative binomial regression is an alternative to model count data, that accounts for overdispersion (147). Our ILI data showed overdispersion and a high proportion of zero (61%). To account for the excess zeros we used a zero inflated model and assumed that our data came from two distributions: a count distribution of positive integers that include zeros (Equation 4.1) and a structural zeros from a binary distribution (Equation 4.2). We assumed that daily ILI data is correlated within hospital therefore the assumption of independence of observations is violated. Incorrect estimates can result if this violation is ignored (148, 149). To account for nonindependence of observations, we used a multilevel model (148). We first determined the best weather model for ILI rates including the predictors: Tmax, Tmin, humidity and precipitation adjusted by hospital. We compared 9 different models based on the Akaike Information Criterion (AIC) as used before for ILI (40). The different models had ILI cases as the outcome and had the form of Equation 4.1,except the linear model that used ILI rates. A logistic regression was incorporated to the count component in zero inflated models that determined the odds of zero cases and had the form of Equation 4.2. Then, count models included only Equation 4.1 and zero-inflated models included Equation 4.1 and Equation 4.2. The multilevel models replaced the variable hospital for a random intercept to account for autocorrelation. The inclusion of a random intercept representing hospitals assuming that data within hospitals are correlated and treats each hospital as a cluster of ILI and weather data. Humidity was excluded from the zero-inflated component due to the presence of non-significant estimates and non-convergence of the models when included. The models compared are presented in Table 4.2. The predictors for the final weather model were selected using backward elimination using AIC, Bayesian information criteria (BIC) and likelihood ratio test (LRT). Finally, to determine the association of pollution

and ILI we included PM10, PM2.5, SO2 and O3 to the weather model and applied the same backward elimination method used for the weather model.

We used R environment and the R packages glmmTMB for analysis and model selection (89, 150, 151).

**Equation 4.1: Count component for weather model selection.**

$$log(\mu_t) = \beta_0 + log(n_t) + \beta_1(tmax_t) + \beta_2(tmin_t) + \beta_3(hum_t) + \beta_4(prec_t) + \beta_5(hospital)$$

**Equation 4.2: Zero-inflation component for weather model selection.**

$$logit(p_{0t}) = \beta_0 + log(n_t) + \beta_1(tmax_t) + \beta_2(tmin_t) + \beta_3(prec_t)$$

Where, μ is the expected number of ILI cases for the day t. tmax, tmin, hum and prec are maximum temperature, minimum temperature, humidity and precipitation, respectively. For multilevel models β3(hospital) was replaced by $\mathcal{U}$ (hospital) that represented the random intercept for hospitals and all variables changed the subscript t, to subscript t,h representing the relation for a given time in a specific hospital. P0t is the probability of zero ILI cases at day t and nt is the population assigned to a hospital at time t. For the linear models, we replaced log(μt) by rate of ILI per 100.000 population.

## 4.4 RESULTS

### 4.4.1 Selected Hospitals

A total of 105,898 daily observations were registered in 42 hospitals. Table 4.1 shows the data characteristics. The number of cases and rate showed an important number of zero cases and justified the use of a zero-inflated model. Further, ILI cases variance ($\sigma 2 = 24.83$) was greater than the mean ($\mu = 1.69$) supporting the use of a Negative Binomial model. Variables Tmax, Tmin and humidity had a distribution closer to normal and a poison distribution was found for precipitation PM10, PM2.5, So2 and O3.

**Table 4.1. Summary of daily ILI counts, rates, weather and pollution variables across Chilean hospitals from January 2010 to December 2016**

| | Mean (95% CI) | Min | Q1 | Median | Q3 | Max | Missing (n) |
|---|---|---|---|---|---|---|---|
| *Influenza-like illness in emergency rooms* | | | | | | | |
| Cases (n) | 1.69 (1.66-1.72) | 0 | 0 | 0 | 2 | 154 | 0 |
| Rate (per 100.000pop) | 7.09 (6.88-7.29) | 0 | 0 | 0 | 2.1 | 2088 | 0 |
| *Meteorological measures* | | | | | | | |
| Minimum Temperature (c°) | 8.42 (8.38-8.45) | -38 | 5.11 | 8.7 | 11.7 | 33.4 | 23445 |
| Maximum Temperature (c ) | 19.89 (19.84-19.9) | -13.9 | 15 | 19.9 | 25 | 41.2 | 23410 |
| Relative Humidity (%) | 60.93 (60.75-61-09) | 0 | 50 | 63.42 | 75.08 | 105 | 53635 |
| Precipitation (mm) | 1.34 (1.30-1.37) | 0 | 0 | 0 | 0 | 80 | 9329 |
| *Pollution Measures* | | | | | | | |
| PM10 (µg/m3) | 58.03 (57.7-58.36) | 0 | 33 | 50 | 72 | 845 | 50098 |
| PM2.5 (µg/m3) | 29.8 (29.5-30.14) | 0 | 13 | 21 | 35 | 960 | 62829 |
| SO2 (ppbv) | 1.76 (1.73-1.79) | 0 | 1 | 1 | 2 | 79 | 75702 |
| O3 (ppbv) | 13.89 (13.72-14.05) | 0 | 7 | 14 | 19 | 500 | 72572 |

We found similar temporal pattern of ILI rates with increased rates in 2010 corresponding to the second season of H1N1 after 2009 pandemic. Vertical patterns in the raster plot showed

synchrony of annual seasons for ILI cases and ILI rates (Figure 4.1a and Figure 4.1b respectively). Higher rates were present in southern hospitals, as the population covered is smaller, few cases results in higher daily rates compared to other hospital with larger population size.

Tmax and Tmin also had marked seasonal pattern across the country. In the northern and central zones of the country higher minimum and maximum temperatures were found. Southern hospitals had a similar patter, but with lower temperatures (Figure 4.1c and Figure 4.1d). Lower relative humidity was present in the north of the country, associated to cities in the desertic regions of the country (Figure 4.1e). Precipitation also presented differences between northern and southern hospitals. A seasonal pattern was present for precipitation, but lower humidity was found in the north (with few days with precipitation) compared to the southern hospitals (Figure 4.1f). PM10, PM2.5, and O3 showed a seasonal pattern across the country with a more consistent seasonality in the northern regions compared to the southern regions of the country (Figure 4.1g, Figure 4.1h, Figure 4.1i). On the contrary, So2 did not presented a clear seasonal pattern across the country (Figure 4.1j).

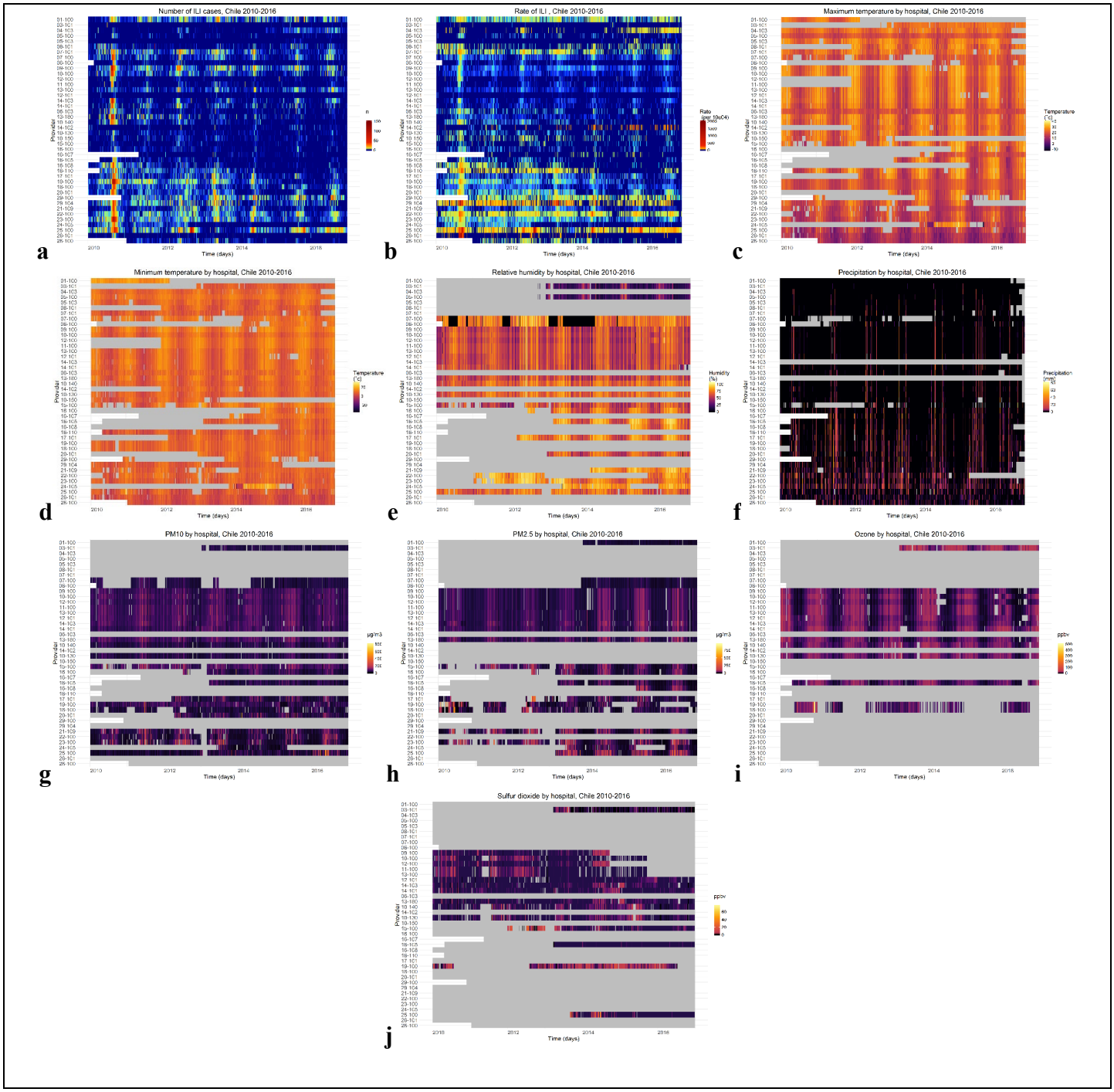


**Figure 4.1. Daily ILI cases in Emergency rooms, rates, weather, and pollution variables in providers by latitude, Chile 2010-2016**

Daily ILI cases, ILI rate, weather, and pollution variables in hospitals ordered by latitude in the y axis (north to south) 2010-2016. Gray represents missing data. Colors denote the value of each variable: **a.** Number of ILI cases. **b.** Rates per 100.000 population. **c.** Maximum temperature C∘. **d.** Minimum temperature in C∘. **e.** Relative Humidity in %. **f.** Precipitation in mm. **g.** PM10 in µg/m3. **h**. PM2.5 in µg/m3. **i.** SO2 in ppbv. **j.** O3 in ppbv.

### 4.4.2 Weather Model

We selected a Multilevel Zero-inflated Negative binomial model as the weather model with the lowest AIC (Table 4.2). The model components that resulted from the backward elimination are presented in Equation 4.1and Equation 4.2. A total of 24 hospitals had enough data to build the weather model (Tmax, Tmin, humidity, and precipitation). The hospitals included were from different latitudes and from 11 regions (Figure 4.2). The estimate's exponent ($e\beta$) of the zero-inflated part of the model can be interpreted as the odds ratio of a day presenting zero ILI cases versus non-zero cases. An increase in 1-degree Celsius of Tmax and Tmin decreased the odds of zero ILI cases by 15% and 33% respectively adjusting by precipitation, and population size (Table 4.3). On the other hand, the odds non-ILI cases increased 4% for every 1 mm of precipitation increase ($p = 0.007$).

In the count component $e\beta$ can be interpreted as the relative change in the number of cases for every one-unit change in the predictor, among days with non-zero ILI cases. For every 1-degree Celsius increase of Tmin or Tmax there is a decline of 1 ILI case (Tmin: e-0.45= 0.95; Tmax: e-0.039= 0.96) adjusting by relative humidity, precipitation and for correlation within hospitals (Table 4.3, Figure 4.3a and Figure 4.3b). A 1% increase in humidity and one mm increase of precipitation increased one ILI case, although these associations were non-significant (hum: e-0.001= 1; prec: e-0.001= 1) (Table 4.3 and Figure 4.3c).

The predicted fixed effects of the complete weather model, including both the count and the zero-inflated component, are shown in Figure 4.3d to Figure 4.3.f for Tmin, Tmax and precipitation. The y axis $\mu*(1-P)$ reflects the combination of both components: ILI number of cases ($\mu$) and the probability of non-zero cases (1-P). ILI cases decrease as Tmin increase. At lower temperatures, people gather together indoor when, increase contact rate, and increase

transmission (Figure 4.3a). Tmax showed a quadratic shape (inverted U) that could be explained by the increased odds of finding zero cases in days with low Tmax. Precipitation showed a small and direct association with ILI cases influenced by the zero-inflated component (Figure 4.3c). Finally, the random effects of the weather model showed the same effects with variation between hospitals (Figure 4.3h, i, j). The y axis is represented in logarithm scale for visualization purposes.

**Table 4.2. AIC scores for 9 models to determine the association between ILI rates and weather variables: minimum and maximum temperature, relative humidity and precipitation in 42 hospitals from Chile, 2010-2016. Sorted from Smaller to larger AIC**

| Model | AIC |
|---|---|
| Multilevel Zero-inflated Negative Binomial | 167242 |
| Zero-inflated Negative Binomial | 169317 |
| Negative Binomial | 169449 |
| Multilevel Negative Binomial | 169602 |
| Zero-inflated Poisson | 251668 |
| Multilevel Zero-inflated Poisson | 292319 |
| Poisson | 292682 |
| Multilevel Poisson | 292868 |
| Multilevel Linear | 561937 |

**Equation 4.3: Count component of weather model.**

$$log(\mu_{t,h}) = \beta_0 - \beta_1(tmax_{t,h}) - \beta_2(tmin_{t,h}) + \beta_3(hum_{t,h}) + \beta_4(prec_{t,h}) + \mathcal{U}_h$$

**Equation 4.4: Zero-inflation component of the weather model.**

$$logit(p_{0t}) = \beta_0 + log(n_t) - \beta_1(tmax_t) - \beta_2(tmin_t) - \beta_3(prec_t)$$

Were, μ is the expected number of ILI cases for day t in hospital h. tmax, tmin, hum and prec are maximum temperature, minimum temperature, humidity and precipitation, respectively. $u$

represents the random intercept for hospitals. $P_{0t}$ is the probability of zero ILI cases at day t and $n_t$ is the population assigned to a hospital at time t.

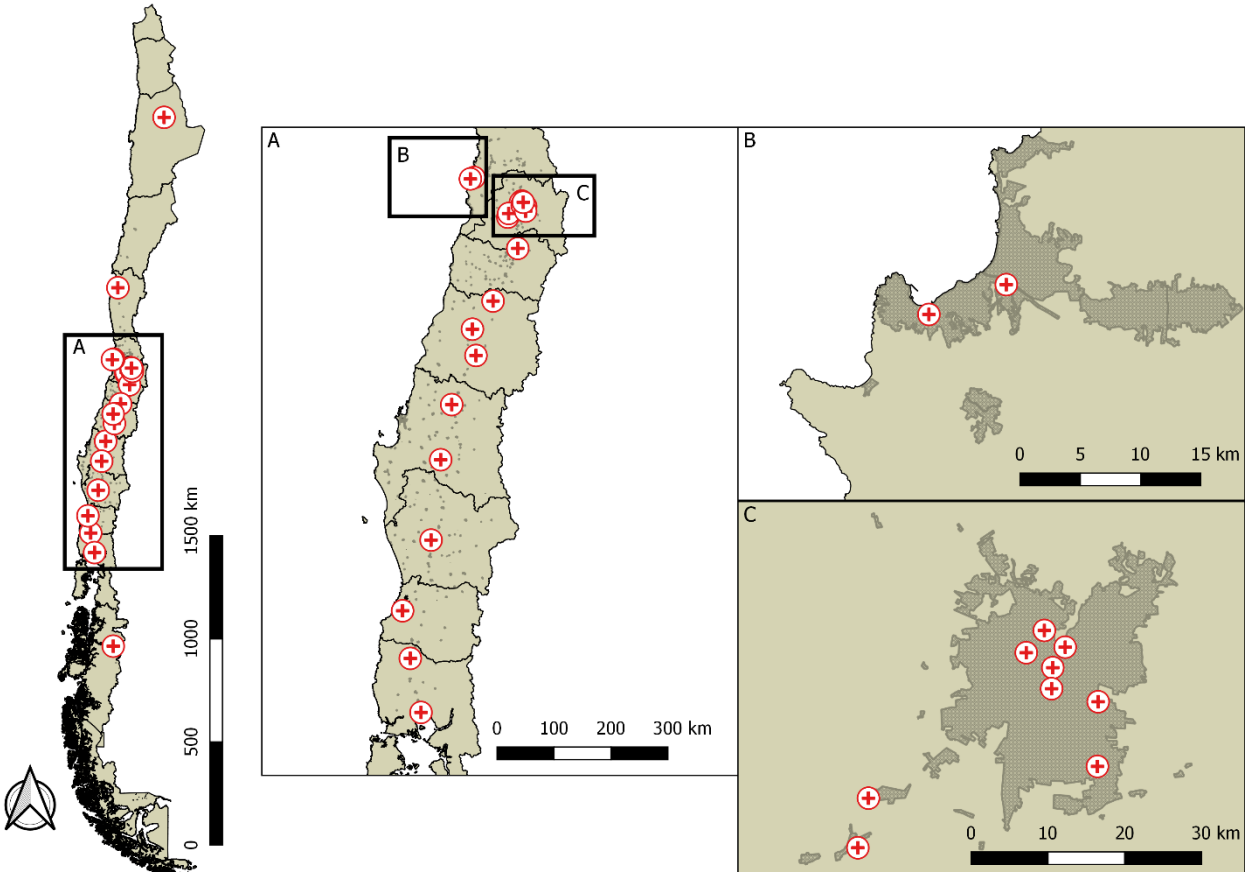


**Figure 4.2. Location of the 24 Hospitals included in the Weather Model, Chile 2010-2016**

**Table 4.3. Association between daily ILI and weather measures across 24 Chilean hospitals from January 2010 to December 2016 in a Multilevel Zero-Inflated Negative Binomial model, with random intercept for Hospital**

| Variable and Unit | β (95% CI) | p-value |
|---|---|---|
| *Fixed Effect* | | |
| *Count component* | | |
| *Meteorological measures* | | |
| Minimum Temperature (c°) | -0.045 (-0.049,-0.041) | <0.001 |
| Maximum Temperature (c°) | -0.039 (-0.043,-0.036) | <0.001 |
| Relative Humidity (%) | 0.001 (-0.0002,0.0017) | 0.13 |
| Precipitation (mm) | 0.001 (-0.001,0.003) | 0.302 |
| *Zero-Inflated component* | **OR (95% CI)** | **p-value** |
| *Meteorological measures* | | |
| Minimum Temperature (c°) | 0.856 (0.815,0.898) | <0.001 |
| Maximum Temperature (c°) | 0.677 (0.620,0.738) | <0.001 |
| Precipitation (mm) | 1.040 (1.010,1.070) | 0.00694 |
| *Random Effect* | | |
| Hospital (Intercept) | 1.382 (1.040,1.834) | <0.001 |

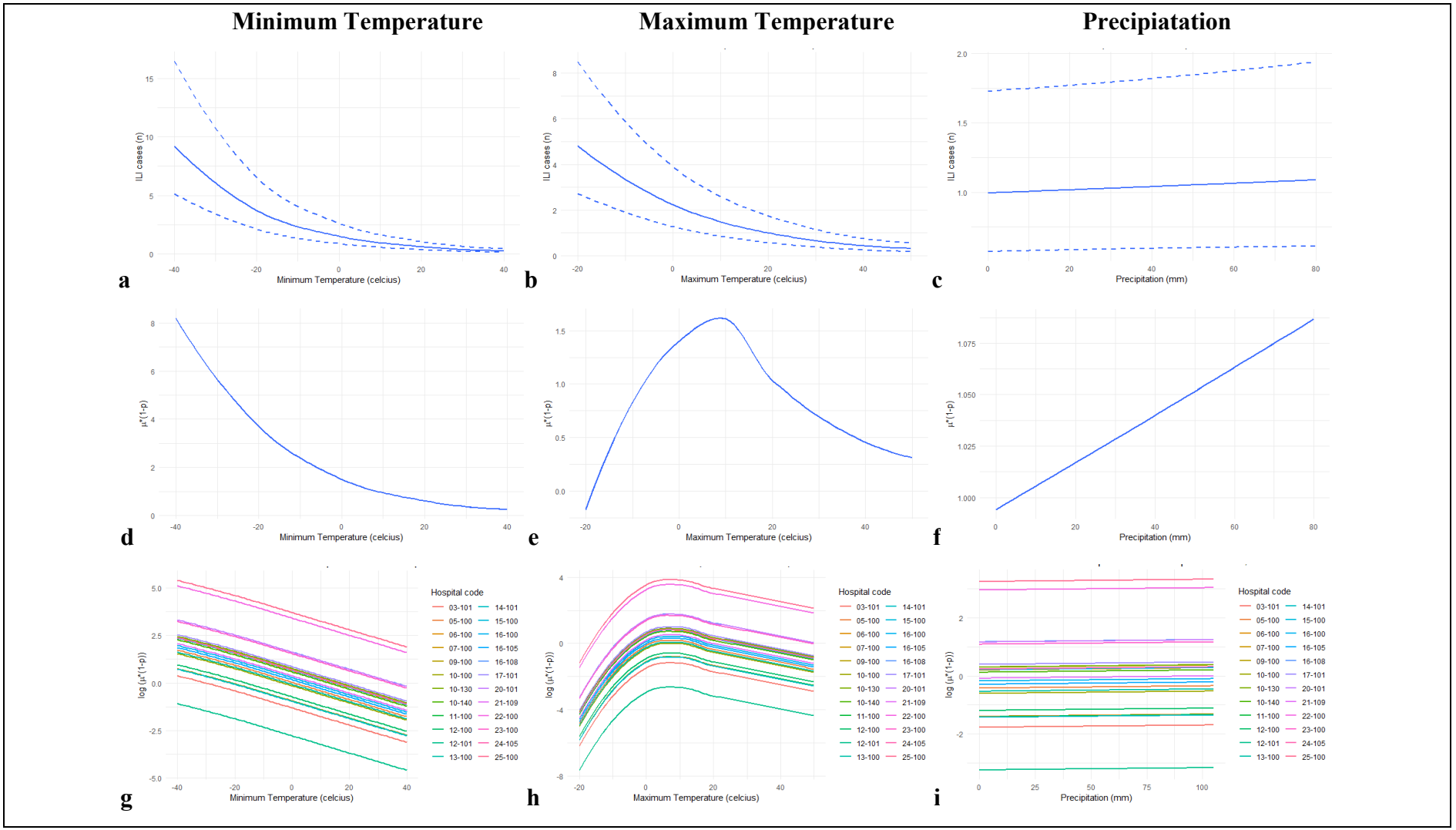


**Figure 4.3. Weather model predicted effects for ILI cases vs minimum temperature, maximum temperature and precipitation in 24 hospitals in Chile 2010-2016**

**Top line:** Predicted fixed effects of the count component on ILI cases of the Multilevel Zero-inflated Negative Binomial weather model for a) Minimum Temperature in C∘, b) Maximum Temperature in C∘ and c) Precipitation in mm. Dashed lines represent upper and lower limits of the 95% CI.
**Middle line:** Predicted fixed effects of complete Multilevel Zero-inflated Negative Binomial weather model presented in μ*(1-P) as the combination of both components: count ILI number of cases (μ) and the probability of non-zero cases (1-P). d) Minimum Temperature in C∘, e) Maximum Temperature in C∘ and f) Precipitation in mm.
**Bottom line:** Predicted random effects of the complete weather model presented in log10(μ*(1-P)) in the y axis. The effects are the combination of both components: ILI number of cases (μ) and the probability of non-zero cases (1-P) for each hospital. g) Minimum Temperature in C∘, i) Maximum Temperature in C∘ h) and i) Precipitation in mm. The y axis is represented in logarithm scale for visualization purposes.

### 4.4.3 Pollution Model

A total of 10 hospitals had enough pollution and weather data to build the pollution model, 7 from the capital Santiago, 2 from the center and one from the south of the country (Figure 4.4). Equation 4.5 and Equation 4.6 show the final pollution model that resulted from the backward elimination. The estimates of the model are presented in Table 4.4. In the zero-inflated component, only Tmax was significantly associated to zero cases (OR 0.57, CI95% 0.41, 0.78). In the count component, similar to the weather model, Tmin and Tmax had a significant inverse association to ILI cases (Tmin: e-0.48= 0.95; Tmax: e-0.038= 0.96) (Figure 4.5a and Figure 4.5b). On the other hand, PM2.5 and SO2 were included in the pollution model, with PM2.5 resulting in a direct and significant association to ILI cases. For one μg/m3 increase in PM2.5 there was an increase of 1 case of ILI (e0.001=1.001, CI95% 1.0003-1.001) adjusting by SO2, temperature, relative humidity and correlation within hospitals (Figure 4.5c). O3 showed a positive, but non-significant association to ILI cases ($e^{0.005}$=1.005, CI95% 0.99-1.01) (Table 4.4). PM10 and O3 were excluded in the backward elimination process and showed a non-significant association in the univariate models adjusting by weather variables. The predicted fixed and random effects of the pollution model were similar to the weather model: An inverse relation of ILI and Tmin and a quadratic shape for Tmax (Figure 4.5d,e,g,h). PM2.5 showed a positive association to ILI cases in the three effects estimated: Count component, fixed, and random effect (Figure 4.5c,f,i).

**Equation 4.5: Count component of the pollution model**

$$log(\mu_{t,h}) = \beta_0 - \beta_1(tmax_{t,h}) - \beta_2(tmin_{t,h}) + \beta_3(hum_{t,h}) + \beta_4(PM2.5_{t,h}) + \beta_4(SO2_{t,h}) + \mathcal{U}_h$$

**Equation 4.6: Zero-inflation component of the pollution model.**

$$logit(p_{0t}) = \beta_0 + log(n_t) - \beta_1(tmax_t) - \beta_2(tmin_t) - \beta_3(prec_t)$$

Where, μ is the expected number of ILI cases for day t in hospital h. tmax, tmin, hum and prec are maximum temperature, minimum temperature, humidity and precipitation, respectively. $\mathcal{U}$ represents the random intercept for hospitals. P0t is the probability of zero ILI cases at day t and nt is the population assigned to a hospital at time t.

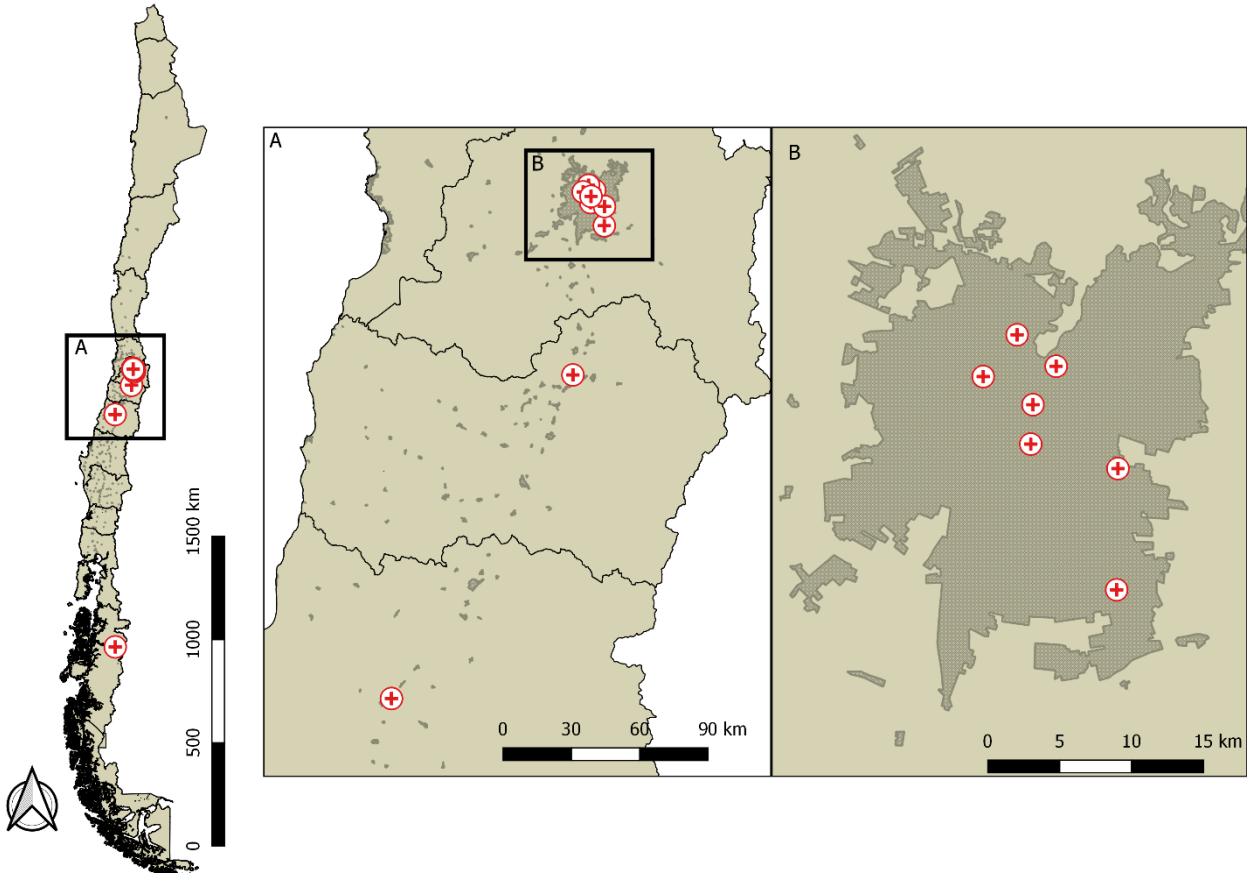


**Figure 4.4. Location of the 10 hospitals included in the Pollution Model, Chile 2010-2016**

**Table 4.4. Association between daily ILI, weather and pollution measures across 10 Chilean hospitals from January 2010 to December 2016 in a Multilevel Zero-Inflated Negative Binomial model, with random intercept for Hospital**

| Variable and Unit | β (95% CI) | p-value |
|---|---|---|
| *Count component* | | |
| *Pollution Measures* | | |
| PM2.5 (µg/m3) | 0.001 (0.0003,0.001) | <0.01 |
| SO2 (ppbv) | 0.005 (-0.0028,0.0127) | 0.2129 |
| *Meteorological measures* | | |
| Minimum Temperature (c°) | -0.048 (-0.0536,-0.0427) | <0.01 |
| Maximum Temperature (c°) | -0.038 (-0.0434,-0.0328) | <0.01 |
| Relative Humidity (%) | -0.002 (-0.0036,0.0005) | 0.1433 |
| *Zero-Inflated component* | **OR (95% CI)** | **p-value** |
| *Meteorological measures* | | |
| Minimum Temperature (c°) | 0.864 (0.7274,1.0273) | 0.0981 |
| Maximum Temperature (c°) | 0.571 (0.4169,0.7832) | <0.001 |
| Precipitation (mm) | 1.012 (0.8984,1.1402) | 0.8434 |
| *Random Effect* | | |
| Hospital (Intercept) | 1.128 (0.7094,1.7929) | <0.001 |

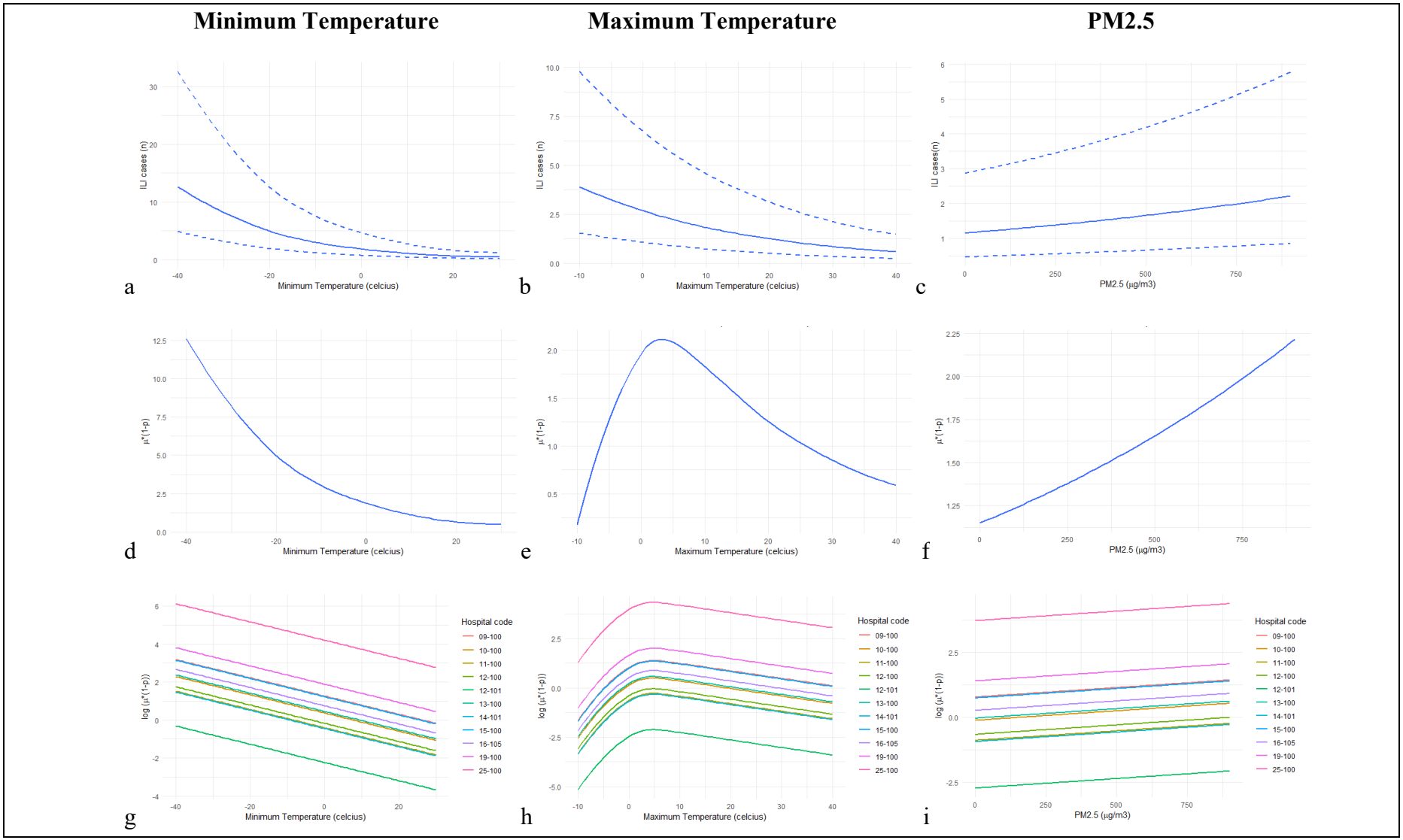


**Figure 4.5. Pollution model predicted effects for ILI cases vs minimum temperature, maximum temperature and PM2.5 in 10 hospitals in Chile 2010-2016**

**Top line:** Predicted fixed effects of the count component on ILI cases of the Multilevel Zero-inflated Negative Binomial pollution model **a**) Minimum Temperature in C∘, **b**) Maximum Temperature in C∘ and **c**) Precipitation in mm. Dashed lines represent upper and lower limits of the 95% CI.
**Middle line:** Predicted fixed effects of complete Multilevel Zero-inflated Negative Binomial pollution model presented in μ*(1-P) as the combination of both components: ILI number of cases (μ) and the probability of non-zero cases (1-P). **d**) Minimum Temperature in C∘, **e**) Maximum Temperature in C∘ and **f**) Precipitation in mm.
**Bottom line:** Predicted random effects of the complete pollution model presented in log10(μ*(1-P)) as the combination of both components: ILI number of cases (μ) and the probability of non-zero cases (1-P) for each hospital. **g**) Minimum Temperature in C∘, **h**) Maximum Temperature in C∘ and **i**) Precipitation in mm. The y axis is represented in logarithm scale for visualization purposes.

## 4.5 DISCUSSION

We found a negative association between Tmin and influenza in both weather and pollution models. These results coincide with international and national findings (11, 17-19, 92, 95, 117, 144, 152). A slightly different effect was found for Tmax. The positive association between Tmax and ILI for negative temperatures turned into a negative association after 0C∘ (32F∘). A possible explanation is that Tmax is normally measured in the afternoon, thus is more closely related to chances of commuting to an Emergency room compared to Tmin, that is normally measured early in the morning. For extreme low temperatures that chance might be reduced, with a predomination of the zero-inflation component (153). On the other hand, when a tolerable temperature is reached, the chances of commuting to an ED settles giving the count component predominance reflecting the negative association to Tmax.

We did not find an association between humidity and ILI cases in concordance with previous studies in the country (144). The lack of association may be explained because we measured relative humidity (Absolute humidity / maximum humidity given the same temperature), but absolute humidity (water content in the air in g/m3 vapor) has been found to be more strongly associated to influenza cases (17). Chile is a country that has different weather and lower humidity compared to other countries. The low humidity and adjusting by other weather variables could diminish the association between humidity and influenza.

Fine particulate matter, like PM2.5 increases the risk of ILI even after controlling for the weather conditions (39, 40). The pollution model showed a positive association between PM2.5 and ILI cases. The relationship found was small, but significant. We believe that the association is

real given that the fixed effects were calculated using diverse hospital locations with different air conditions. Further, some hospitals shared the same pollution station, increasing the variance that could result in underestimating the real effect. Nevertheless, our findings are in line with the accepted hypotheses about the relation of PM2.5 and influenza, and similar findings were reported for the one Chilean Region (144). PM2.5 causes direct tissue damage, local inflammation, reduced capacity of the immune system, and increase transmission by transporting viruses in minuscule droplets present in the particles (113, 135-139). These individual level effects of pollution should be addressed in future studies to determine the association and to explain the mechanisms involved in the relation between PM and influenza.

Our study has limitations. First, we calculated exposure using weather and pollution stations. The stations rather than measure individual exposure, represent a proxy of exposure. Second, we did not include age structure and assumed a constant spread in all age groups, regardless that is feasible that temperature and PM2.5 might have different effects in different age groups. This differential effect could determine a different transmission pattern in zones with different age structure (40). Third, the selection of cities for the pollution model may be biased given that cities with higher air pollution are more likely to have stations. Consequently, these results must be interpreted with caution given that they cannot be generalized. Fourth, some hospitals were paired to the same stations. This could underestimate the effect given that outcome variance might increase for equivalent exposures. Even though this could underestimate the associations, we found significant relations between temperatures, PM2.5 and influenza, supporting the existence of a real association in the locations studied.

In this manuscript, we obtained a large amount of ILI, weather and pollution data from different locations across the country. Data came from established and reliable surveillance systems, for example ILI surveillance operates year-round with centralized report and national

guidelines. All data were obtained from publicly available reports from the Ministry of Health, meteorological services and air quality surveillance. We compared different models and handled overdispersion, excess zeros, and adjusted by autocorrelation within hospitals. Overdispersion, excess zeros and autocorrelation are common characteristics in ILI data, but not always accounted for. Few studies have evaluated the relation between PM2.5 and ILI (40). Even, fewer used different locations to determine the association. In that matter, our study contributes a small step in understanding the complex relations between weather, pollution and influenza in temperate regions.

## 4.6 CONCLUSION

To our knowledge, this is the first study that address the relation between weather, pollution and ILI across different locations in Chile. Our findings showed a positive association between ILI and PM2.5 and a negative association with Tmin. Tmax showed an inverted U shape relation with negative temperature providing a positive association and the opposite for temperature > 0∘ Celsius. Our results could help decision-makers prepare vaccination campaigns, stablish pollution standards and to calculate health effects of policies that reduce particulate matter. Additionally, this study could be a baseline to compare effects of weather and pollution on influenza across Chile.

# 5.0 DISSERTATION DISCUSSION

## 5.1 MAJOR FINDINGS

Influenza causes an important burden of morbidity and mortality every year in Chile and the rest of the world. However, the dynamics of influenza at global and local scale are not fully understood. This investigation aimed to understand the spatial relation of influenza between different regions in Chile and the association to weather and pollution. For our purpose, we presented three complementary studies. The first explores the influenza surveillance system in Chile and determine the timing association between ILI and 7 laboratory confirmed viruses. The second assesses the seasonality of influenza and spatial relationships across the country, including the analysis of local traveling waves between health networks. Finally, the third study assesses the association between influenza, weather and air pollution.

The study presented in chapter two found that the timing of ILI in emergency rooms is closely related to the incidence of influenza A. There were no significant differences on timing across different hospitals that participated in both laboratory and ILI surveillance systems. Further, we compared ILI timing to different laboratory-confirmed viruses to confirm our findings. Our results support the use of ILI as a reliable measure of influenza A timing in Chile.

The results on spatial dependencies of influenza and travelling waves was presented in chapter three of this dissertation. Here, we demonstrated that influenza has a predominant periodicity (seasonality) in Chile of 50 weeks. Also, we found a north to south latitudinal gradient

of influenza that was related to the central zone of the country and associated to health networks with larger population size. Similarly, local travelling waves of influenza were present in health networks from the center of the country and were also associated with population size. Our findings suggest that the larger population located in the center of the country drives seasonal influenza epidemics in Chile.

Finally, the results from the association between influenza, weather and pollution are presented in chapter four. Lower minimum and maximum temperature were associated with fewer influenza cases and a small positive association was found between influenza and PM2.5. These findings can help to understand the complex relation between influenza, weather and pollution.

## 5.2 PUBLIC HEALTH SIGNIFICANCE

The Chilean Ministry of Health, public health networks and local public health departments have the constitutional mandate to protect the population from health threats. Influenza causes high morbidity and mortality. Decision-makers need to be informed about influenza dynamics and the factors associated to allocate resources more efficiently and to reduce the burden of influenza.

The results of the three complementary studies are a step forward to the understanding of the complex relationships that govern seasonal influenza epidemics in Chile. Influenza season preparation is fundamental to reduce influenza mortality and morbidity. We present new information that can help prepare vaccination campaigns by prioritizing areas with larger populations from the center of the country. Although we studied seasonal influenza epidemics in a "normal" scenario, it should be considered in future pandemics associated with new influenza strains, in situations of vaccine shortages, and to allocate human resources in these cases. Influenza spread and impact in the population can be reduced in Chile if earlier actions are taken in zones with larger populations and where influenza starts earlier. Finally, weather and pollution should be considered in the design of influenza campaigns. Our results are inputs to establish pollution standards to calculate the effect of pollution policies on health. Further, the results established a baseline to compare future effects of weather on influenza in Chile in the context of global warming.

## 5.3 FUTURE DIRECTIONS

Influenza affects the population differently across age groups. Young children and the elderly are at higher risk of developing the disease and presenting complications. Temperature and pollution effects on influenza vary across age groups. Future analysis should include age structure of the population to account for this differential risk and to shed light on the local influenza dynamics.

Age groups have different contact rates that result in differential impact on influenza spread. Contact rate is fundamental to simulate infectious diseases with person-to-person transmission, like influenza. Contact rate surveys could be a central input to develop better models for the understanding of influenza spread at the local and national level.

Humans are the principal host of influenza and the main source of transmission. There is little knowledge on how human movement across Chile could affect transmission of influenza and other diseases. Although the study of travel patterns and its relation to disease in Chile is a complex endeavor, we think that substantial advances could be made by incorporating professionals from different disciplines and international collaborators with experience in this research topic.

Finally, our research is unique in South America. A major body of knowledge could be built for the understanding of global influenza dynamics by initially including neighboring countries followed by countries from all the Americas and, why not, the rest of the world.

## APPENDIX A: Cross wavelet power spectrum for ILI versus laboratory-confirmed viruses by hospital, Chile 2011-2016

### 1. Cross wavelet power spectrum for ILI versus laboratory-confirmed influenza A by hospital

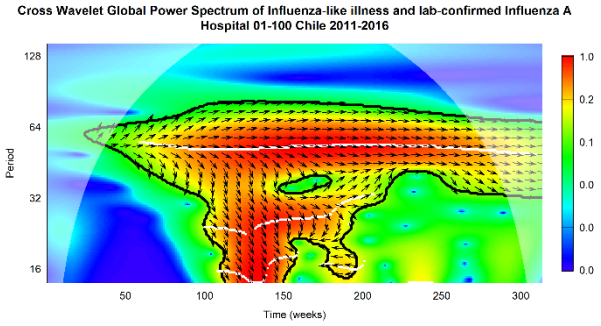


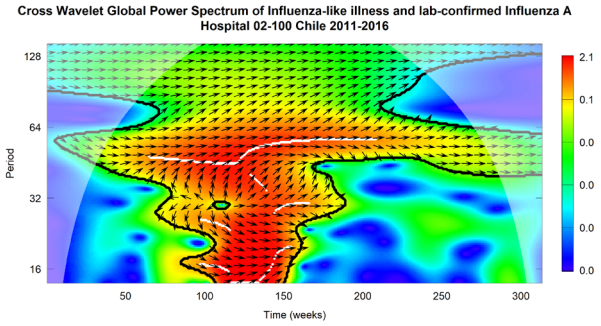


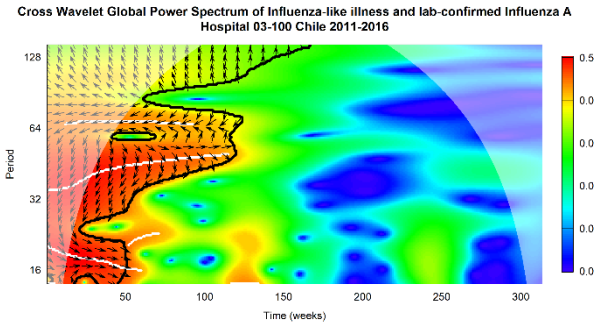


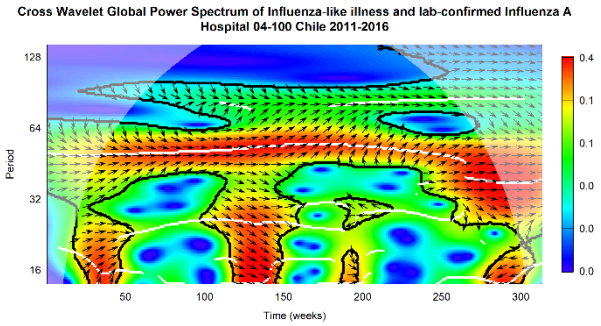


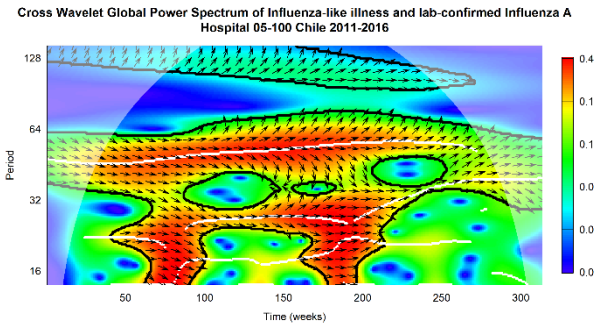


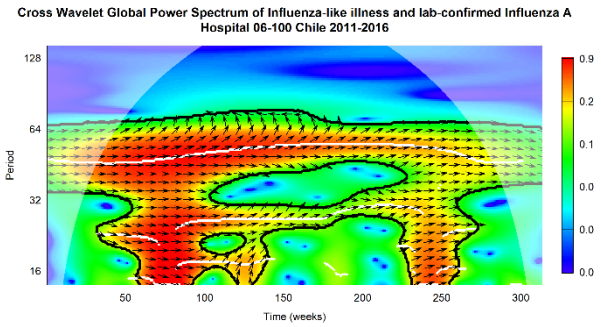

Cross Wavelet Global Power Spectrum of Influenza-like illness and lab-confirmed Influenza A
Hospital 06-103 Chile 2011-2016

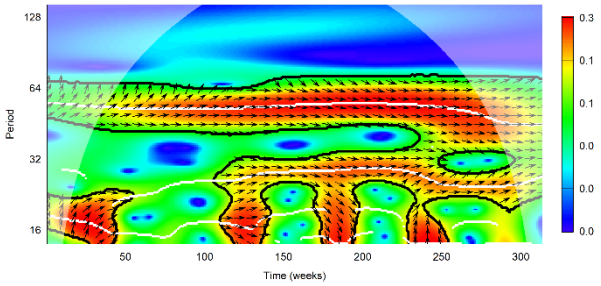


Cross Wavelet Global Power Spectrum of Influenza-like illness and lab-confirmed Influenza A
Hospital 07-100 Chile 2011-2016

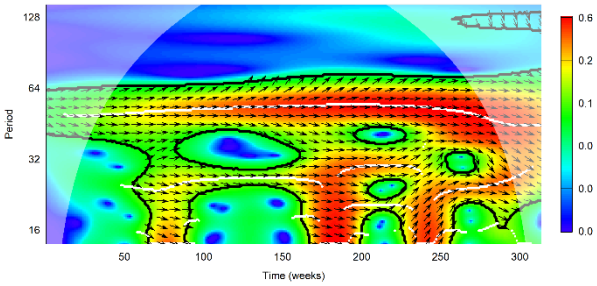


Cross Wavelet Global Power Spectrum of Influenza-like illness and lab-confirmed Influenza A
Hospital 08-100 Chile 2011-2016

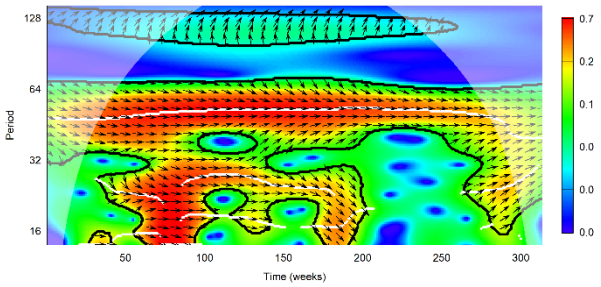


Cross Wavelet Global Power Spectrum of Influenza-like illness and lab-confirmed Influenza A
Hospital 10-100 Chile 2011-2016

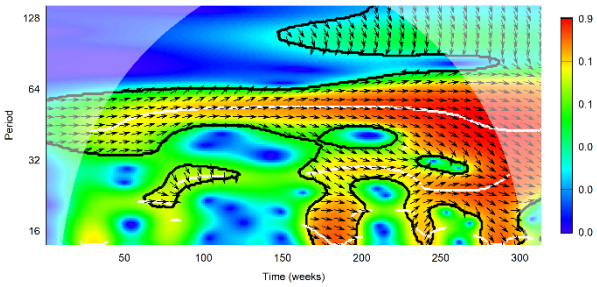


Cross Wavelet Global Power Spectrum of Influenza-like illness and lab-confirmed Influenza A
Hospital 14-103 Chile 2011-2016

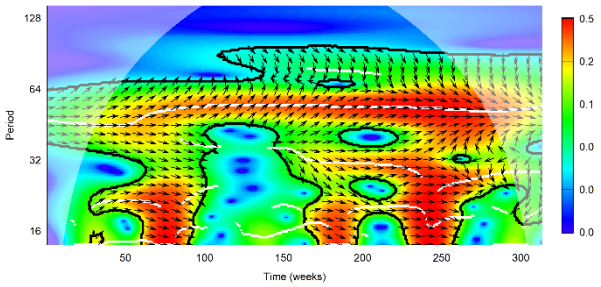


Cross Wavelet Global Power Spectrum of Influenza-like illness and lab-confirmed Influenza A
Hospital 15-100 Chile 2011-2016

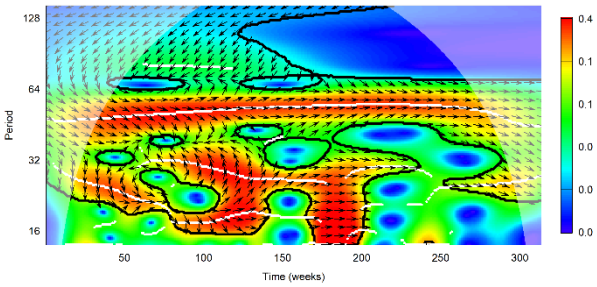


Cross Wavelet Global Power Spectrum of Influenza-like illness and lab-confirmed Influenza A
Hospital 16-100 Chile 2011-2016

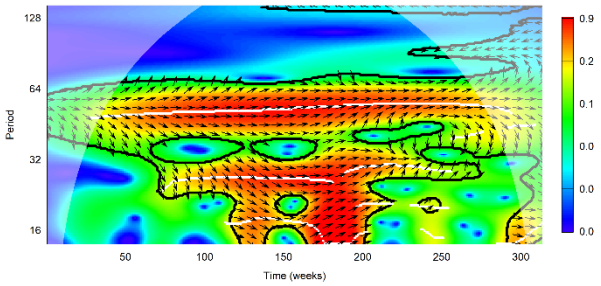


Cross Wavelet Global Power Spectrum of Influenza-like illness and lab-confirmed Influenza A
Hospital 16-105 Chile 2011-2016

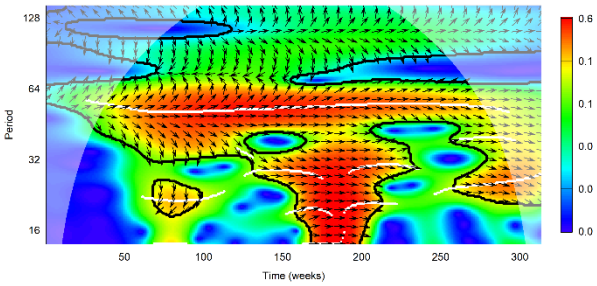

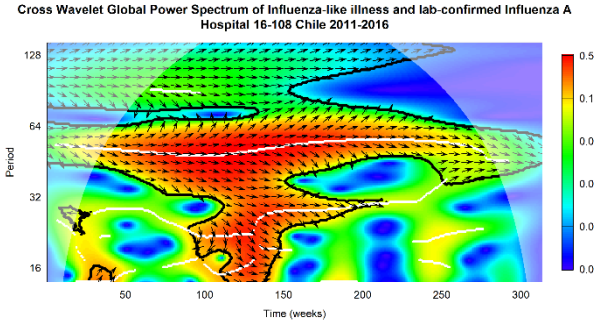
Cross Wavelet Global Power Spectrum of Influenza-like illness and lab-confirmed Influenza A
Hospital 16-108 Chile 2011-2016
Period
Time (weeks)

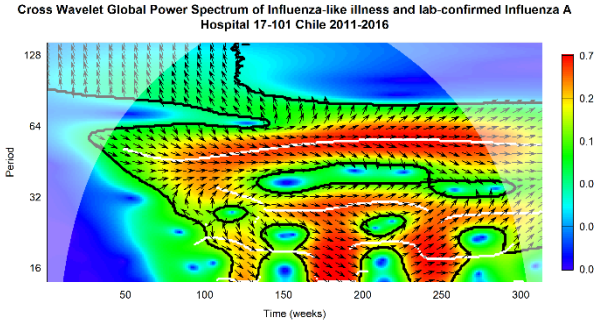
Cross Wavelet Global Power Spectrum of Influenza-like illness and lab-confirmed Influenza A
Hospital 17-101 Chile 2011-2016
Period
Time (weeks)

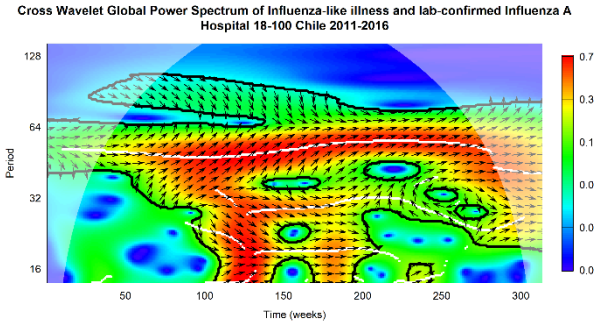
Cross Wavelet Global Power Spectrum of Influenza-like illness and lab-confirmed Influenza A
Hospital 18-100 Chile 2011-2016
Period
Time (weeks)

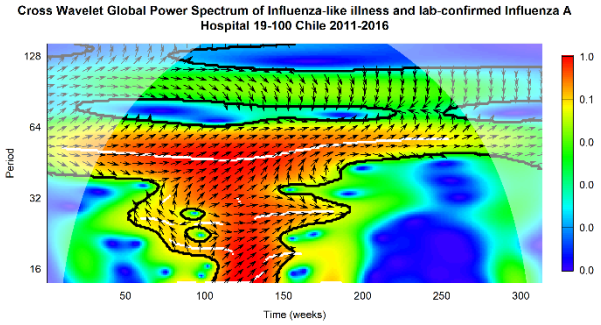
Cross Wavelet Global Power Spectrum of Influenza-like illness and lab-confirmed Influenza A
Hospital 19-100 Chile 2011-2016
Period
Time (weeks)

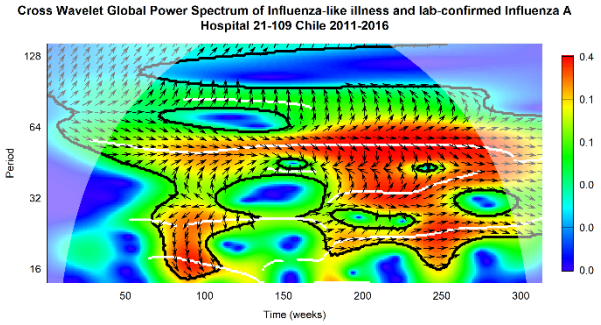
Cross Wavelet Global Power Spectrum of Influenza-like illness and lab-confirmed Influenza A
Hospital 21-109 Chile 2011-2016
Period
Time (weeks)

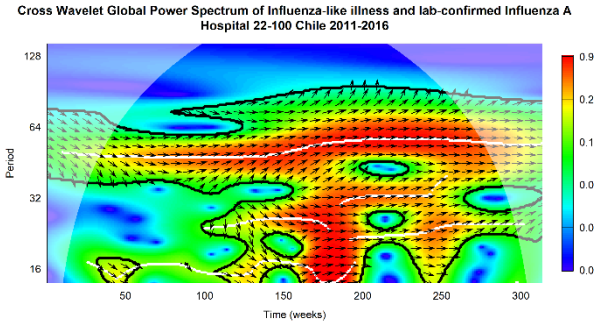
Cross Wavelet Global Power Spectrum of Influenza-like illness and lab-confirmed Influenza A
Hospital 22-100 Chile 2011-2016
Period
Time (weeks)

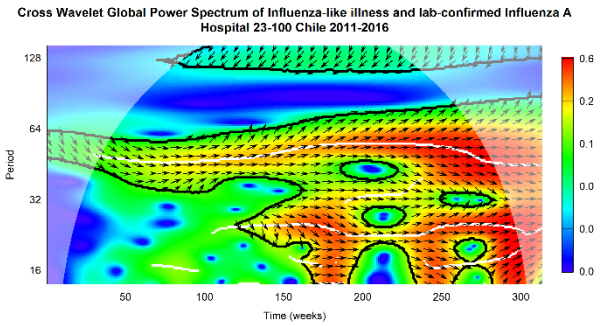
Cross Wavelet Global Power Spectrum of Influenza-like illness and lab-confirmed Influenza A
Hospital 23-100 Chile 2011-2016
Period
Time (weeks)

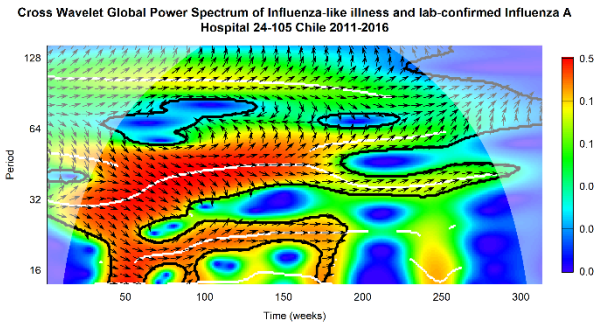
Cross Wavelet Global Power Spectrum of Influenza-like illness and lab-confirmed Influenza A
Hospital 24-105 Chile 2011-2016
Period
Time (weeks)

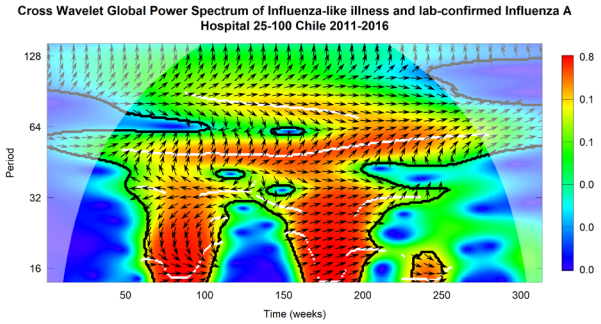


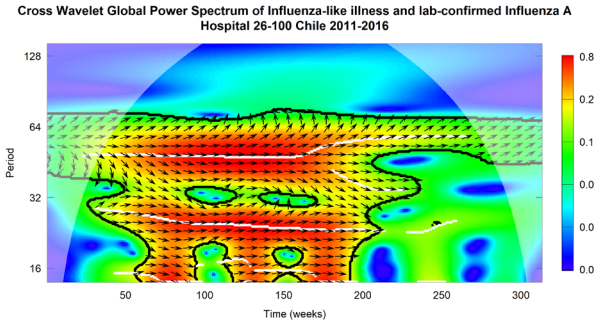


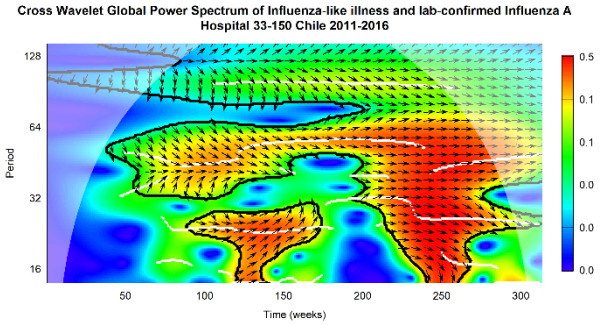


## 2. Cross wavelet power spectrum for ILI versus laboratory-confirmed influenza B by hospital

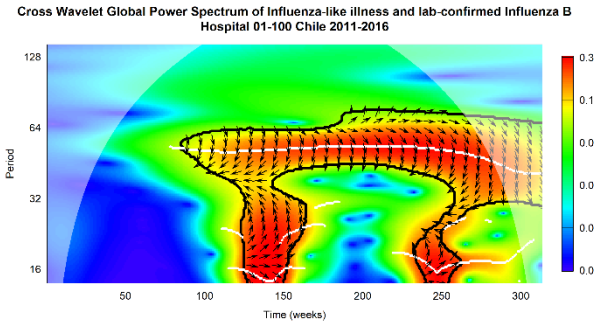


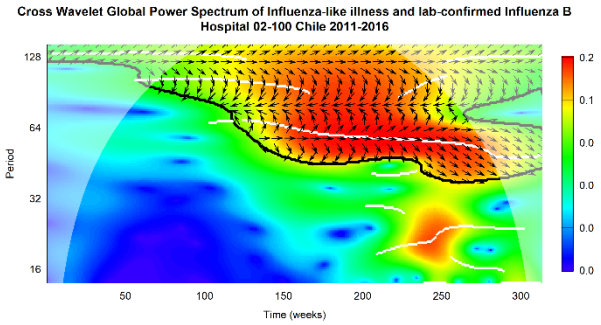


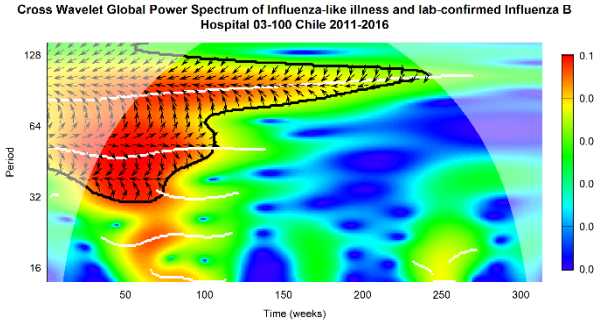


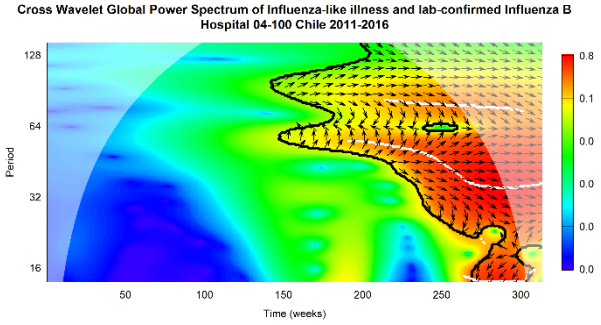

Cross Wavelet Global Power Spectrum of Influenza-like illness and lab-confirmed Influenza B
Hospital 05-100 Chile 2011-2016

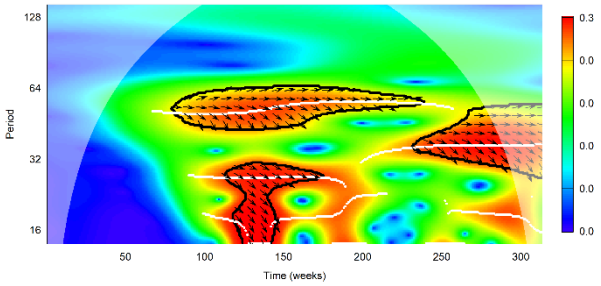


Cross Wavelet Global Power Spectrum of Influenza-like illness and lab-confirmed Influenza B
Hospital 06-100 Chile 2011-2016

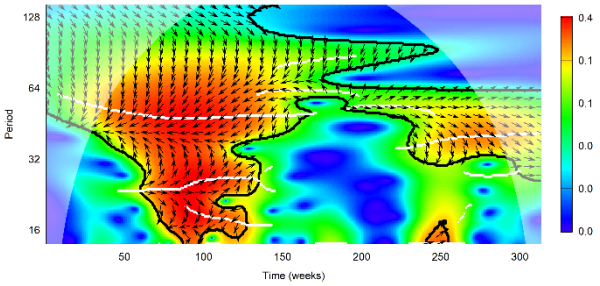


Cross Wavelet Global Power Spectrum of Influenza-like illness and lab-confirmed Influenza B
Hospital 06-103 Chile 2011-2016

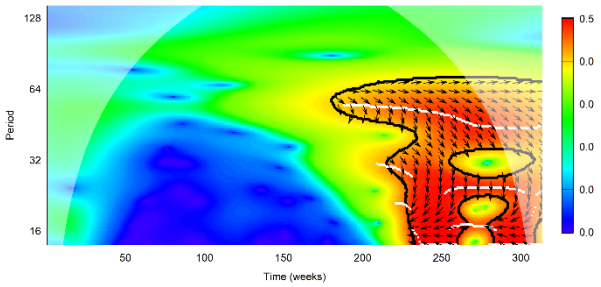


Cross Wavelet Global Power Spectrum of Influenza-like illness and lab-confirmed Influenza B
Hospital 07-100 Chile 2011-2016

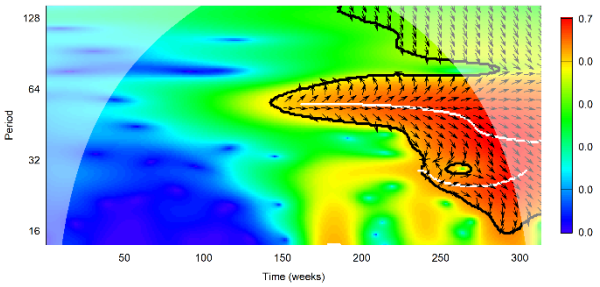


Cross Wavelet Global Power Spectrum of Influenza-like illness and lab-confirmed Influenza B
Hospital 08-100 Chile 2011-2016

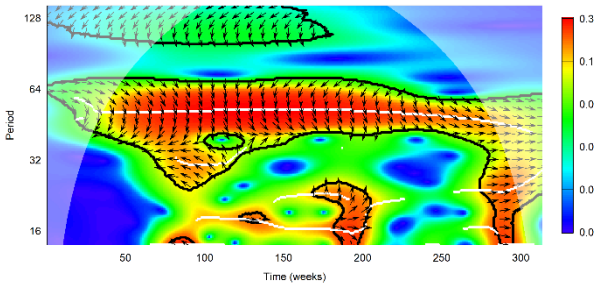


Cross Wavelet Global Power Spectrum of Influenza-like illness and lab-confirmed Influenza B
Hospital 10-100 Chile 2011-2016

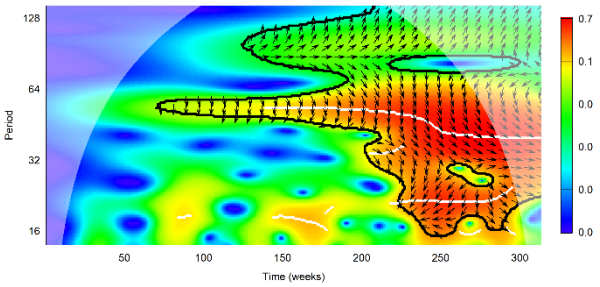


Cross Wavelet Global Power Spectrum of Influenza-like illness and lab-confirmed Influenza B
Hospital 14-103 Chile 2011-2016

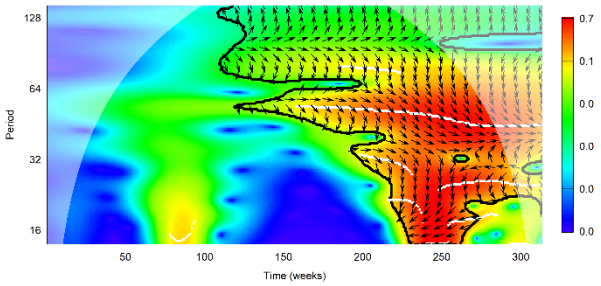


Cross Wavelet Global Power Spectrum of Influenza-like illness and lab-confirmed Influenza B
Hospital 15-100 Chile 2011-2016

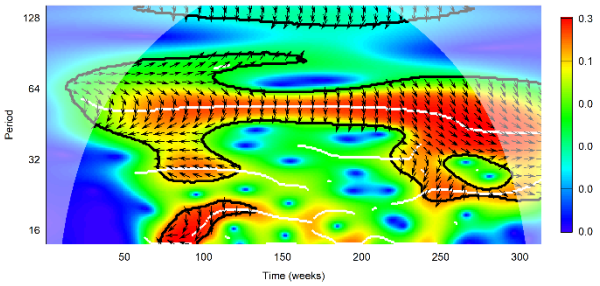

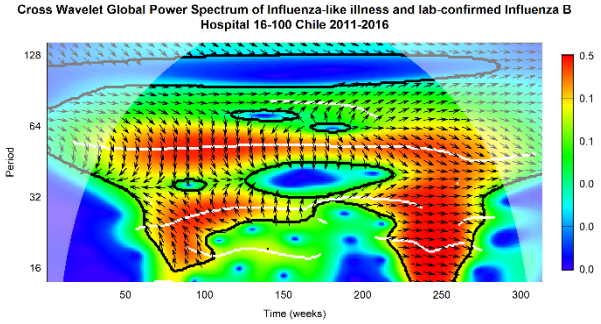
Cross Wavelet Global Power Spectrum of Influenza-like illness and lab-confirmed Influenza B
Hospital 16-100 Chile 2011-2016
Period
Time (weeks)

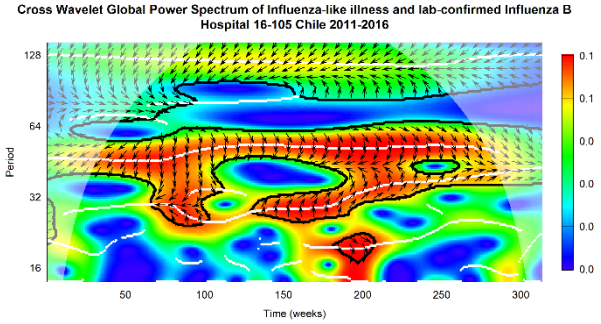
Cross Wavelet Global Power Spectrum of Influenza-like illness and lab-confirmed Influenza B
Hospital 16-105 Chile 2011-2016
Period
Time (weeks)

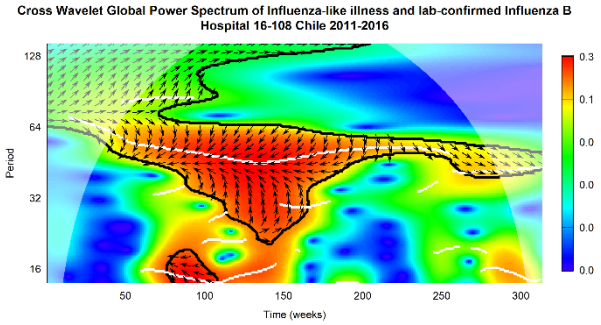
Cross Wavelet Global Power Spectrum of Influenza-like illness and lab-confirmed Influenza B
Hospital 16-108 Chile 2011-2016
Period
Time (weeks)

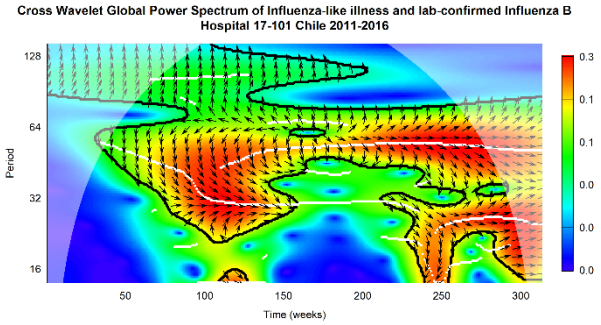
Cross Wavelet Global Power Spectrum of Influenza-like illness and lab-confirmed Influenza B
Hospital 17-101 Chile 2011-2016
Period
Time (weeks)

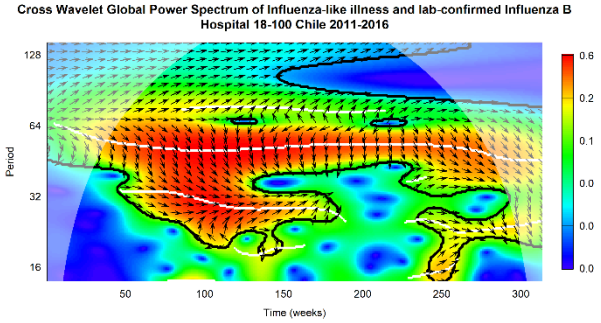
Cross Wavelet Global Power Spectrum of Influenza-like illness and lab-confirmed Influenza B
Hospital 18-100 Chile 2011-2016
Period
Time (weeks)

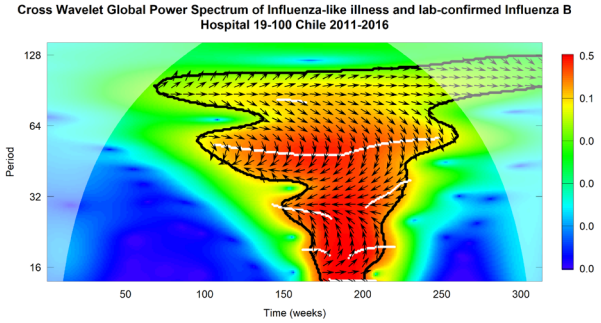
Cross Wavelet Global Power Spectrum of Influenza-like illness and lab-confirmed Influenza B
Hospital 19-100 Chile 2011-2016
Period
Time (weeks)

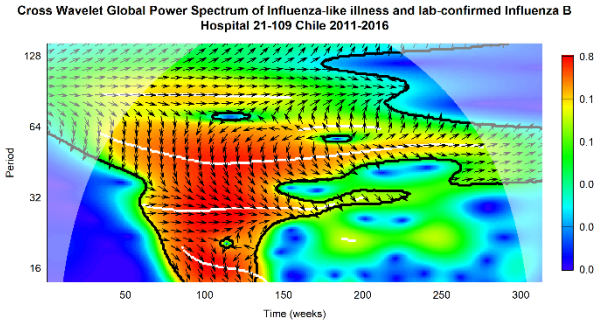
Cross Wavelet Global Power Spectrum of Influenza-like illness and lab-confirmed Influenza B
Hospital 21-109 Chile 2011-2016
Period
Time (weeks)

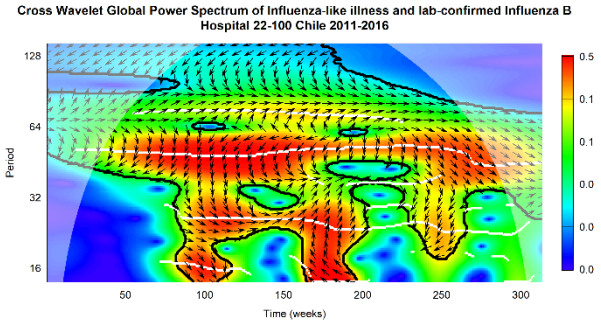
Cross Wavelet Global Power Spectrum of Influenza-like illness and lab-confirmed Influenza B
Hospital 22-100 Chile 2011-2016
Period
Time (weeks)

Cross Wavelet Global Power Spectrum of Influenza-like illness and lab-confirmed Influenza B
Hospital 23-100 Chile 2011-2016

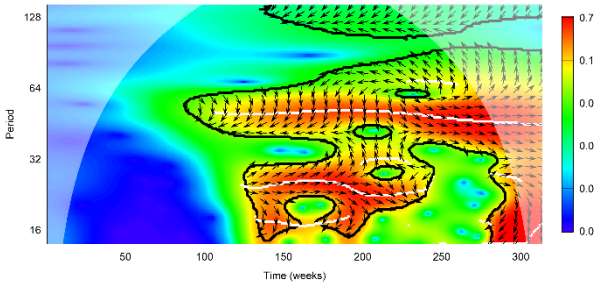


Cross Wavelet Global Power Spectrum of Influenza-like illness and lab-confirmed Influenza B
Hospital 24-105 Chile 2011-2016

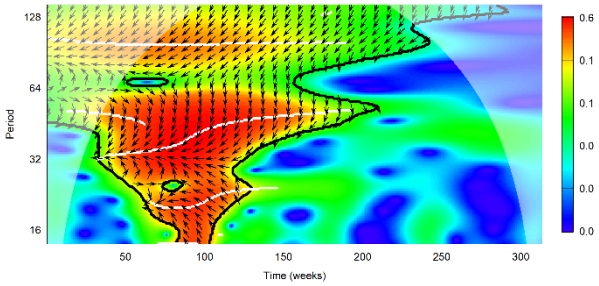


Cross Wavelet Global Power Spectrum of Influenza-like illness and lab-confirmed Influenza B
Hospital 25-100 Chile 2011-2016

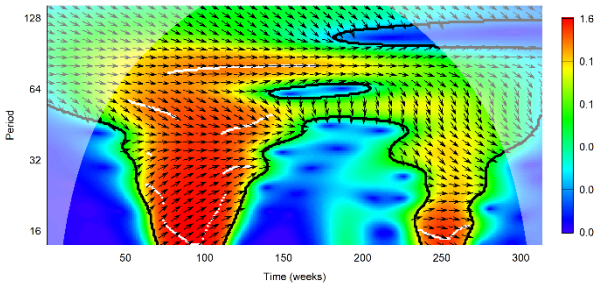


Cross Wavelet Global Power Spectrum of Influenza-like illness and lab-confirmed Influenza B
Hospital 26-100 Chile 2011-2016

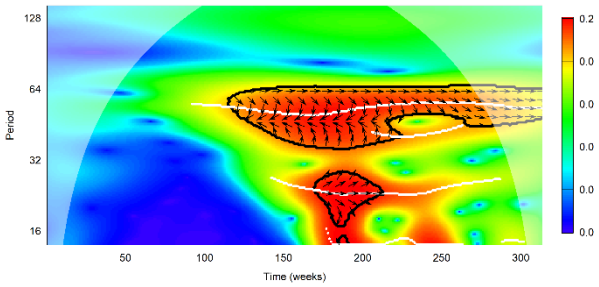


Cross Wavelet Global Power Spectrum of Influenza-like illness and lab-confirmed Influenza B
Hospital 33-150 Chile 2011-2016

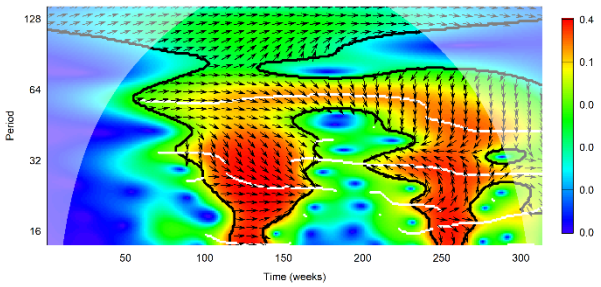

## 3. Cross wavelet power spectrum for ILI versus laboratory-confirmed influenza A plus influenza B by hospital

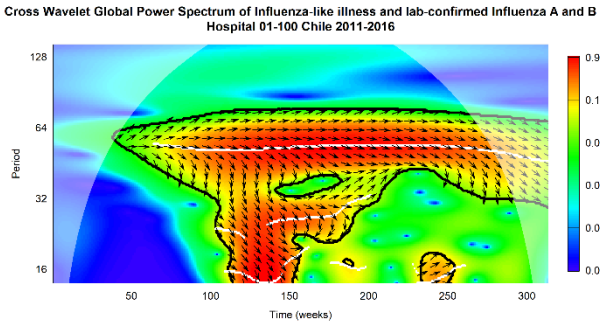


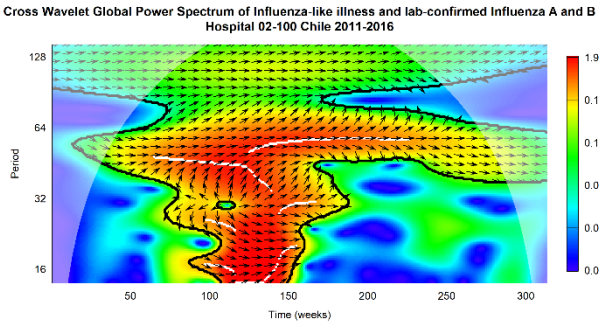


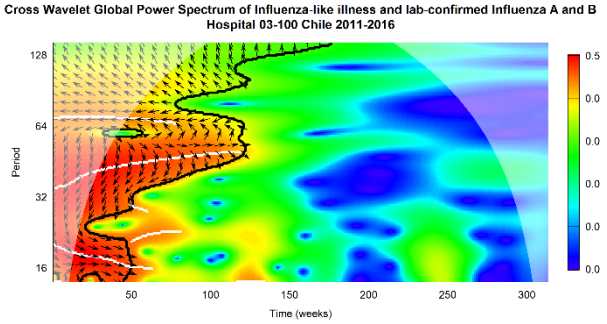


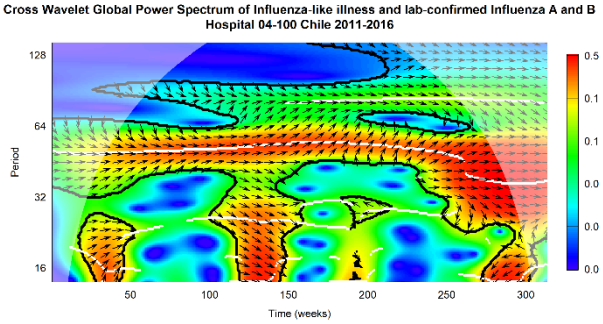


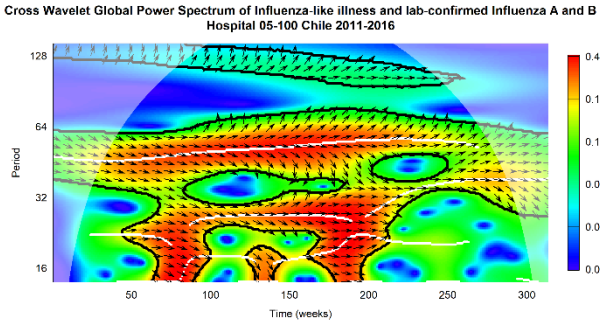


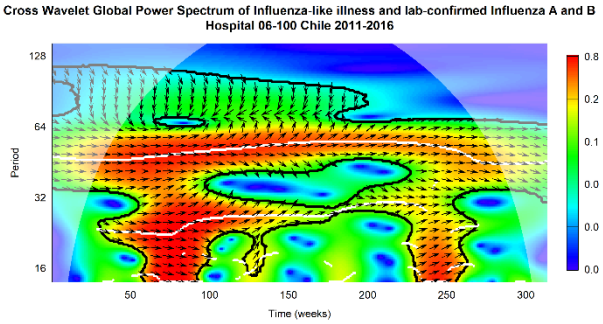


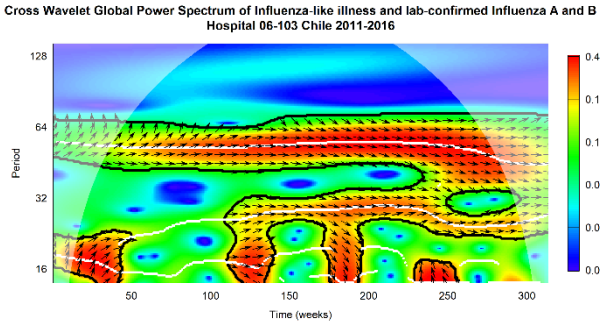


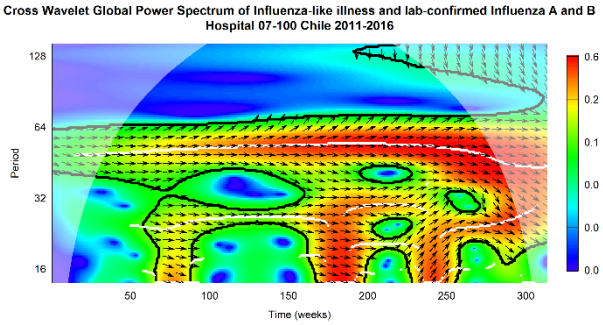

Cross Wavelet Global Power Spectrum of Influenza-like illness and lab-confirmed Influenza A and B
Hospital 08-100 Chile 2011-2016

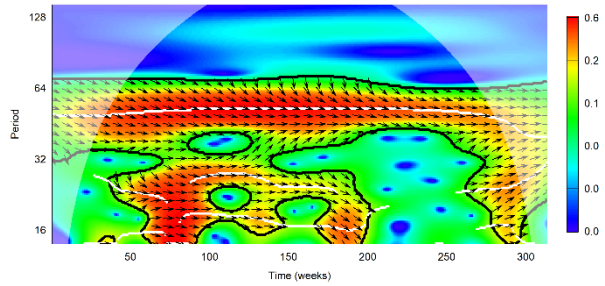


Cross Wavelet Global Power Spectrum of Influenza-like illness and lab-confirmed Influenza A and B
Hospital 14-103 Chile 2011-2016

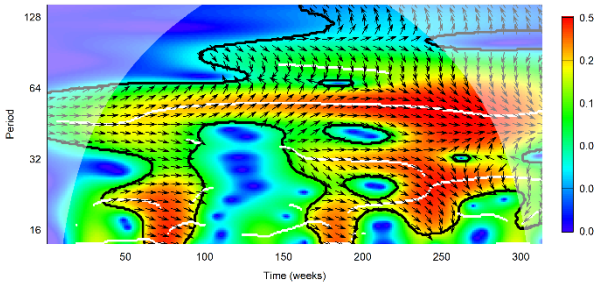


Cross Wavelet Global Power Spectrum of Influenza-like illness and lab-confirmed Influenza A and B
Hospital 15-100 Chile 2011-2016

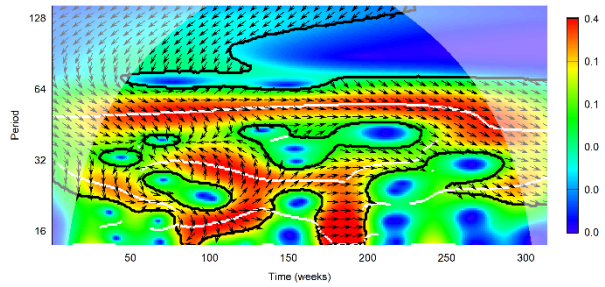


Cross Wavelet Global Power Spectrum of Influenza-like illness and lab-confirmed Influenza A and B
Hospital 16-100 Chile 2011-2016

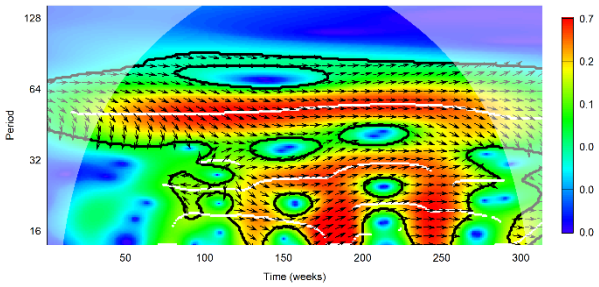


Cross Wavelet Global Power Spectrum of Influenza-like illness and lab-confirmed Influenza A and B
Hospital 16-105 Chile 2011-2016

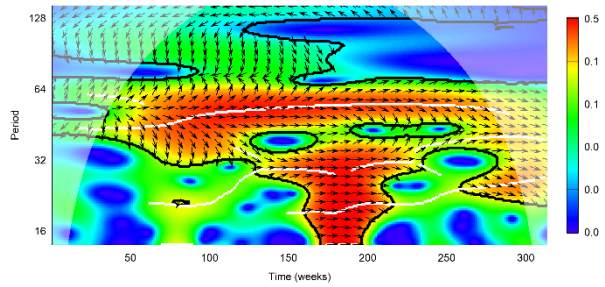


Cross Wavelet Global Power Spectrum of Influenza-like illness and lab-confirmed Influenza A and B
Hospital 16-108 Chile 2011-2016

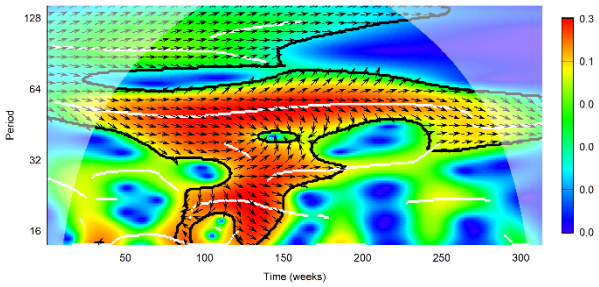


Cross Wavelet Global Power Spectrum of Influenza-like illness and lab-confirmed Influenza A and B
Hospital 17-101 Chile 2011-2016

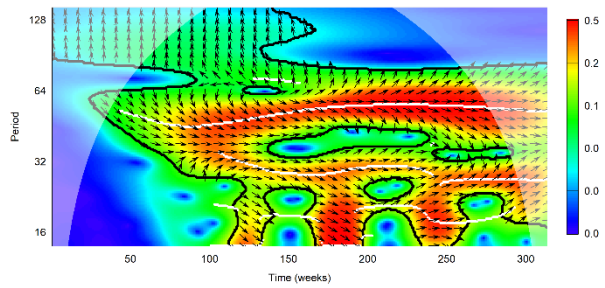


Cross Wavelet Global Power Spectrum of Influenza-like illness and lab-confirmed Influenza A and B
Hospital 18-100 Chile 2011-2016

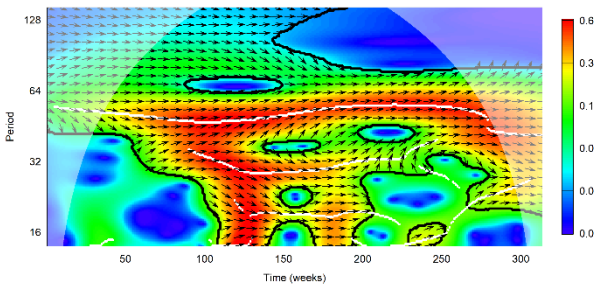

Cross Wavelet Global Power Spectrum of Influenza-like illness and lab-confirmed Influenza A and B
Hospital 19-100 Chile 2011-2016

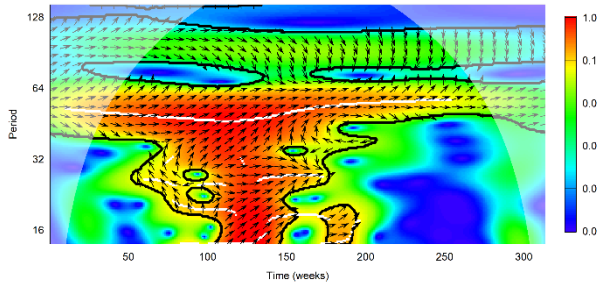


Cross Wavelet Global Power Spectrum of Influenza-like illness and lab-confirmed Influenza A and B
Hospital 21-109 Chile 2011-2016

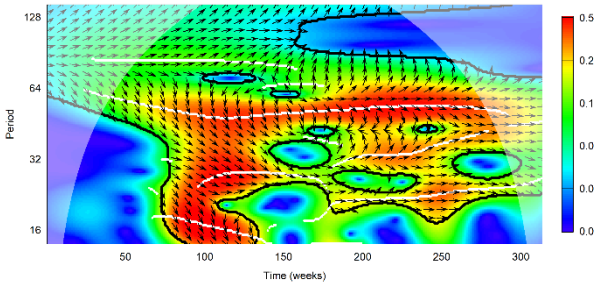


Cross Wavelet Global Power Spectrum of Influenza-like illness and lab-confirmed Influenza A and B
Hospital 22-100 Chile 2011-2016

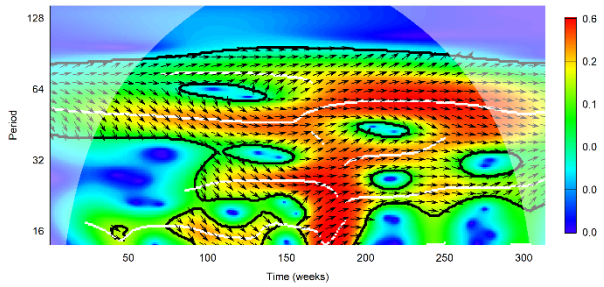


Cross Wavelet Global Power Spectrum of Influenza-like illness and lab-confirmed Influenza A and B
Hospital 23-100 Chile 2011-2016

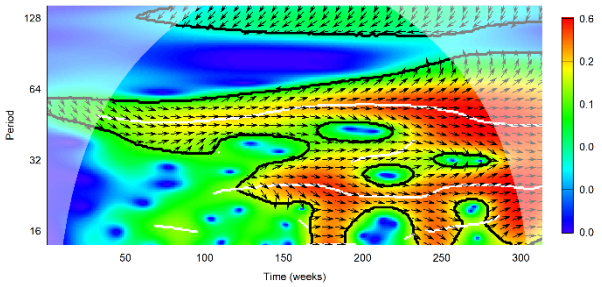


Cross Wavelet Global Power Spectrum of Influenza-like illness and lab-confirmed Influenza A and B
Hospital 24-105 Chile 2011-2016

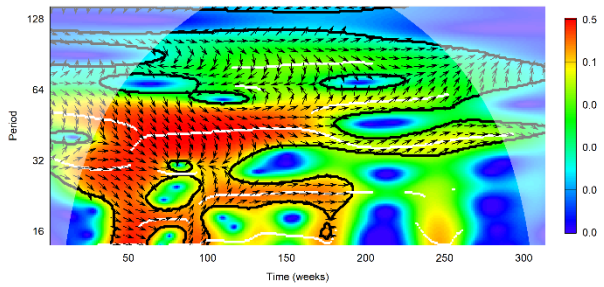


Cross Wavelet Global Power Spectrum of Influenza-like illness and lab-confirmed Influenza A and B
Hospital 25-100 Chile 2011-2016

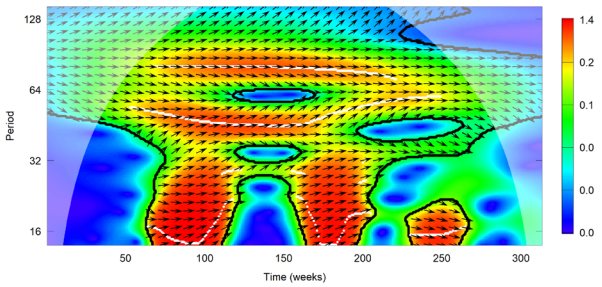


Cross Wavelet Global Power Spectrum of Influenza-like illness and lab-confirmed Influenza A and B
Hospital 26-100 Chile 2011-2016

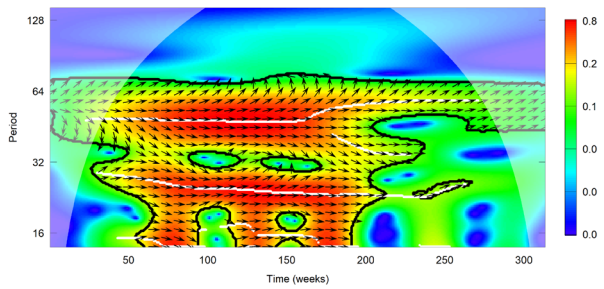


Cross Wavelet Global Power Spectrum of Influenza-like illness and lab-confirmed Influenza A and B
Hospital 33-150 Chile 2011-2016

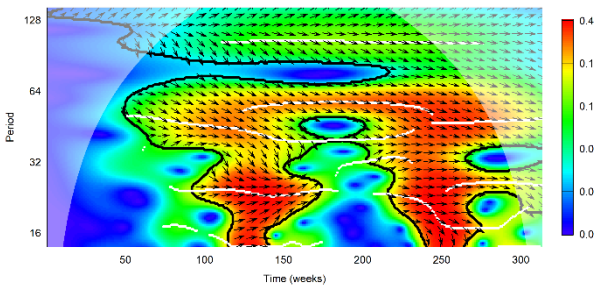

## 4. Cross wavelet power spectrum for ILI versus laboratory-confirmed respiratory syncytial virus by hospital

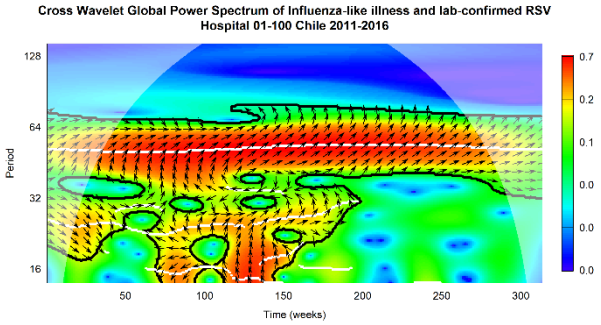


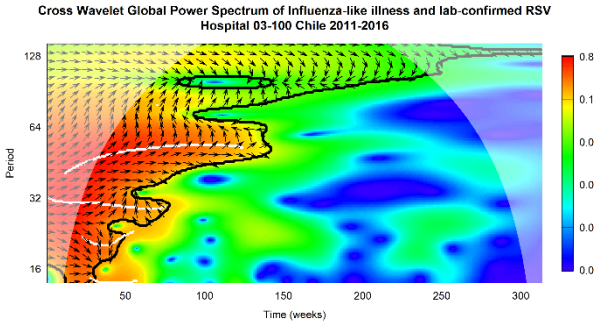


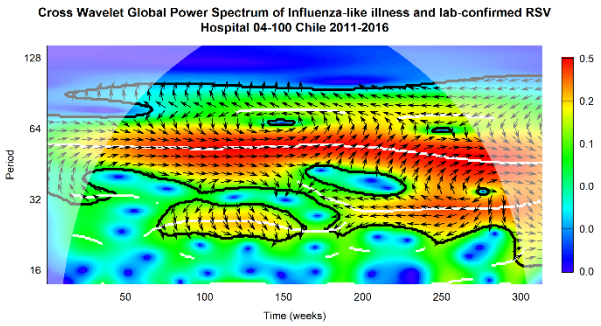


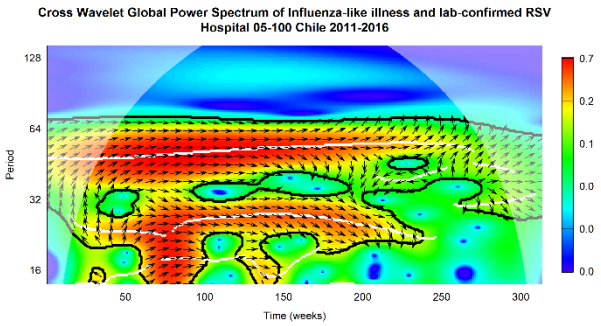


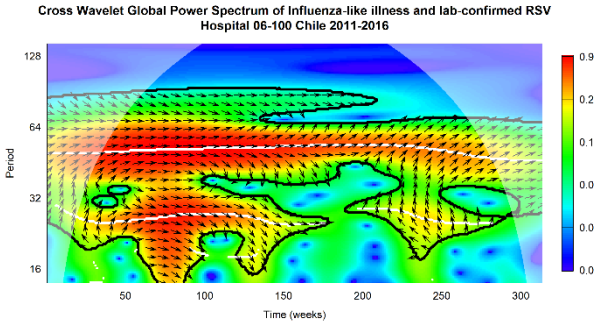


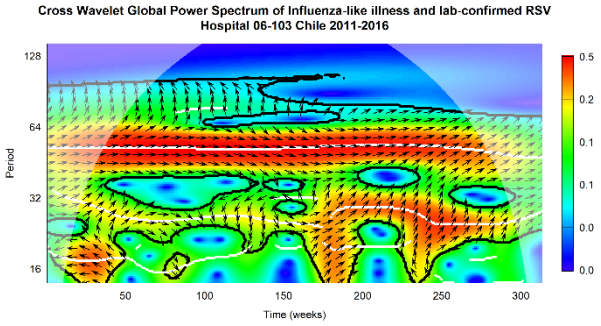


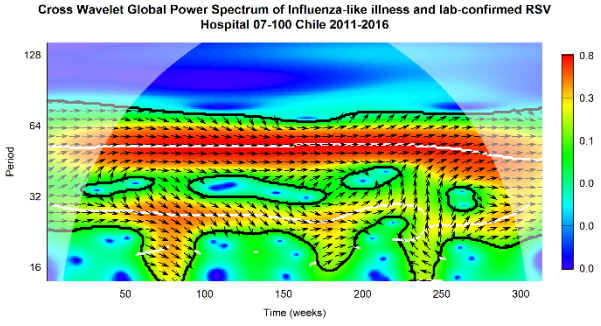


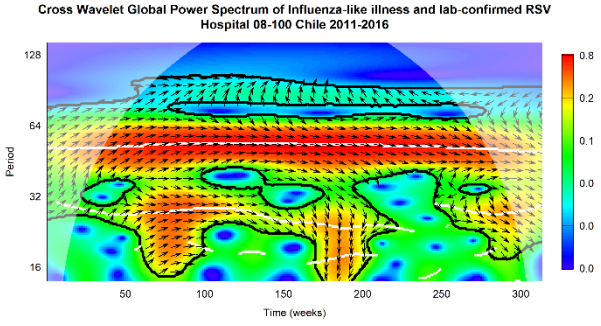

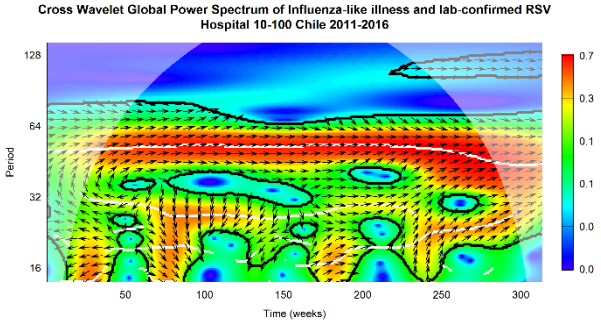
Cross Wavelet Global Power Spectrum of Influenza-like illness and lab-confirmed RSV
Hospital 10-100 Chile 2011-2016
Period
Time (weeks)

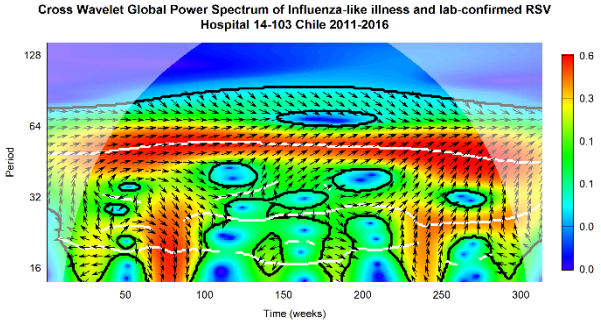
Cross Wavelet Global Power Spectrum of Influenza-like illness and lab-confirmed RSV
Hospital 14-103 Chile 2011-2016
Period
Time (weeks)

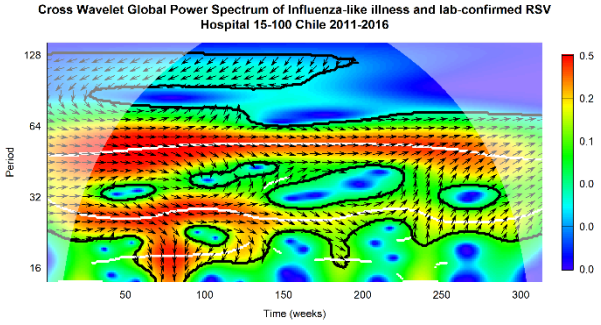
Cross Wavelet Global Power Spectrum of Influenza-like illness and lab-confirmed RSV
Hospital 15-100 Chile 2011-2016
Period
Time (weeks)

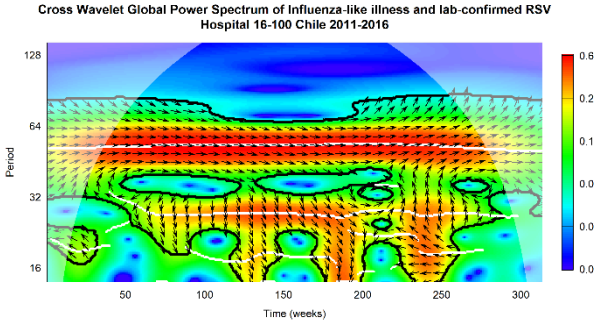
Cross Wavelet Global Power Spectrum of Influenza-like illness and lab-confirmed RSV
Hospital 16-100 Chile 2011-2016
Period
Time (weeks)

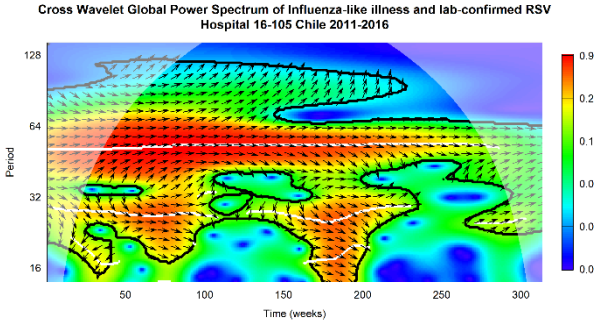
Cross Wavelet Global Power Spectrum of Influenza-like illness and lab-confirmed RSV
Hospital 16-105 Chile 2011-2016
Period
Time (weeks)

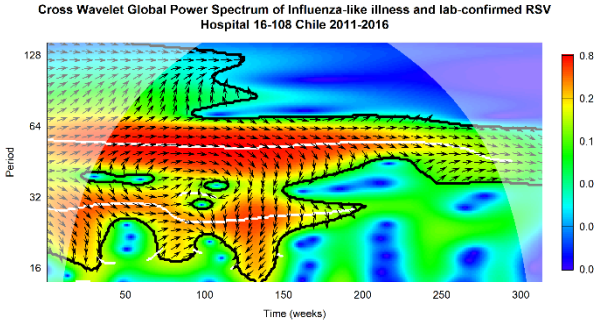
Cross Wavelet Global Power Spectrum of Influenza-like illness and lab-confirmed RSV
Hospital 16-108 Chile 2011-2016
Period
Time (weeks)

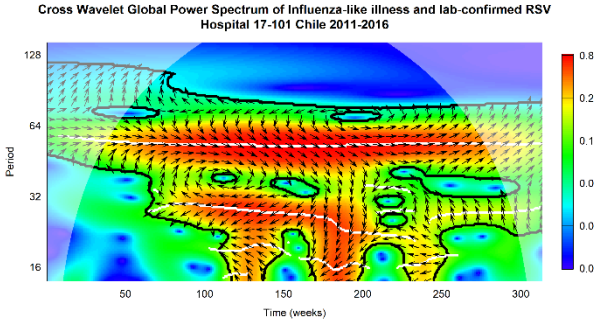
Cross Wavelet Global Power Spectrum of Influenza-like illness and lab-confirmed RSV
Hospital 17-101 Chile 2011-2016
Period
Time (weeks)

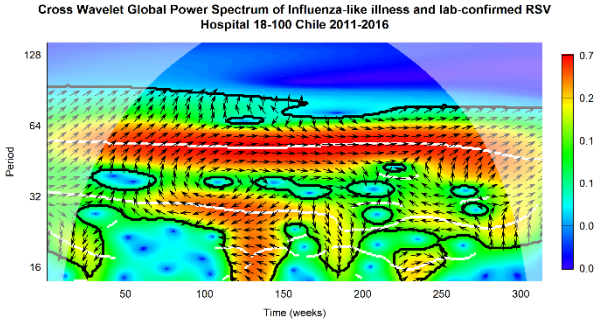
Cross Wavelet Global Power Spectrum of Influenza-like illness and lab-confirmed RSV
Hospital 18-100 Chile 2011-2016
Period
Time (weeks)

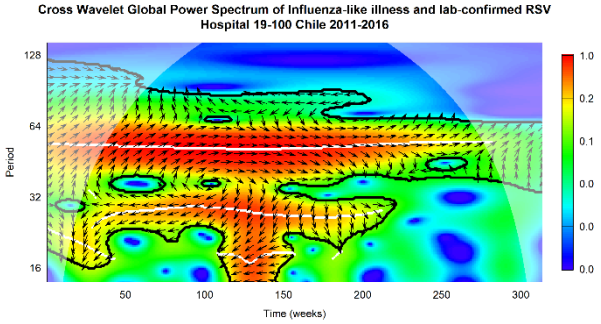
Cross Wavelet Global Power Spectrum of Influenza-like illness and lab-confirmed RSV
Hospital 19-100 Chile 2011-2016
Period
Time (weeks)

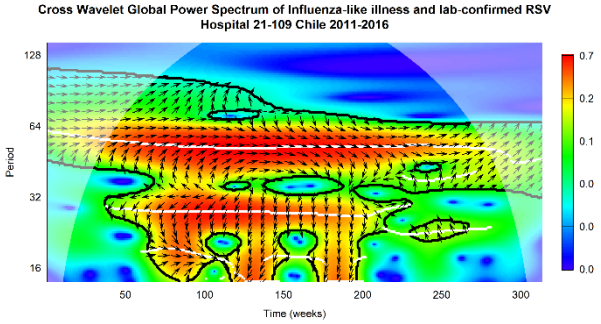
Cross Wavelet Global Power Spectrum of Influenza-like illness and lab-confirmed RSV
Hospital 21-109 Chile 2011-2016
Period
Time (weeks)

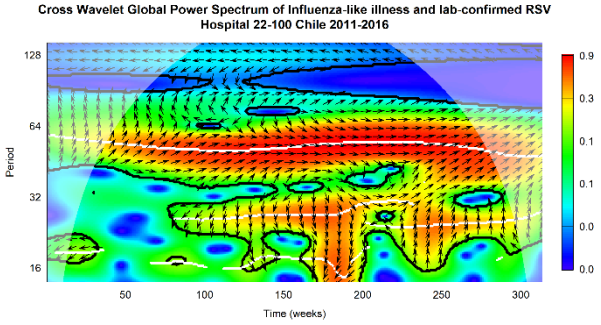
Cross Wavelet Global Power Spectrum of Influenza-like illness and lab-confirmed RSV
Hospital 22-100 Chile 2011-2016
Period
Time (weeks)

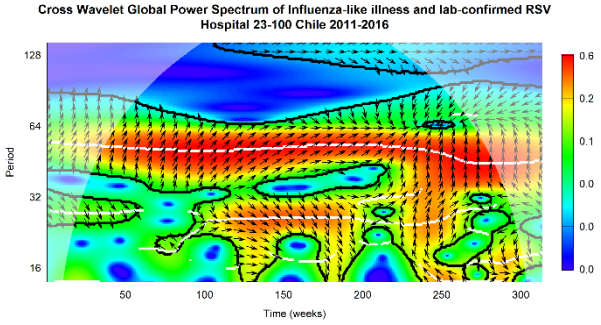
Cross Wavelet Global Power Spectrum of Influenza-like illness and lab-confirmed RSV
Hospital 23-100 Chile 2011-2016
Period
Time (weeks)

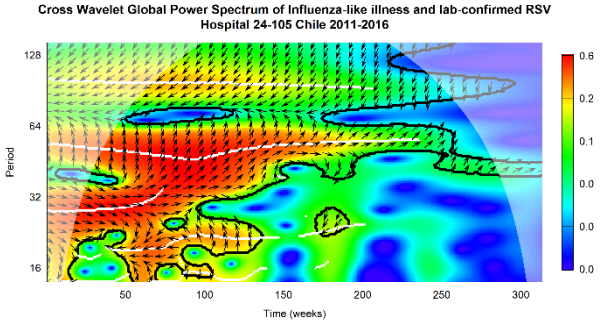
Cross Wavelet Global Power Spectrum of Influenza-like illness and lab-confirmed RSV
Hospital 24-105 Chile 2011-2016
Period
Time (weeks)

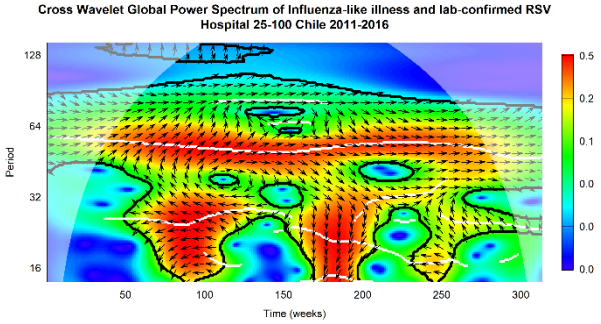
Cross Wavelet Global Power Spectrum of Influenza-like illness and lab-confirmed RSV
Hospital 25-100 Chile 2011-2016
Period
Time (weeks)

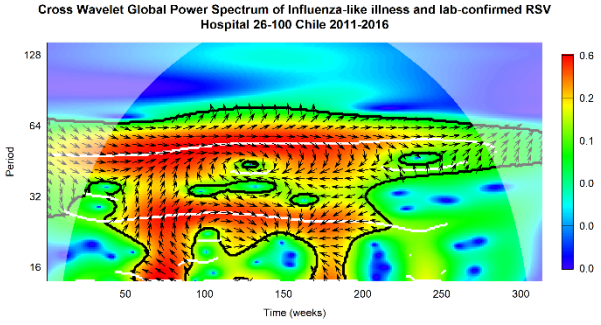
Cross Wavelet Global Power Spectrum of Influenza-like illness and lab-confirmed RSV
Hospital 26-100 Chile 2011-2016
Period
Time (weeks)

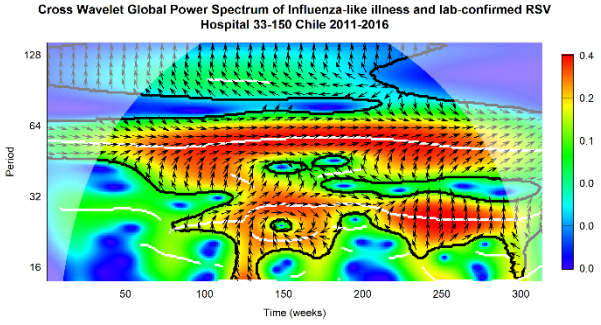
Cross Wavelet Global Power Spectrum of Influenza-like illness and lab-confirmed RSV
Hospital 33-150 Chile 2011-2016
Period
Time (weeks)

## 5. Cross wavelet power spectrum for ILI versus laboratory-confirmed parainfluenza by hospital

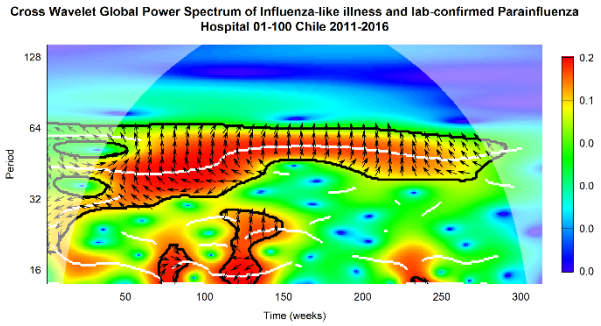


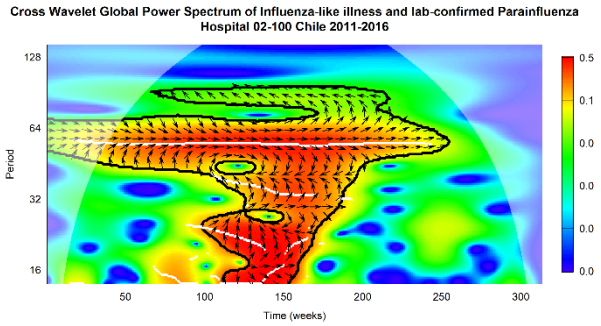


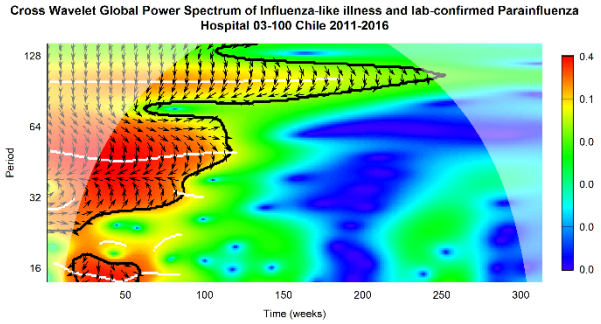


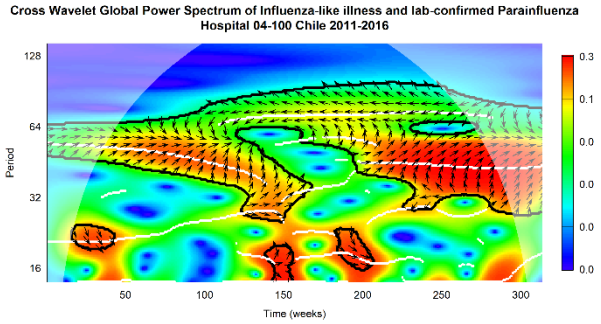


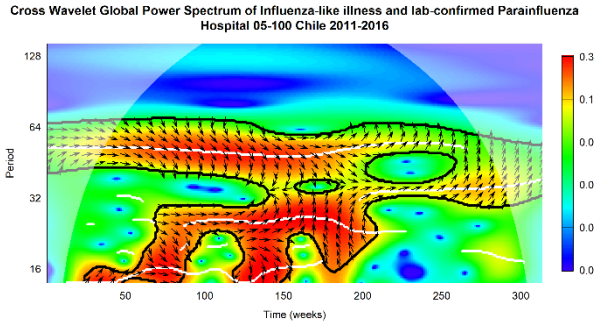


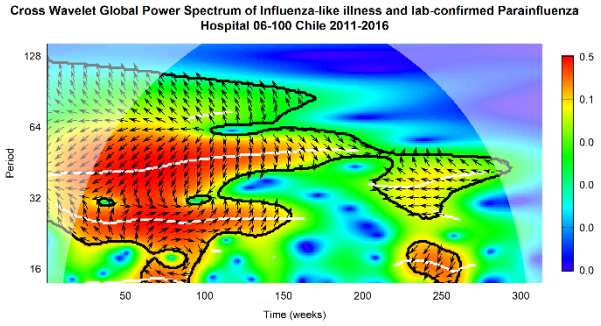


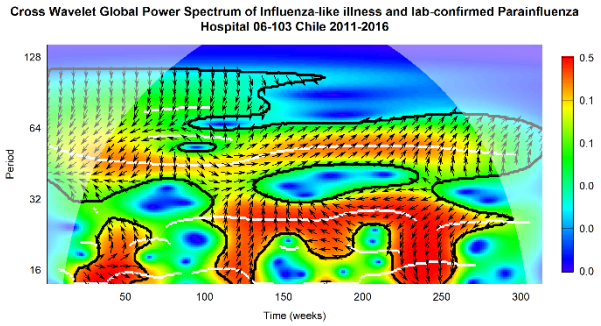


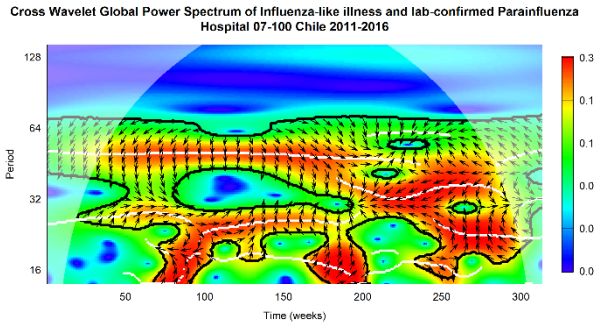

Cross Wavelet Global Power Spectrum of Influenza-like illness and lab-confirmed Parainfluenza Hospital 08-100 Chile 2011-2016

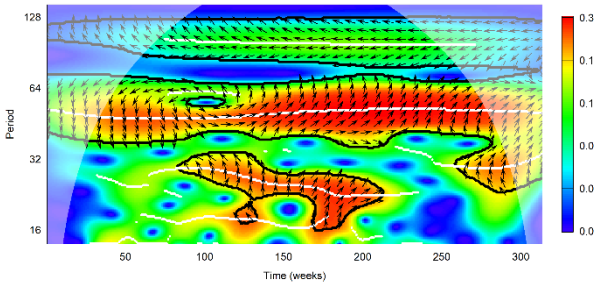


Cross Wavelet Global Power Spectrum of Influenza-like illness and lab-confirmed Parainfluenza Hospital 10-100 Chile 2011-2016

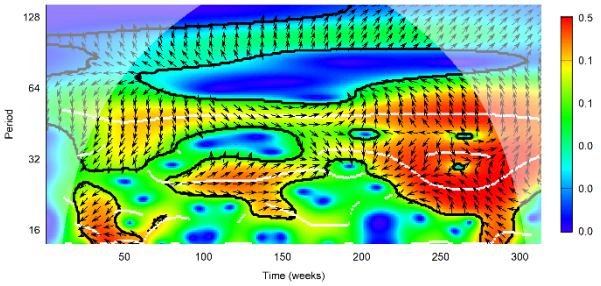


Cross Wavelet Global Power Spectrum of Influenza-like illness and lab-confirmed Parainfluenza Hospital 14-103 Chile 2011-2016

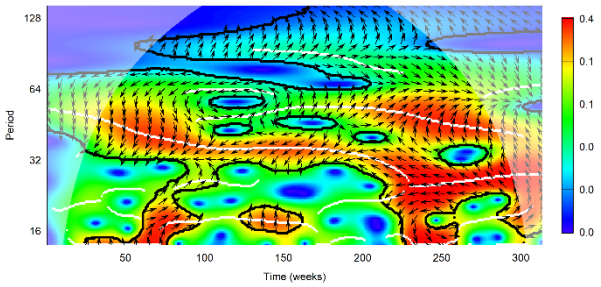


Cross Wavelet Global Power Spectrum of Influenza-like illness and lab-confirmed Parainfluenza Hospital 15-100 Chile 2011-2016

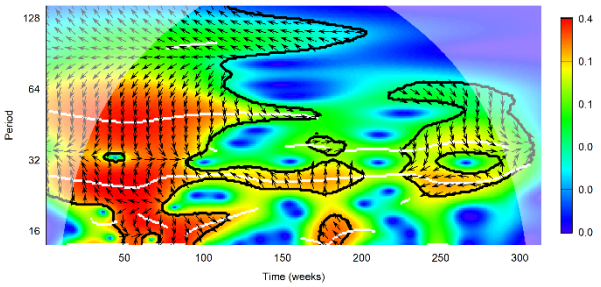


Cross Wavelet Global Power Spectrum of Influenza-like illness and lab-confirmed Parainfluenza Hospital 16-100 Chile 2011-2016

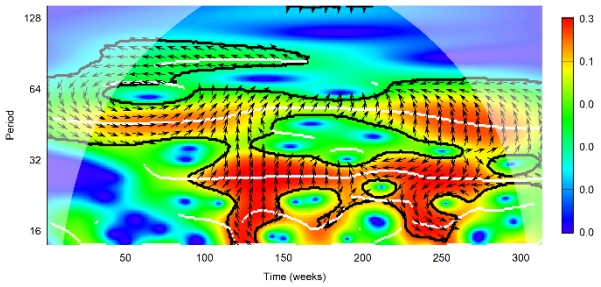


Cross Wavelet Global Power Spectrum of Influenza-like illness and lab-confirmed Parainfluenza Hospital 16-105 Chile 2011-2016

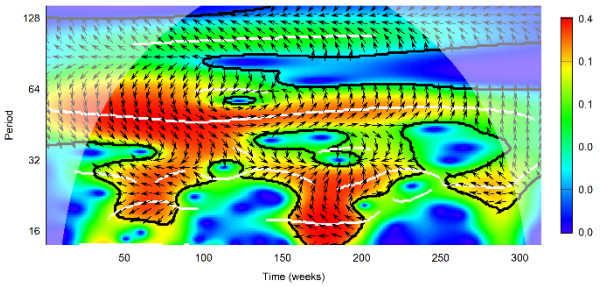


Cross Wavelet Global Power Spectrum of Influenza-like illness and lab-confirmed Parainfluenza Hospital 16-108 Chile 2011-2016

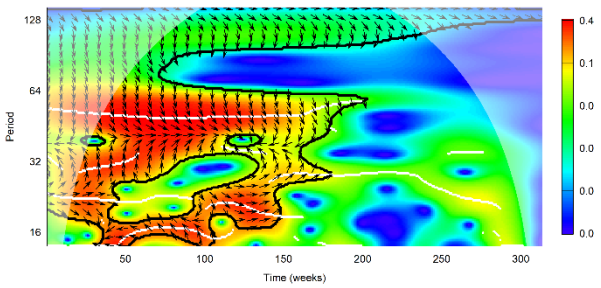


Cross Wavelet Global Power Spectrum of Influenza-like illness and lab-confirmed Parainfluenza Hospital 17-101 Chile 2011-2016

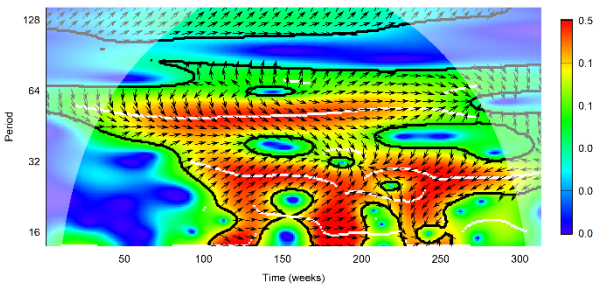

Cross Wavelet Global Power Spectrum of Influenza-like illness and lab-confirmed Parainfluenza
Hospital 18-100 Chile 2011-2016

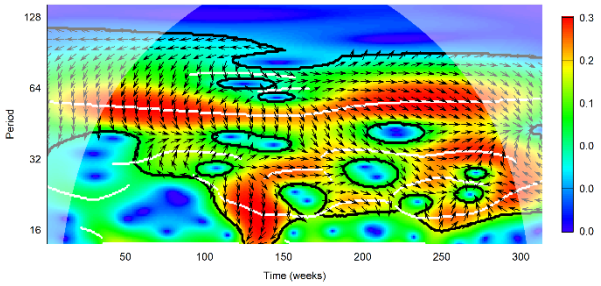


Cross Wavelet Global Power Spectrum of Influenza-like illness and lab-confirmed Parainfluenza
Hospital 19-100 Chile 2011-2016

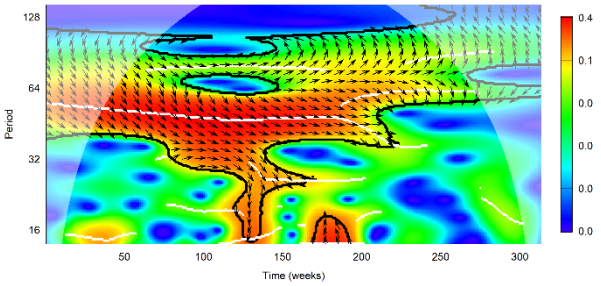


Cross Wavelet Global Power Spectrum of Influenza-like illness and lab-confirmed Parainfluenza
Hospital 21-109 Chile 2011-2016

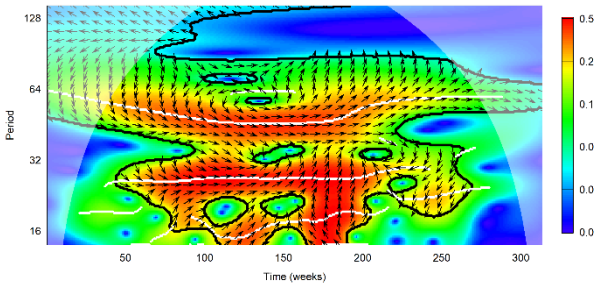


Cross Wavelet Global Power Spectrum of Influenza-like illness and lab-confirmed Parainfluenza
Hospital 22-100 Chile 2011-2016

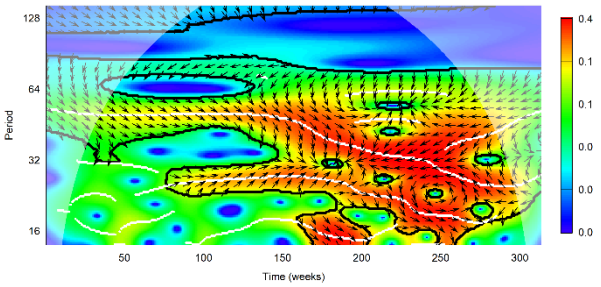


Cross Wavelet Global Power Spectrum of Influenza-like illness and lab-confirmed Parainfluenza
Hospital 23-100 Chile 2011-2016

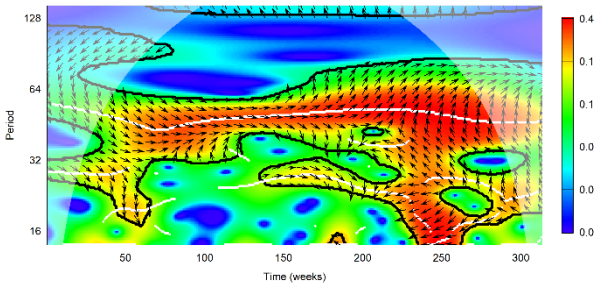


Cross Wavelet Global Power Spectrum of Influenza-like illness and lab-confirmed Parainfluenza
Hospital 24-105 Chile 2011-2016

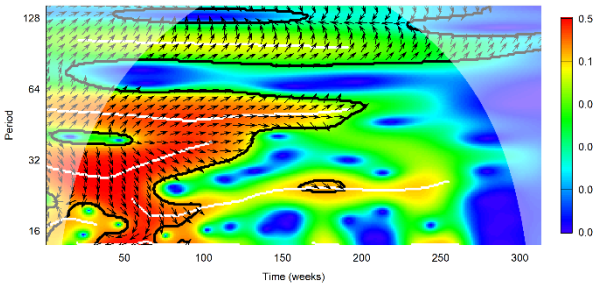


Cross Wavelet Global Power Spectrum of Influenza-like illness and lab-confirmed Parainfluenza
Hospital 25-100 Chile 2011-2016

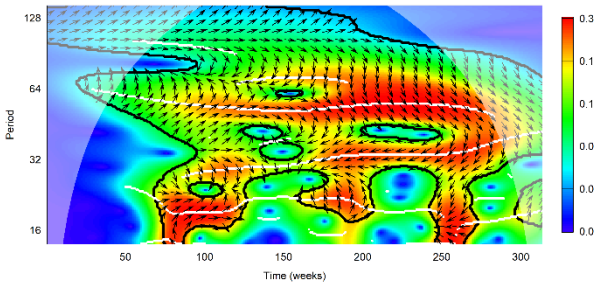


Cross Wavelet Global Power Spectrum of Influenza-like illness and lab-confirmed Parainfluenza
Hospital 26-100 Chile 2011-2016

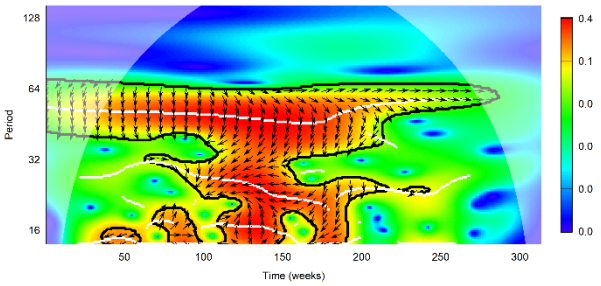

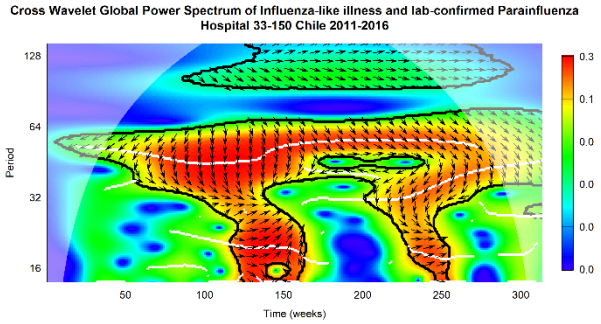


## 6. Cross wavelet power spectrum for ILI versus laboratory-confirmed adenovirus by hospital

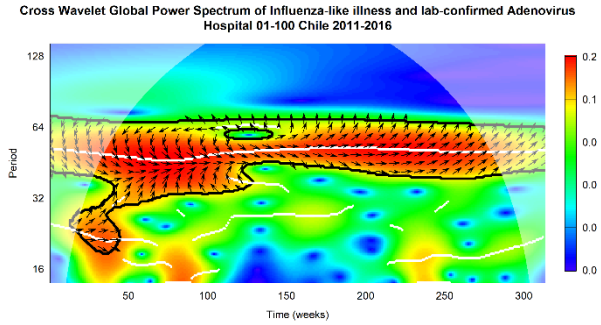


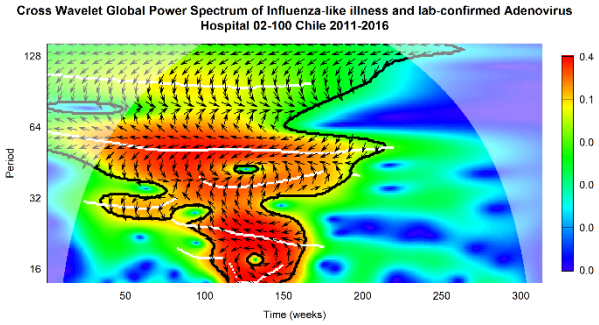


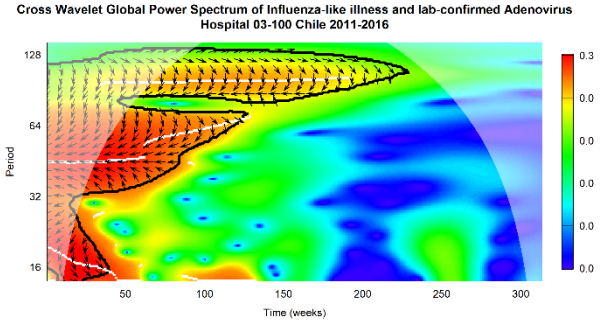


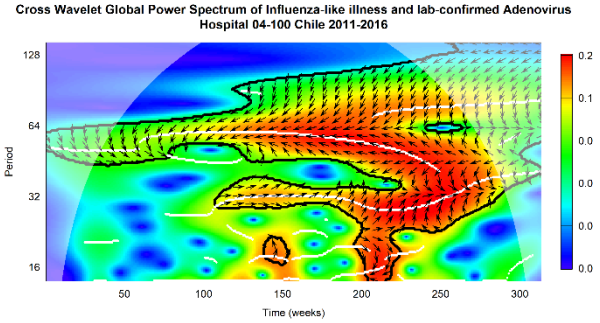


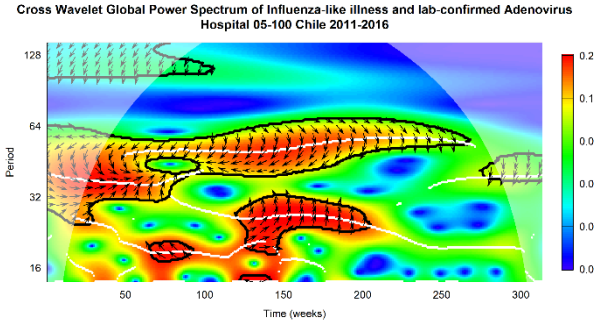


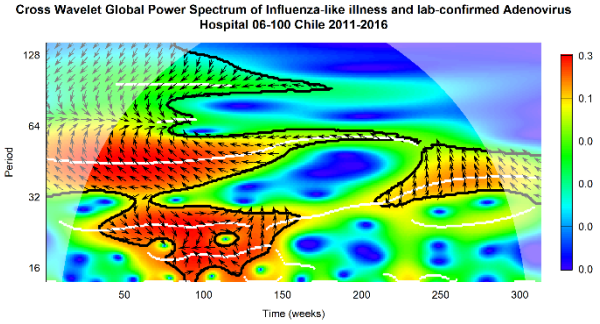

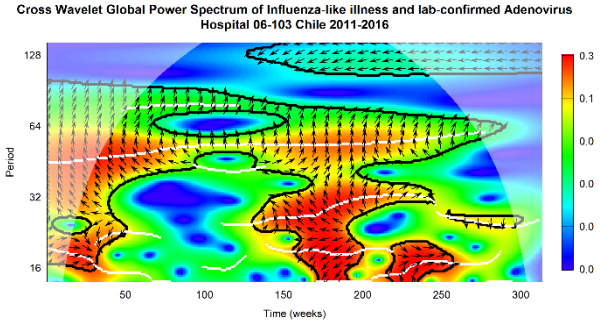
Cross Wavelet Global Power Spectrum of Influenza-like illness and lab-confirmed Adenovirus
Hospital 06-103 Chile 2011-2016
Period
Time (weeks)

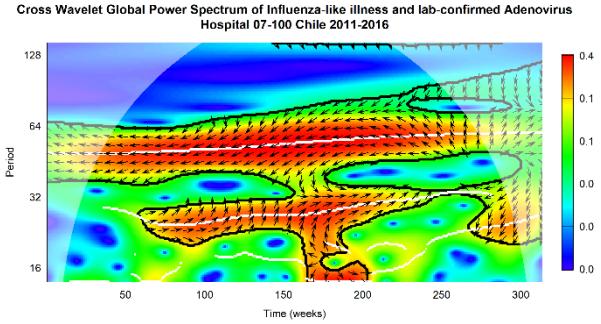
Cross Wavelet Global Power Spectrum of Influenza-like illness and lab-confirmed Adenovirus
Hospital 07-100 Chile 2011-2016
Period
Time (weeks)

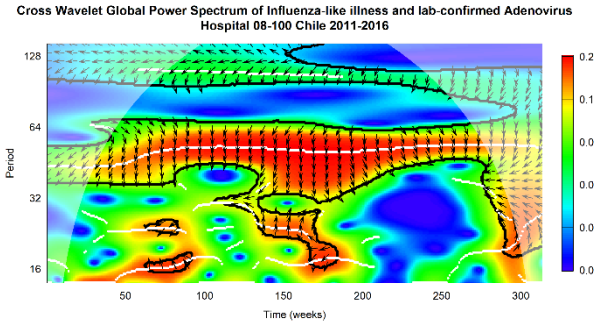
Cross Wavelet Global Power Spectrum of Influenza-like illness and lab-confirmed Adenovirus
Hospital 08-100 Chile 2011-2016
Period
Time (weeks)

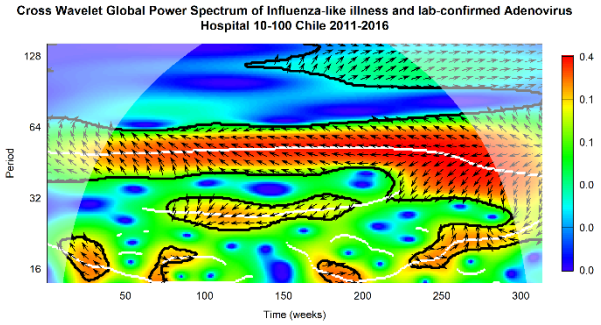
Cross Wavelet Global Power Spectrum of Influenza-like illness and lab-confirmed Adenovirus
Hospital 10-100 Chile 2011-2016
Period
Time (weeks)

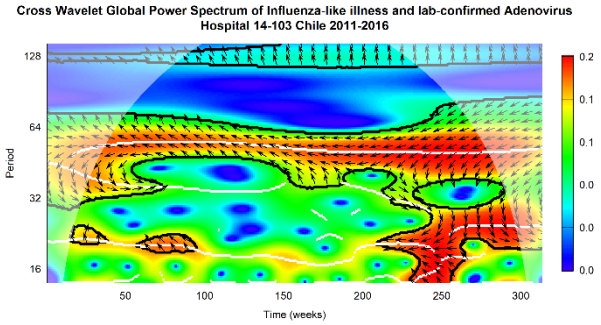
Cross Wavelet Global Power Spectrum of Influenza-like illness and lab-confirmed Adenovirus
Hospital 14-103 Chile 2011-2016
Period
Time (weeks)

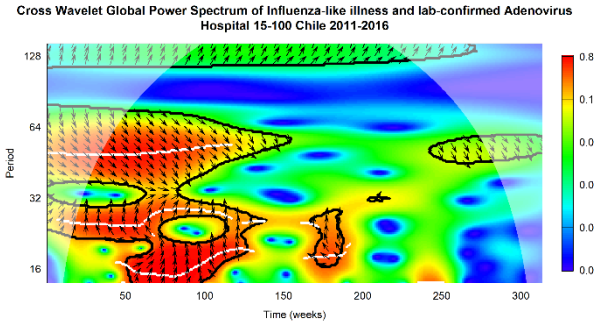
Cross Wavelet Global Power Spectrum of Influenza-like illness and lab-confirmed Adenovirus
Hospital 15-100 Chile 2011-2016
Period
Time (weeks)

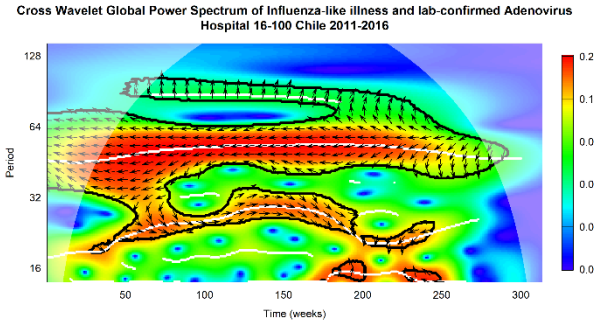
Cross Wavelet Global Power Spectrum of Influenza-like illness and lab-confirmed Adenovirus
Hospital 16-100 Chile 2011-2016
Period
Time (weeks)

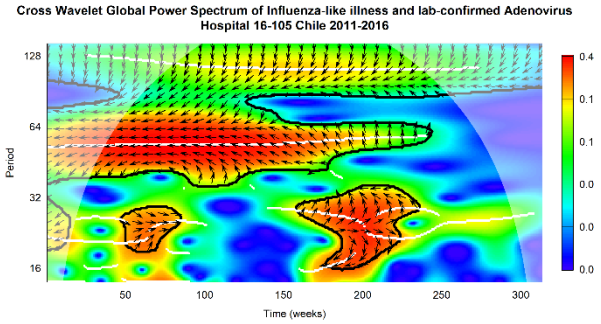
Cross Wavelet Global Power Spectrum of Influenza-like illness and lab-confirmed Adenovirus
Hospital 16-105 Chile 2011-2016
Period
Time (weeks)

Cross Wavelet Global Power Spectrum of Influenza-like illness and lab-confirmed Adenovirus
Hospital 16-108 Chile 2011-2016

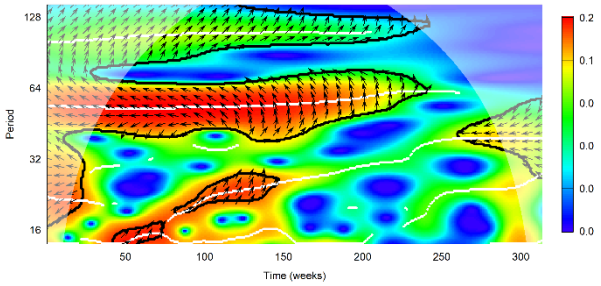


Cross Wavelet Global Power Spectrum of Influenza-like illness and lab-confirmed Adenovirus
Hospital 17-101 Chile 2011-2016

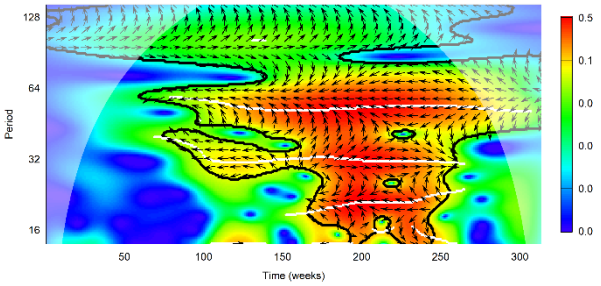


Cross Wavelet Global Power Spectrum of Influenza-like illness and lab-confirmed Adenovirus
Hospital 18-100 Chile 2011-2016

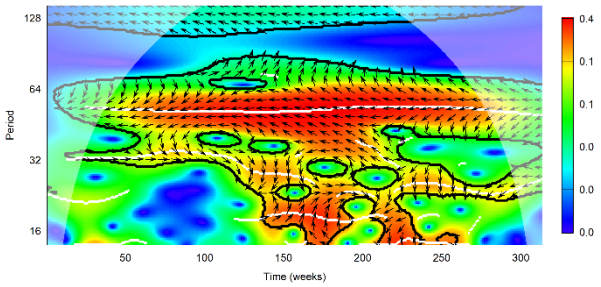


Cross Wavelet Global Power Spectrum of Influenza-like illness and lab-confirmed Adenovirus
Hospital 19-100 Chile 2011-2016

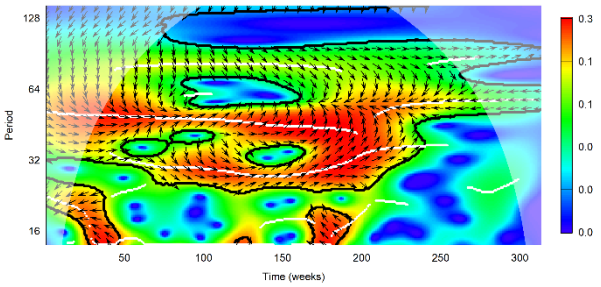


Cross Wavelet Global Power Spectrum of Influenza-like illness and lab-confirmed Adenovirus
Hospital 21-109 Chile 2011-2016

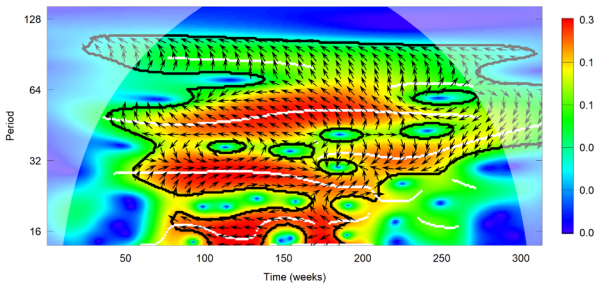


Cross Wavelet Global Power Spectrum of Influenza-like illness and lab-confirmed Adenovirus
Hospital 22-100 Chile 2011-2016

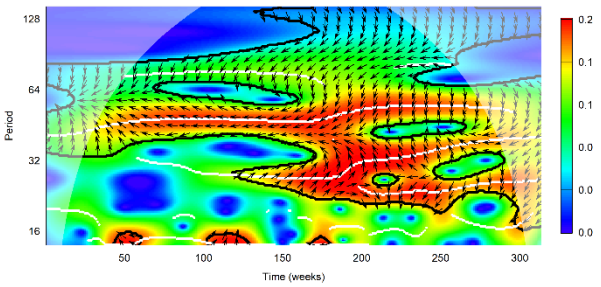


Cross Wavelet Global Power Spectrum of Influenza-like illness and lab-confirmed Adenovirus
Hospital 23-100 Chile 2011-2016

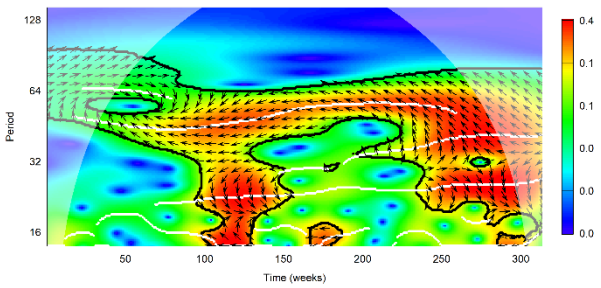


Cross Wavelet Global Power Spectrum of Influenza-like illness and lab-confirmed Adenovirus
Hospital 24-105 Chile 2011-2016

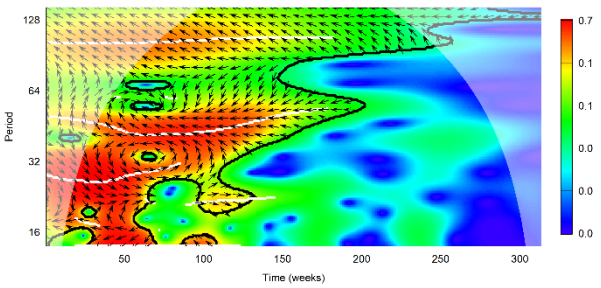

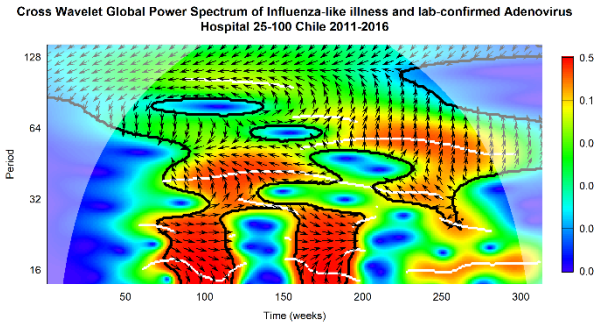


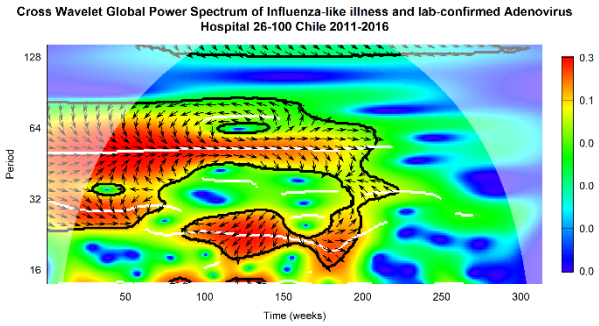


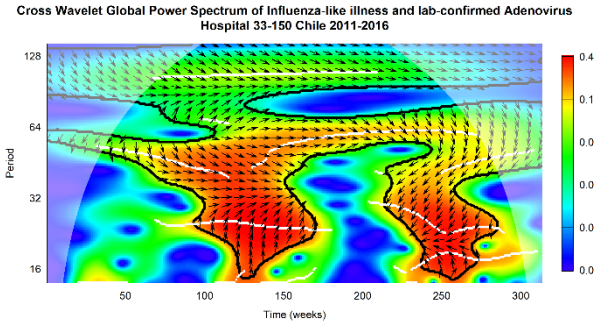


## 7. Cross wavelet power spectrum for ILI versus laboratory-confirmed metapneumovirus by hospital

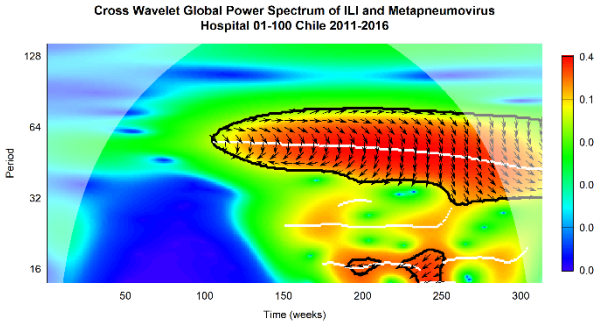


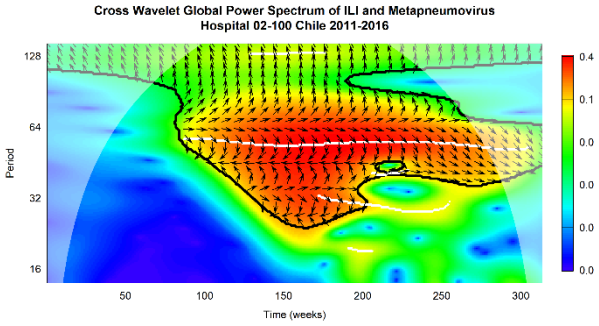


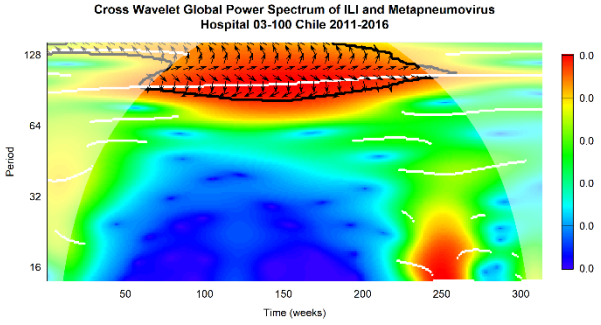


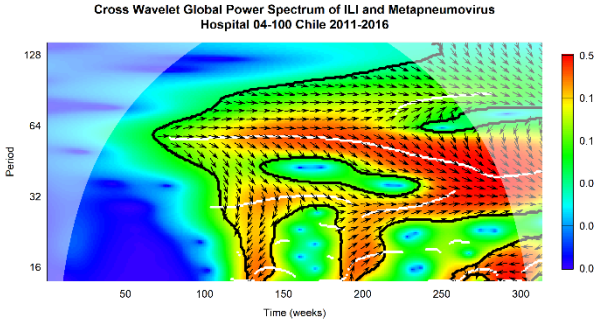

Cross Wavelet Global Power Spectrum of ILI and Metapneumovirus
Hospital 05-100 Chile 2011-2016

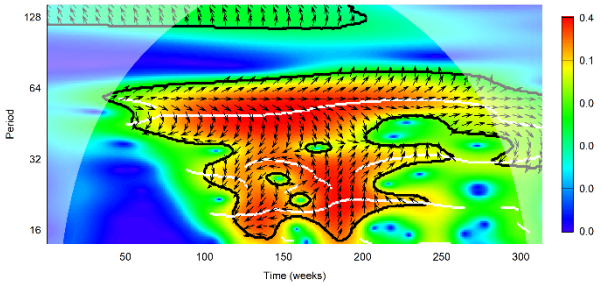


Cross Wavelet Global Power Spectrum of ILI and Metapneumovirus
Hospital 07-100 Chile 2011-2016

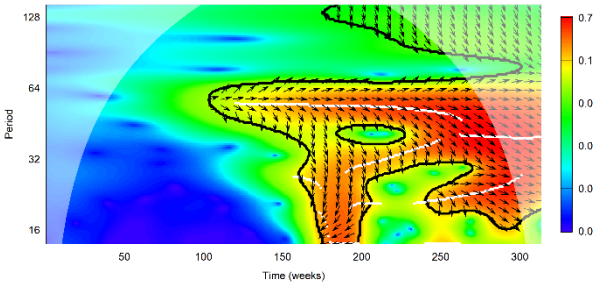


Cross Wavelet Global Power Spectrum of ILI and Metapneumovirus
Hospital 08-100 Chile 2011-2016

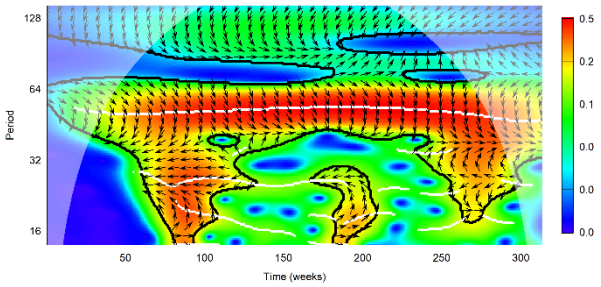


Cross Wavelet Global Power Spectrum of ILI and Metapneumovirus
Hospital 10-100 Chile 2011-2016

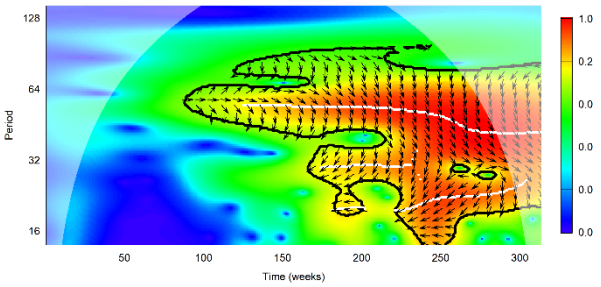


Cross Wavelet Global Power Spectrum of ILI and Metapneumovirus
Hospital 14-103 Chile 2011-2016

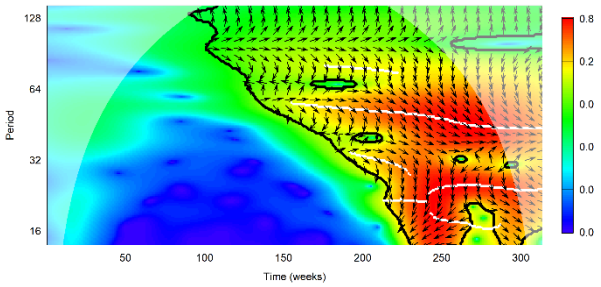


Cross Wavelet Global Power Spectrum of ILI and Metapneumovirus
Hospital 15-100 Chile 2011-2016

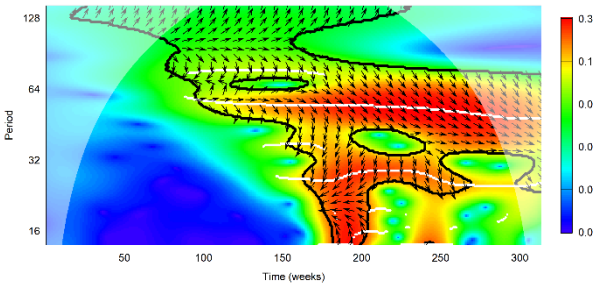


Cross Wavelet Global Power Spectrum of ILI and Metapneumovirus
Hospital 16-100 Chile 2011-2016

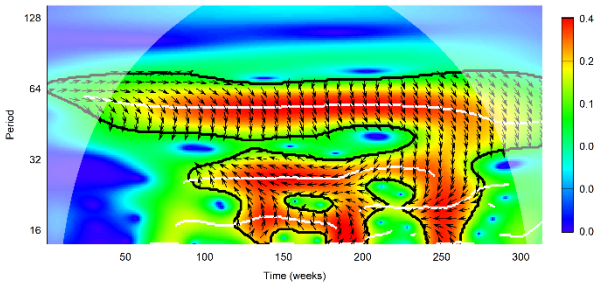


Cross Wavelet Global Power Spectrum of ILI and Metapneumovirus
Hospital 16-105 Chile 2011-2016

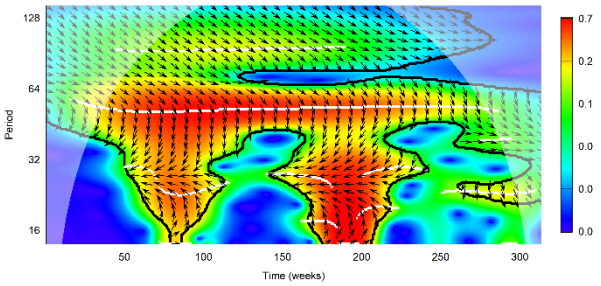

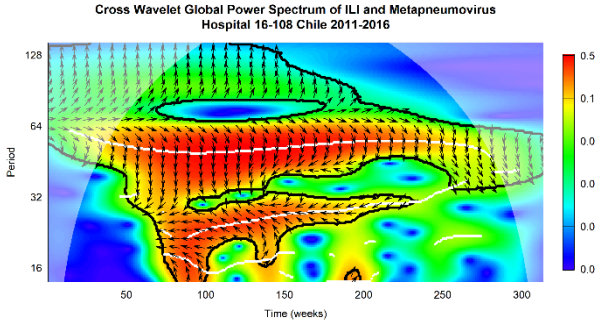
Cross Wavelet Global Power Spectrum of ILI and Metapneumovirus
Hospital 16-108 Chile 2011-2016
Period
Time (weeks)

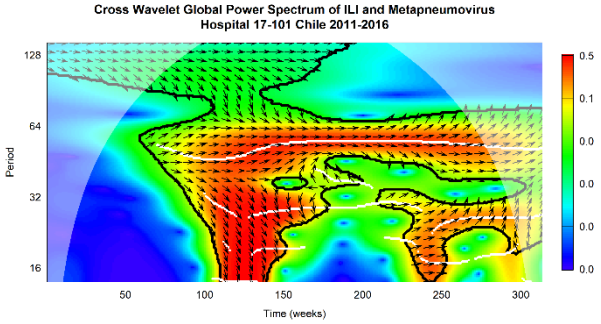
Cross Wavelet Global Power Spectrum of ILI and Metapneumovirus
Hospital 17-101 Chile 2011-2016
Period
Time (weeks)

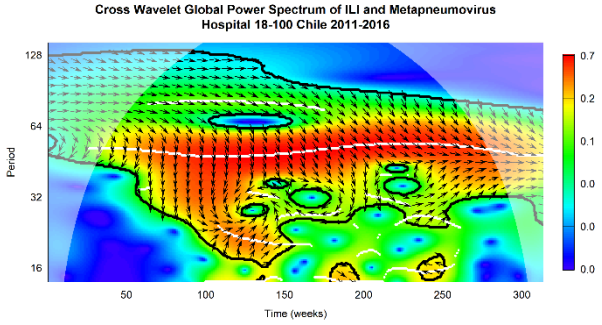
Cross Wavelet Global Power Spectrum of ILI and Metapneumovirus
Hospital 18-100 Chile 2011-2016
Period
Time (weeks)

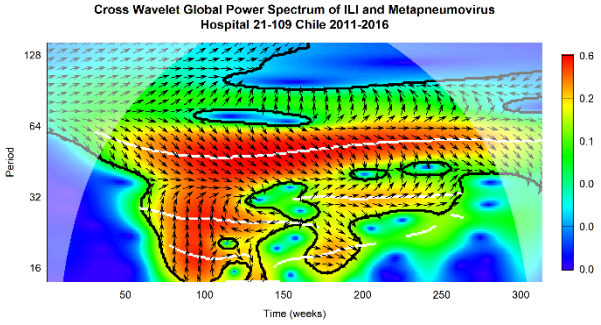
Cross Wavelet Global Power Spectrum of ILI and Metapneumovirus
Hospital 21-109 Chile 2011-2016
Period
Time (weeks)

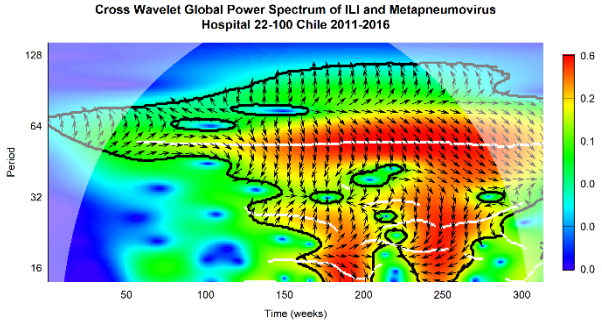
Cross Wavelet Global Power Spectrum of ILI and Metapneumovirus
Hospital 22-100 Chile 2011-2016
Period
Time (weeks)

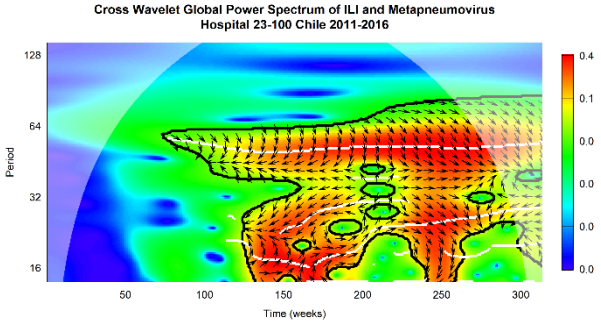
Cross Wavelet Global Power Spectrum of ILI and Metapneumovirus
Hospital 23-100 Chile 2011-2016
Period
Time (weeks)

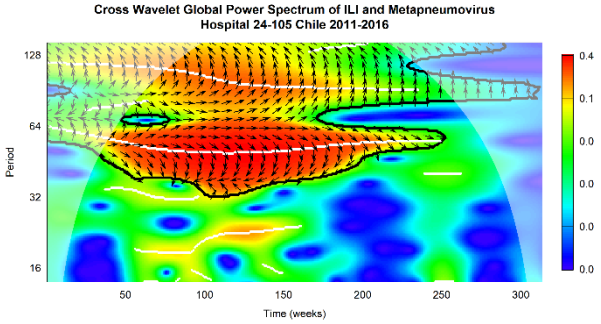
Cross Wavelet Global Power Spectrum of ILI and Metapneumovirus
Hospital 24-105 Chile 2011-2016
Period
128
64
32
16
50
100
150
200
250
300
Time (weeks)
0.4
0.1
0.0
0.0
0.0
0.0

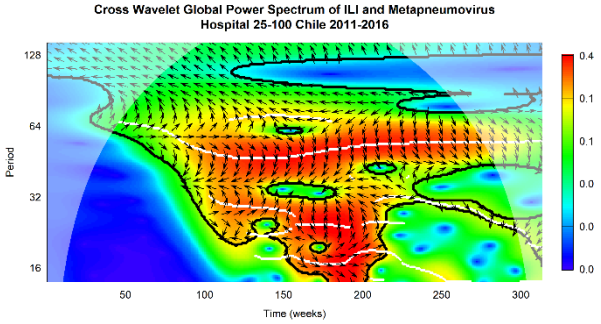
Cross Wavelet Global Power Spectrum of ILI and Metapneumovirus
Hospital 25-100 Chile 2011-2016
Period
128
64
32
16
50
100
150
200
250
300
Time (weeks)
0.4
0.1
0.1
0.0
0.0
0.0

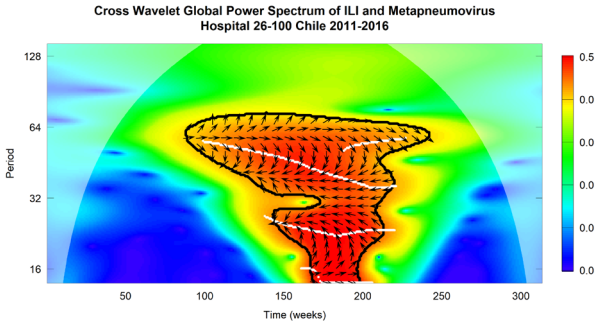
Cross Wavelet Global Power Spectrum of ILI and Metapneumovirus
Hospital 26-100 Chile 2011-2016
Period
128
64
32
16
50
100
150
200
250
300
Time (weeks)
0.5
0.0
0.0
0.0
0.0
0.0

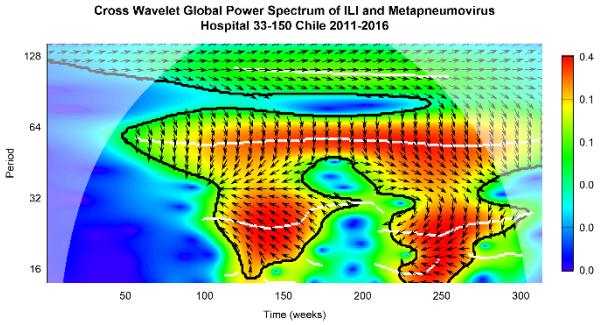
Cross Wavelet Global Power Spectrum of ILI and Metapneumovirus
Hospital 33-150 Chile 2011-2016
Period
128
64
32
16
50
100
150
200
250
300
Time (weeks)
0.4
0.1
0.1
0.0
0.0
0.0

## APPENDIX B: Detrended rate time series, wavelet transformed rates and phases of ILI and viruses by hospital, Chile 2011-2016

### 1. Detrended rate time series, wavelet transformed rates and phases of ILI and influenza A by hospital

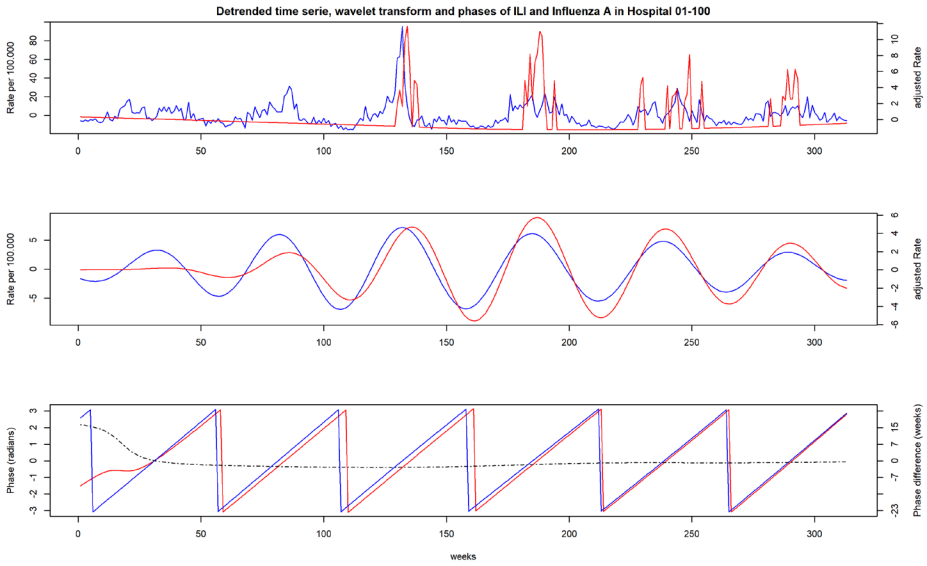


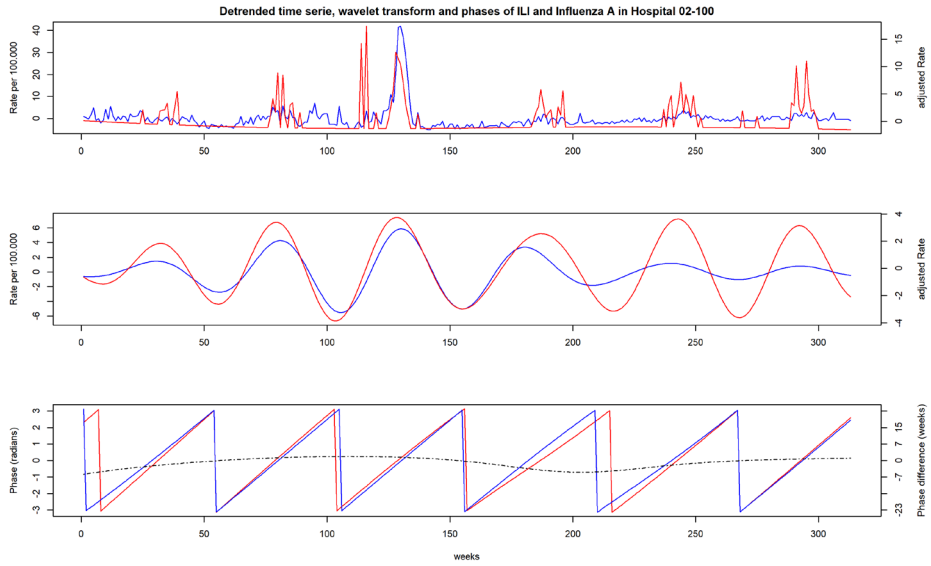

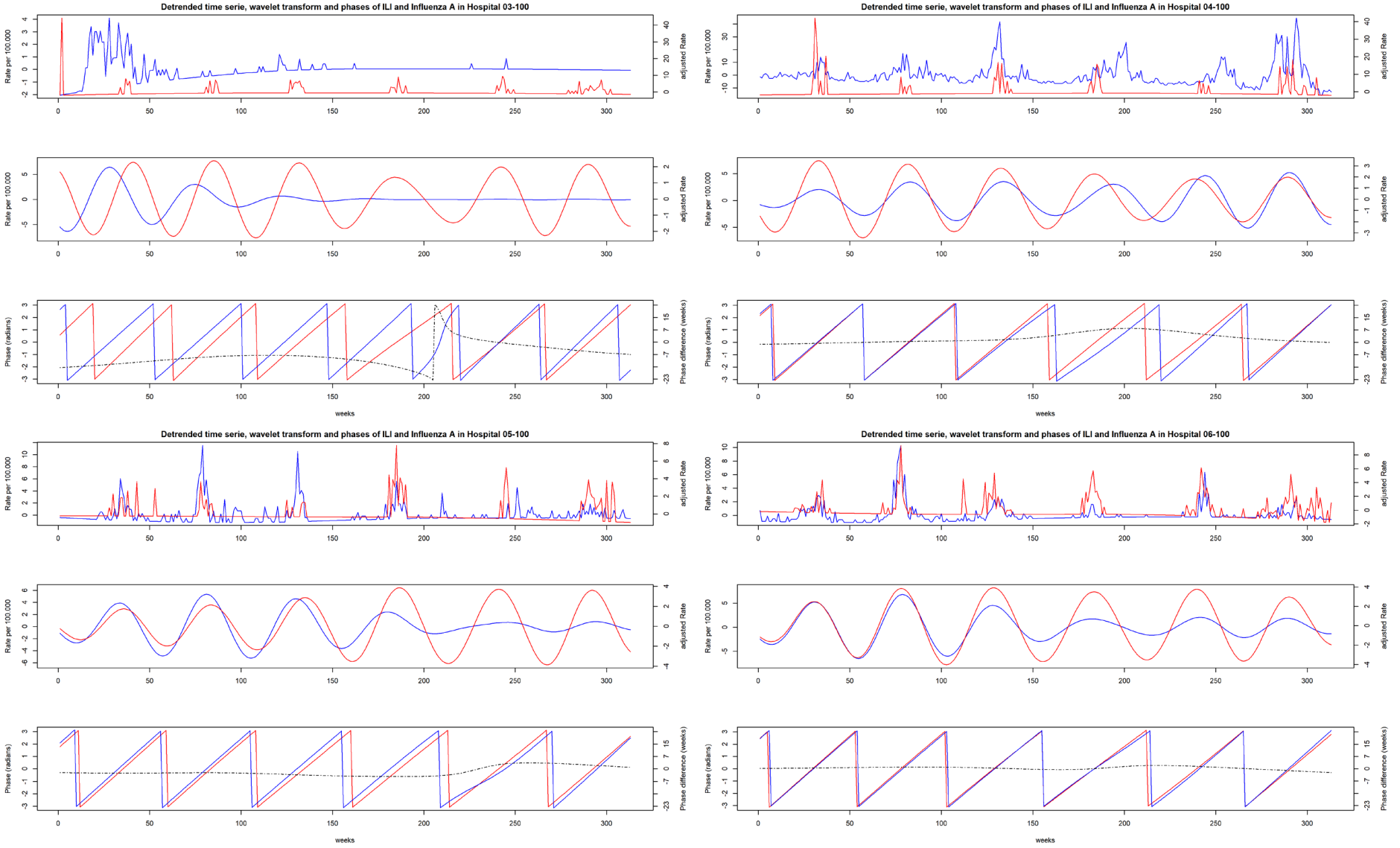
Detrended time serie, wavelet transform and phases of ILI and Influenza A in Hospital 03-100
Rate per 100,000
adjusted Rate
Phase (radians)
Phase difference (weeks)
weeks
Detrended time serie, wavelet transform and phases of ILI and Influenza A in Hospital 04-100
Rate per 100,000
adjusted Rate
Phase (radians)
Phase difference (weeks)
weeks
Detrended time serie, wavelet transform and phases of ILI and Influenza A in Hospital 05-100
Rate per 100,000
adjusted Rate
Phase (radians)
Phase difference (weeks)
weeks
Detrended time serie, wavelet transform and phases of ILI and Influenza A in Hospital 06-100
Rate per 100,000
adjusted Rate
Phase (radians)
Phase difference (weeks)
weeks

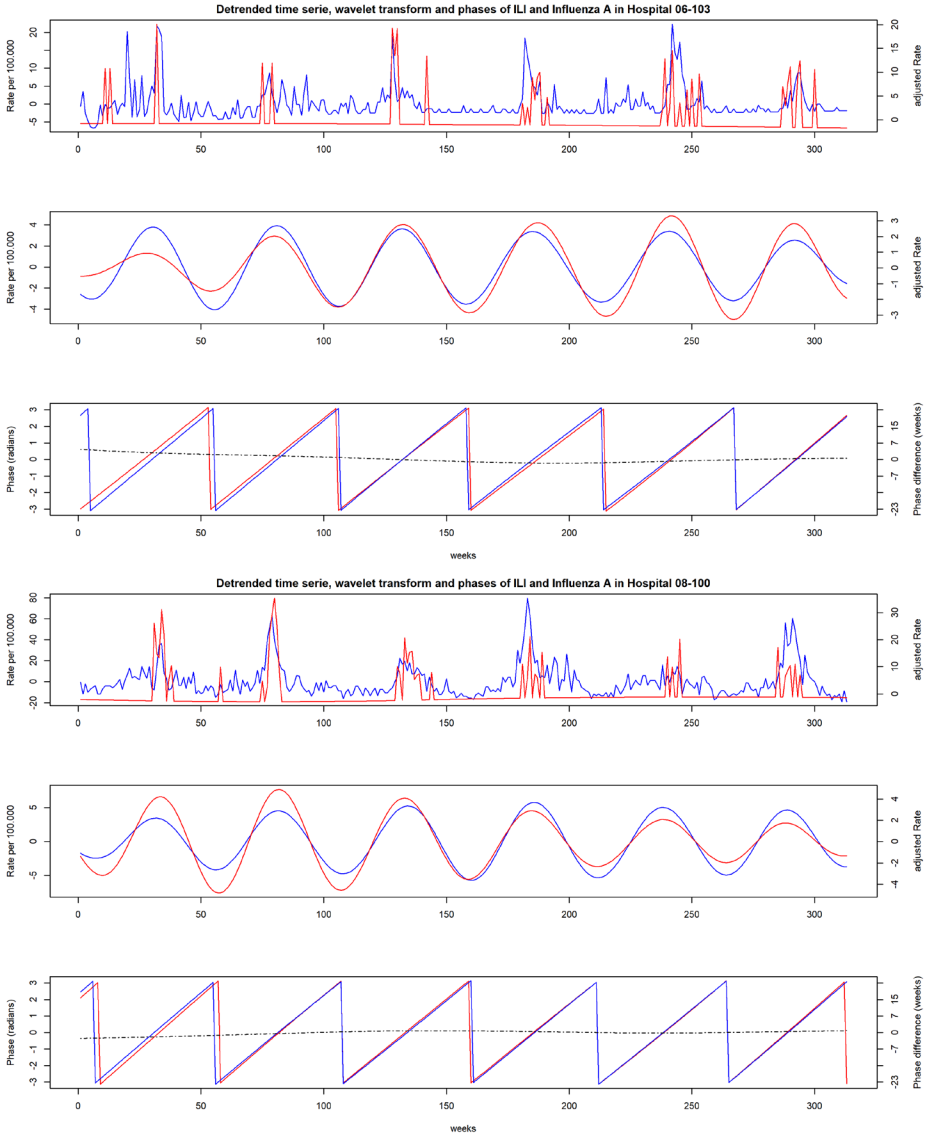
Detrended time serie, wavelet transform and phases of ILI and Influenza A in Hospital 06-103
Rate per 100,000
adjusted Rate
Phase (radians)
Phase difference (weeks)
weeks

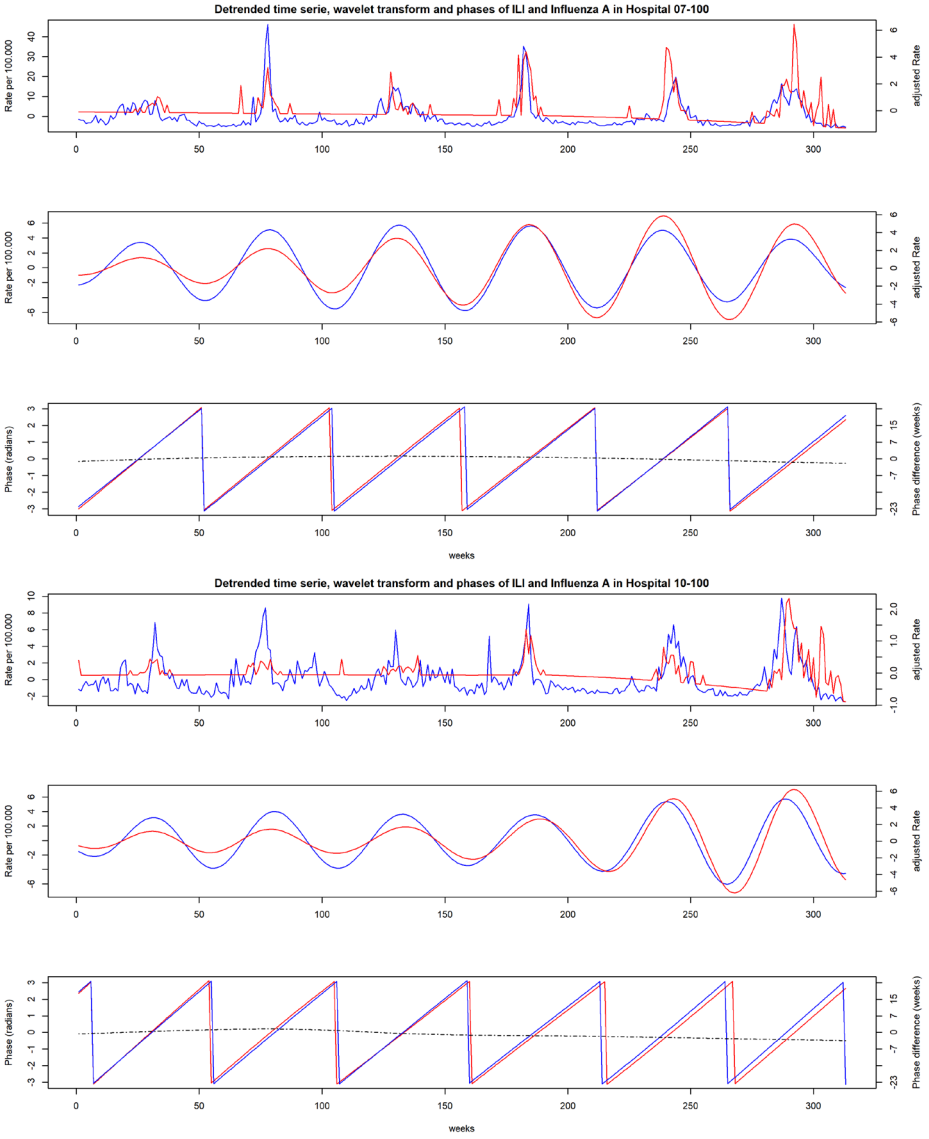
Detrended time serie, wavelet transform and phases of ILI and Influenza A in Hospital 07-100
Rate per 100,000
adjusted Rate
Phase (radians)
Phase difference (weeks)
weeks


Detrended time serie, wavelet transform and phases of ILI and Influenza A in Hospital 08-100
Rate per 100,000
adjusted Rate
Phase (radians)
Phase difference (weeks)
weeks


Detrended time serie, wavelet transform and phases of ILI and Influenza A in Hospital 10-100
Rate per 100,000
adjusted Rate
Phase (radians)
Phase difference (weeks)
weeks

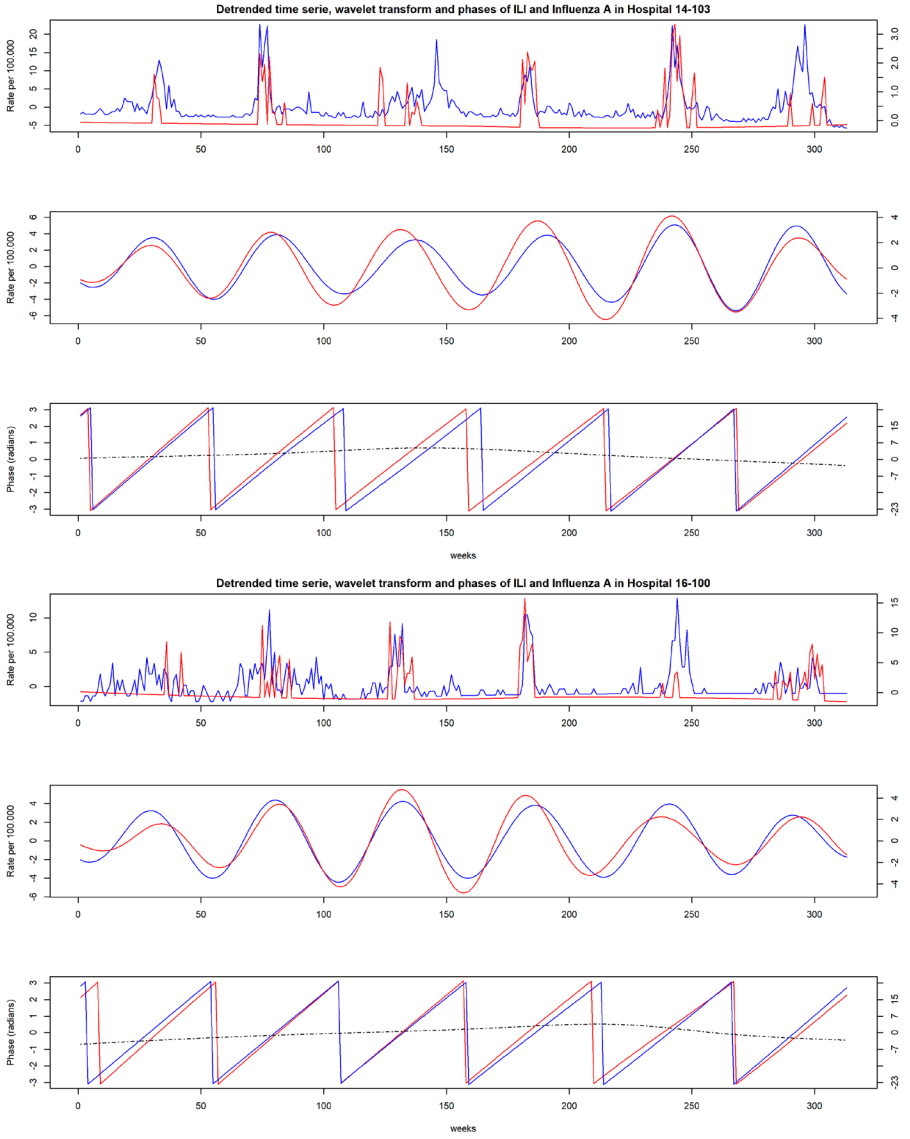
Detrended time serie, wavelet transform and phases of ILI and Influenza A in Hospital 14-103
Rate per 100,000
adjusted Rate
Phase (radians)
Phase difference (weeks)
weeks

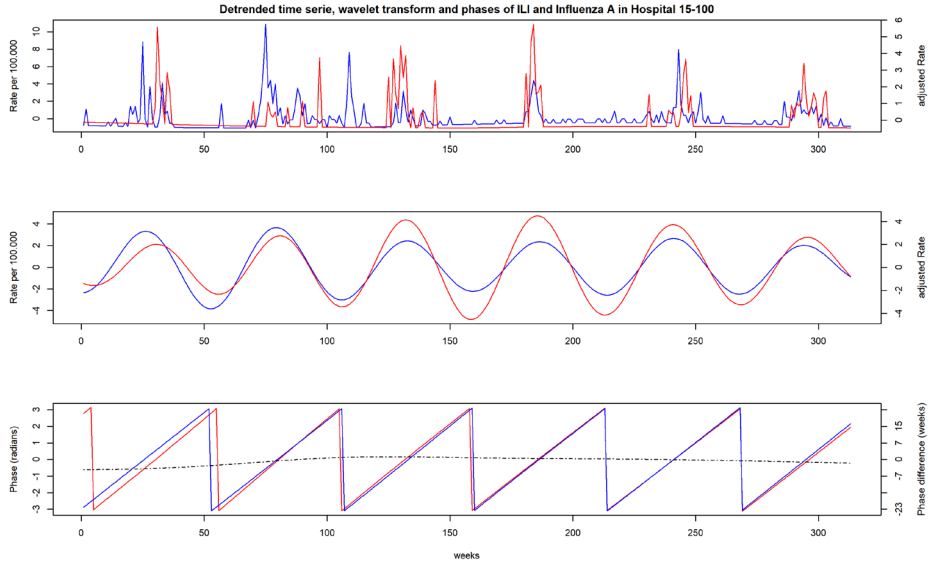
Detrended time serie, wavelet transform and phases of ILI and Influenza A in Hospital 15-100
Rate per 100,000
adjusted Rate
Phase (radians)
Phase difference (weeks)
weeks


Detrended time serie, wavelet transform and phases of ILI and Influenza A in Hospital 16-100
Rate per 100,000
adjusted Rate
Phase (radians)
Phase difference (weeks)
weeks

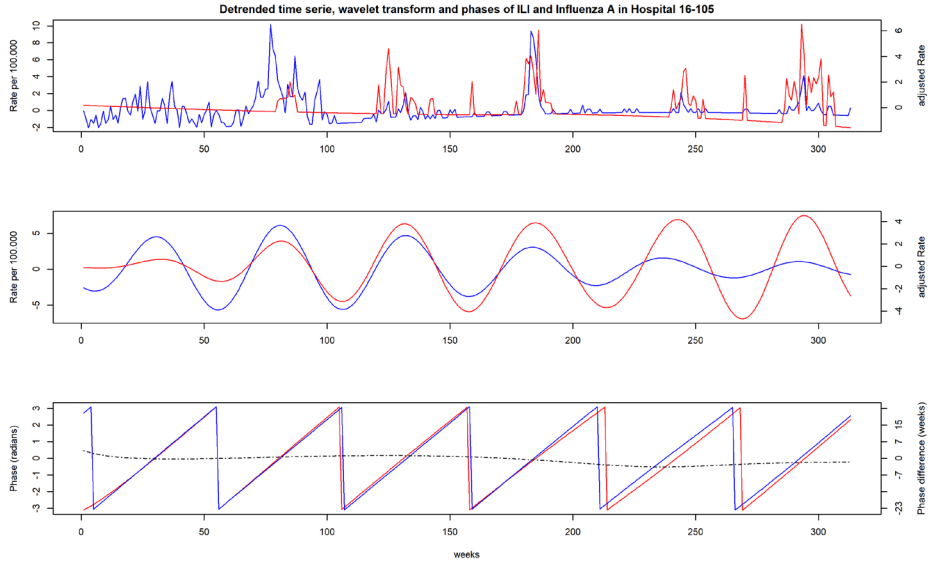
Detrended time serie, wavelet transform and phases of ILI and Influenza A in Hospital 16-105
Rate per 100,000
adjusted Rate
Phase (radians)
Phase difference (weeks)
weeks

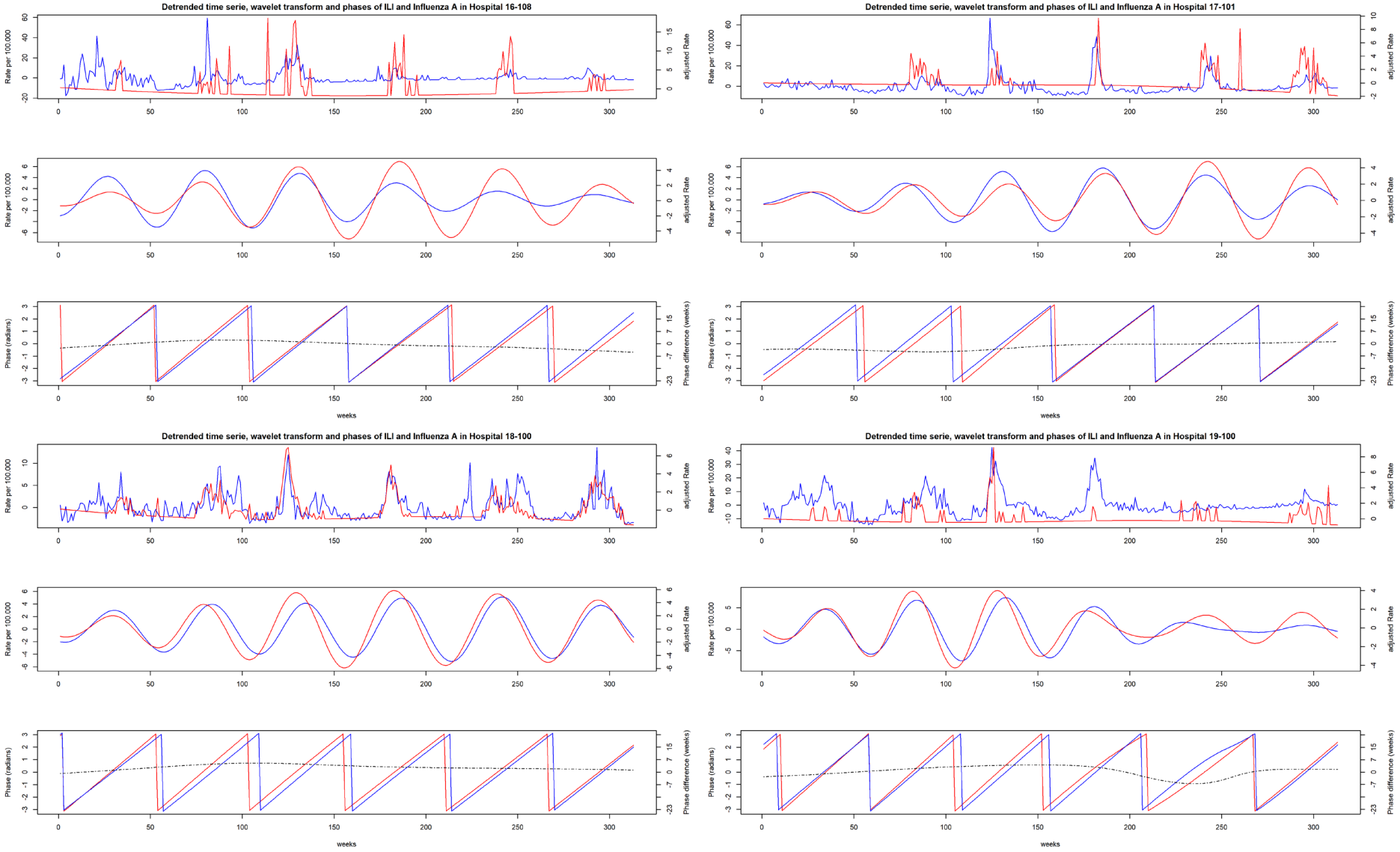
Detrended time serie, wavelet transform and phases of ILI and Influenza A in Hospital 16-108
Detrended time serie, wavelet transform and phases of ILI and Influenza A in Hospital 17-101
Detrended time serie, wavelet transform and phases of ILI and Influenza A in Hospital 18-100
Detrended time serie, wavelet transform and phases of ILI and Influenza A in Hospital 19-100
Rate per 100,000
adjusted Rate
Phase (radians)
Phase difference (weeks)
weeks

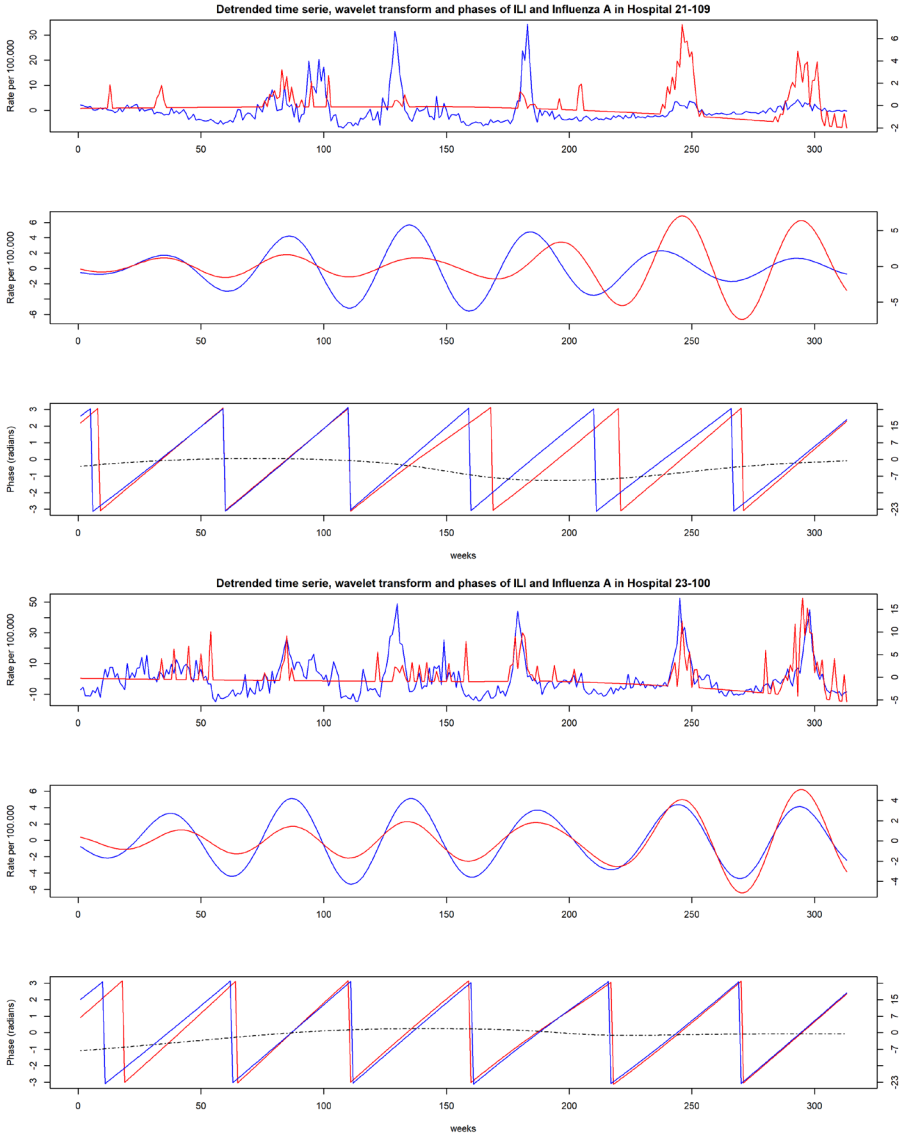
Detrended time serie, wavelet transform and phases of ILI and Influenza A in Hospital 21-109
Rate per 100,000
adjusted Rate
Phase (radians)
Phase difference (weeks)
weeks

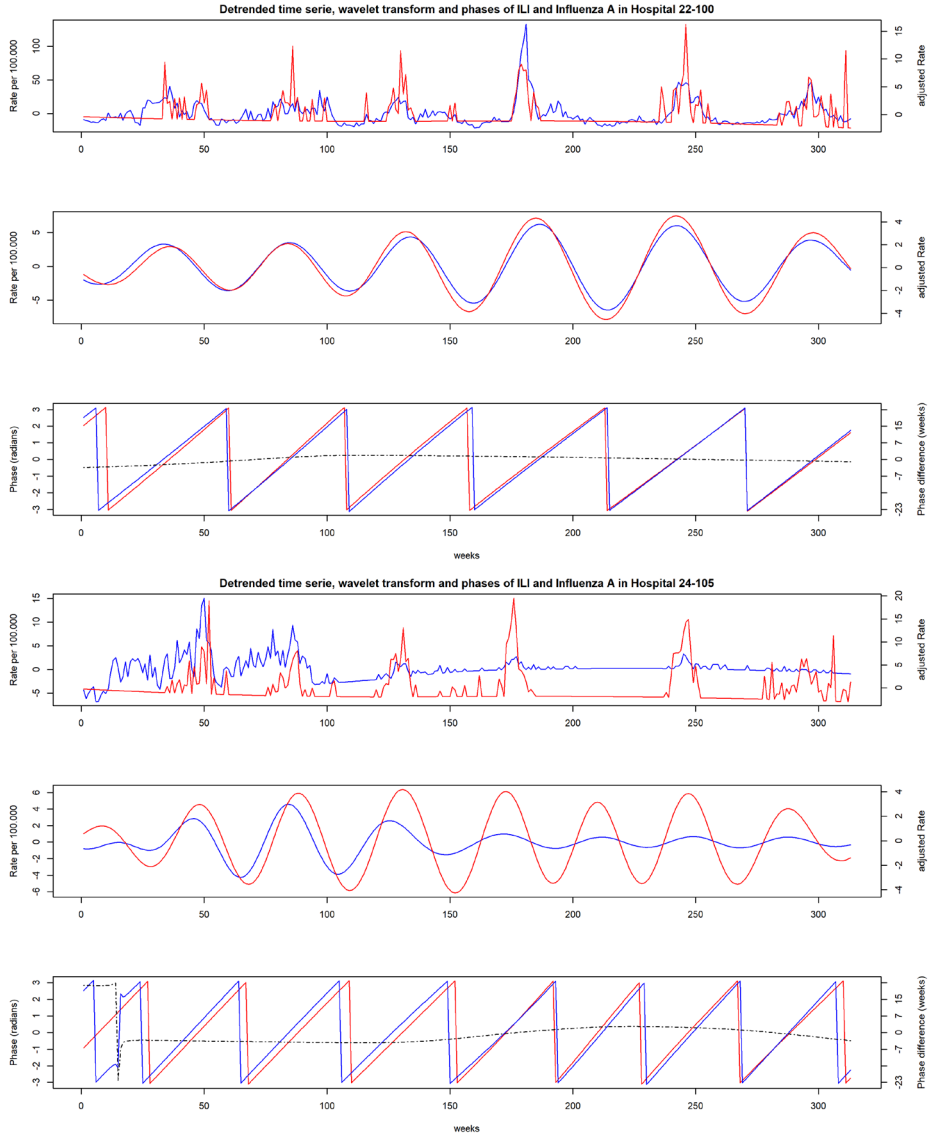
Detrended time serie, wavelet transform and phases of ILI and Influenza A in Hospital 22-100
Rate per 100,000
adjusted Rate
Phase (radians)
Phase difference (weeks)
weeks


Detrended time serie, wavelet transform and phases of ILI and Influenza A in Hospital 23-100
Rate per 100,000
adjusted Rate
Phase (radians)
Phase difference (weeks)
weeks


Detrended time serie, wavelet transform and phases of ILI and Influenza A in Hospital 24-105
Rate per 100,000
adjusted Rate
Phase (radians)
Phase difference (weeks)
weeks

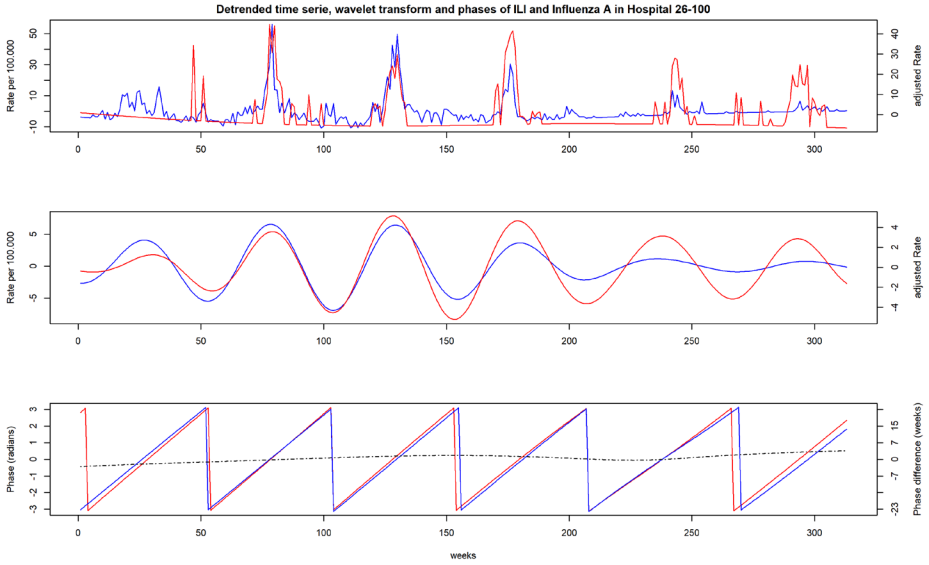
Detrended time serie, wavelet transform and phases of ILI and Influenza A in Hospital 26-100
Rate per 100,000
adjusted Rate
Phase (radians)
Phase difference (weeks)
weeks

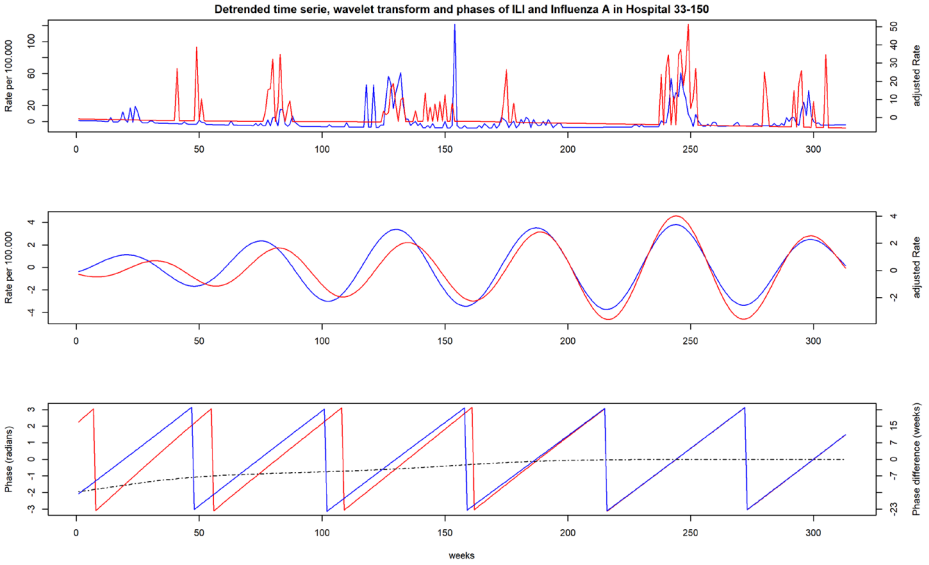
Detrended time serie, wavelet transform and phases of ILI and Influenza A in Hospital 33-150
Rate per 100,000
adjusted Rate
Phase (radians)
Phase difference (weeks)
weeks

## 2. Detrended rate time series, wavelet transformed rates and phases of ILI and influenza B by hospital

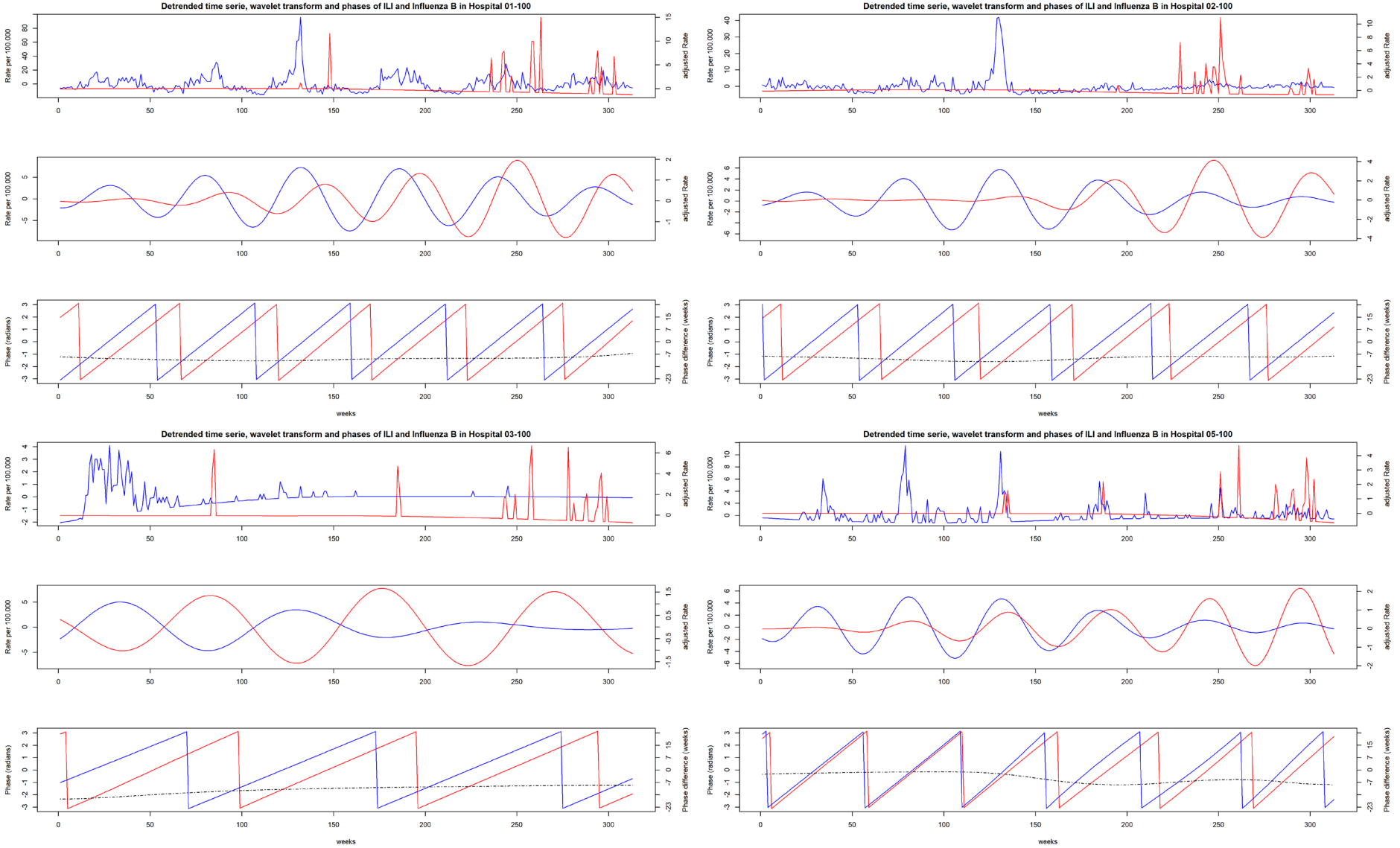

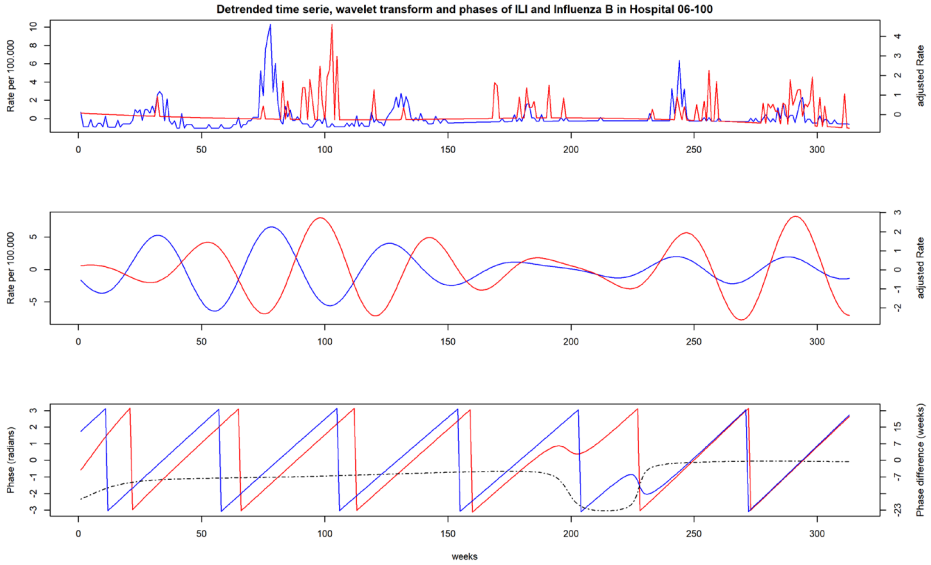
Detrended time serie, wavelet transform and phases of ILI and Influenza B in Hospital 06-100
Rate per 100.000
adjusted Rate
Phase (radians)
Phase difference (weeks)
weeks

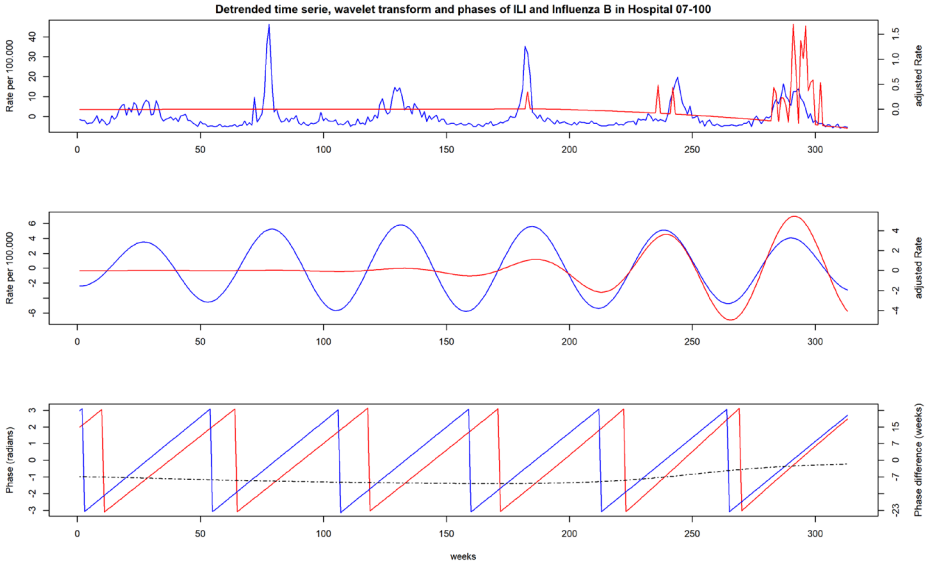
Detrended time serie, wavelet transform and phases of ILI and Influenza B in Hospital 07-100
Rate per 100.000
adjusted Rate
Phase (radians)
Phase difference (weeks)
weeks

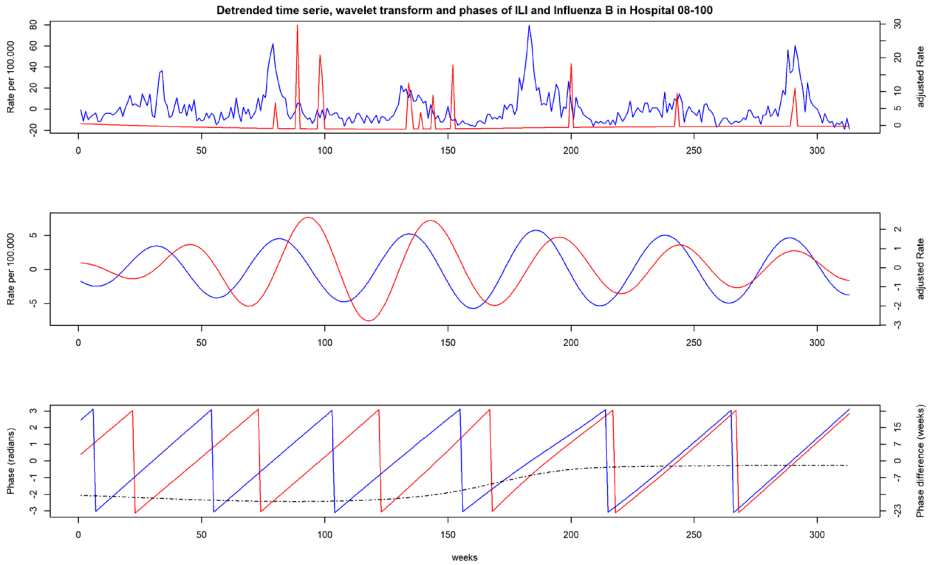
Detrended time serie, wavelet transform and phases of ILI and Influenza B in Hospital 08-100
Rate per 100.000
adjusted Rate
Phase (radians)
Phase difference (weeks)
weeks

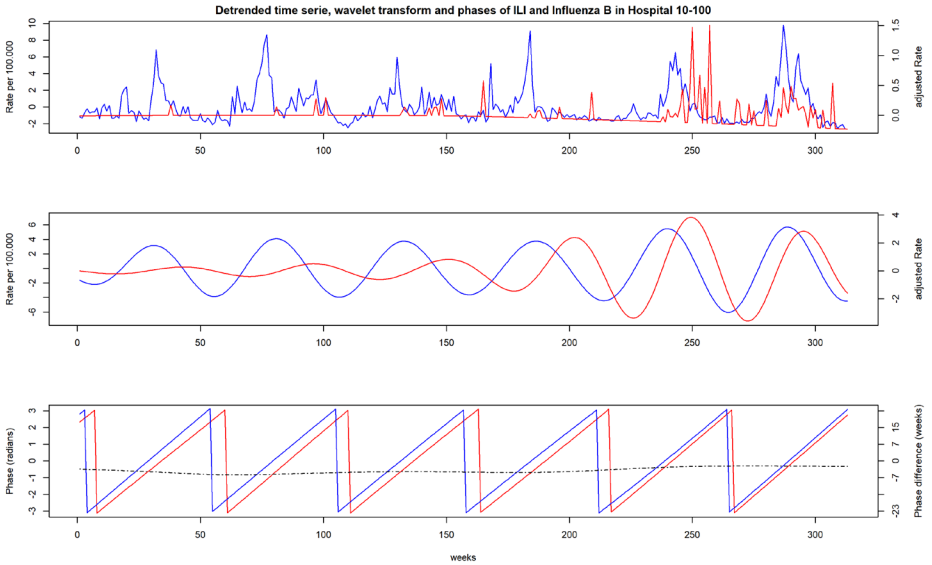
Detrended time serie, wavelet transform and phases of ILI and Influenza B in Hospital 10-100
Rate per 100.000
adjusted Rate
Phase (radians)
Phase difference (weeks)
weeks

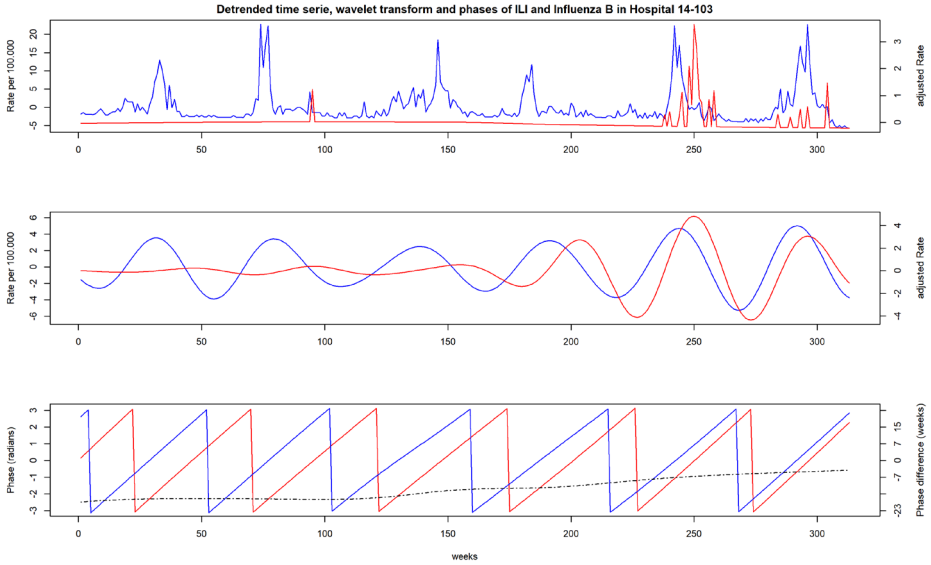
Detrended time serie, wavelet transform and phases of ILI and Influenza B in Hospital 14-103
Rate per 100.000
adjusted Rate
Phase (radians)
Phase difference (weeks)
weeks

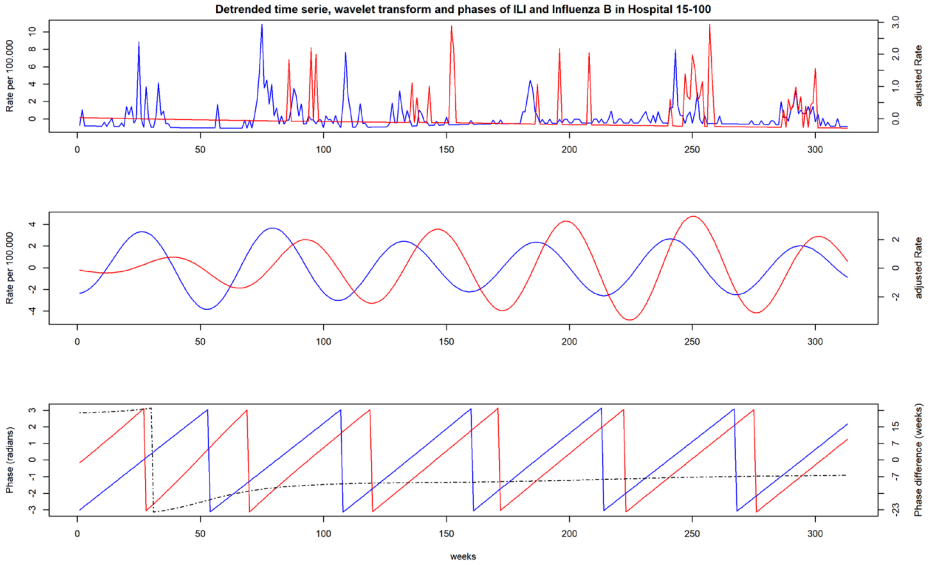
Detrended time serie, wavelet transform and phases of ILI and Influenza B in Hospital 15-100
Rate per 100.000
adjusted Rate
Phase (radians)
Phase difference (weeks)
weeks

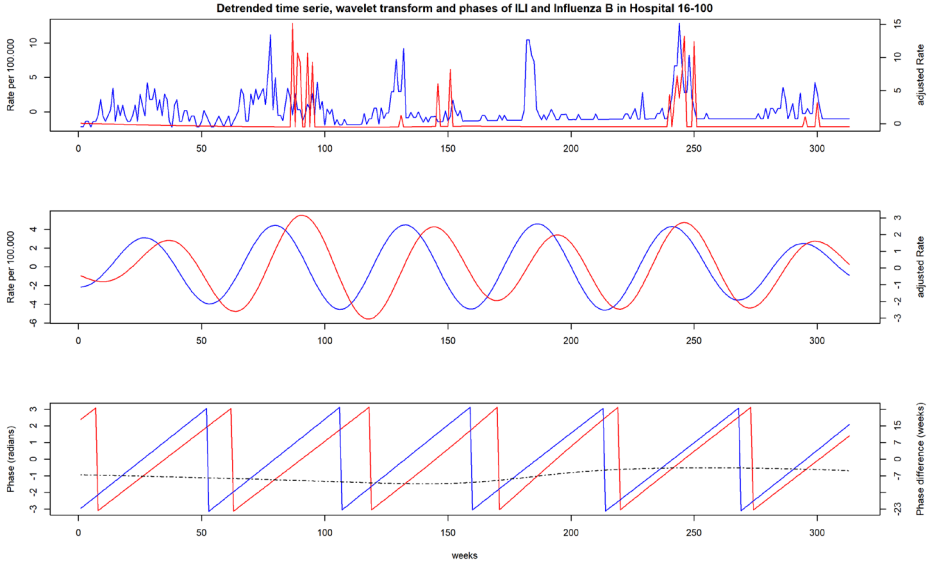
Detrended time serie, wavelet transform and phases of ILI and Influenza B in Hospital 16-100
Rate per 100.000
adjusted Rate
Phase (radians)
Phase difference (weeks)
weeks

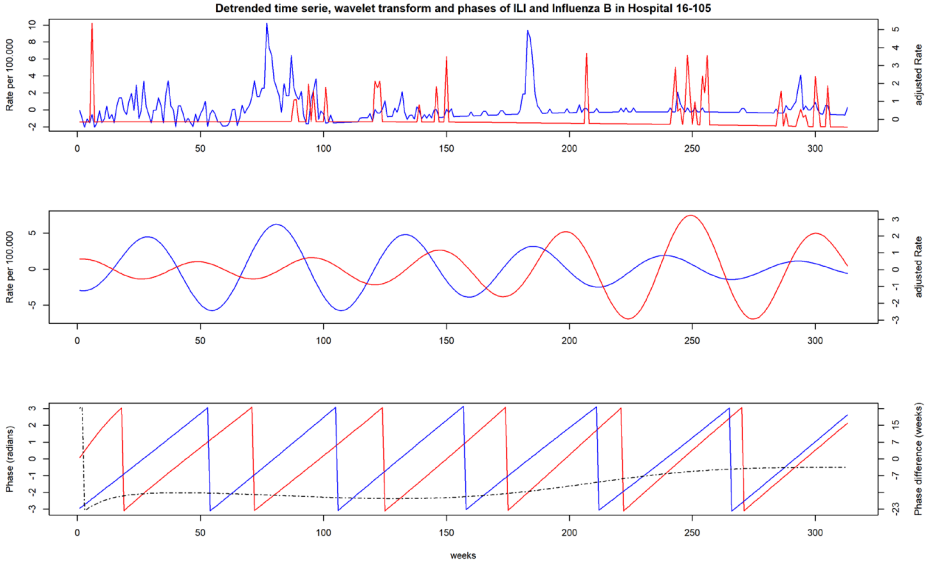
Detrended time serie, wavelet transform and phases of ILI and Influenza B in Hospital 16-105
Rate per 100.000
adjusted Rate
Phase (radians)
Phase difference (weeks)
weeks

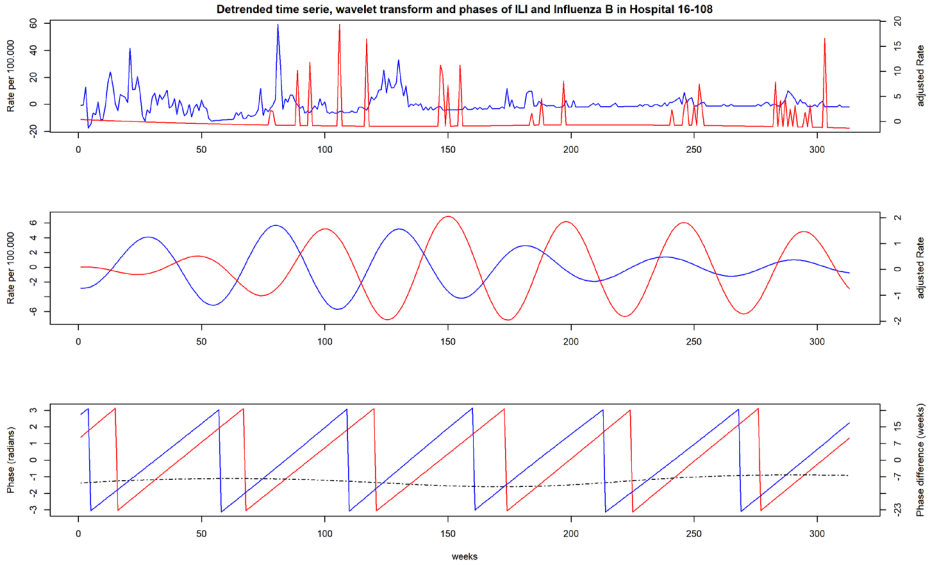
Detrended time serie, wavelet transform and phases of ILI and Influenza B in Hospital 16-108
Rate per 100.000
adjusted Rate
Phase (radians)
Phase difference (weeks)
weeks

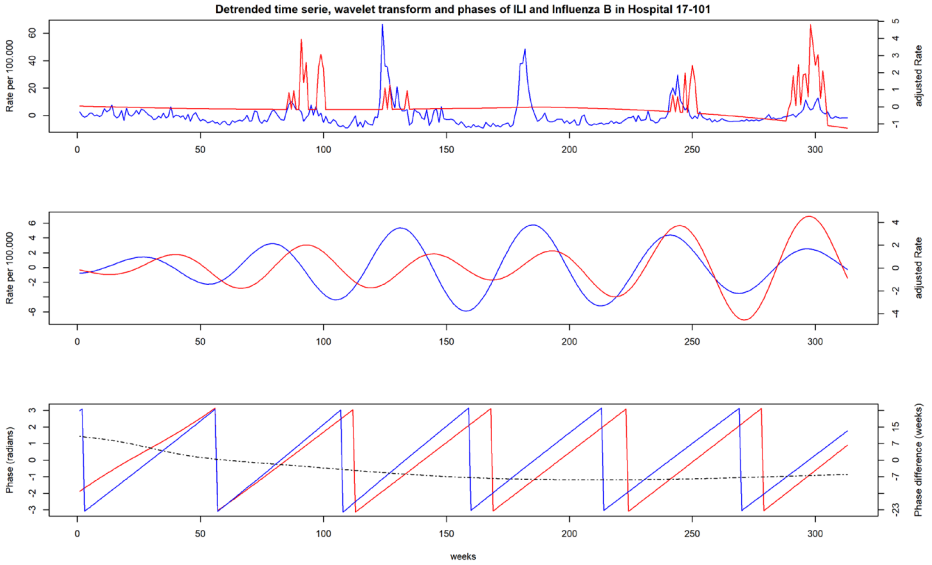
Detrended time serie, wavelet transform and phases of ILI and Influenza B in Hospital 17-101
Rate per 100.000
adjusted Rate
Phase (radians)
Phase difference (weeks)
weeks

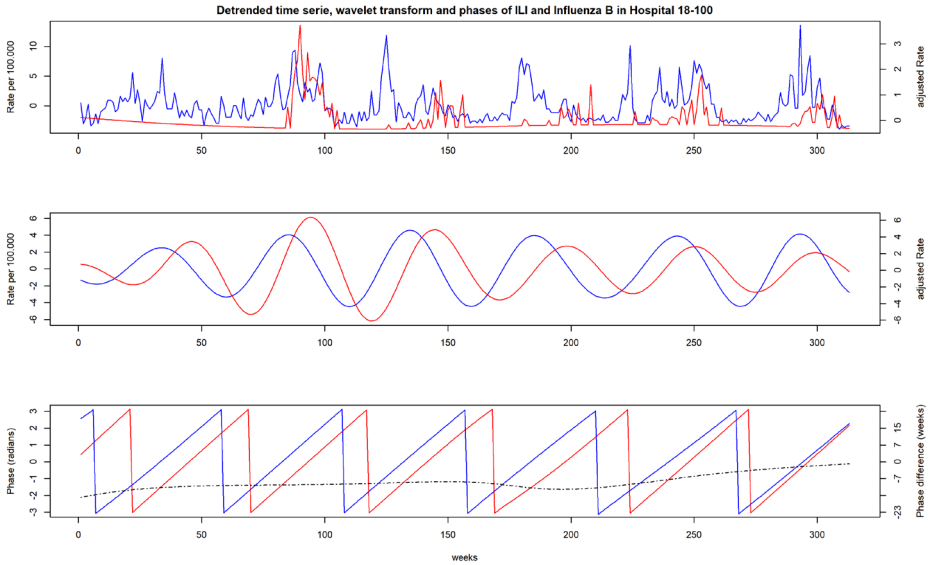
Detrended time serie, wavelet transform and phases of ILI and Influenza B in Hospital 18-100
Rate per 100.000
adjusted Rate
Phase (radians)
Phase difference (weeks)
weeks

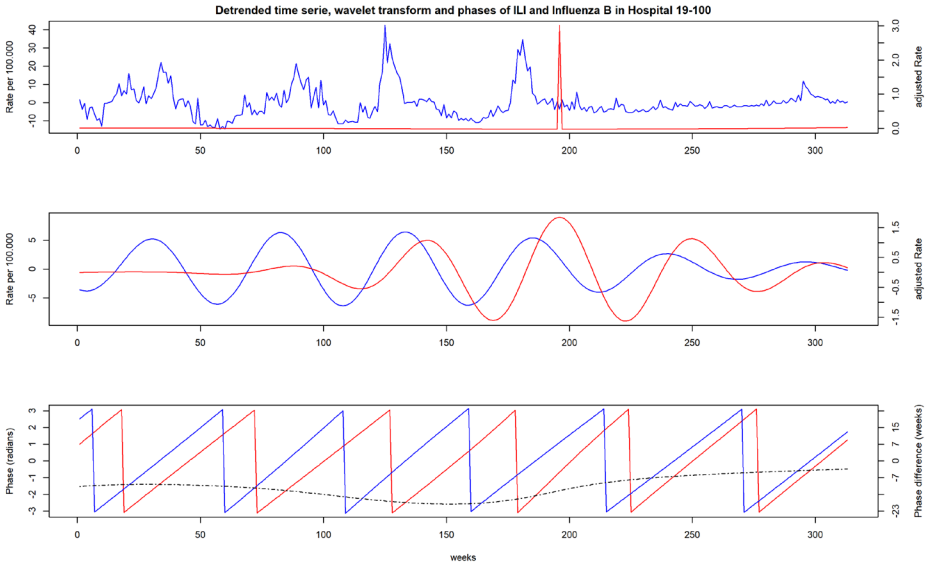
Detrended time serie, wavelet transform and phases of ILI and Influenza B in Hospital 19-100
Rate per 100.000
adjusted Rate
Phase (radians)
Phase difference (weeks)
weeks

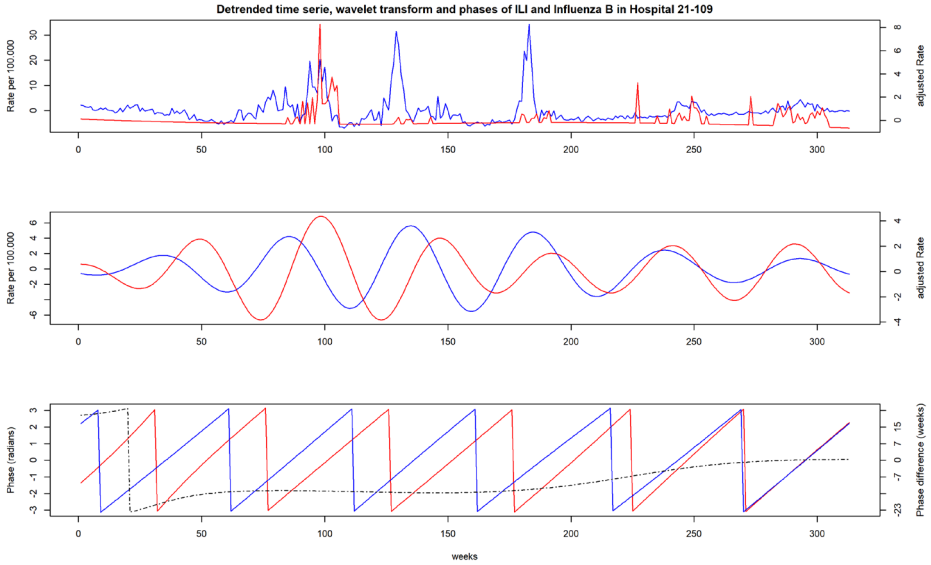
Detrended time serie, wavelet transform and phases of ILI and Influenza B in Hospital 21-109
Rate per 100.000
adjusted Rate
Phase (radians)
Phase difference (weeks)
weeks

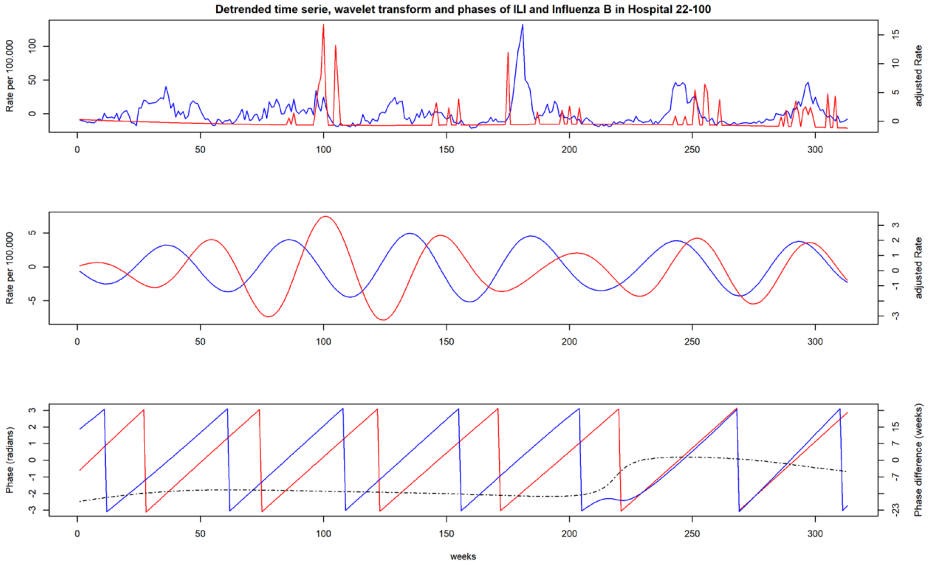
Detrended time serie, wavelet transform and phases of ILI and Influenza B in Hospital 22-100
Rate per 100.000
adjusted Rate
Phase (radians)
Phase difference (weeks)
weeks

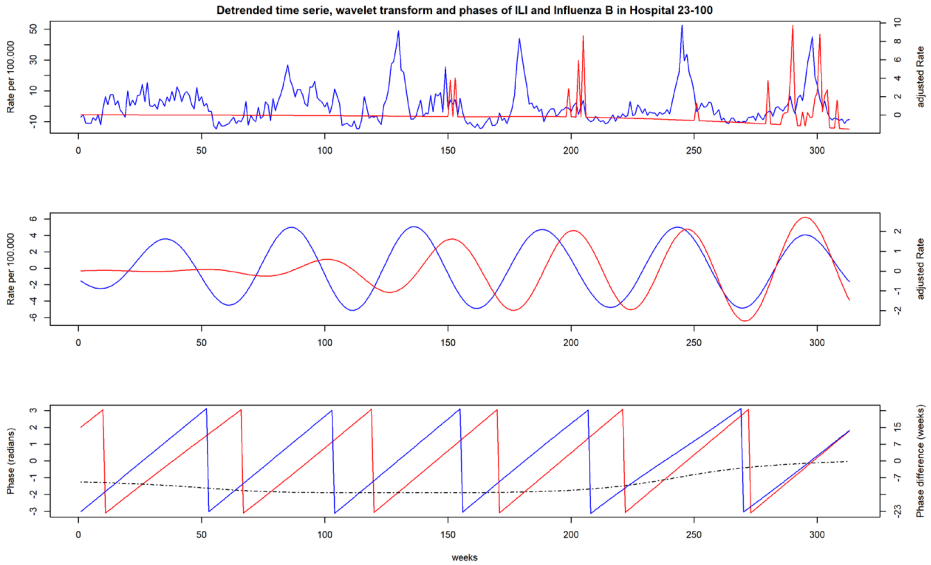
Detrended time serie, wavelet transform and phases of ILI and Influenza B in Hospital 23-100
Rate per 100.000
adjusted Rate
Phase (radians)
Phase difference (weeks)
weeks

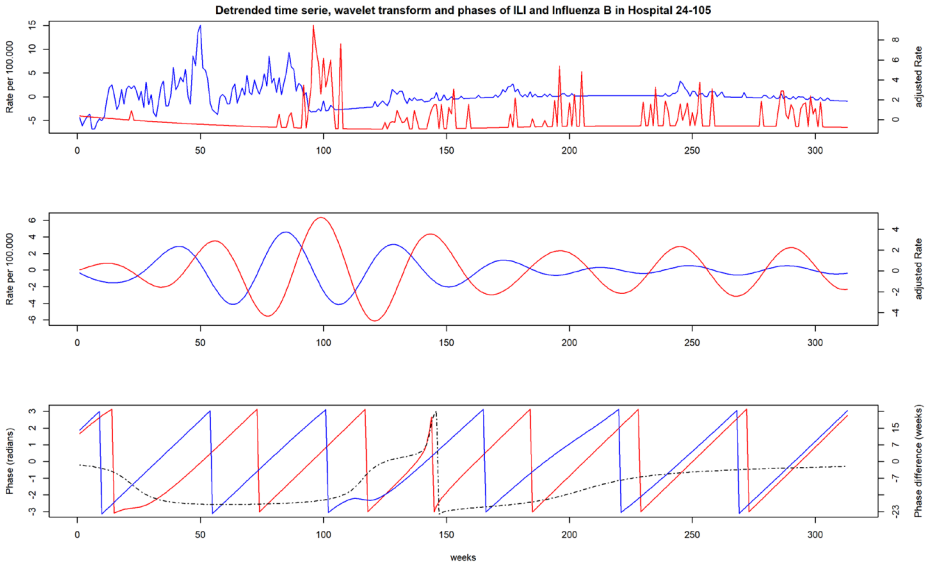
Detrended time serie, wavelet transform and phases of ILI and Influenza B in Hospital 24-105
Rate per 100.000
adjusted Rate
Phase (radians)
Phase difference (weeks)
weeks

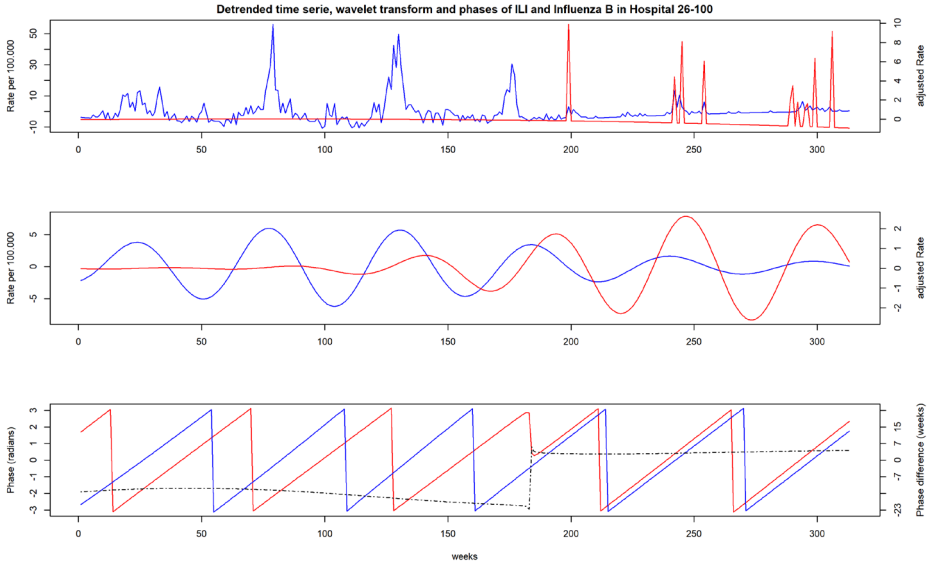
Detrended time serie, wavelet transform and phases of ILI and Influenza B in Hospital 26-100
Rate per 100,000
adjusted Rate
Rate per 100,000
adjusted Rate
Phase (radians)
Phase difference (weeks)
weeks

## 3. Detrended rate time series, wavelet transformed rates and phases of ILI and infuenza A plus influenza B by hospital

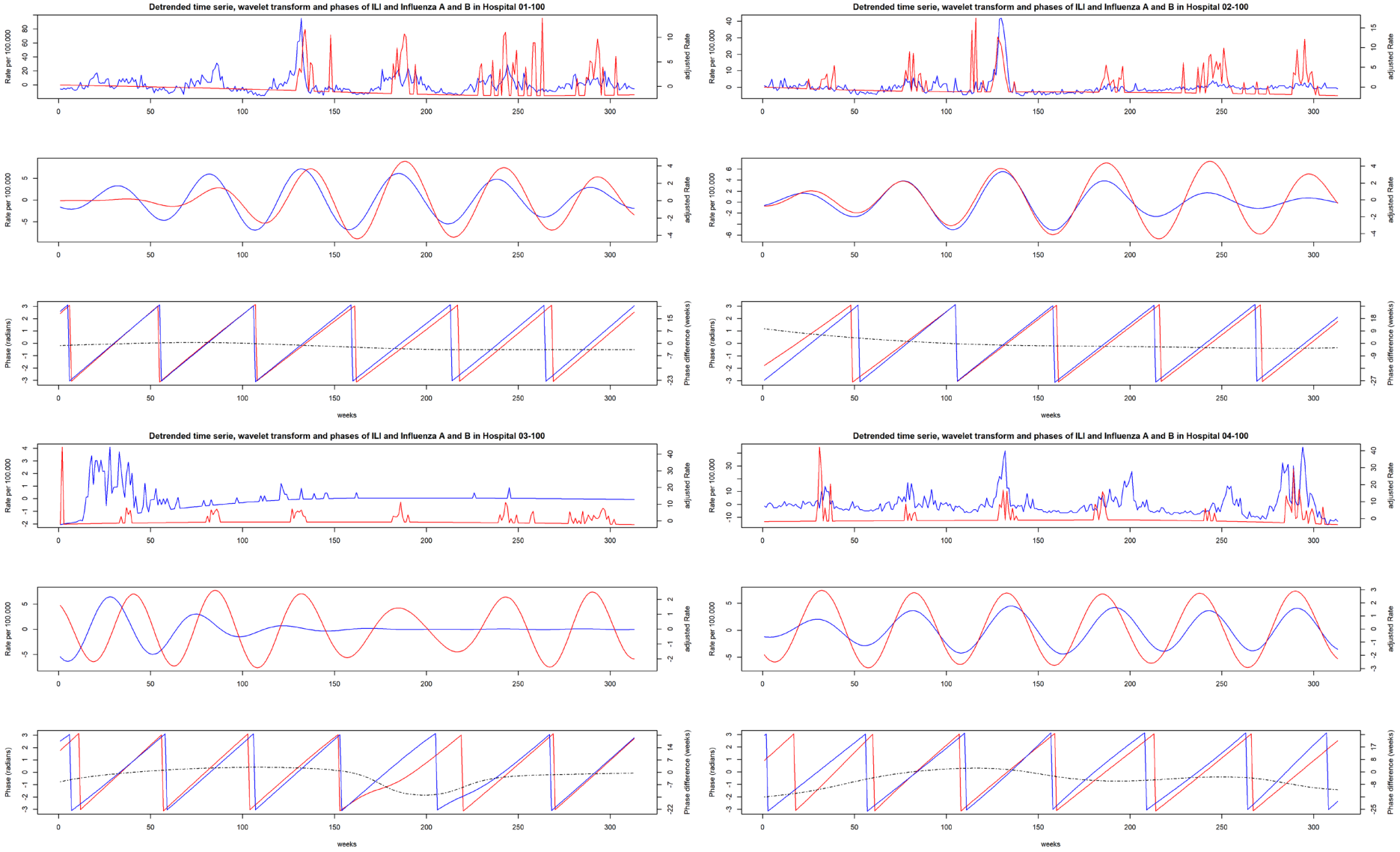

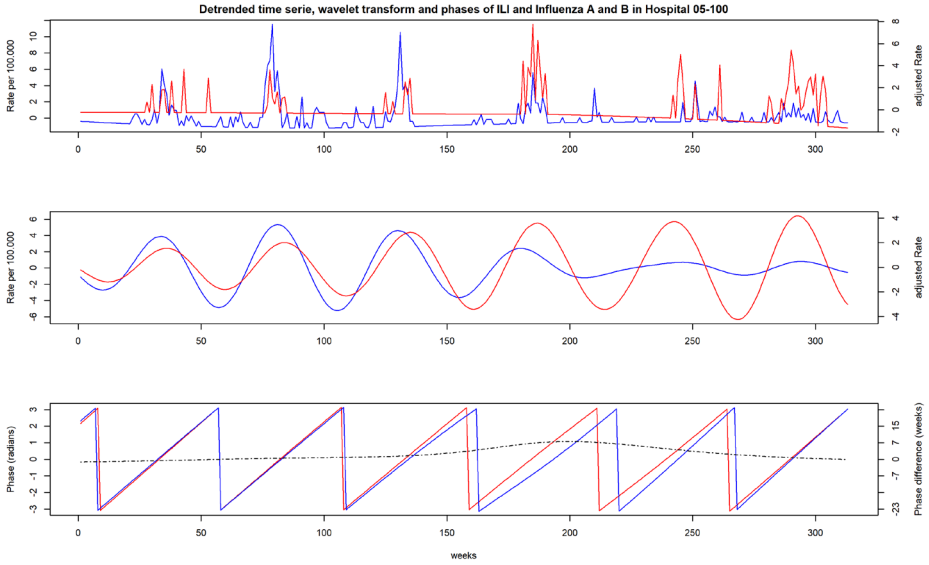
Detrended time serie, wavelet transform and phases of ILI and Influenza A and B in Hospital 05-100
Rate per 100,000
adjusted Rate
Phase (radians)
Phase difference (weeks)
weeks

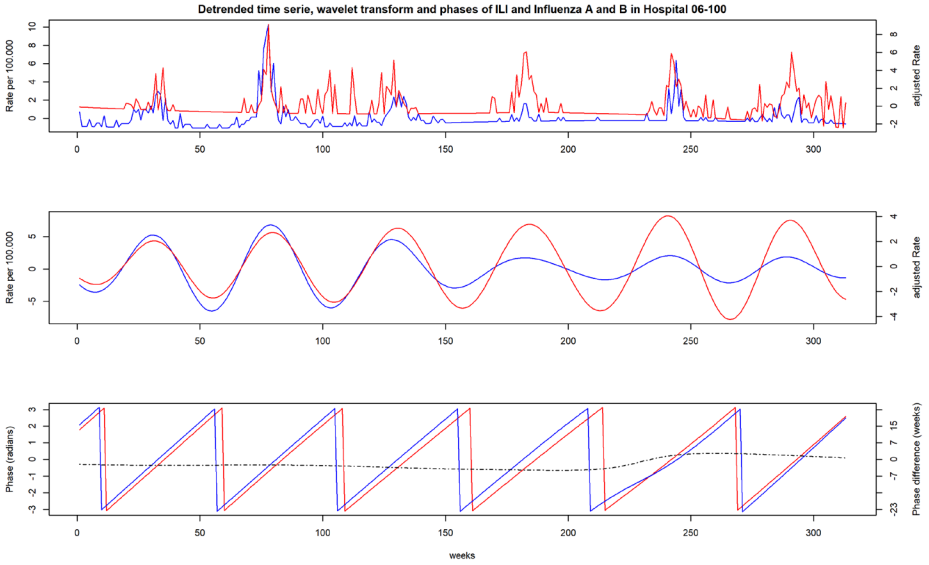
Detrended time serie, wavelet transform and phases of ILI and Influenza A and B in Hospital 06-100
Rate per 100,000
adjusted Rate
Phase (radians)
Phase difference (weeks)
weeks

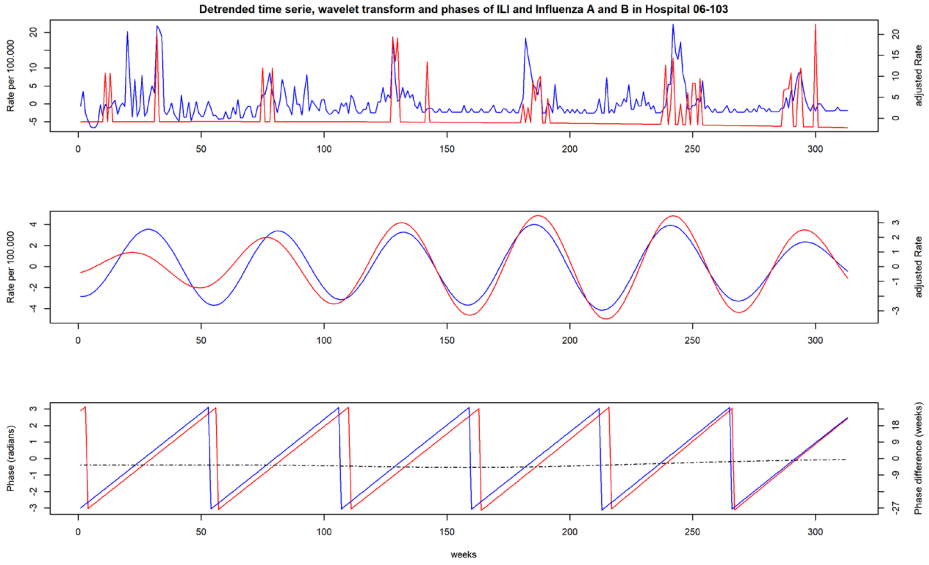
Detrended time serie, wavelet transform and phases of ILI and Influenza A and B in Hospital 06-103
Rate per 100,000
adjusted Rate
Phase (radians)
Phase difference (weeks)
weeks

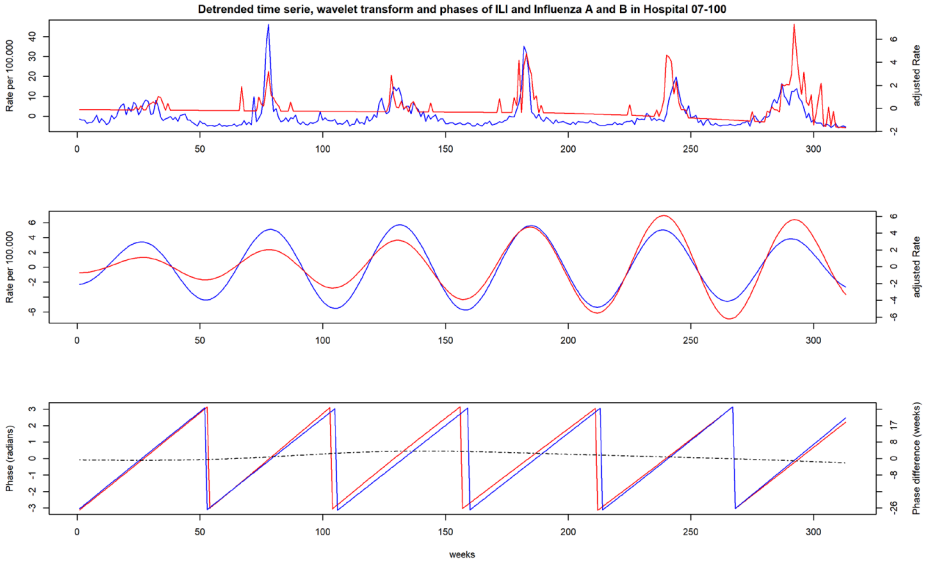
Detrended time serie, wavelet transform and phases of ILI and Influenza A and B in Hospital 07-100
Rate per 100,000
adjusted Rate
Phase (radians)
Phase difference (weeks)
weeks

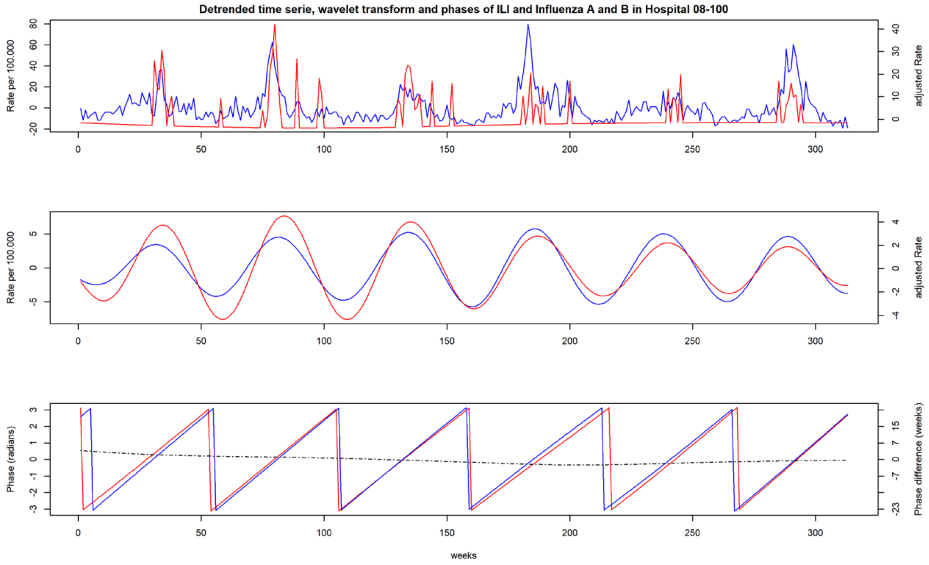
Detrended time serie, wavelet transform and phases of ILI and Influenza A and B in Hospital 08-100
Rate per 100,000
adjusted Rate
Phase (radians)
Phase difference (weeks)
weeks

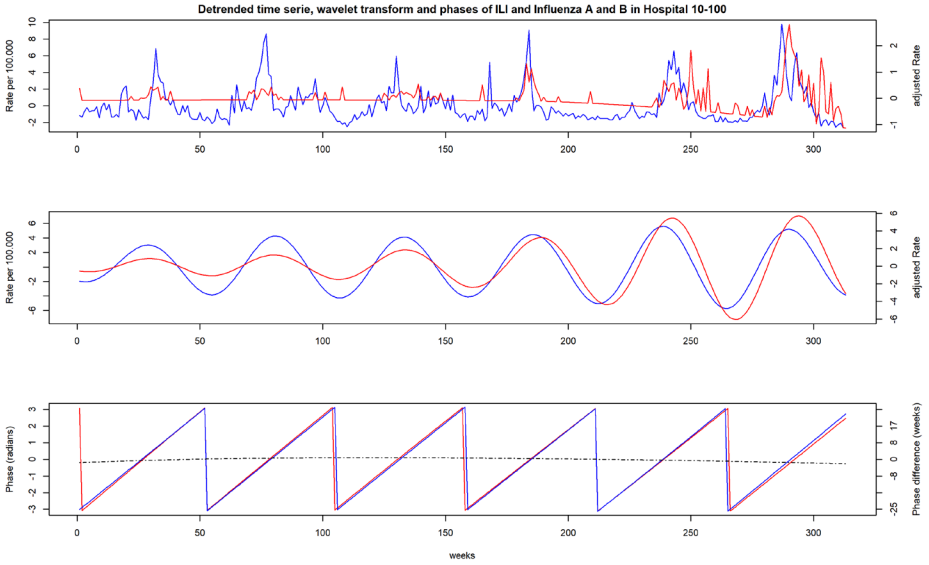
Detrended time serie, wavelet transform and phases of ILI and Influenza A and B in Hospital 10-100
Rate per 100,000
adjusted Rate
Phase (radians)
Phase difference (weeks)
weeks

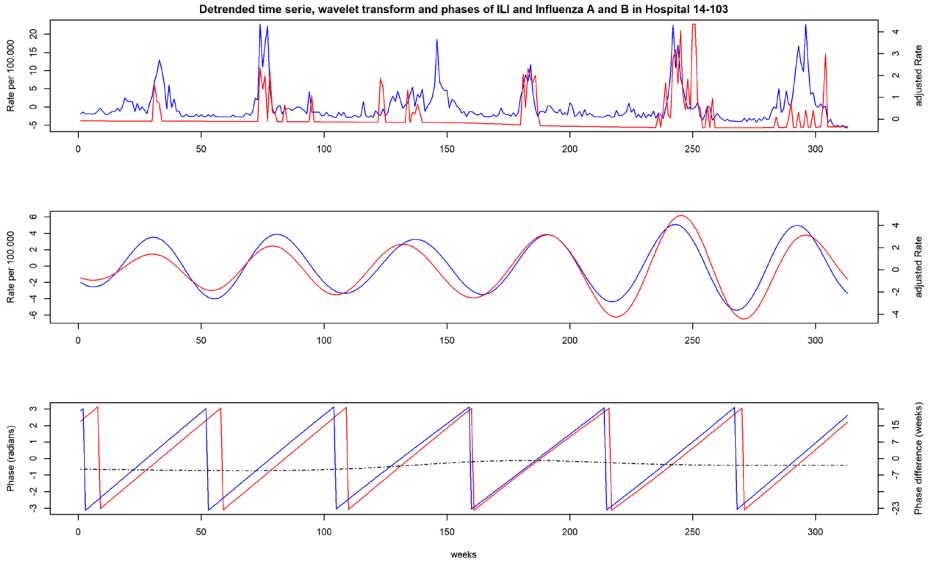
Detrended time serie, wavelet transform and phases of ILI and Influenza A and B in Hospital 14-103
Rate per 100,000
adjusted Rate
Phase (radians)
Phase difference (weeks)
weeks

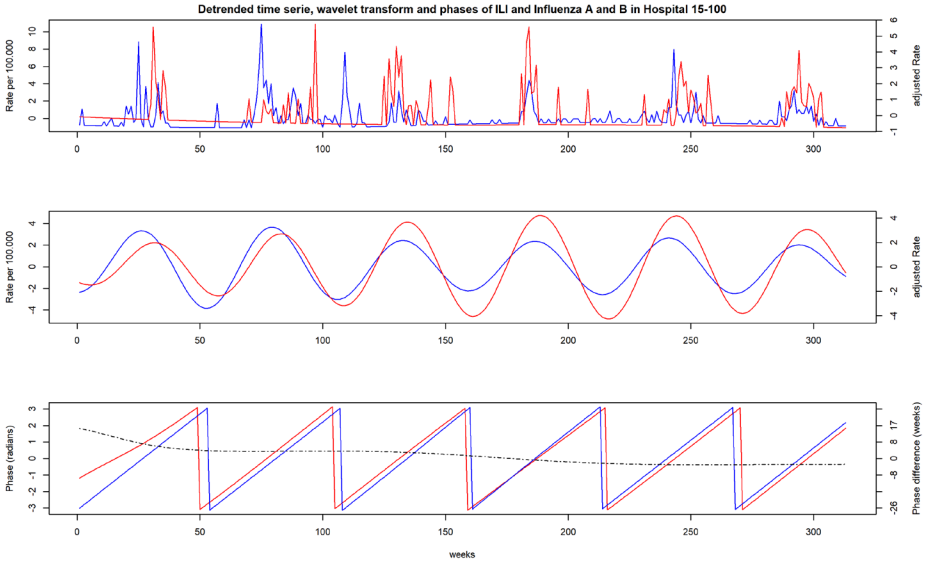
Detrended time serie, wavelet transform and phases of ILI and Influenza A and B in Hospital 15-100
Rate per 100,000
adjusted Rate
Phase (radians)
Phase difference (weeks)
weeks

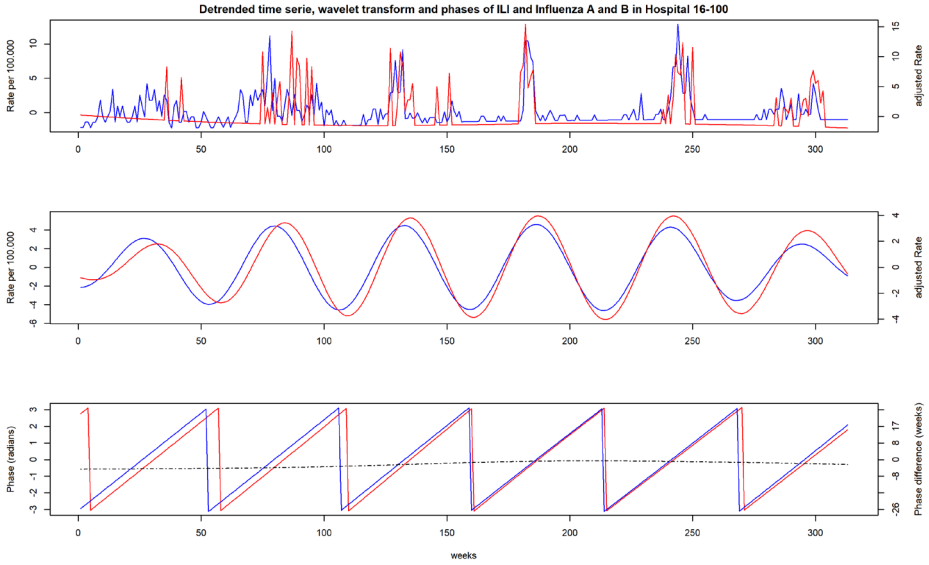
Detrended time serie, wavelet transform and phases of ILI and Influenza A and B in Hospital 16-100
Rate per 100,000
adjusted Rate
Phase (radians)
Phase difference (weeks)
weeks

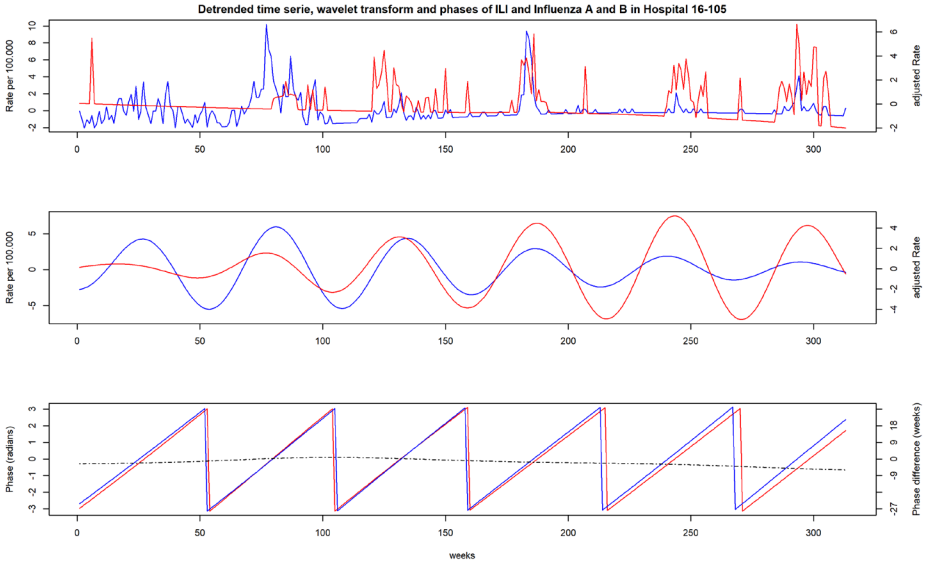
Detrended time serie, wavelet transform and phases of ILI and Influenza A and B in Hospital 16-105
Rate per 100,000
adjusted Rate
Phase (radians)
Phase difference (weeks)
weeks

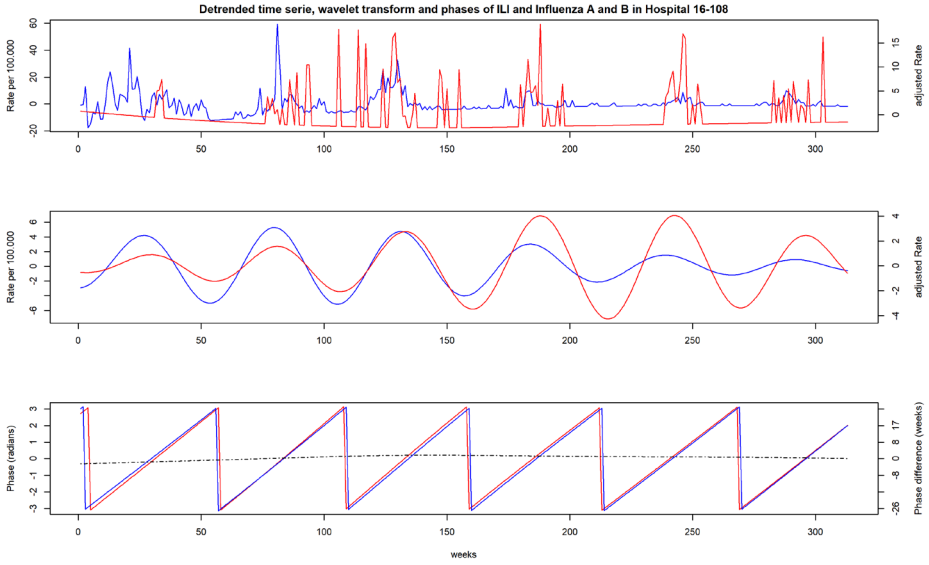
Detrended time serie, wavelet transform and phases of ILI and Influenza A and B in Hospital 16-108
Rate per 100,000
adjusted Rate
Phase (radians)
Phase difference (weeks)
weeks

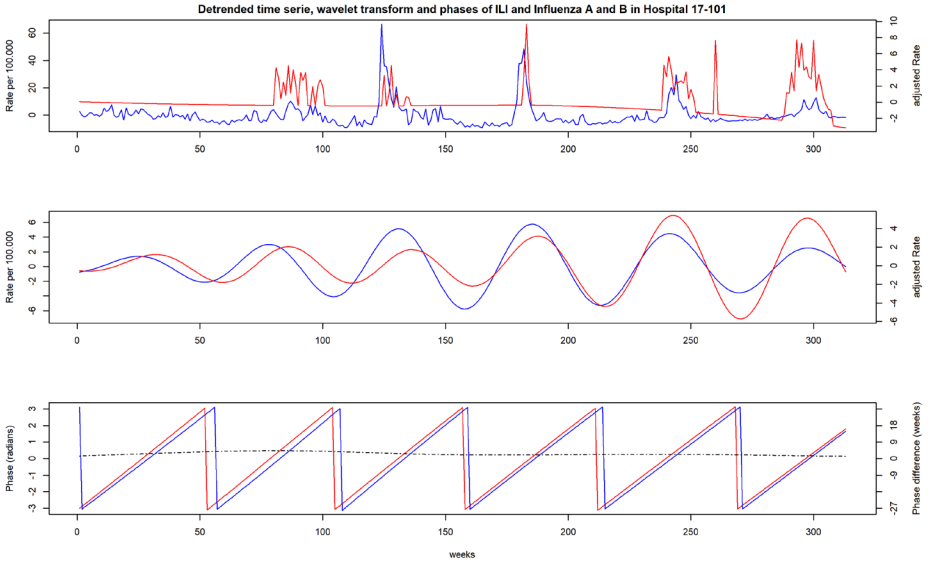
Detrended time serie, wavelet transform and phases of ILI and Influenza A and B in Hospital 17-101
Rate per 100,000
adjusted Rate
Phase (radians)
Phase difference (weeks)
weeks

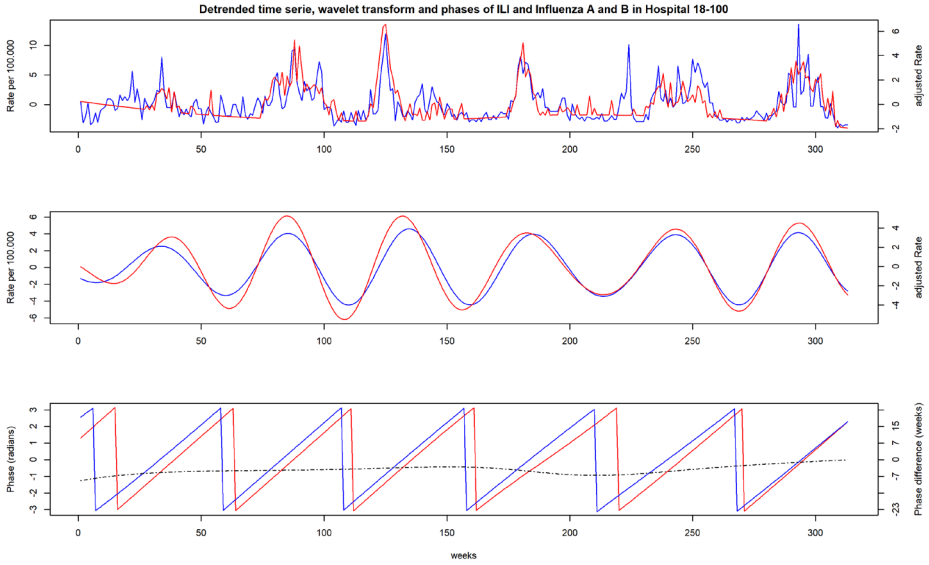
Detrended time serie, wavelet transform and phases of ILI and Influenza A and B in Hospital 18-100
Rate per 100,000
adjusted Rate
Phase (radians)
Phase difference (weeks)
weeks

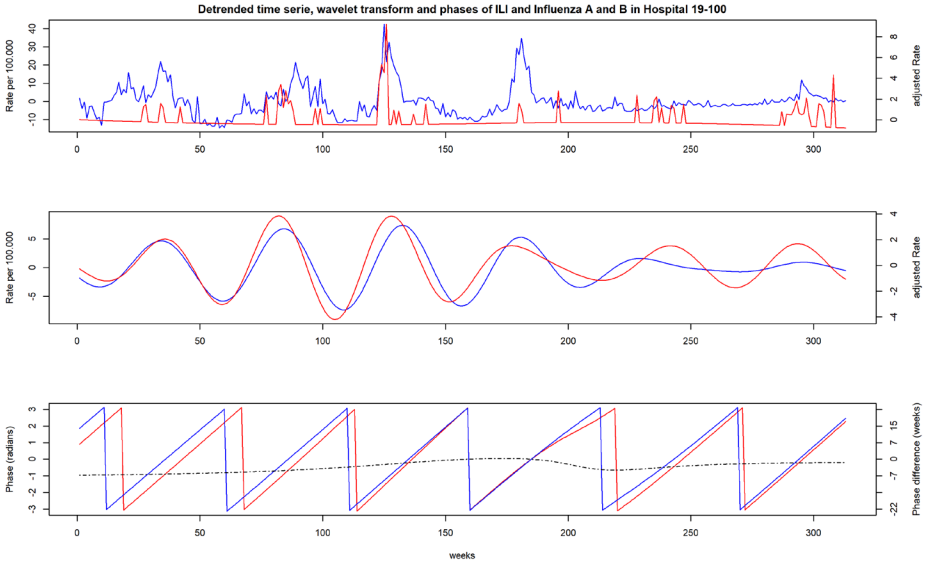
Detrended time serie, wavelet transform and phases of ILI and Influenza A and B in Hospital 19-100
Rate per 100,000
adjusted Rate
Phase (radians)
Phase difference (weeks)
weeks

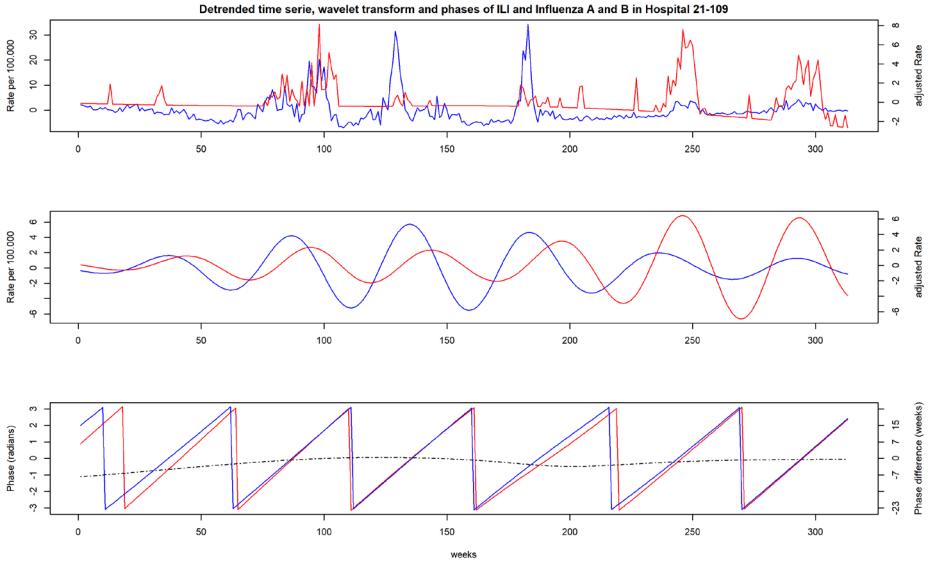
Detrended time serie, wavelet transform and phases of ILI and Influenza A and B in Hospital 21-109
Rate per 100,000
adjusted Rate
Phase (radians)
Phase difference (weeks)
weeks

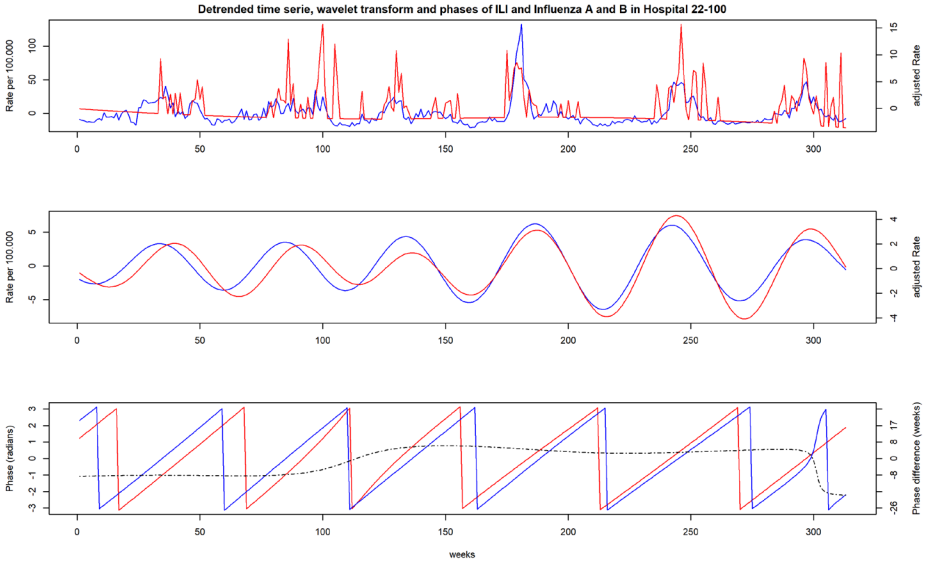
Detrended time serie, wavelet transform and phases of ILI and Influenza A and B in Hospital 22-100
Rate per 100,000
adjusted Rate
Phase (radians)
Phase difference (weeks)
weeks

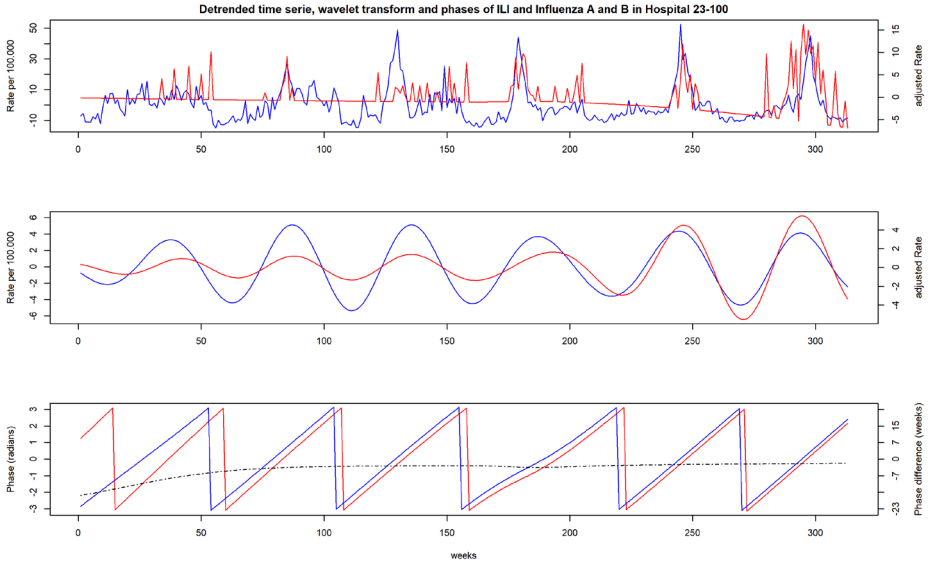
Detrended time serie, wavelet transform and phases of ILI and Influenza A and B in Hospital 23-100
Rate per 100,000
adjusted Rate
Phase (radians)
Phase difference (weeks)
weeks

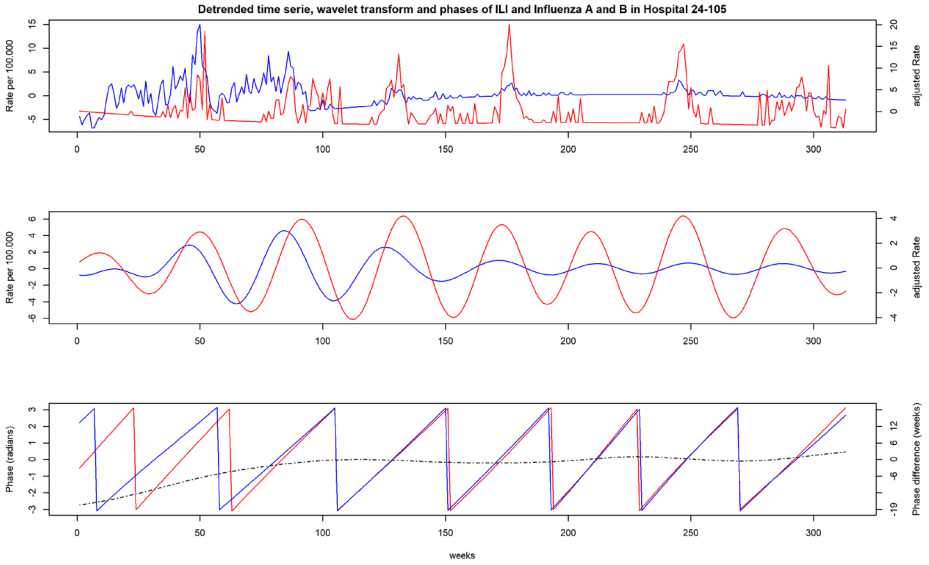
Detrended time serie, wavelet transform and phases of ILI and Influenza A and B in Hospital 24-105
Rate per 100,000
adjusted Rate
Phase (radians)
Phase difference (weeks)
weeks

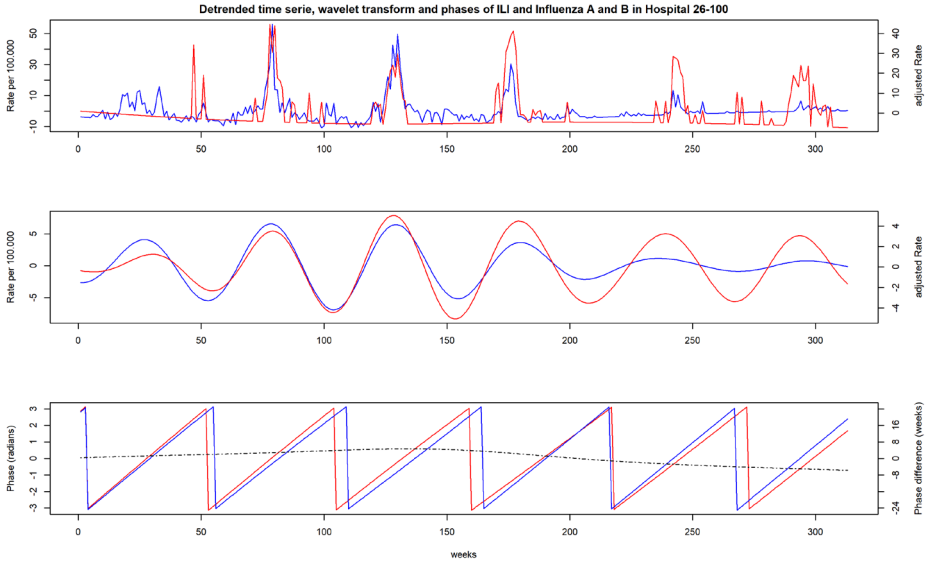
Detrended time serie, wavelet transform and phases of ILI and Influenza A and B in Hospital 26-100
Rate per 100,000
adjusted Rate
Phase (radians)
Phase difference (weeks)
weeks

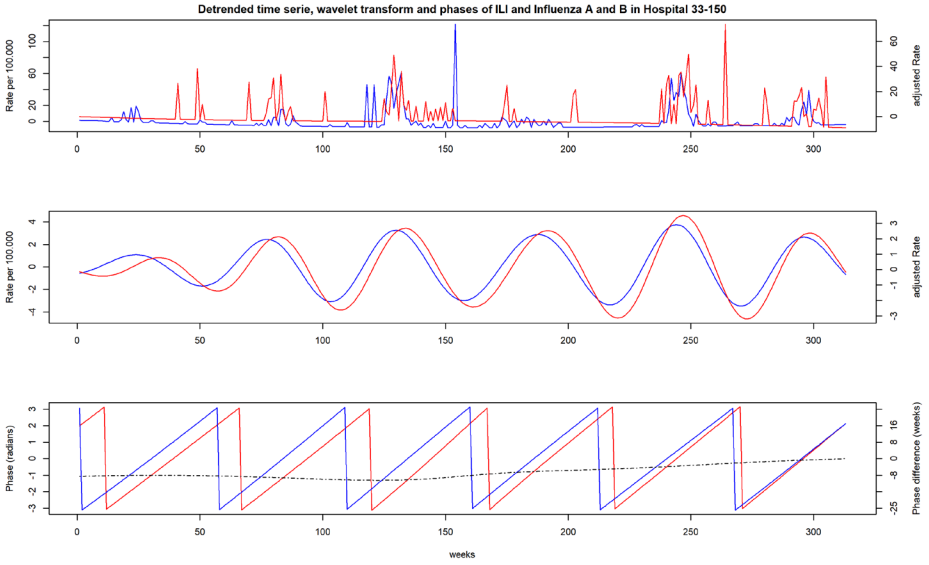
Detrended time serie, wavelet transform and phases of ILI and Influenza A and B in Hospital 33-150
Rate per 100,000
adjusted Rate
Phase (radians)
Phase difference (weeks)
weeks

## 4. Detrended rate time series, wavelet transformed rates and phases of ILI and respiratory syncytial virus by hospital

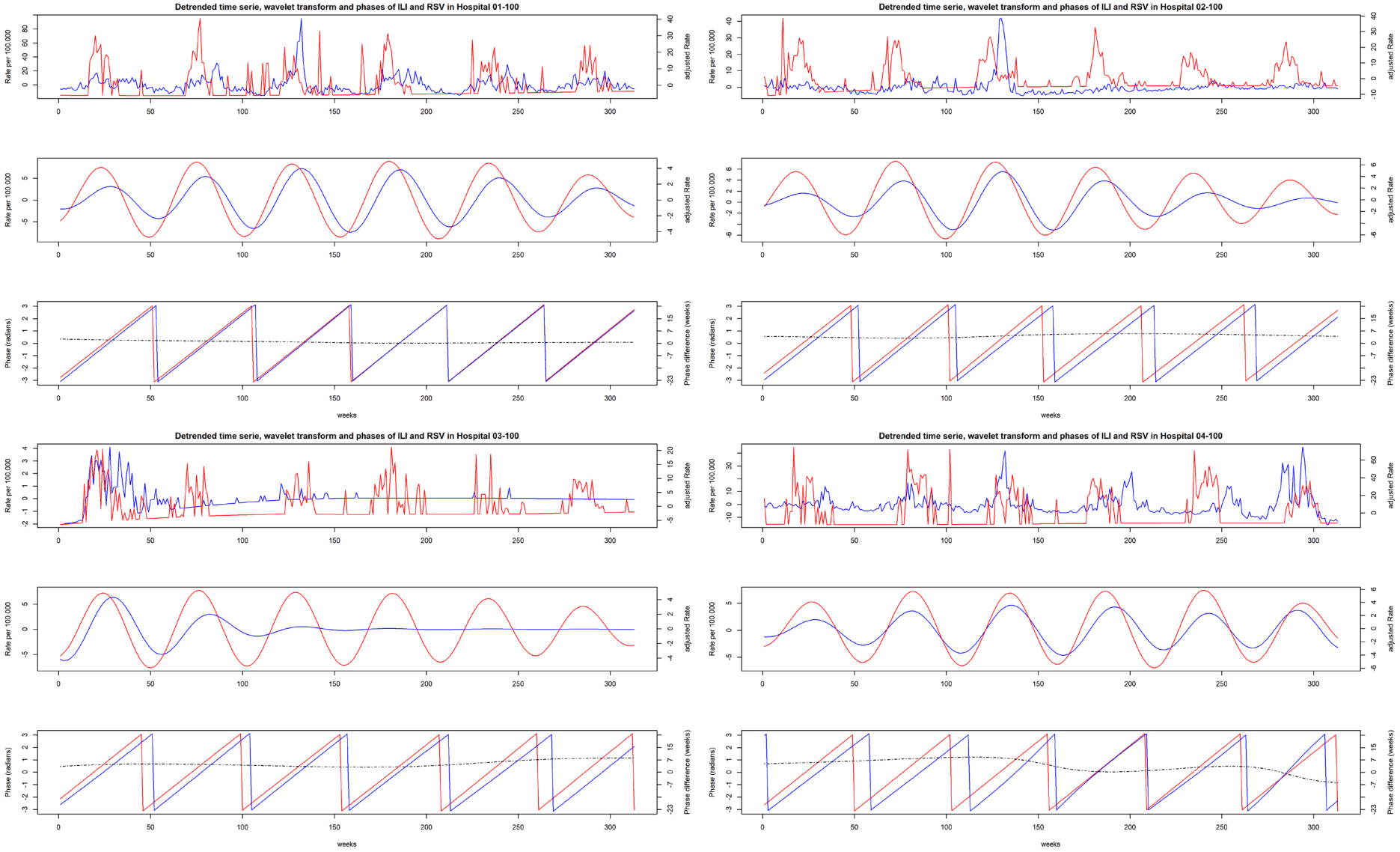

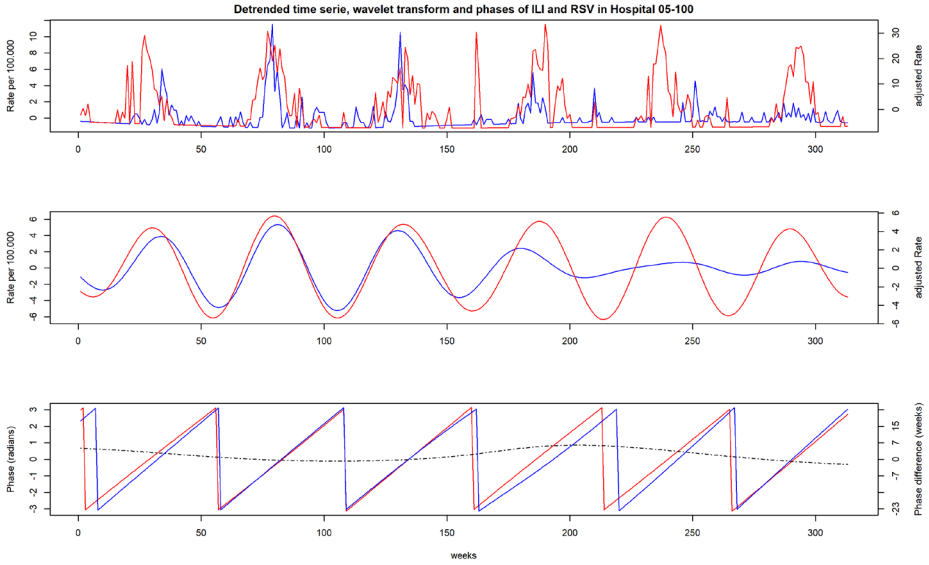
Detrended time serie, wavelet transform and phases of ILI and RSV in Hospital 05-100
Rate per 100.000
adjusted Rate
Phase (radians)
Phase difference (weeks)
weeks

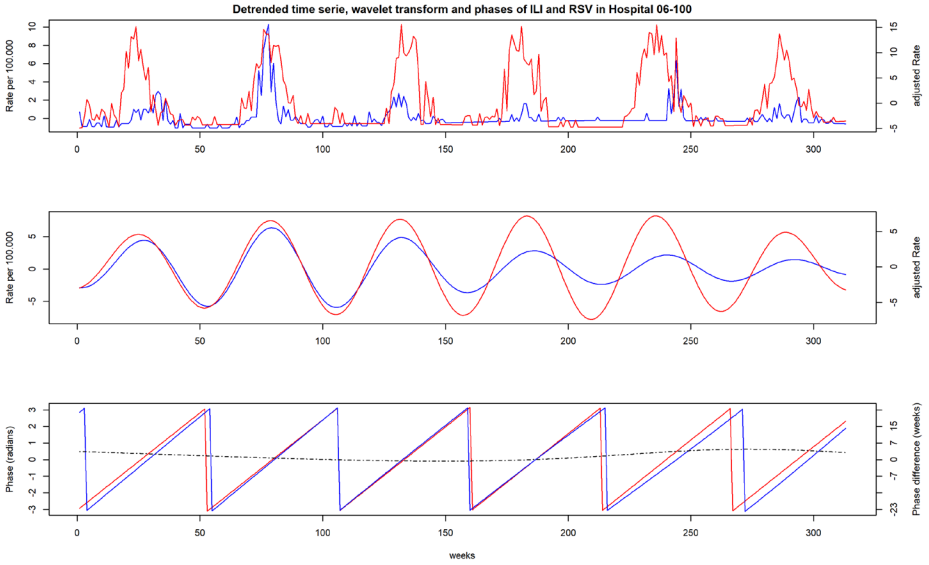
Detrended time serie, wavelet transform and phases of ILI and RSV in Hospital 06-100
Rate per 100.000
adjusted Rate
Phase (radians)
Phase difference (weeks)
weeks

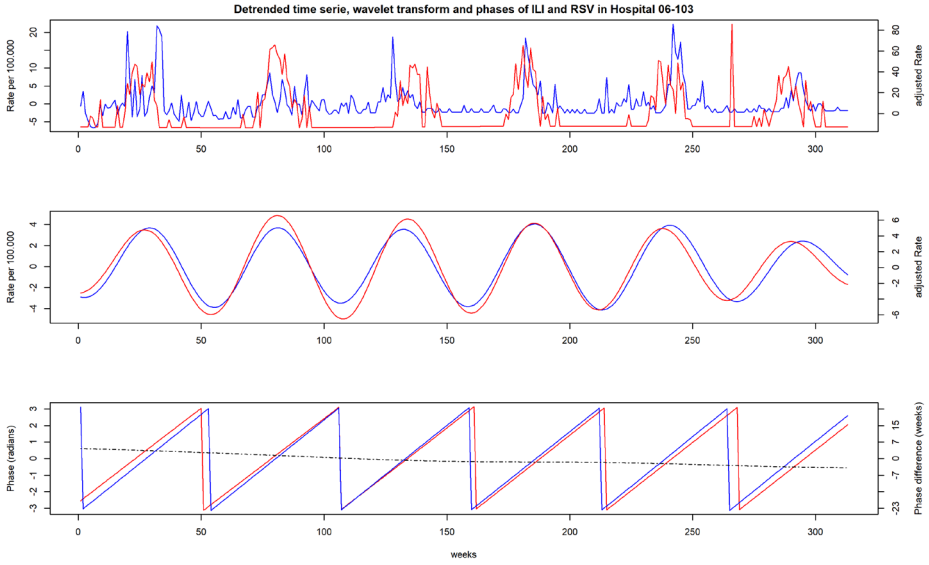
Detrended time serie, wavelet transform and phases of ILI and RSV in Hospital 06-103
Rate per 100.000
adjusted Rate
Phase (radians)
Phase difference (weeks)
weeks

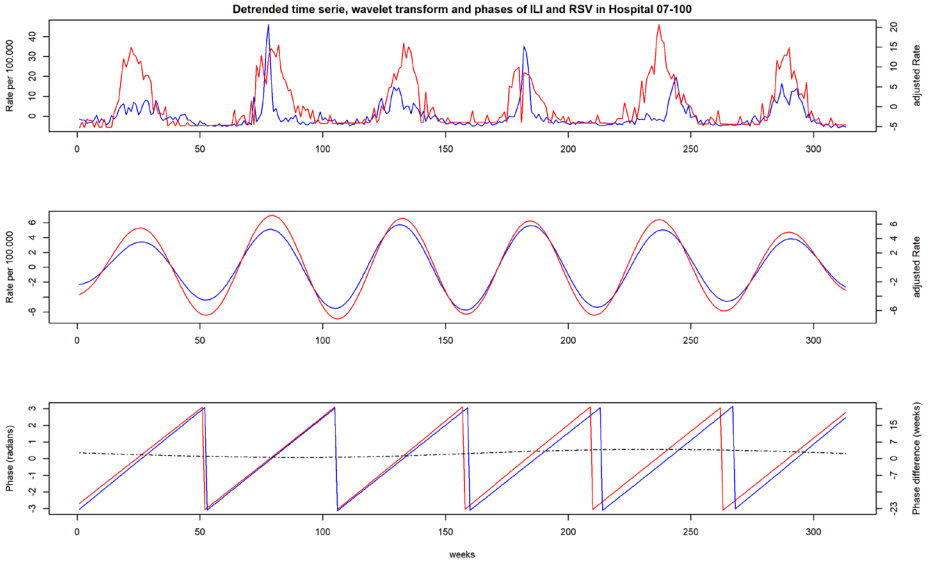
Detrended time serie, wavelet transform and phases of ILI and RSV in Hospital 07-100
Rate per 100.000
adjusted Rate
Phase (radians)
Phase difference (weeks)
weeks

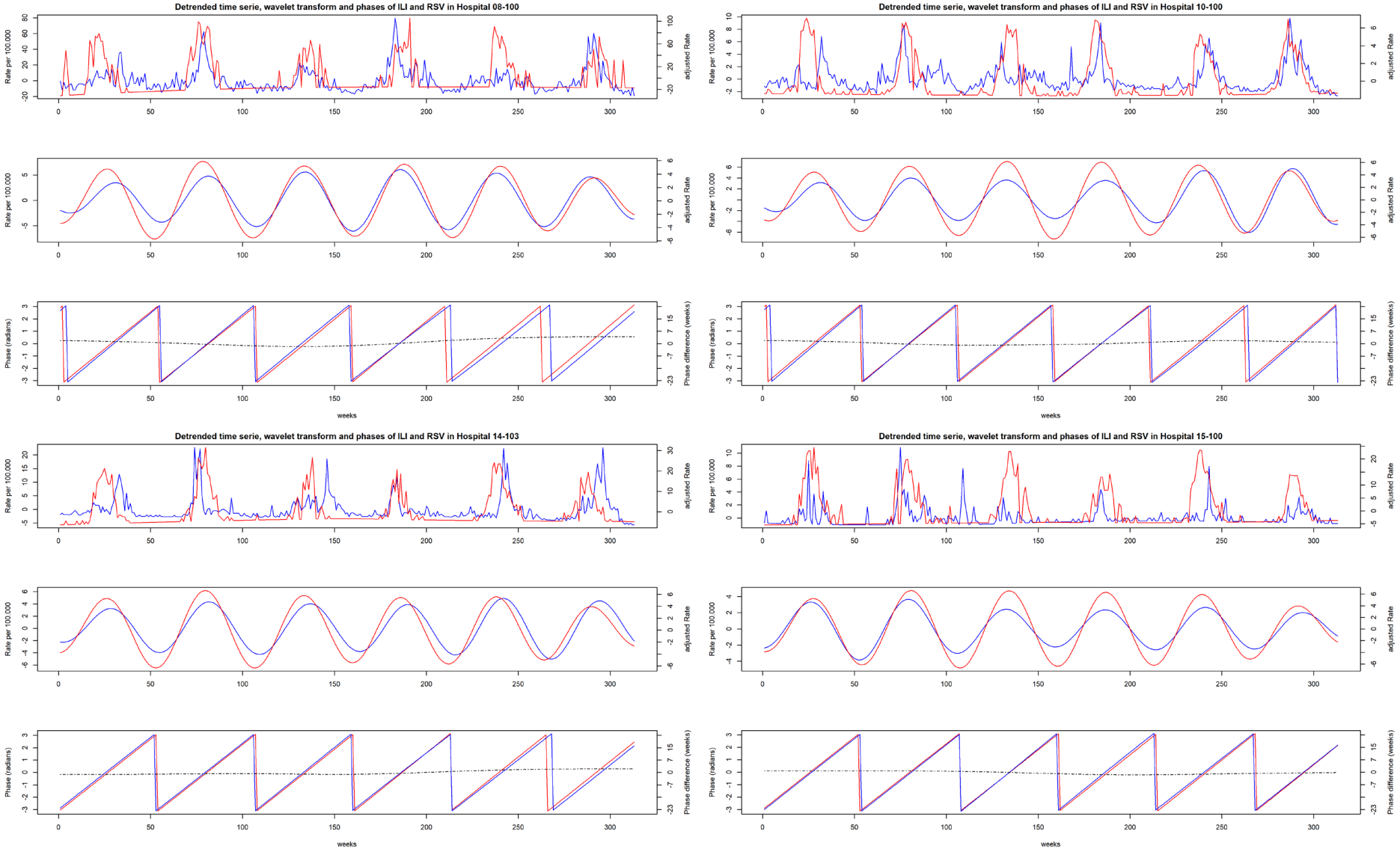
Detrended time serie, wavelet transform and phases of ILI and RSV in Hospital 08-100
Detrended time serie, wavelet transform and phases of ILI and RSV in Hospital 10-100
Detrended time serie, wavelet transform and phases of ILI and RSV in Hospital 14-103
Detrended time serie, wavelet transform and phases of ILI and RSV in Hospital 15-100
Rate per 100,000
adjusted Rate
Phase (radians)
Phase difference (weeks)
weeks

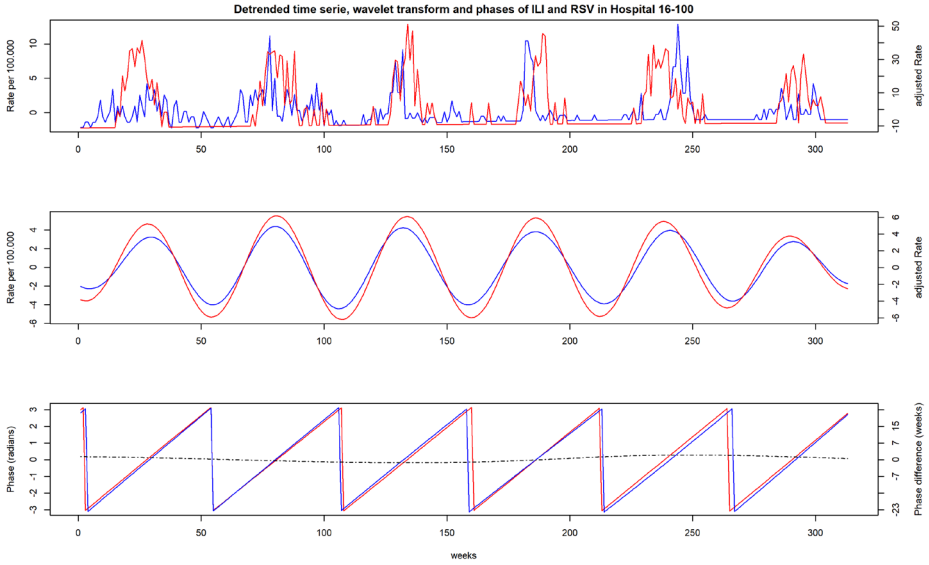
Detrended time serie, wavelet transform and phases of ILI and RSV in Hospital 16-100
Rate per 100,000
adjusted Rate
Phase (radians)
Phase difference (weeks)
weeks

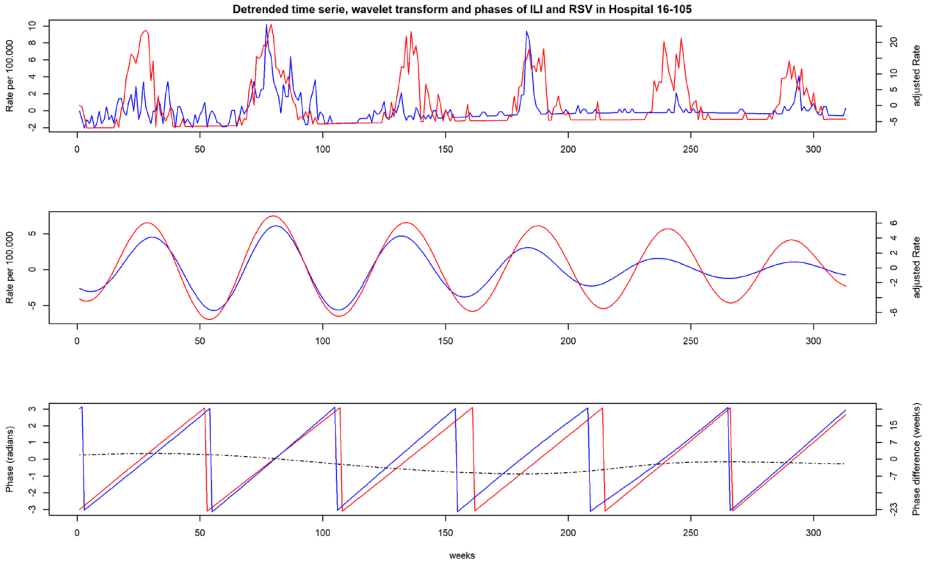
Detrended time serie, wavelet transform and phases of ILI and RSV in Hospital 16-105
Rate per 100,000
adjusted Rate
Phase (radians)
Phase difference (weeks)
weeks

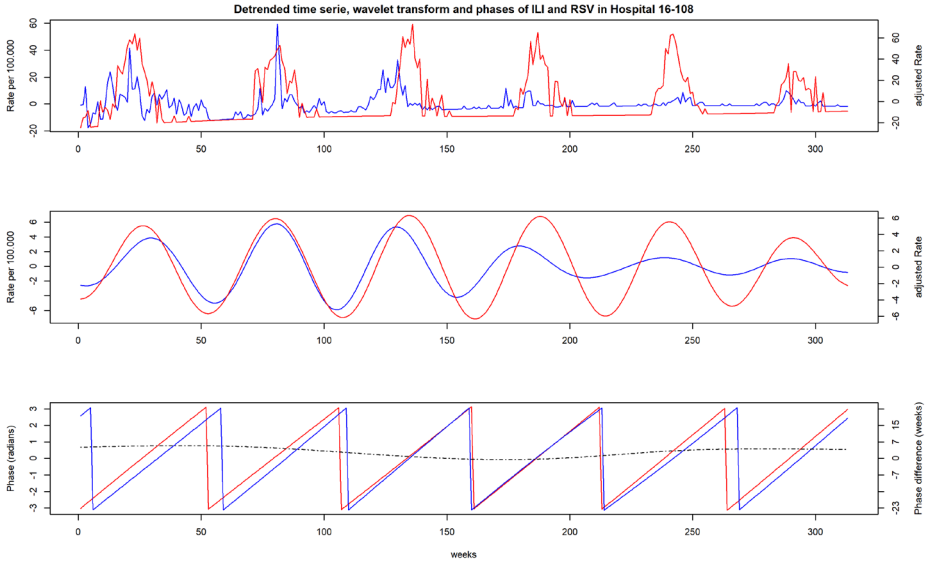
Detrended time serie, wavelet transform and phases of ILI and RSV in Hospital 16-108
Rate per 100,000
adjusted Rate
Phase (radians)
Phase difference (weeks)
weeks

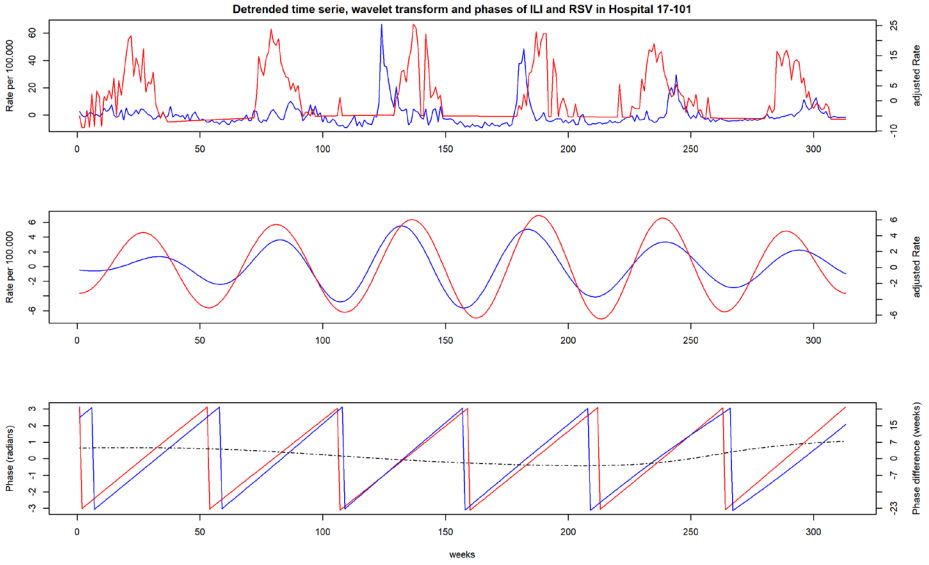
Detrended time serie, wavelet transform and phases of ILI and RSV in Hospital 17-101
Rate per 100,000
adjusted Rate
Phase (radians)
Phase difference (weeks)
weeks

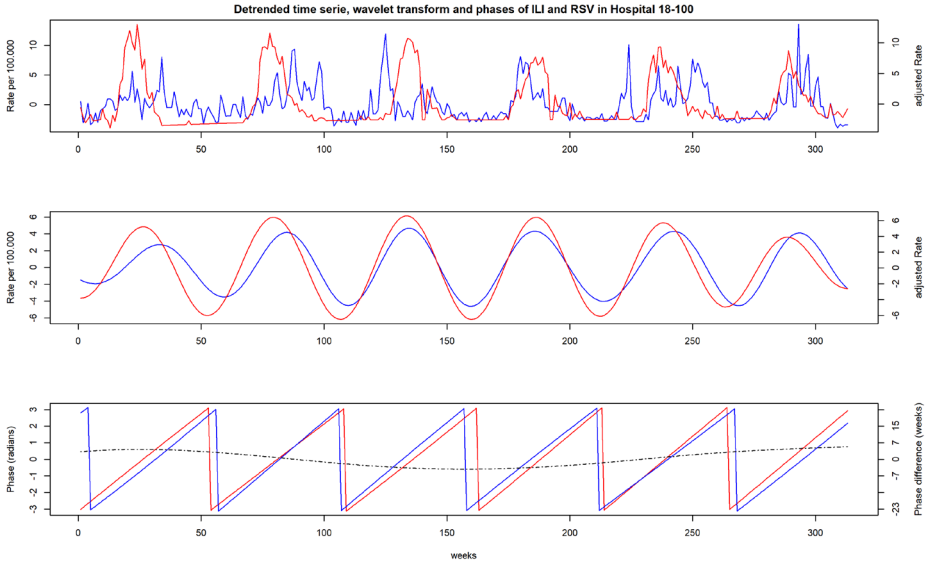
Detrended time serie, wavelet transform and phases of ILI and RSV in Hospital 18-100
Rate per 100,000
adjusted Rate
Phase (radians)
Phase difference (weeks)
weeks

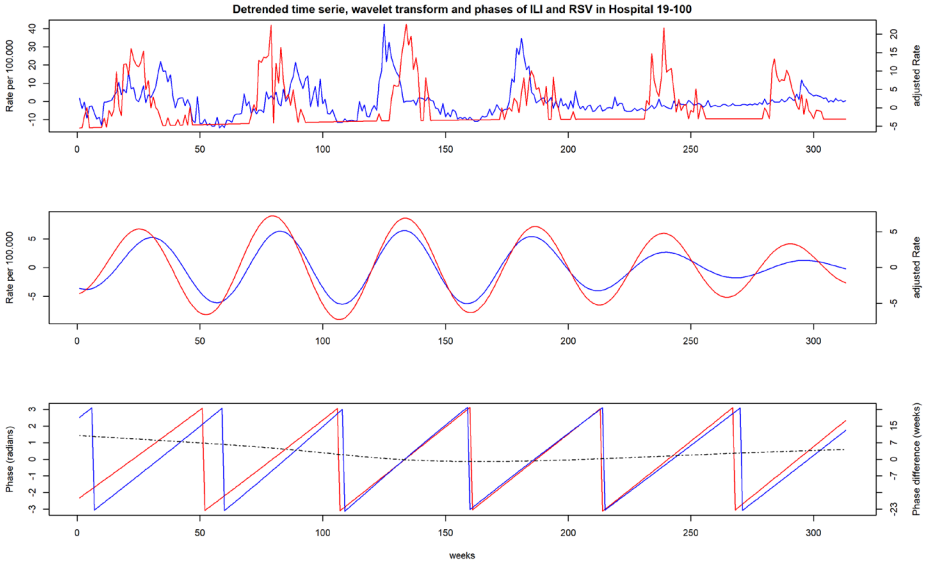
Detrended time serie, wavelet transform and phases of ILI and RSV in Hospital 19-100
Rate per 100,000
adjusted Rate
Phase (radians)
Phase difference (weeks)
weeks

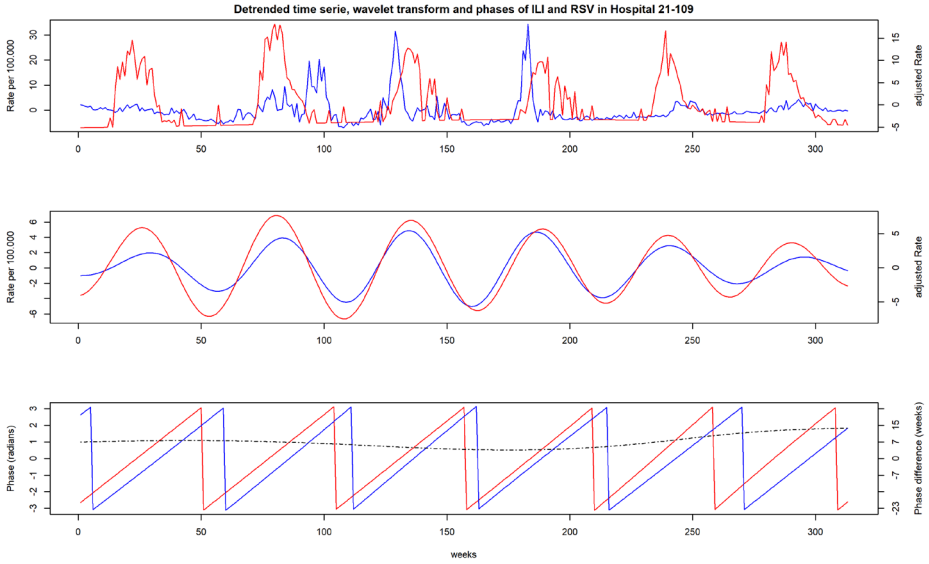
Detrended time serie, wavelet transform and phases of ILI and RSV in Hospital 21-109
Rate per 100,000
adjusted Rate
Phase (radians)
Phase difference (weeks)
weeks

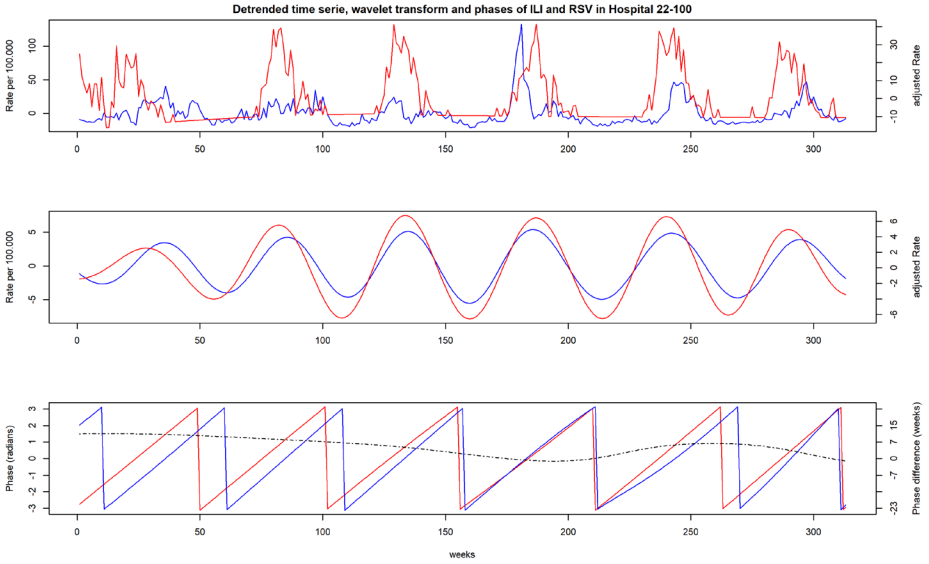
Detrended time serie, wavelet transform and phases of ILI and RSV in Hospital 22-100
Rate per 100,000
adjusted Rate
Phase (radians)
Phase difference (weeks)
weeks

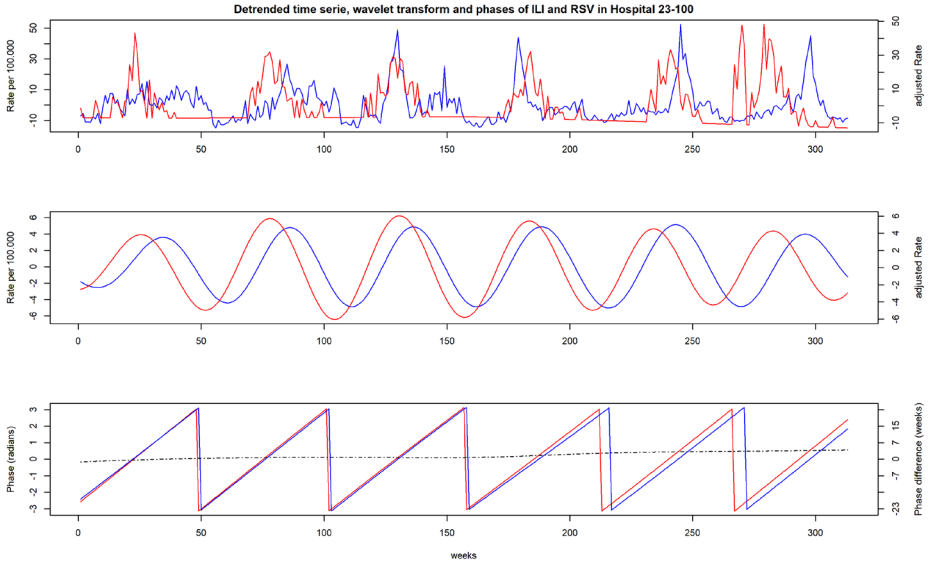
Detrended time serie, wavelet transform and phases of ILI and RSV in Hospital 23-100
Rate per 100,000
adjusted Rate
Phase (radians)
Phase difference (weeks)
weeks

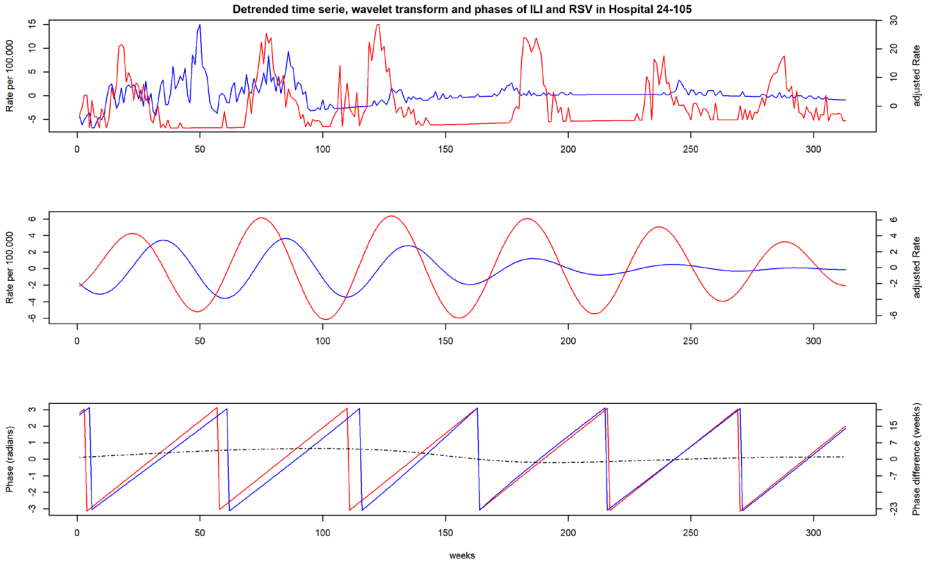
Detrended time serie, wavelet transform and phases of ILI and RSV in Hospital 24-105
Rate per 100,000
adjusted Rate
Phase (radians)
Phase difference (weeks)
weeks

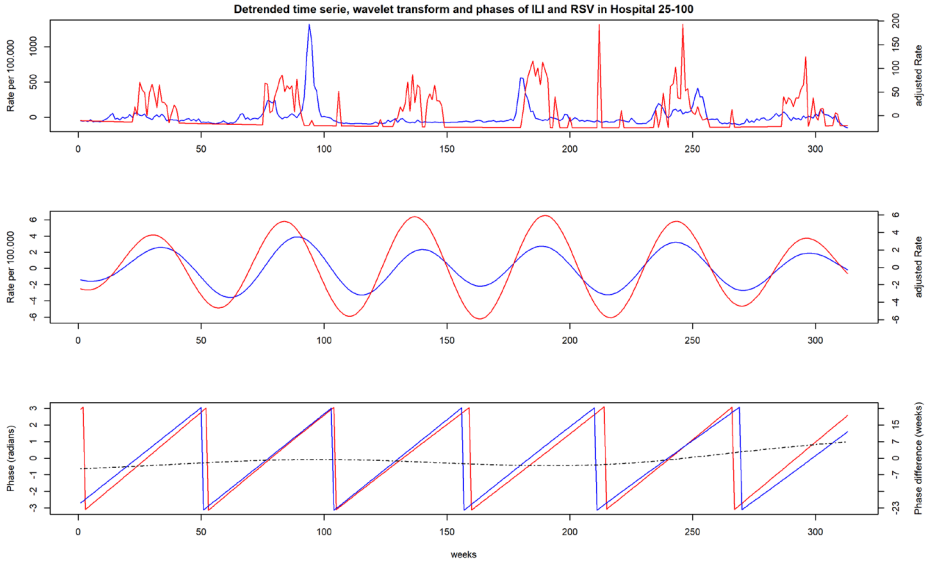
Detrended time serie, wavelet transform and phases of ILI and RSV in Hospital 25-100
Rate per 100,000
adjusted Rate
Phase (radians)
Phase difference (weeks)
weeks

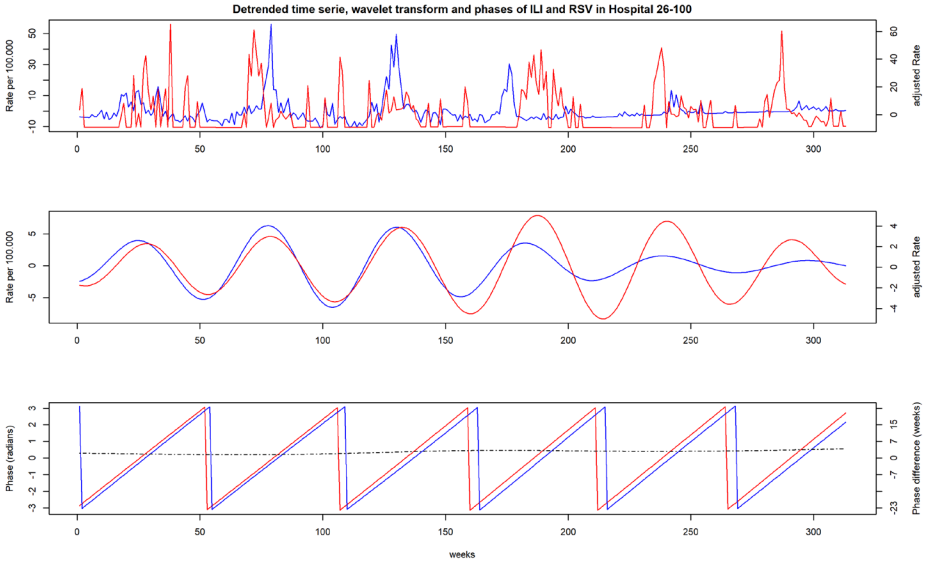
Detrended time serie, wavelet transform and phases of ILI and RSV in Hospital 26-100
Rate per 100,000
adjusted Rate
Phase (radians)
Phase difference (weeks)
weeks

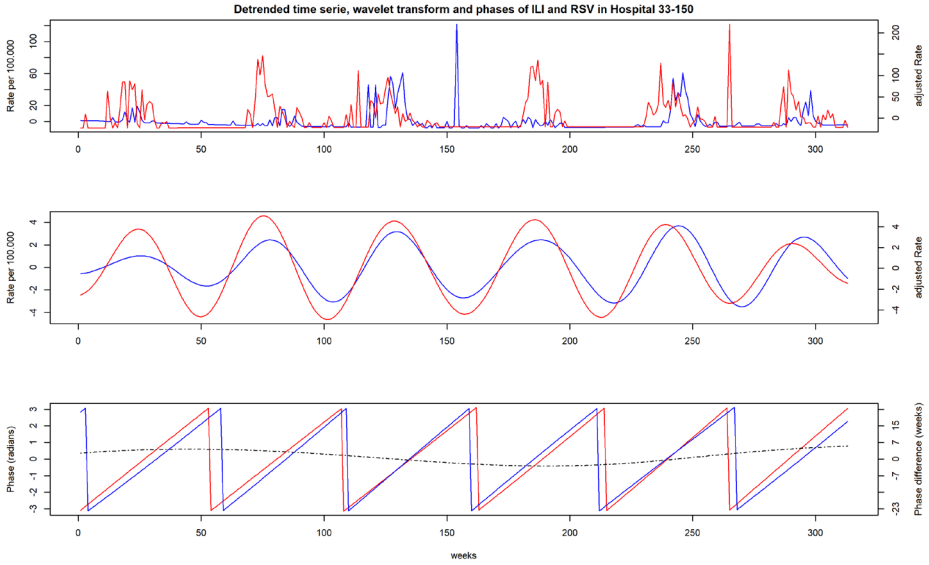
Detrended time serie, wavelet transform and phases of ILI and RSV in Hospital 33-150
Rate per 100,000
adjusted Rate
Phase (radians)
Phase difference (weeks)
weeks

## 5. Detrended rate time series, wavelet transformed rates and phases of ILI and parainfluenza by hospital

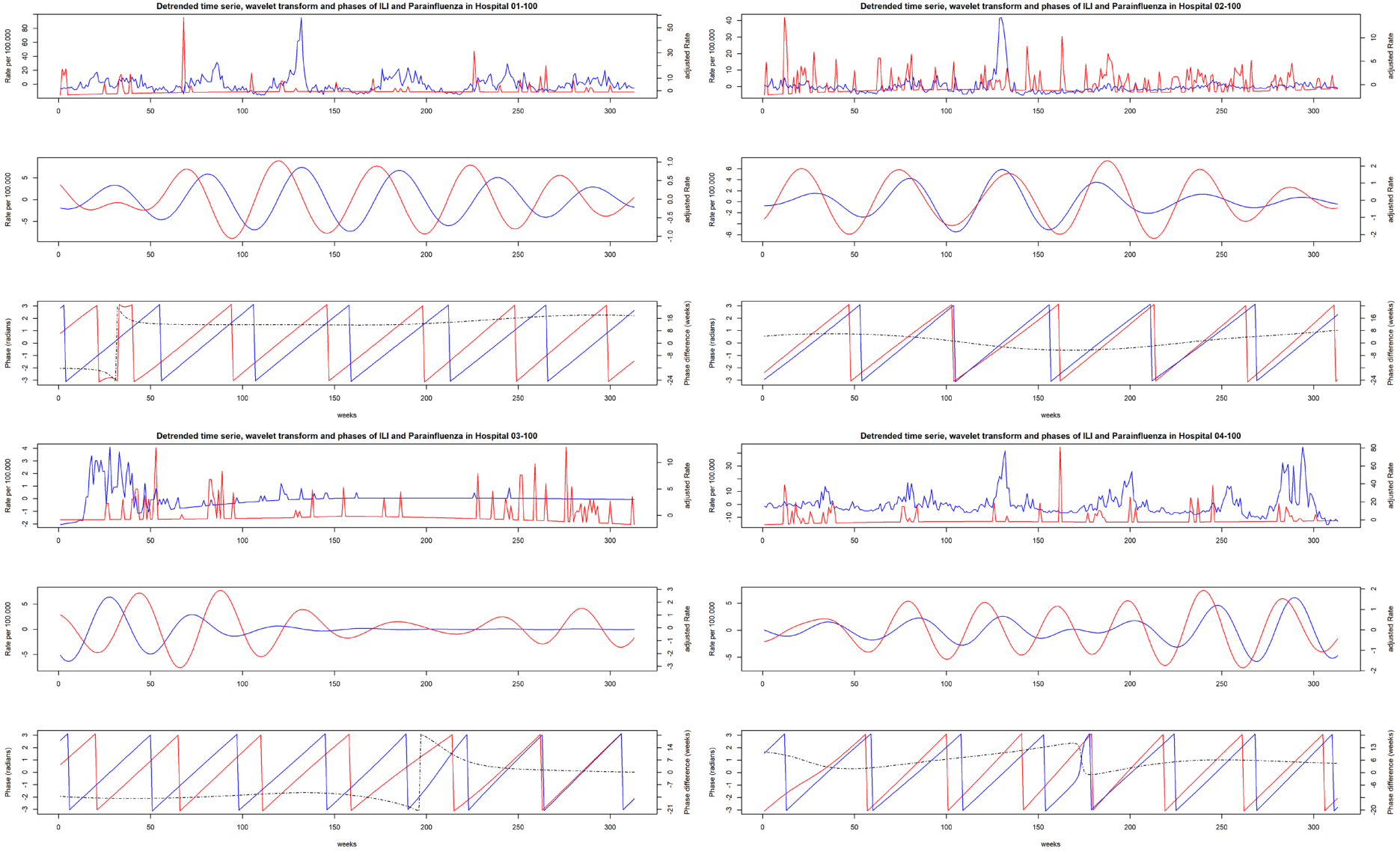

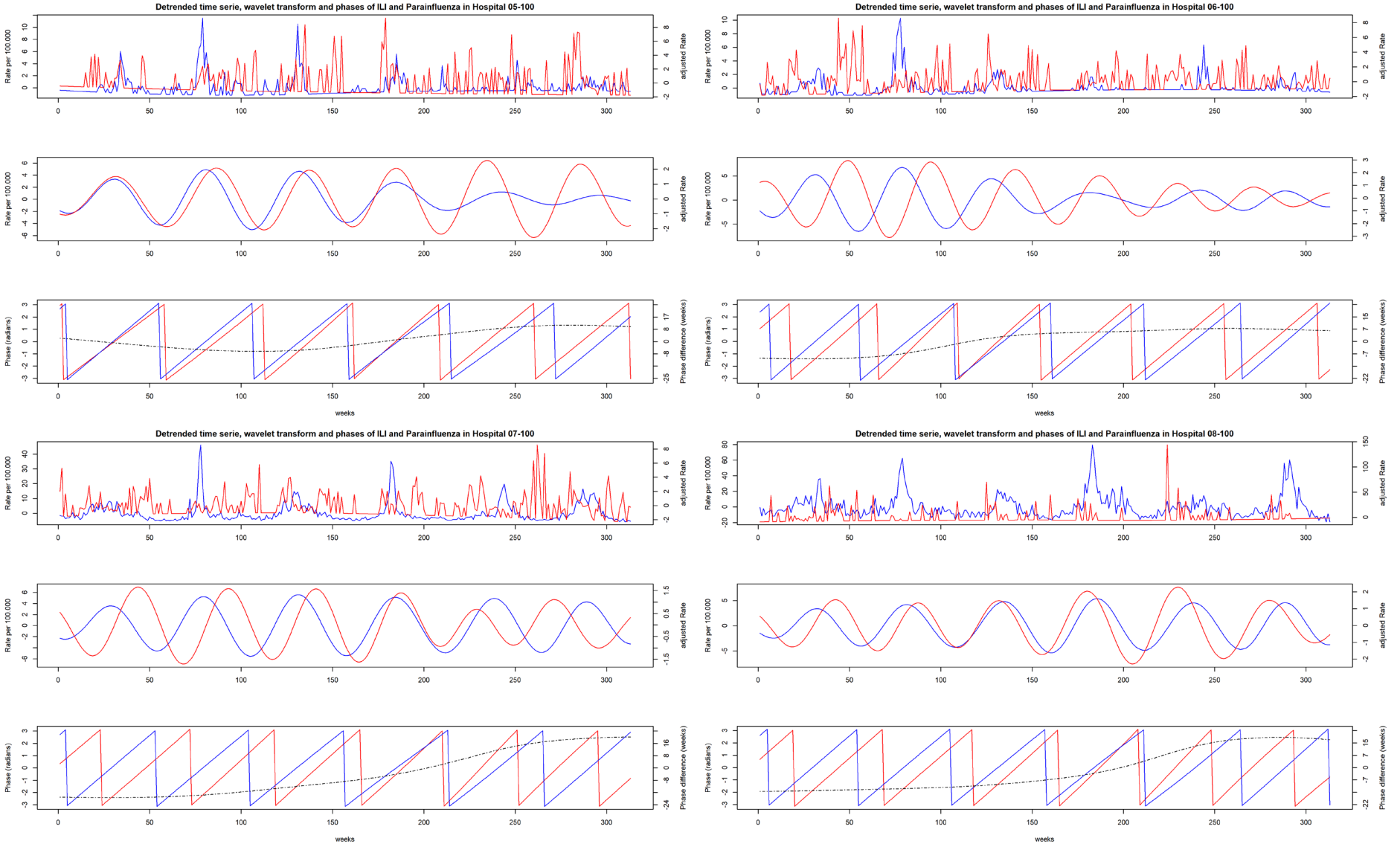
Detrended time serie, wavelet transform and phases of ILI and Parainfluenza in Hospital 05-100
Rate per 100.000
adjusted Rate
Phase (radians)
Phase difference (weeks)
weeks
Detrended time serie, wavelet transform and phases of ILI and Parainfluenza in Hospital 06-100
Rate per 100.000
adjusted Rate
Phase (radians)
Phase difference (weeks)
weeks
Detrended time serie, wavelet transform and phases of ILI and Parainfluenza in Hospital 07-100
Rate per 100.000
adjusted Rate
Phase (radians)
Phase difference (weeks)
weeks
Detrended time serie, wavelet transform and phases of ILI and Parainfluenza in Hospital 08-100
Rate per 100.000
adjusted Rate
Phase (radians)
Phase difference (weeks)
weeks

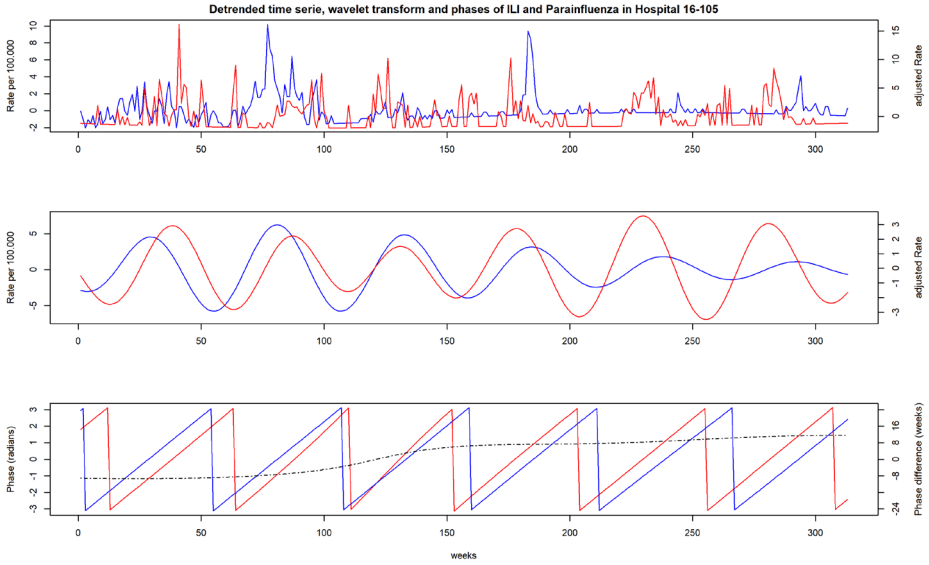
Detrended time serie, wavelet transform and phases of ILI and Parainfluenza in Hospital 16-105
Rate per 100,000
adjusted Rate
Phase (radians)
Phase difference (weeks)
weeks

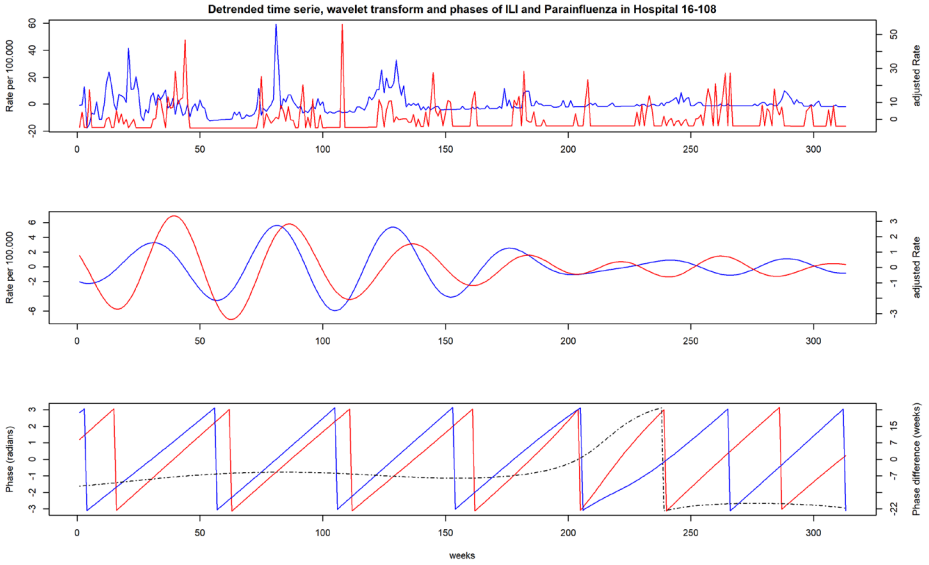
Detrended time serie, wavelet transform and phases of ILI and Parainfluenza in Hospital 16-108
Rate per 100,000
adjusted Rate
Phase (radians)
Phase difference (weeks)
weeks

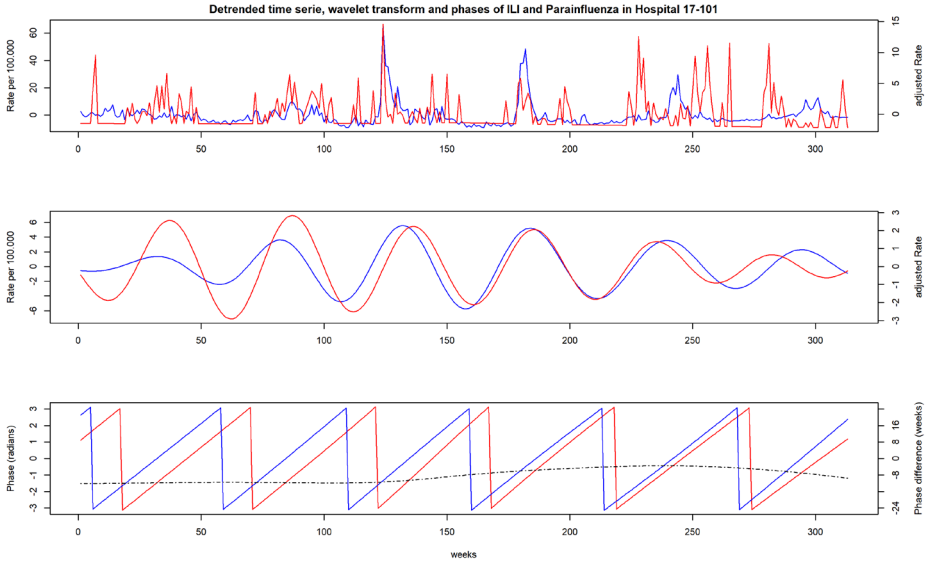
Detrended time serie, wavelet transform and phases of ILI and Parainfluenza in Hospital 17-101
Rate per 100,000
adjusted Rate
Phase (radians)
Phase difference (weeks)
weeks

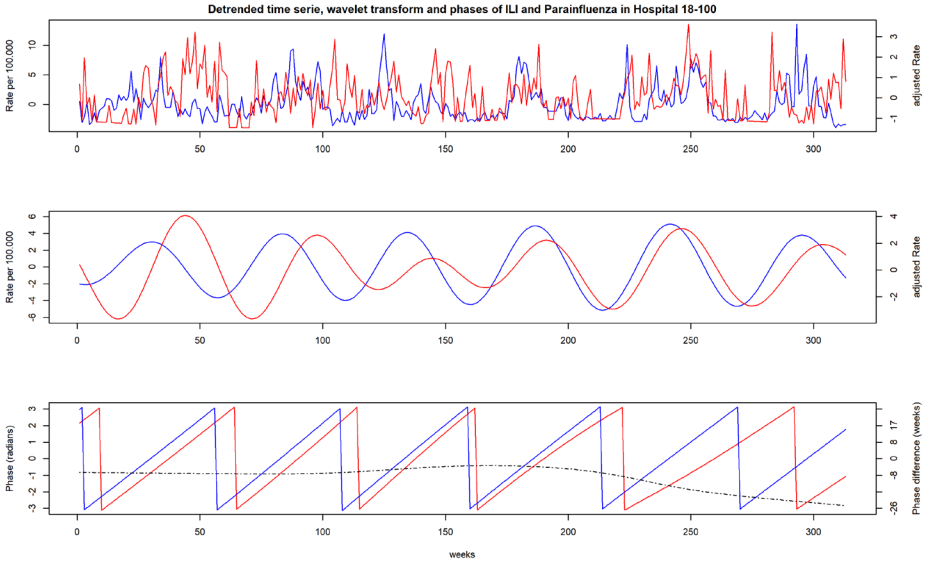
Detrended time serie, wavelet transform and phases of ILI and Parainfluenza in Hospital 18-100
Rate per 100,000
adjusted Rate
Phase (radians)
Phase difference (weeks)
weeks

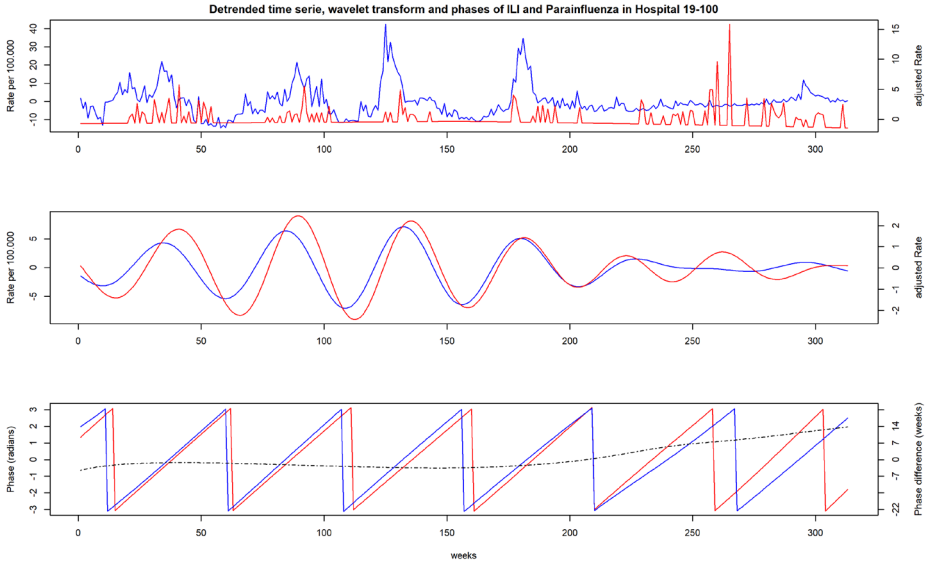
Detrended time serie, wavelet transform and phases of ILI and Parainfluenza in Hospital 19-100
Rate per 100.000
adjusted Rate
Phase (radians)
Phase difference (weeks)
weeks

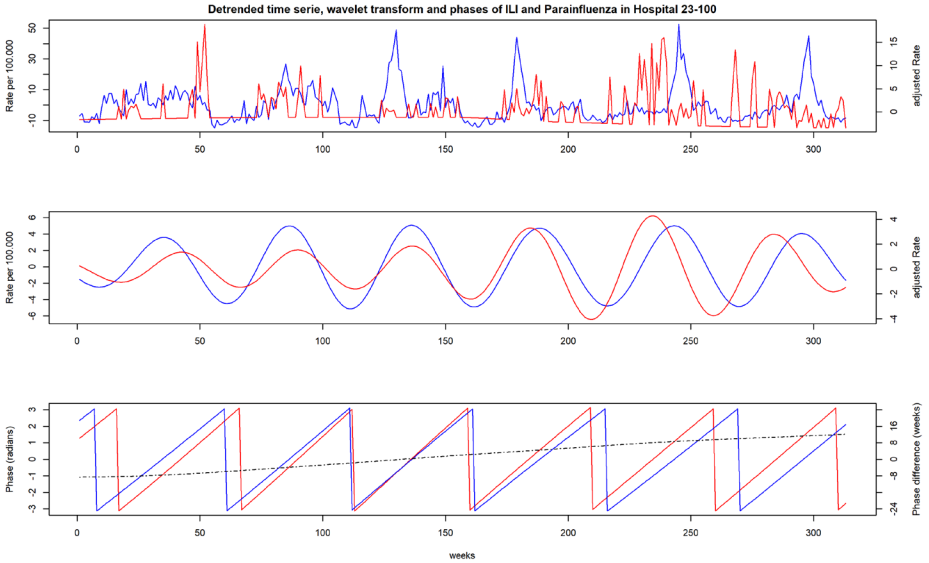
Detrended time serie, wavelet transform and phases of ILI and Parainfluenza in Hospital 23-100
Rate per 100.000
adjusted Rate
Phase (radians)
Phase difference (weeks)
weeks

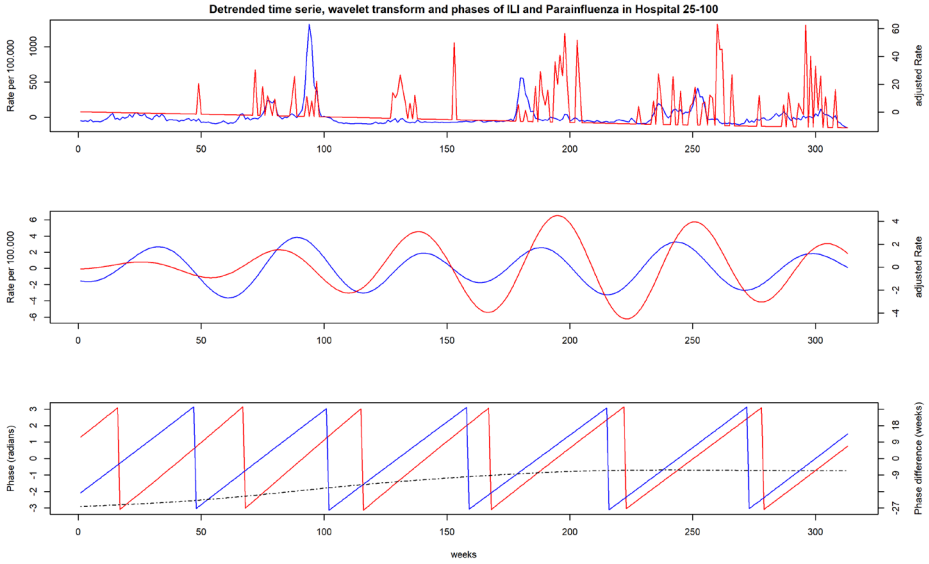
Detrended time serie, wavelet transform and phases of ILI and Parainfluenza in Hospital 25-100
Rate per 100.000
adjusted Rate
Phase (radians)
Phase difference (weeks)
weeks

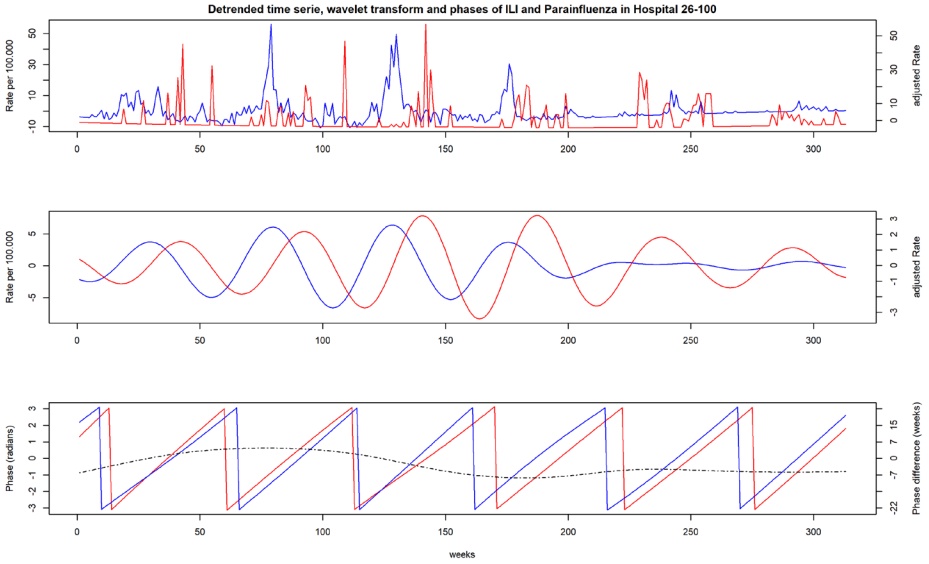
Detrended time serie, wavelet transform and phases of ILI and Parainfluenza in Hospital 26-100
Rate per 100.000
adjusted Rate
Phase (radians)
Phase difference (weeks)
weeks

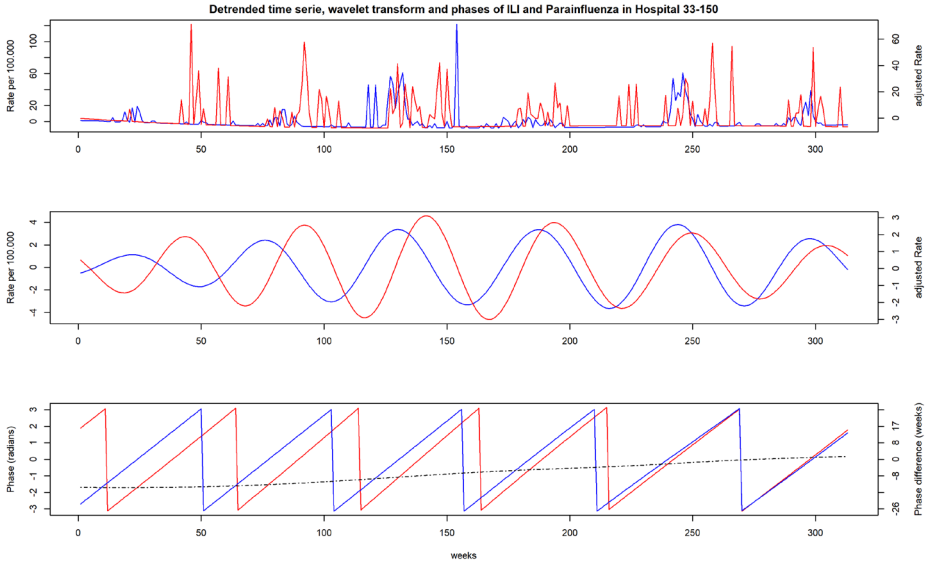
Detrended time serie, wavelet transform and phases of ILI and Parainfluenza in Hospital 33-150
Rate per 100,000
adjusted Rate
Rate per 100,000
adjusted Rate
Phase (radians)
Phase difference (weeks)
weeks

## 6. Detrended rate time series, wavelet transformed rates and phases of ILI and adenovirus by hospital

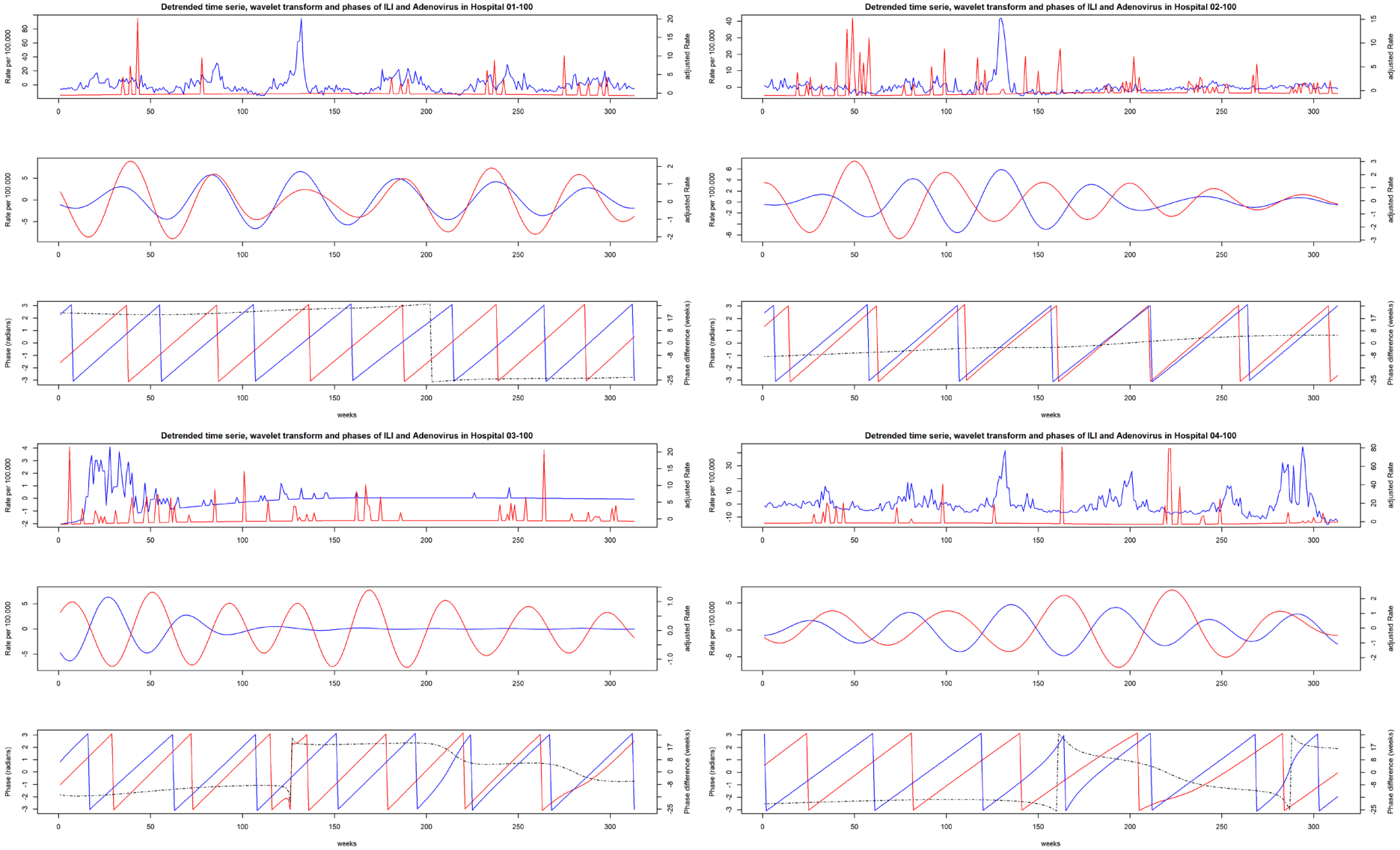

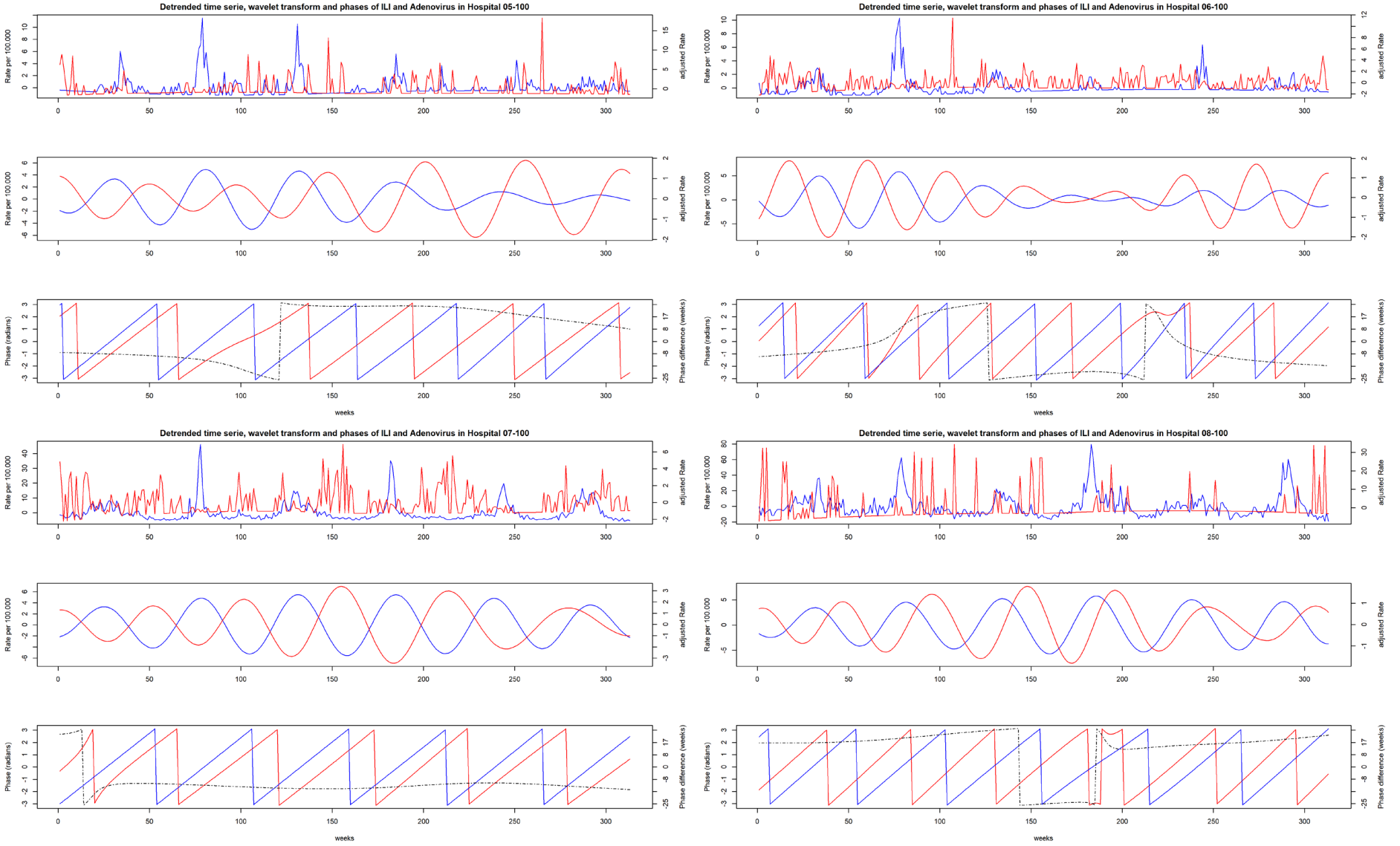
Detrended time serie, wavelet transform and phases of ILI and Adenovirus in Hospital 05-100
Detrended time serie, wavelet transform and phases of ILI and Adenovirus in Hospital 06-100
Detrended time serie, wavelet transform and phases of ILI and Adenovirus in Hospital 07-100
Detrended time serie, wavelet transform and phases of ILI and Adenovirus in Hospital 08-100
Rate per 100,000
adjusted Rate
Phase (radians)
Phase difference (weeks)
weeks

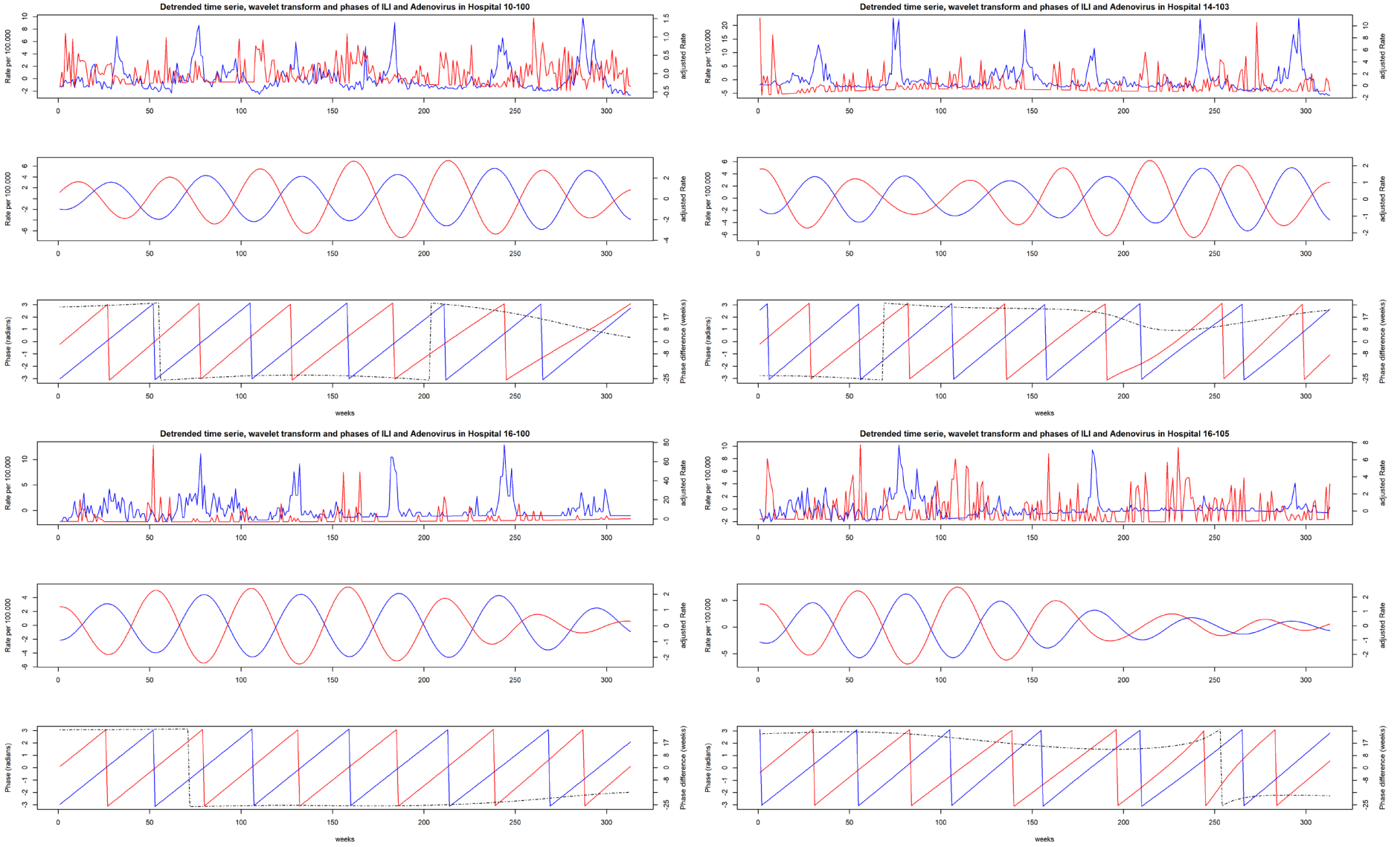
Detrended time serie, wavelet transform and phases of ILI and Adenovirus in Hospital 10-100
Rate per 100,000
adjusted Rate
Phase (radians)
Phase difference (weeks)
weeks
Detrended time serie, wavelet transform and phases of ILI and Adenovirus in Hospital 14-103
Rate per 100,000
adjusted Rate
Phase (radians)
Phase difference (weeks)
weeks
Detrended time serie, wavelet transform and phases of ILI and Adenovirus in Hospital 16-100
Rate per 100,000
adjusted Rate
Phase (radians)
Phase difference (weeks)
weeks
Detrended time serie, wavelet transform and phases of ILI and Adenovirus in Hospital 16-105
Rate per 100,000
adjusted Rate
Phase (radians)
Phase difference (weeks)
weeks

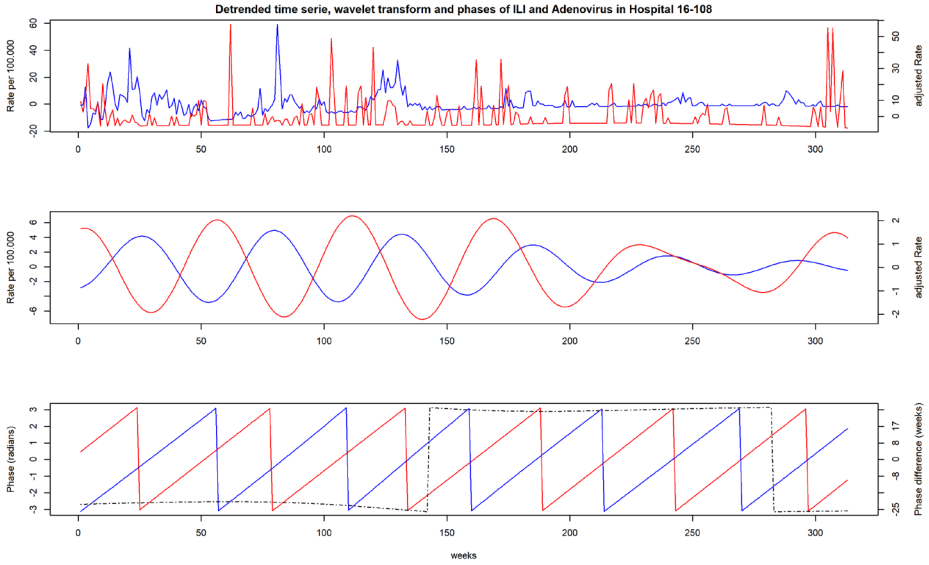
Detrended time serie, wavelet transform and phases of ILI and Adenovirus in Hospital 16-108
Rate per 100.000
adjusted Rate
Phase (radians)
Phase difference (weeks)
weeks

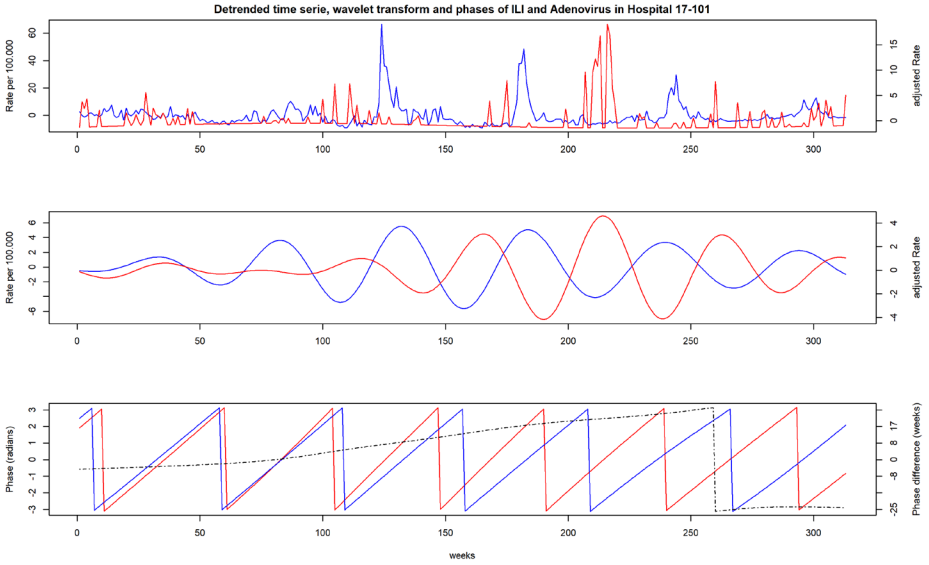
Detrended time serie, wavelet transform and phases of ILI and Adenovirus in Hospital 17-101
Rate per 100.000
adjusted Rate
Phase (radians)
Phase difference (weeks)
weeks

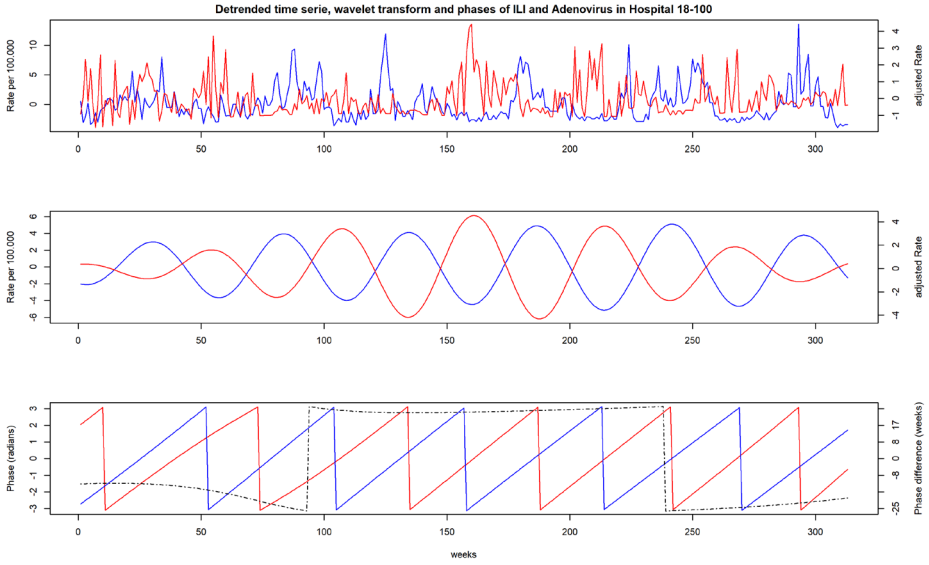
Detrended time serie, wavelet transform and phases of ILI and Adenovirus in Hospital 18-100
Rate per 100.000
adjusted Rate
Phase (radians)
Phase difference (weeks)
weeks

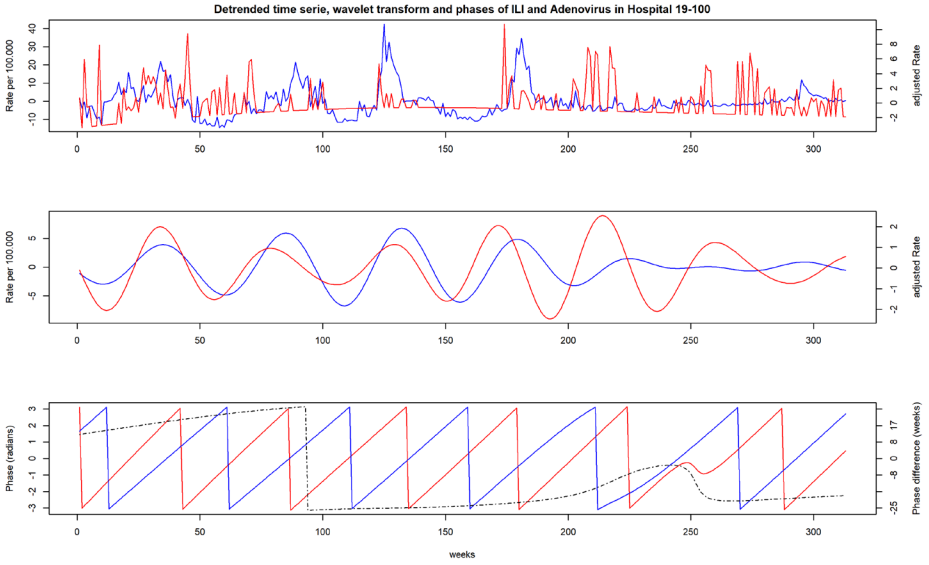
Detrended time serie, wavelet transform and phases of ILI and Adenovirus in Hospital 19-100
Rate per 100.000
adjusted Rate
Phase (radians)
Phase difference (weeks)
weeks

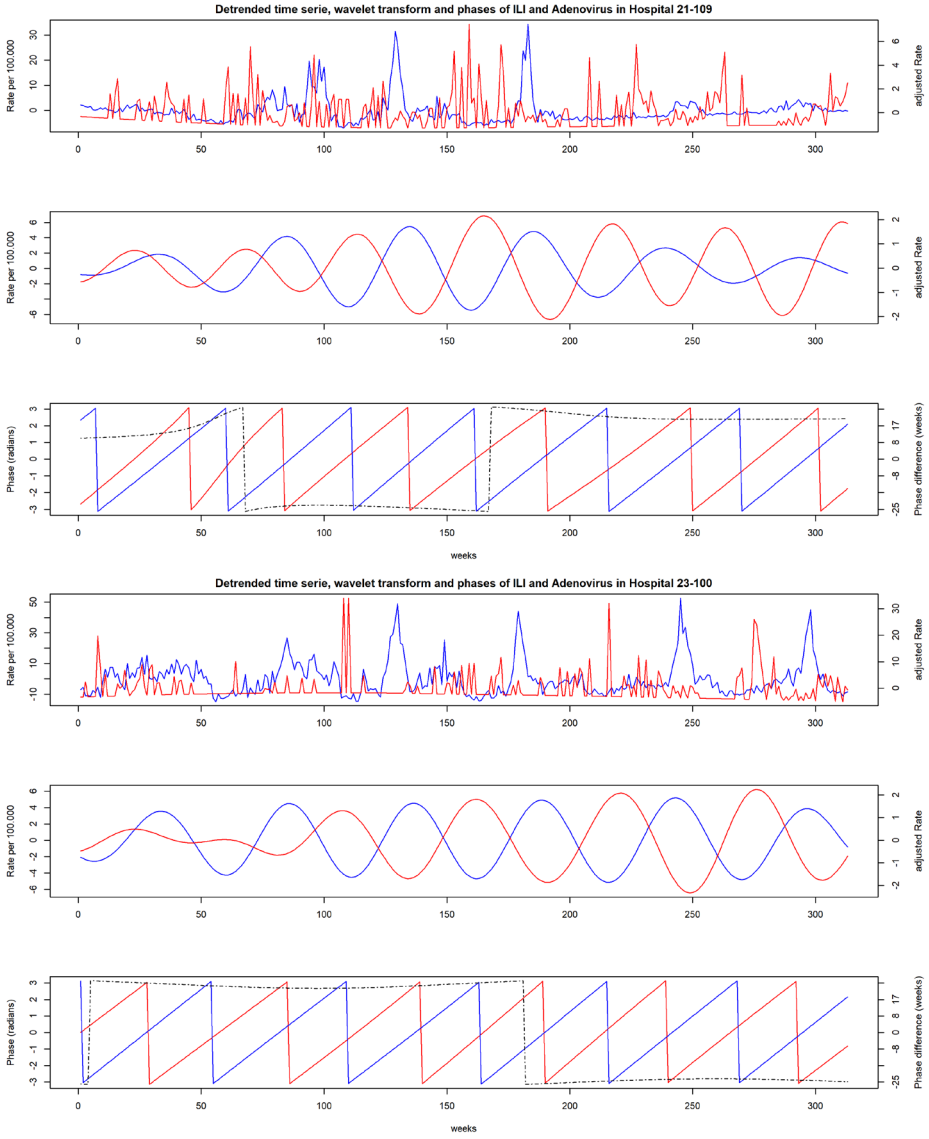
Detrended time serie, wavelet transform and phases of ILI and Adenovirus in Hospital 21-109
Rate per 100,000
adjusted Rate
Phase (radians)
Phase difference (weeks)
weeks

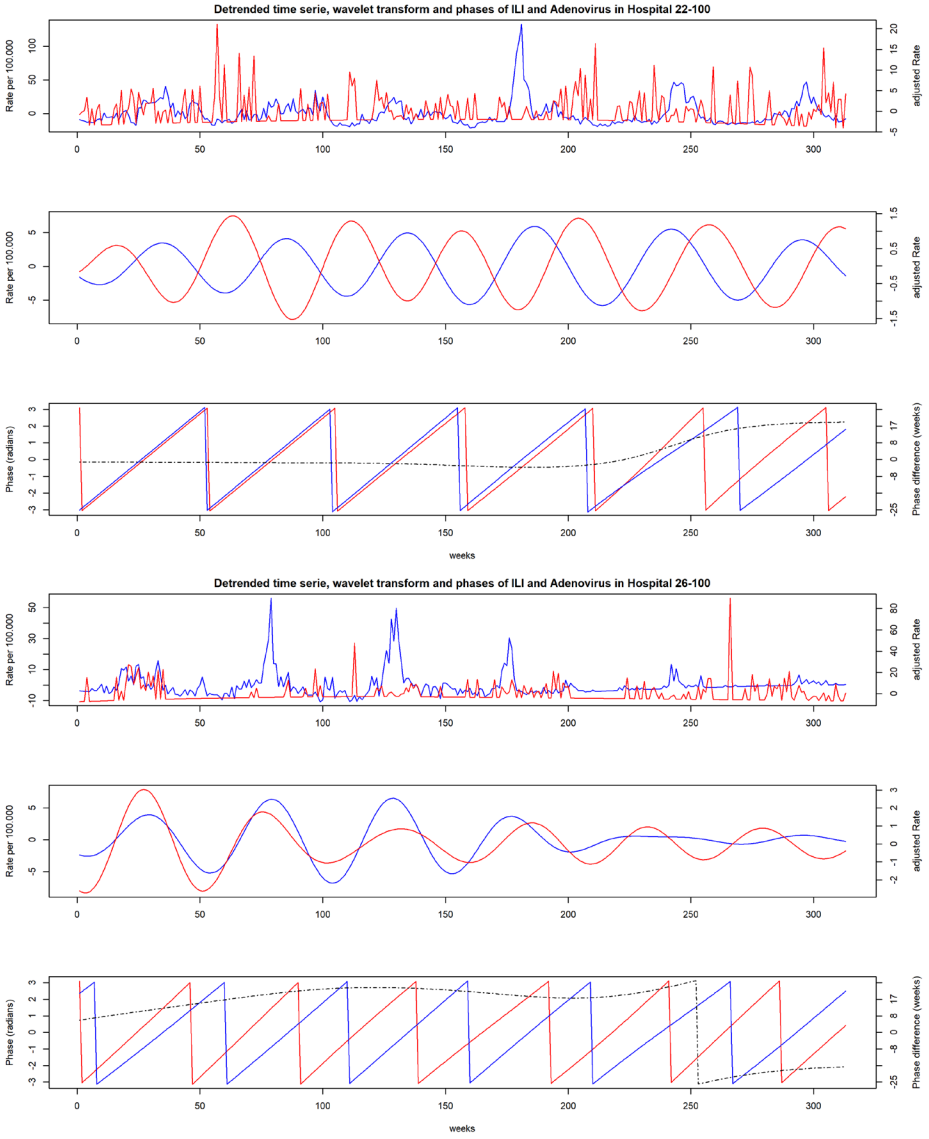
Detrended time serie, wavelet transform and phases of ILI and Adenovirus in Hospital 22-100
Rate per 100,000
adjusted Rate
Phase (radians)
Phase difference (weeks)
weeks


Detrended time serie, wavelet transform and phases of ILI and Adenovirus in Hospital 23-100
Rate per 100,000
adjusted Rate
Phase (radians)
Phase difference (weeks)
weeks


Detrended time serie, wavelet transform and phases of ILI and Adenovirus in Hospital 26-100
Rate per 100,000
adjusted Rate
Phase (radians)
Phase difference (weeks)
weeks

## 7. Detrended rate time series, wavelet transformed rates and phases of ILI and metapneumovirus by hospital

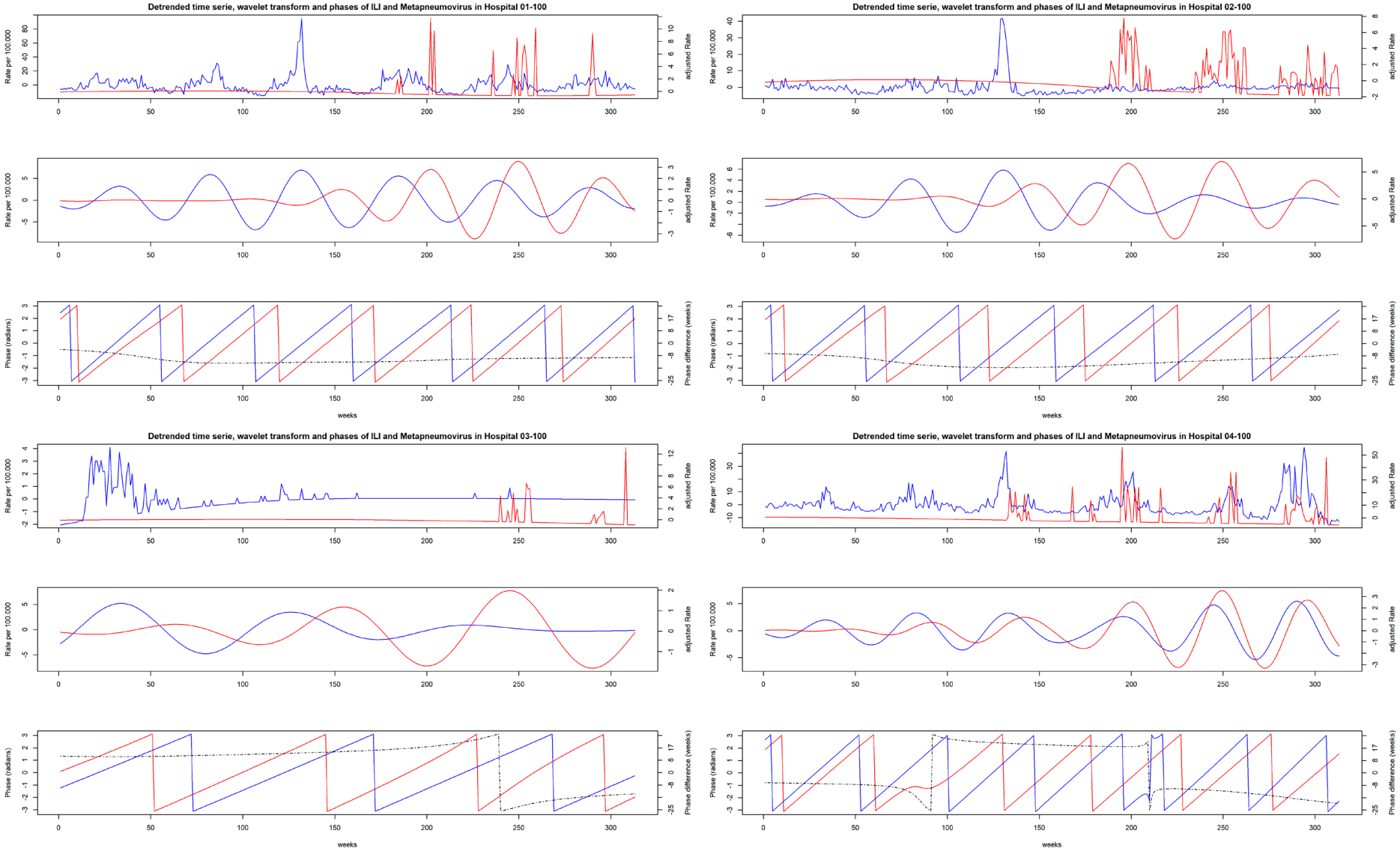

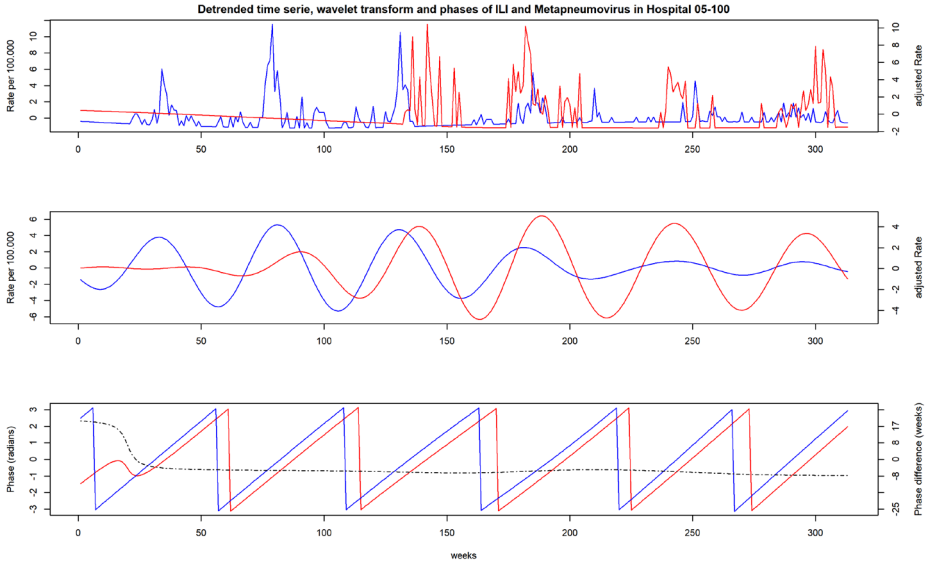
Detrended time serie, wavelet transform and phases of ILI and Metapneumovirus in Hospital 05-100
Rate per 100.000
adjusted Rate
Phase (radians)
Phase difference (weeks)
weeks

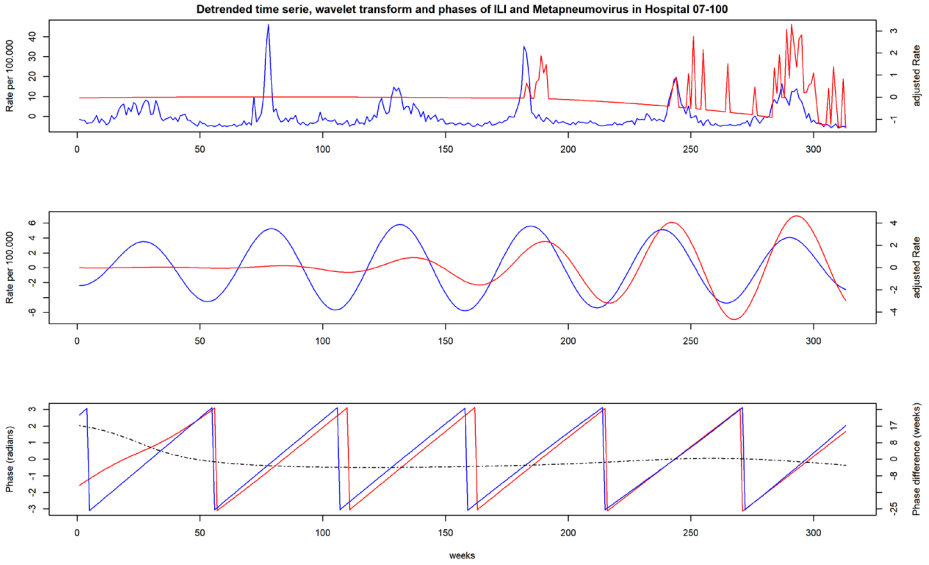
Detrended time serie, wavelet transform and phases of ILI and Metapneumovirus in Hospital 07-100
Rate per 100.000
adjusted Rate
Phase (radians)
Phase difference (weeks)
weeks

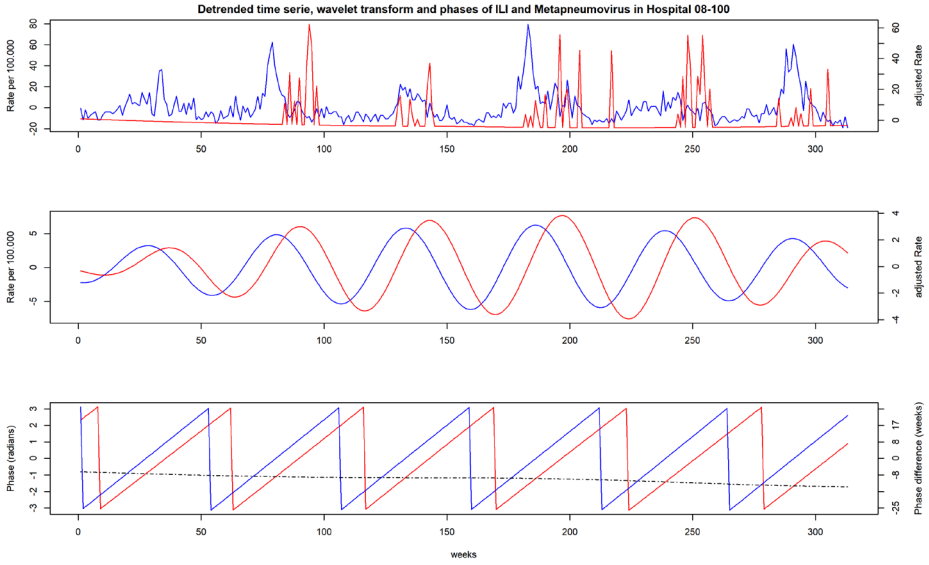
Detrended time serie, wavelet transform and phases of ILI and Metapneumovirus in Hospital 08-100
Rate per 100.000
adjusted Rate
Phase (radians)
Phase difference (weeks)
weeks

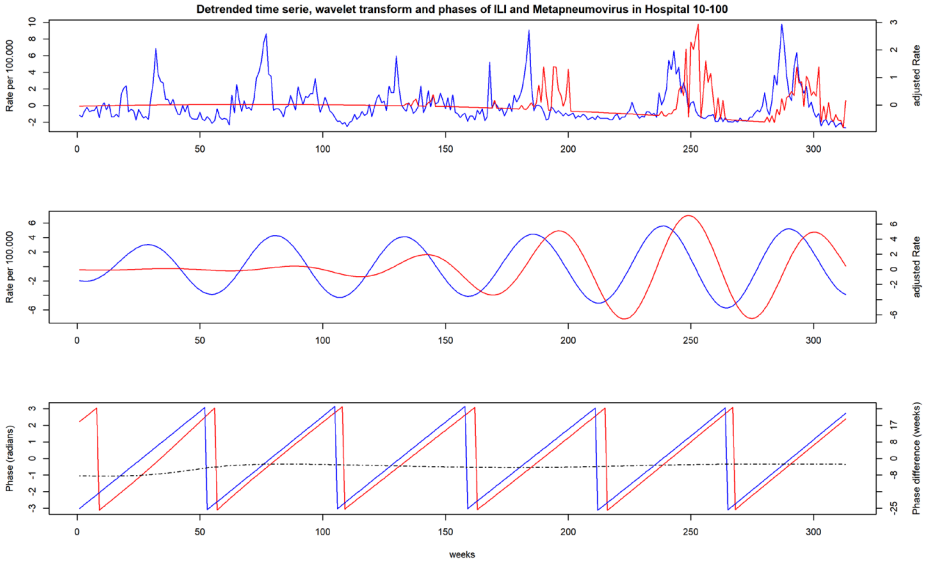
Detrended time serie, wavelet transform and phases of ILI and Metapneumovirus in Hospital 10-100
Rate per 100.000
adjusted Rate
Phase (radians)
Phase difference (weeks)
weeks

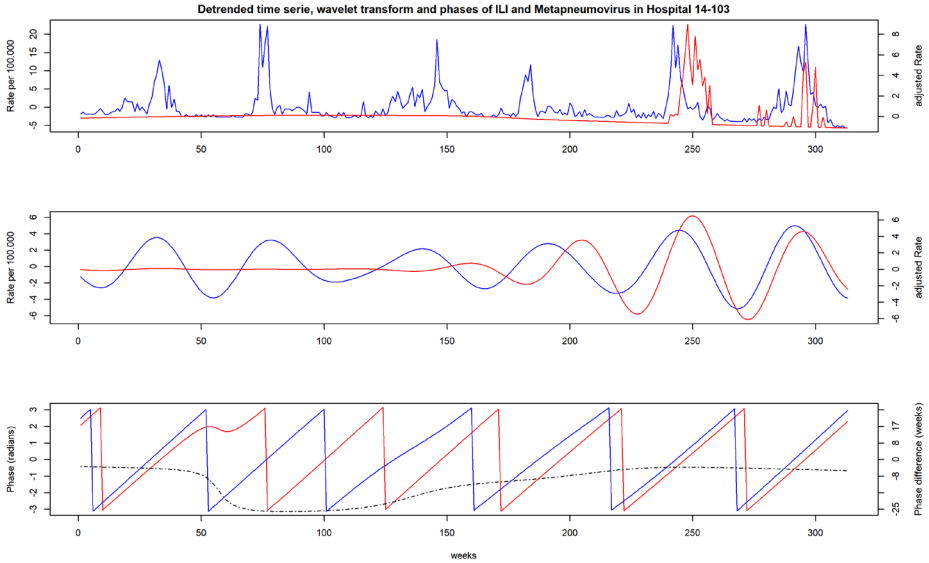
Detrended time serie, wavelet transform and phases of ILI and Metapneumovirus in Hospital 14-103
Rate per 100,000
adjusted Rate
Phase (radians)
Phase difference (weeks)
weeks

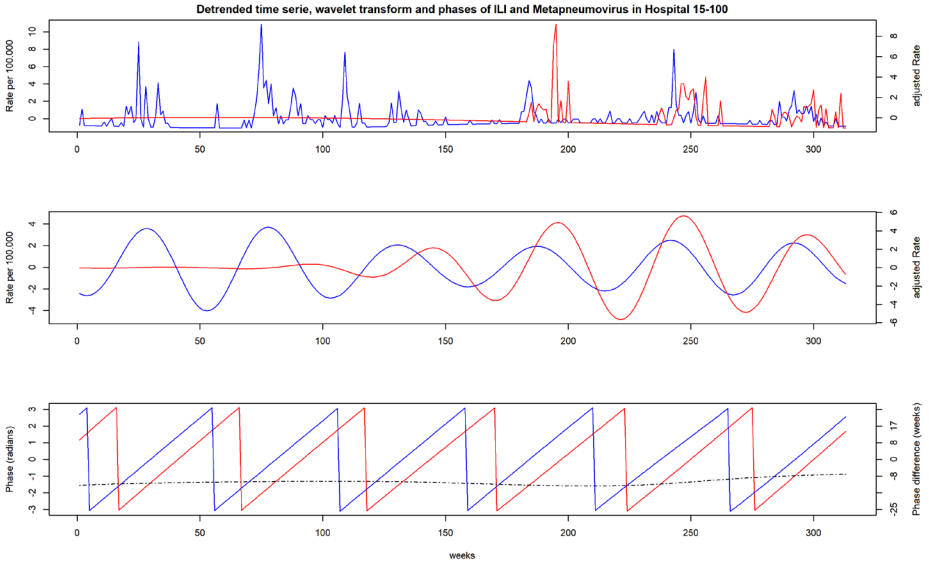
Detrended time serie, wavelet transform and phases of ILI and Metapneumovirus in Hospital 15-100
Rate per 100,000
adjusted Rate
Phase (radians)
Phase difference (weeks)
weeks

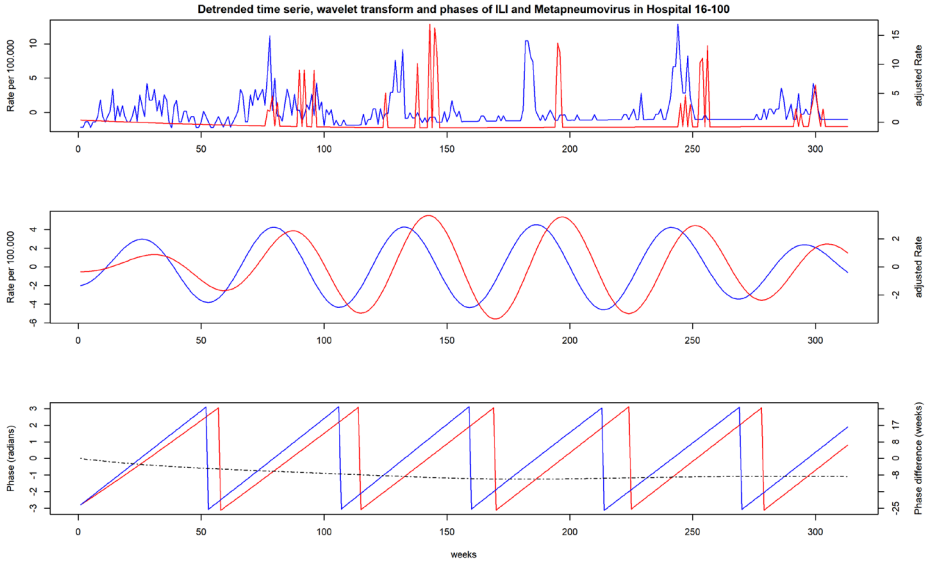
Detrended time serie, wavelet transform and phases of ILI and Metapneumovirus in Hospital 16-100
Rate per 100,000
adjusted Rate
Phase (radians)
Phase difference (weeks)
weeks

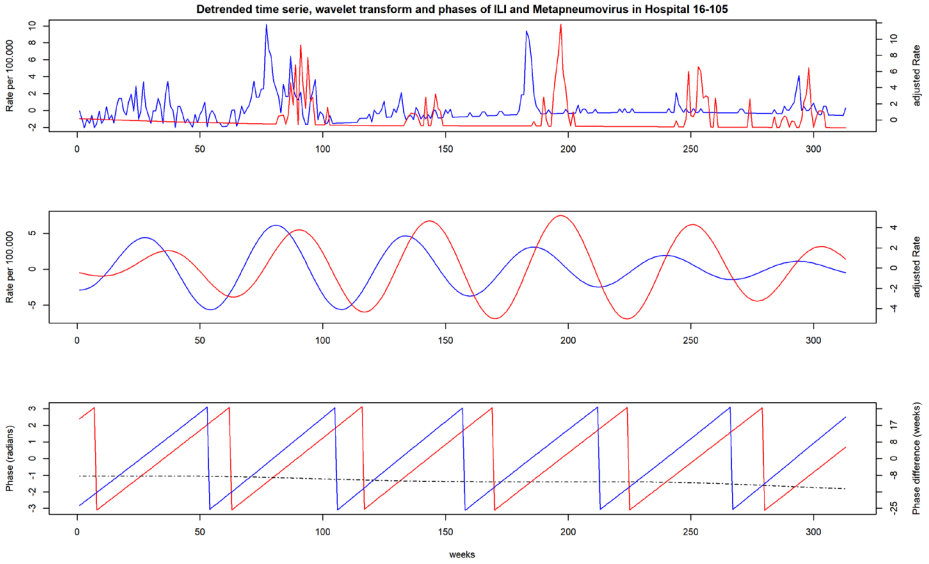
Detrended time serie, wavelet transform and phases of ILI and Metapneumovirus in Hospital 16-105
Rate per 100,000
adjusted Rate
Phase (radians)
Phase difference (weeks)
weeks

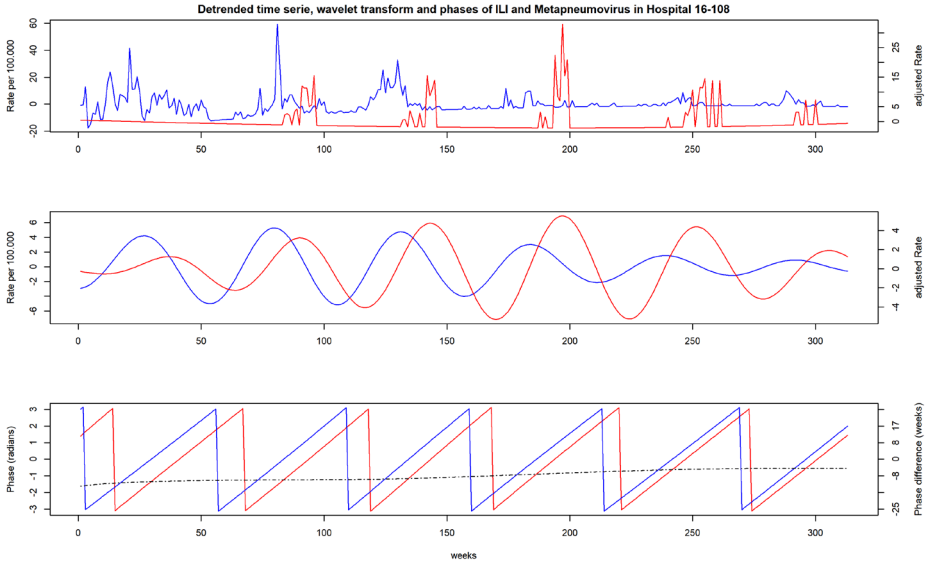
Detrended time serie, wavelet transform and phases of ILI and Metapneumovirus in Hospital 16-108
Rate per 100,000
adjusted Rate
Phase (radians)
Phase difference (weeks)
weeks

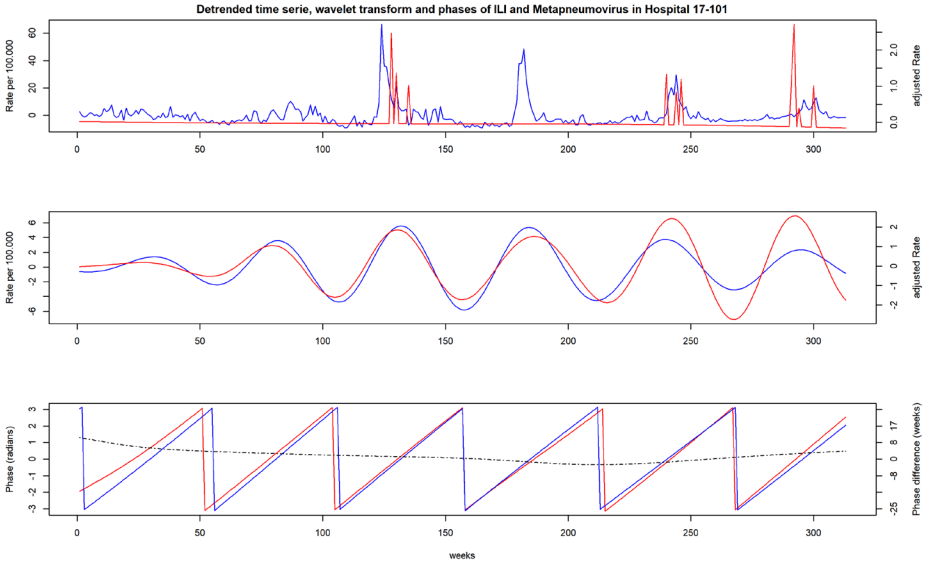
Detrended time serie, wavelet transform and phases of ILI and Metapneumovirus in Hospital 17-101
Rate per 100,000
adjusted Rate
Phase (radians)
Phase difference (weeks)
weeks

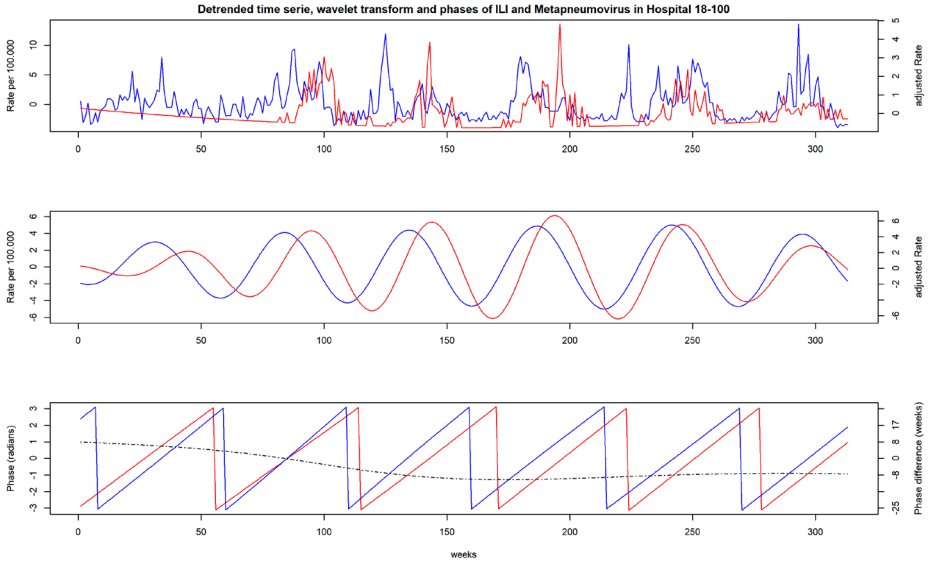
Detrended time serie, wavelet transform and phases of ILI and Metapneumovirus in Hospital 18-100
Rate per 100,000
adjusted Rate
Phase (radians)
Phase difference (weeks)
weeks

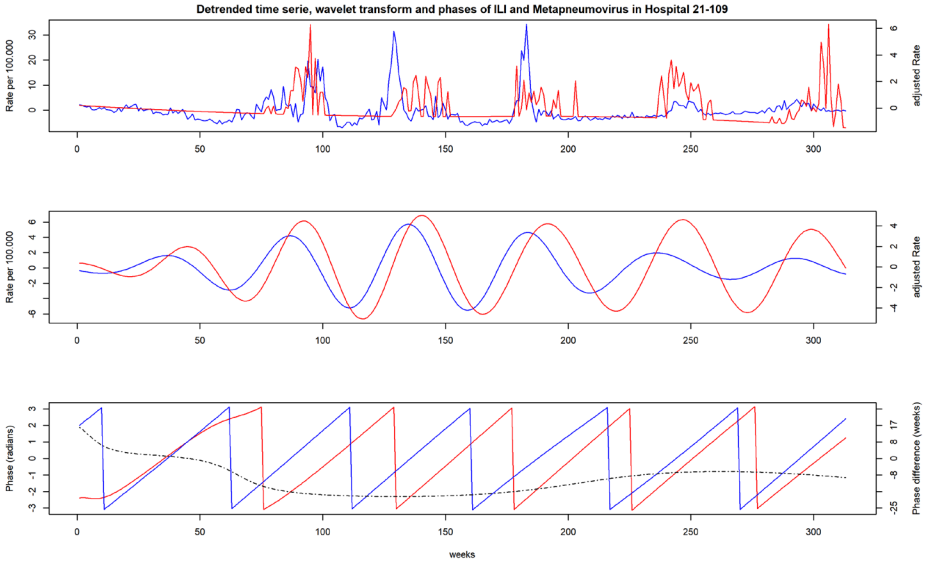
Detrended time serie, wavelet transform and phases of ILI and Metapneumovirus in Hospital 21-109
Rate per 100,000
adjusted Rate
Phase (radians)
Phase difference (weeks)
weeks

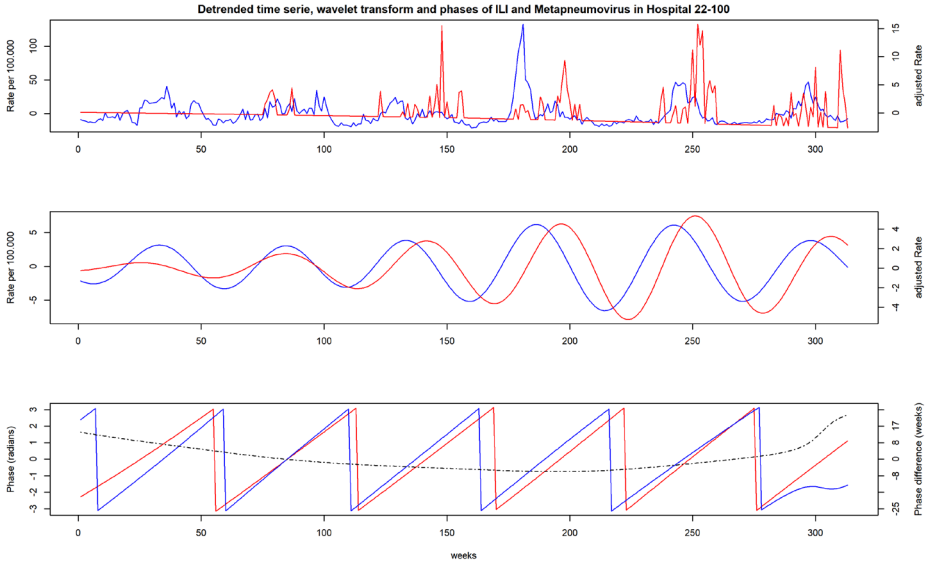
Detrended time serie, wavelet transform and phases of ILI and Metapneumovirus in Hospital 22-100
Rate per 100.000
adjusted Rate
Phase (radians)
Phase difference (weeks)
weeks

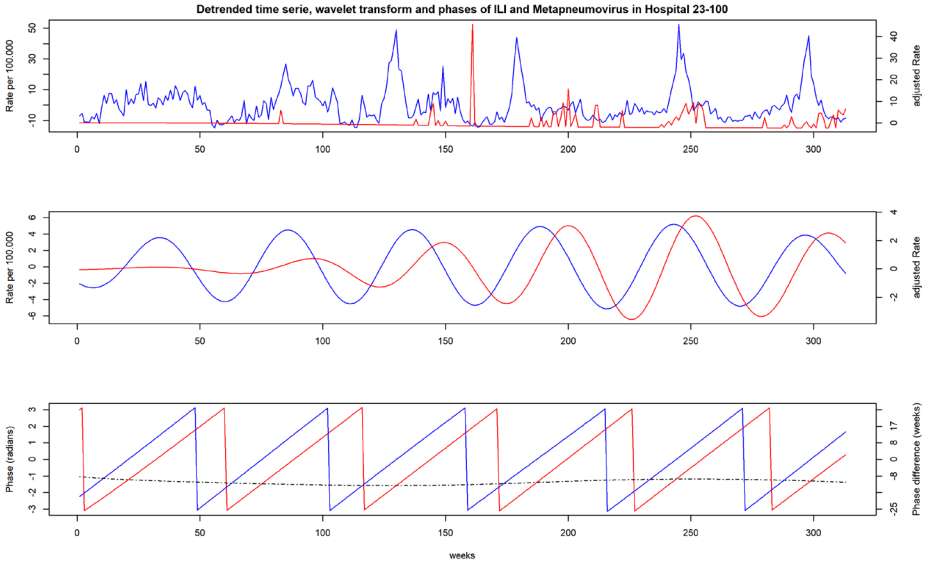
Detrended time serie, wavelet transform and phases of ILI and Metapneumovirus in Hospital 23-100
Rate per 100.000
adjusted Rate
Phase (radians)
Phase difference (weeks)
weeks

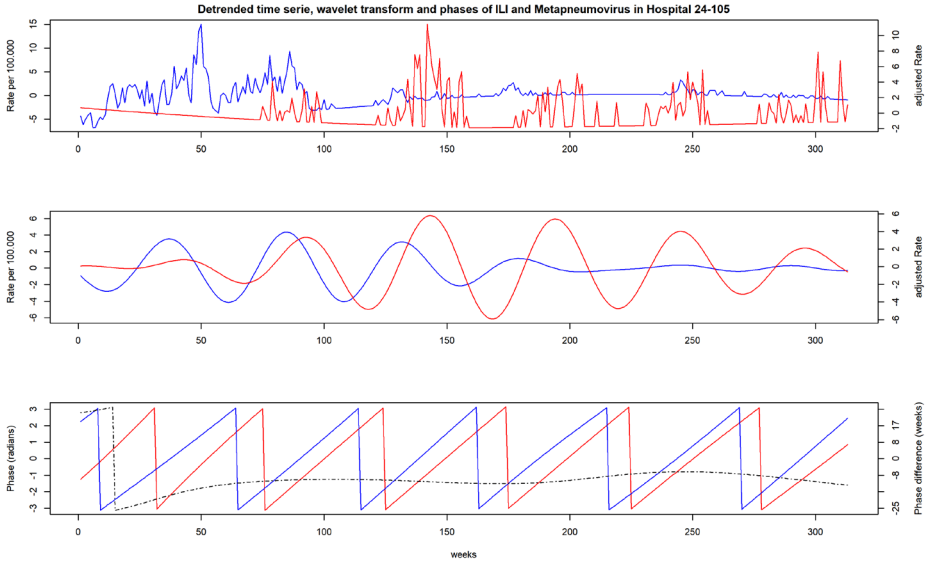
Detrended time serie, wavelet transform and phases of ILI and Metapneumovirus in Hospital 24-105
Rate per 100.000
adjusted Rate
Phase (radians)
Phase difference (weeks)
weeks

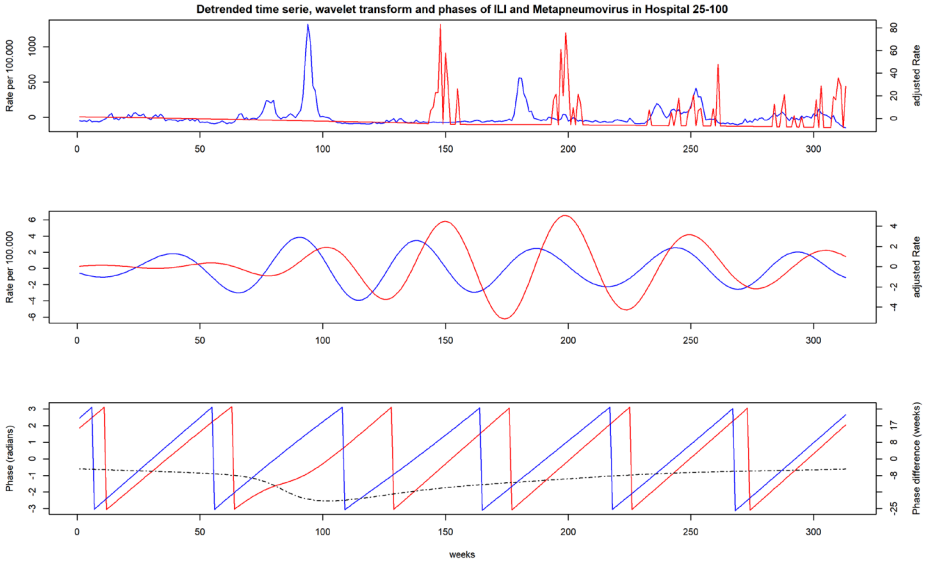
Detrended time serie, wavelet transform and phases of ILI and Metapneumovirus in Hospital 25-100
Rate per 100.000
adjusted Rate
Phase (radians)
Phase difference (weeks)
weeks

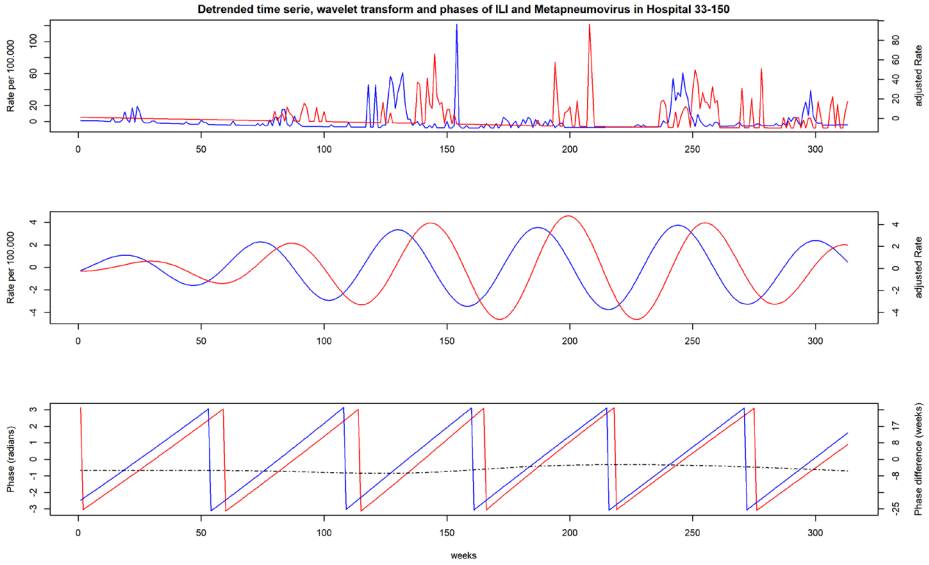
Detrended time serie, wavelet transform and phases of ILI and Metapneumovirus in Hospital 33-150
Rate per 100,000
adjusted Rate
Rate per 100,000
adjusted Rate
Phase (radians)
Phase difference (weeks)
weeks

**APPENDIX C: Selected and combined hospitals in Santiago, Chile 2011-2016**

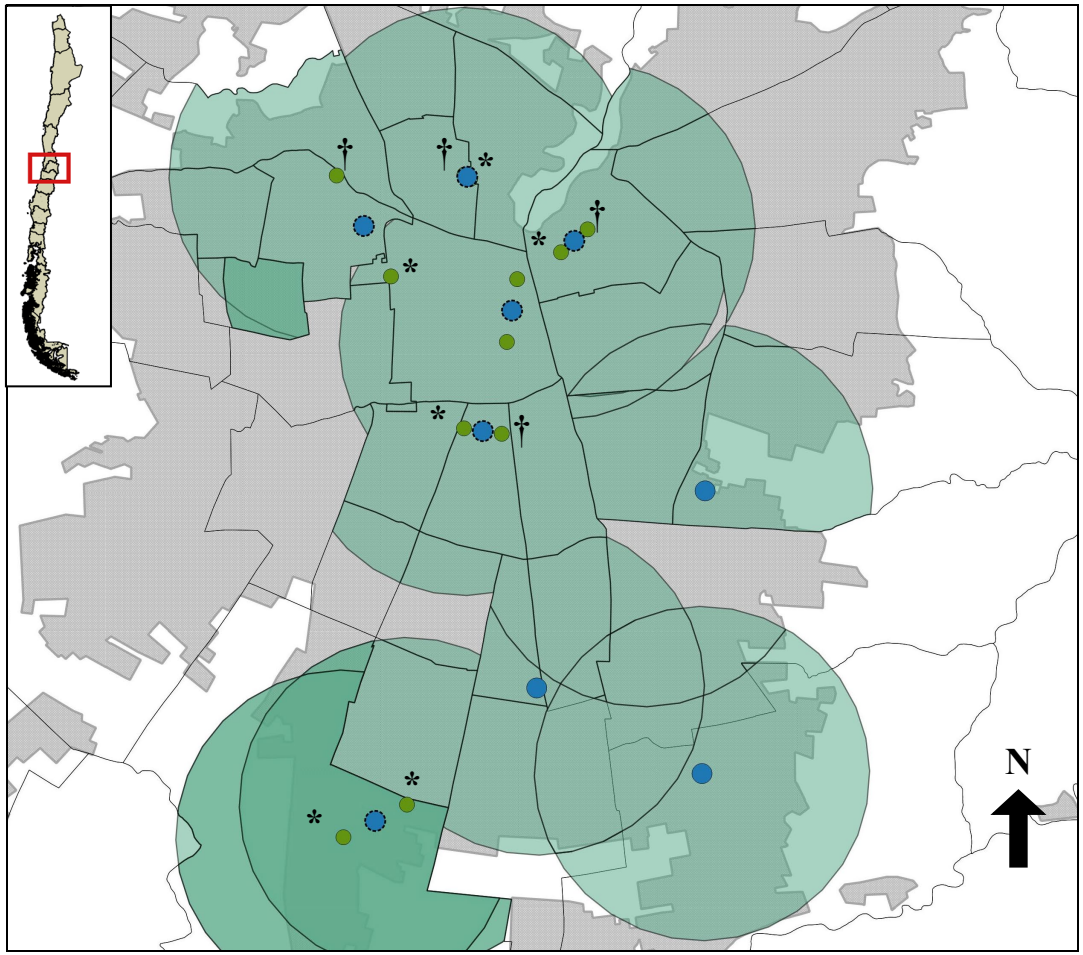


**Selected hospitals from Santiago.**
Blue dots: Hospitals included. Green dots: hospitals that were combined with the nearest green point to form the blue dot between both green hospitals. † Pediatric hospital that were combined, * Adult Hospital that were combined. The upper blue dot with † and * represent the combination of two neighboring hospitals.

# APPENDIX D: Power spectrum for influenza-like illness by health network, Chile 2010-2016

Local Wavelet Power Spectrum of Influenza-like illness in Health network 01, Chile 2011-2016

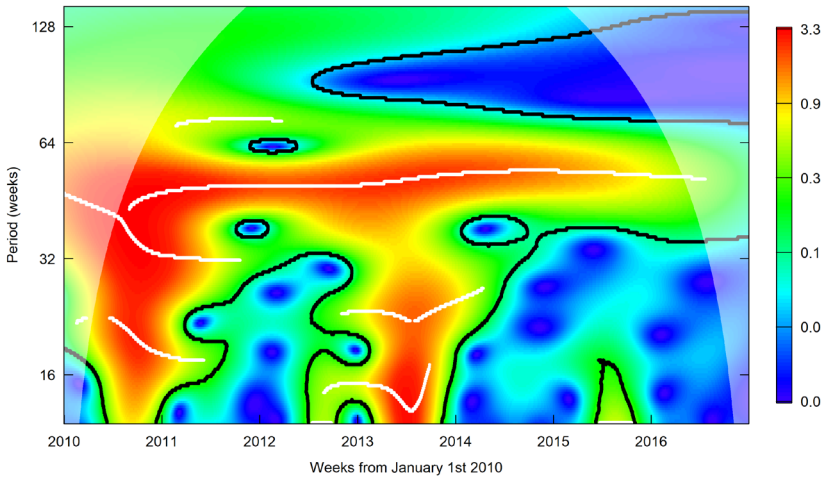


Local Wavelet Power Spectrum of Influenza-like illness in Health network 02, Chile 2011-2016

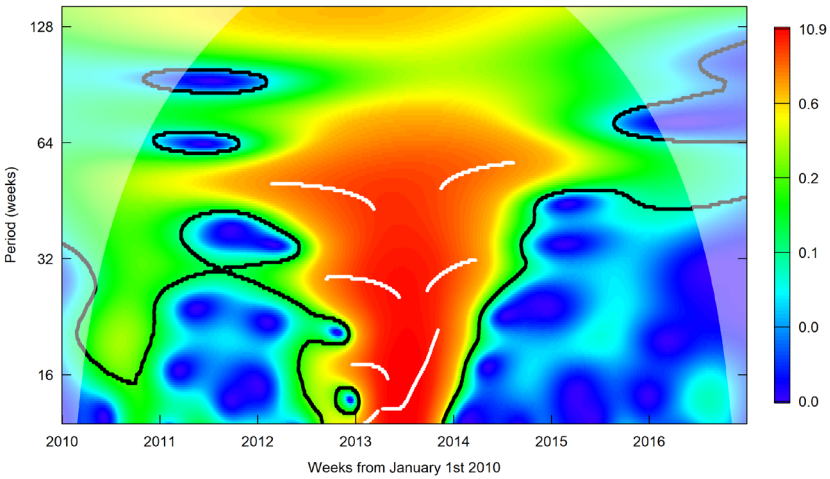


Local Wavelet Power Spectrum of Influenza-like illness in Health network 03, Chile 2011-2016

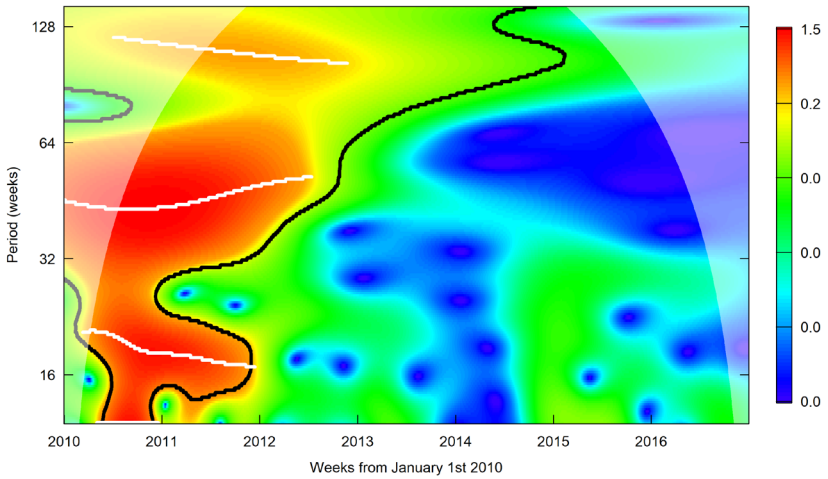


Local Wavelet Power Spectrum of Influenza-like illness in Health network 04, Chile 2011-2016

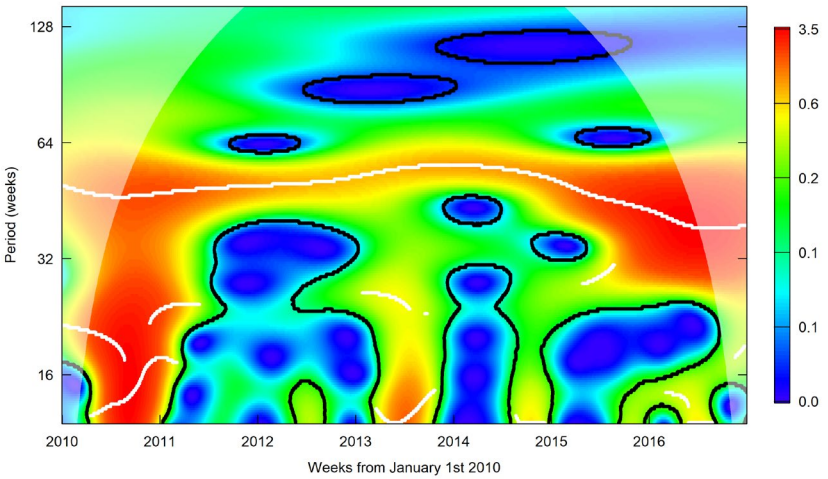

**Local Wavelet Power Spectrum of Influenza-like illness in Health network 05, Chile 2011-2016**

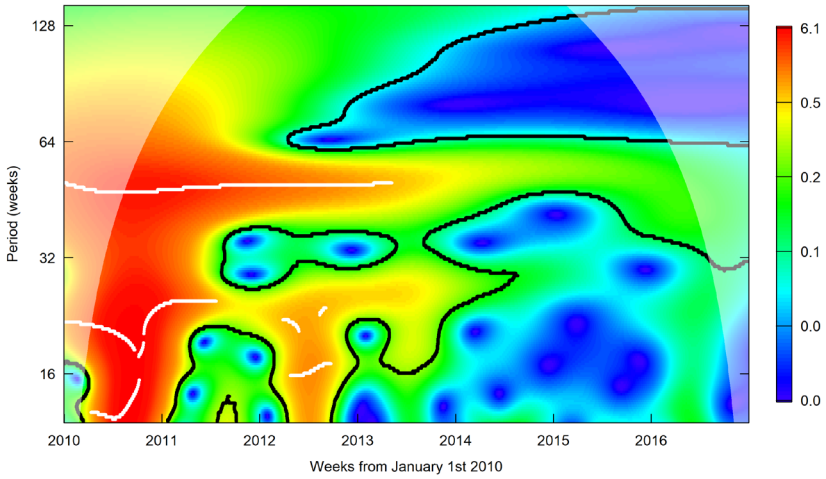


**Local Wavelet Power Spectrum of Influenza-like illness in Health network 06, Chile 2011-2016**

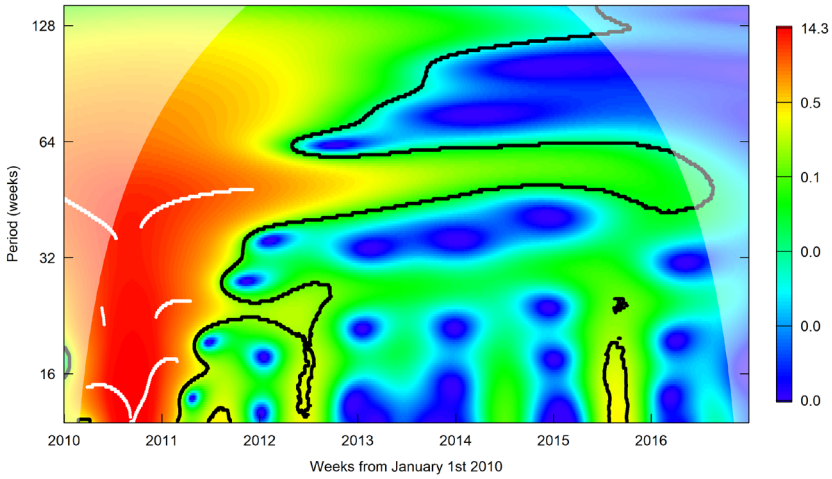


**Local Wavelet Power Spectrum of Influenza-like illness in Health network 07, Chile 2011-2016**

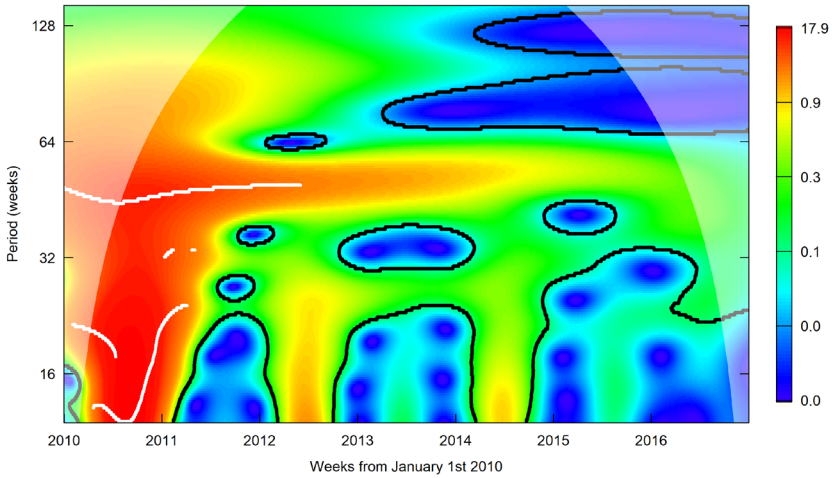


**Local Wavelet Power Spectrum of Influenza-like illness in Health network 08, Chile 2011-2016**

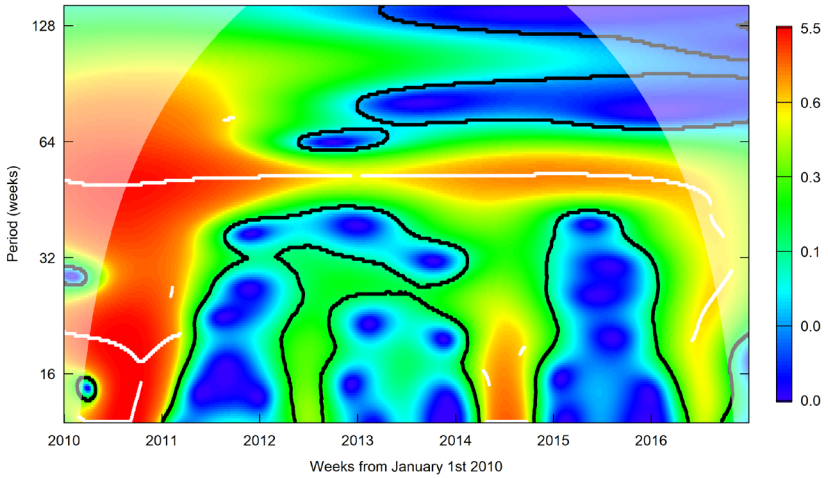

**Local Wavelet Power Spectrum of Influenza-like illness in Health network 09, Chile 2011-2016**

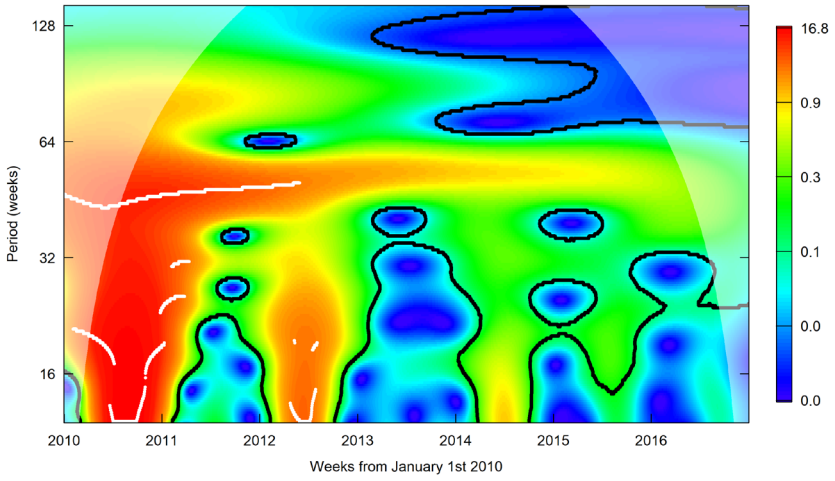


**Local Wavelet Power Spectrum of Influenza-like illness in Health network 10, Chile 2011-2016**

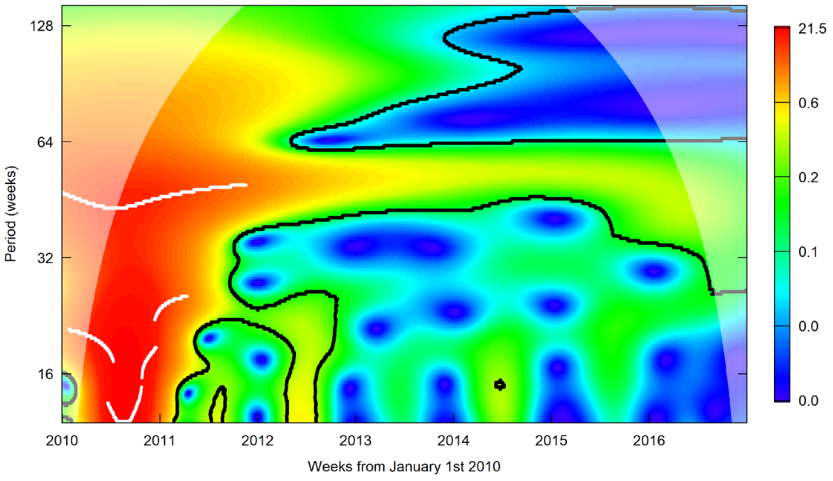


**Local Wavelet Power Spectrum of Influenza-like illness in Health network 11, Chile 2011-2016**

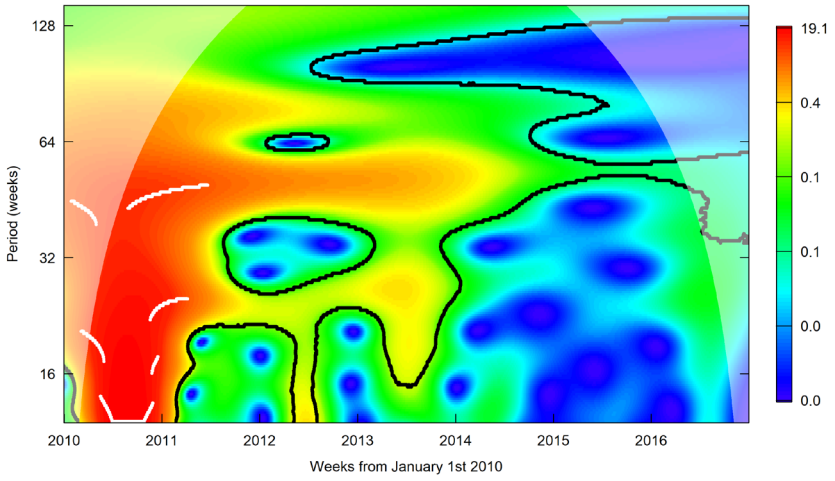


**Local Wavelet Power Spectrum of Influenza-like illness in Health network 12, Chile 2011-2016**

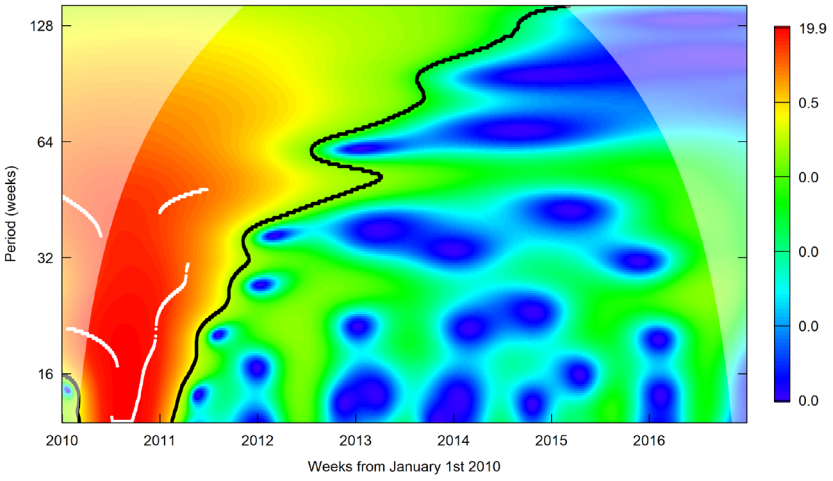

**Local Wavelet Power Spectrum of Influenza-like illness in Health network 13, Chile 2011-2016**

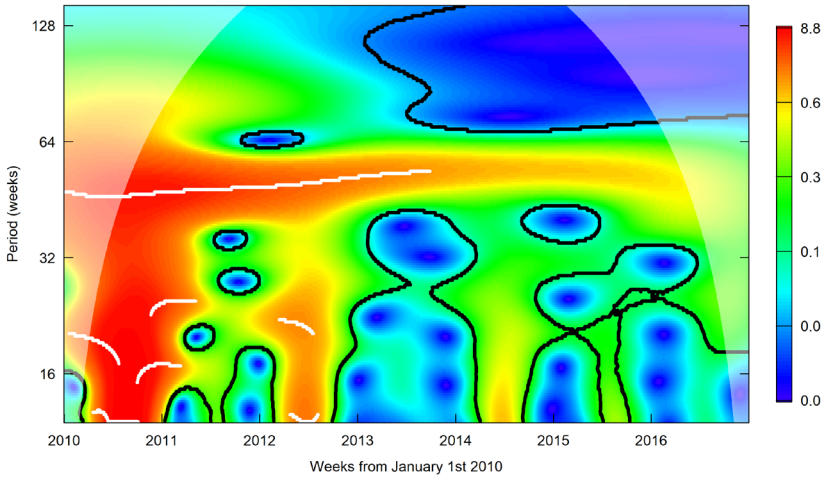


**Local Wavelet Power Spectrum of Influenza-like illness in Health network 14, Chile 2011-2016**

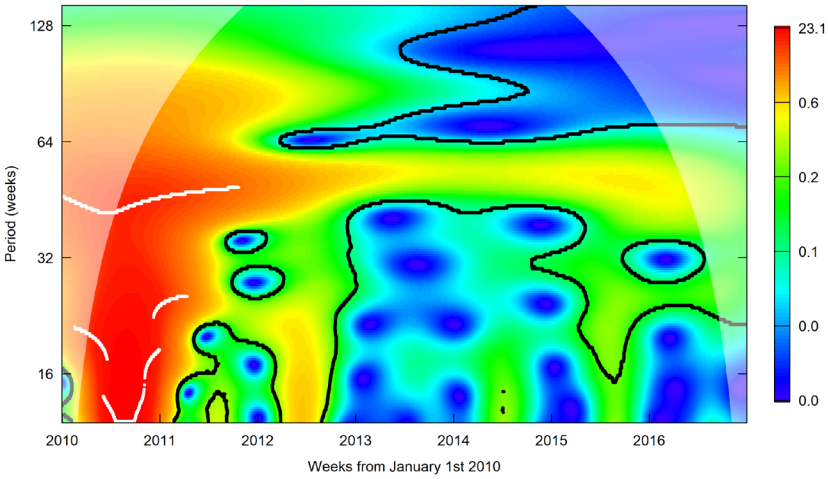


**Local Wavelet Power Spectrum of Influenza-like illness in Health network 15, Chile 2011-2016**

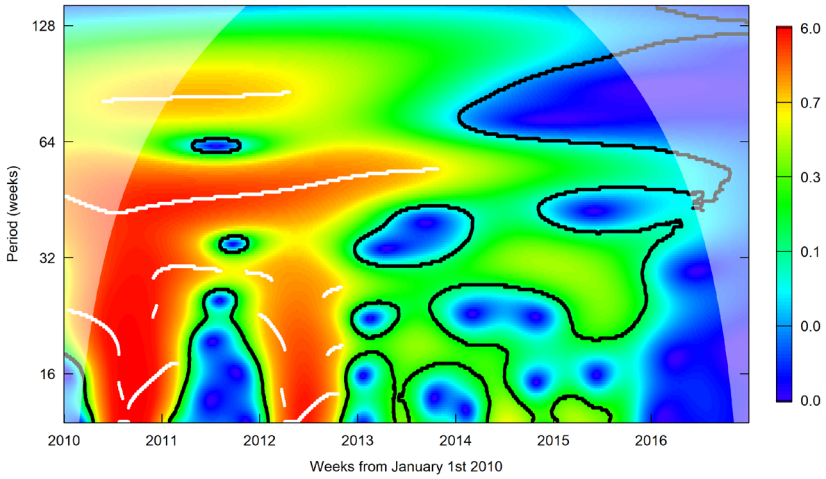


**Local Wavelet Power Spectrum of Influenza-like illness in Health network 16, Chile 2011-2016**

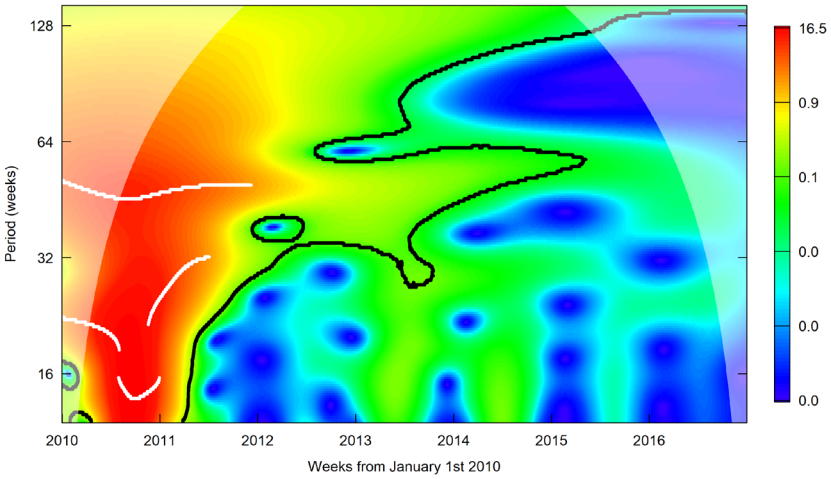

**Local Wavelet Power Spectrum of Influenza-like illness in Health network 17, Chile 2011-2016**

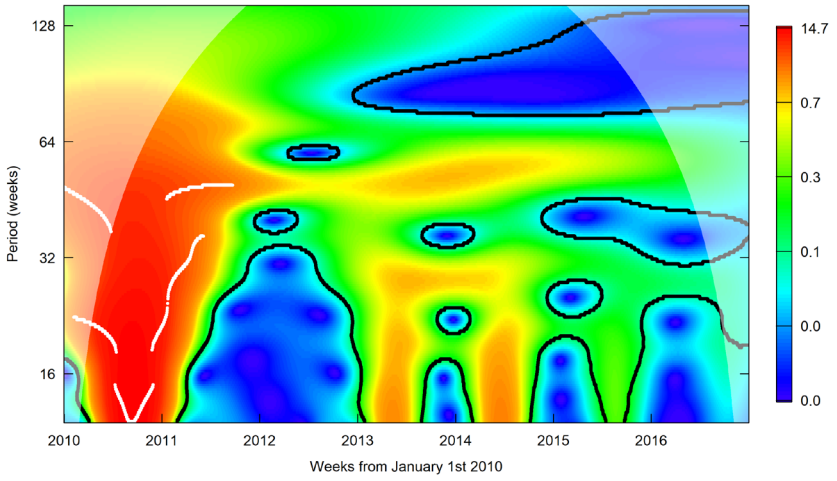


**Local Wavelet Power Spectrum of Influenza-like illness in Health network 18, Chile 2011-2016**

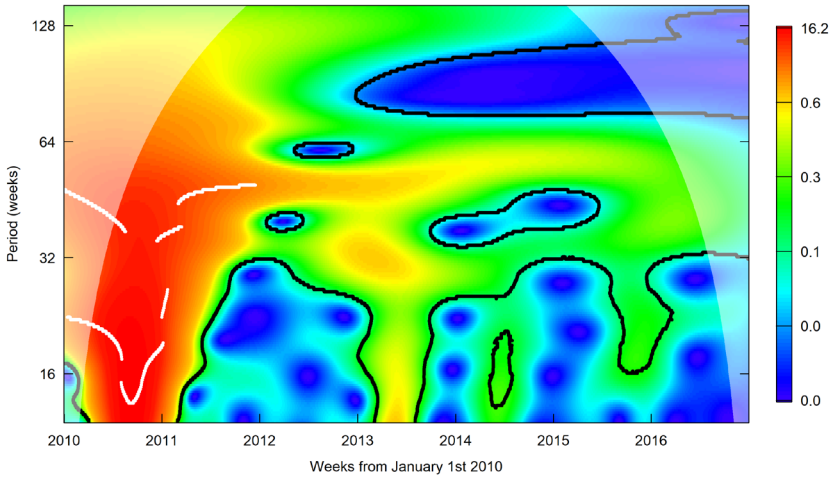


**Local Wavelet Power Spectrum of Influenza-like illness in Health network 19, Chile 2011-2016**

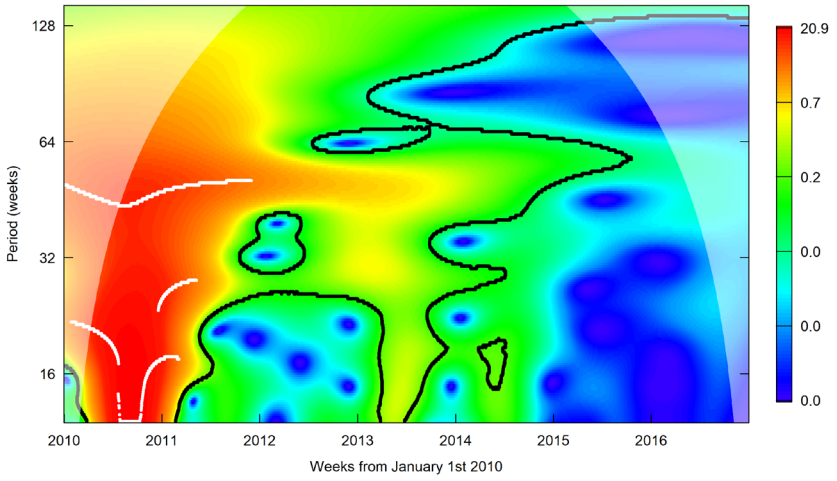


**Local Wavelet Power Spectrum of Influenza-like illness in Health network 20, Chile 2011-2016**

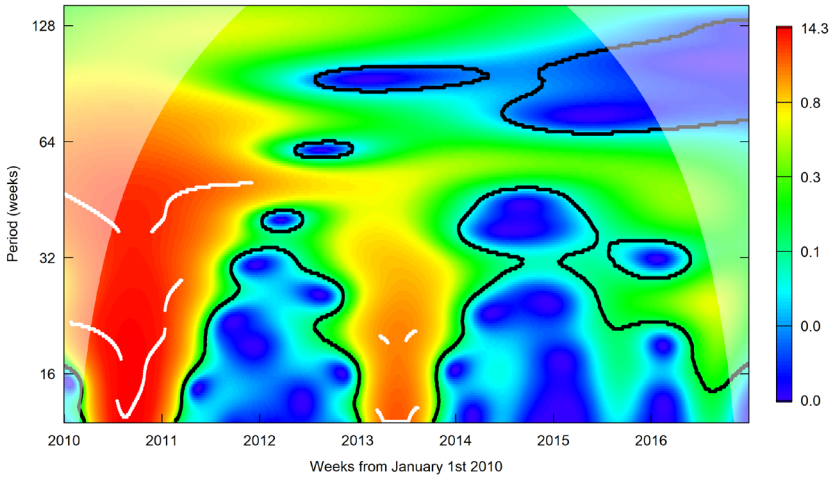

**Local Wavelet Power Spectrum of Influenza-like illness in Health network 21, Chile 2011-2016**

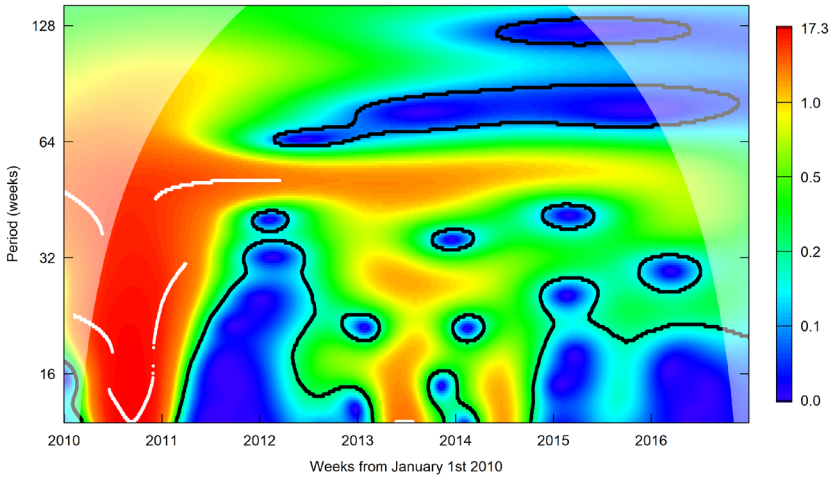


**Local Wavelet Power Spectrum of Influenza-like illness in Health network 22, Chile 2011-2016**

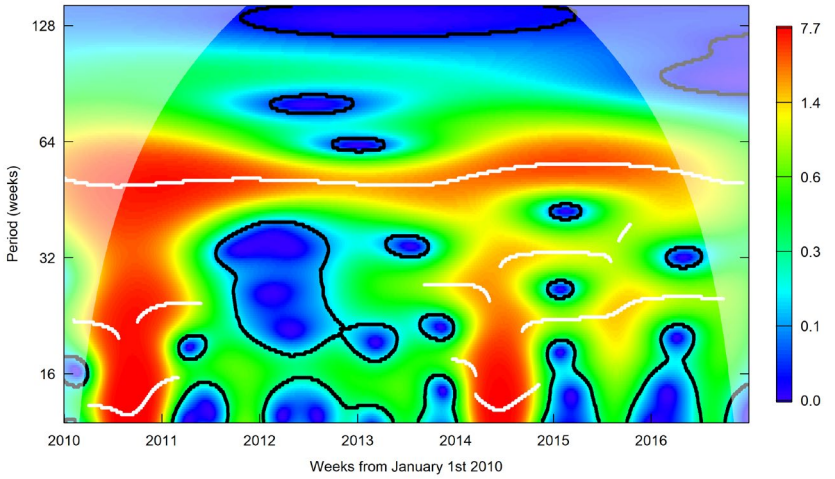


**Local Wavelet Power Spectrum of Influenza-like illness in Health network 23, Chile 2011-2016**

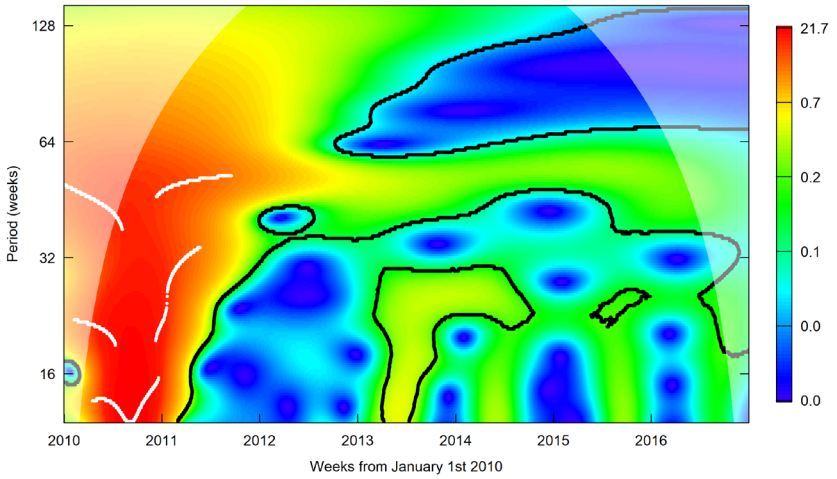


**Local Wavelet Power Spectrum of Influenza-like illness in Health network 24, Chile 2011-2016**

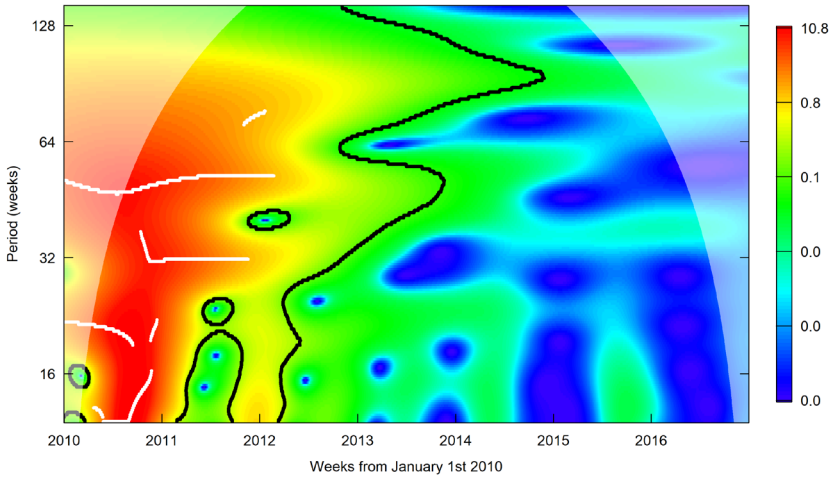

**Local Wavelet Power Spectrum of Influenza-like illness in Health network 25, Chile 2011-2016**

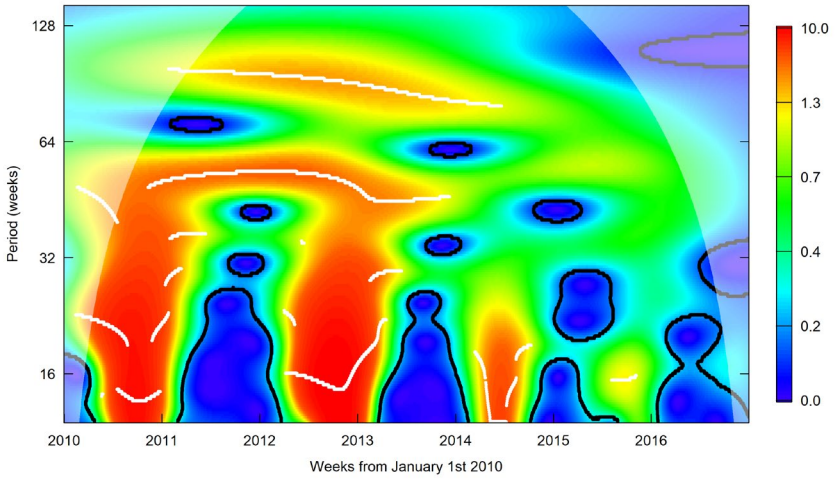


**Local Wavelet Power Spectrum of Influenza-like illness in Health network 26, Chile 2011-2016**

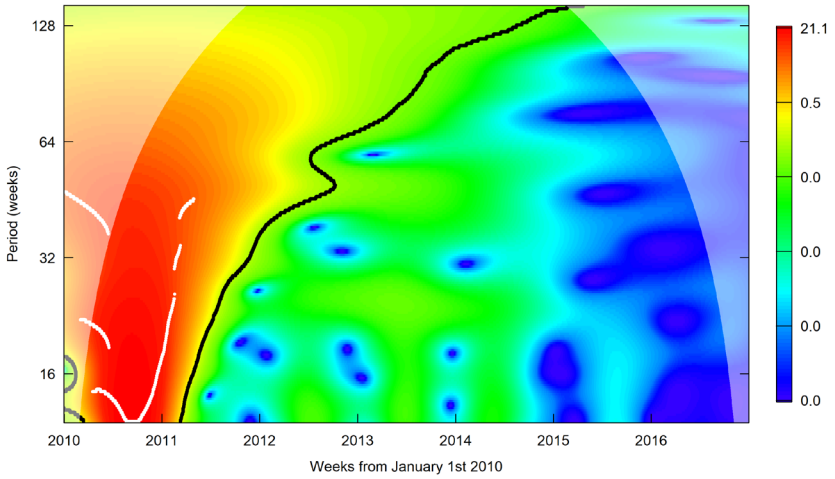


**Local Wavelet Power Spectrum of Influenza-like illness in Health network 28, Chile 2011-2016**

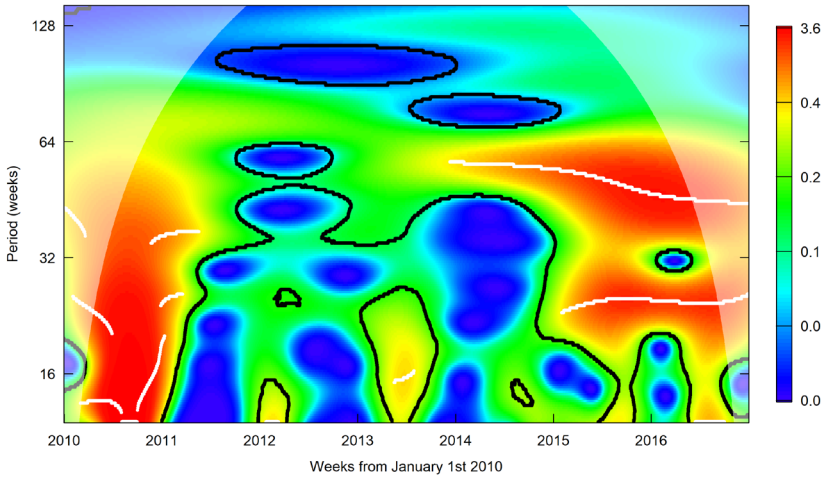


**Local Wavelet Power Spectrum of Influenza-like illness in Health network 29, Chile 2011-2016**

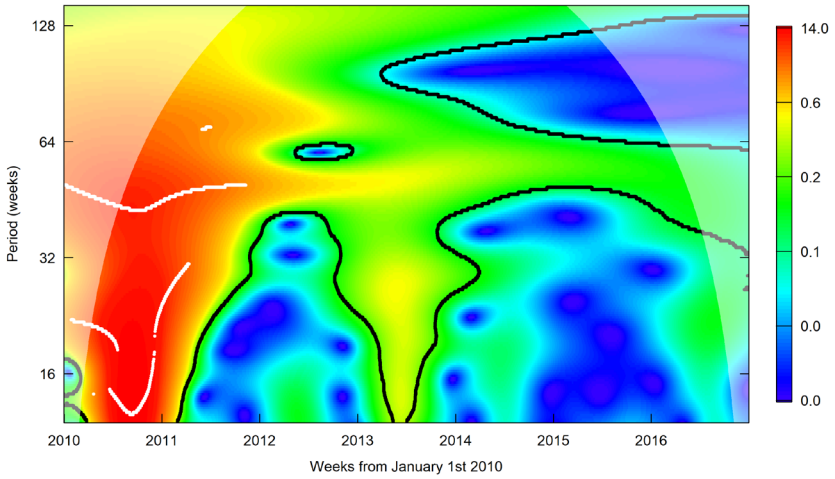

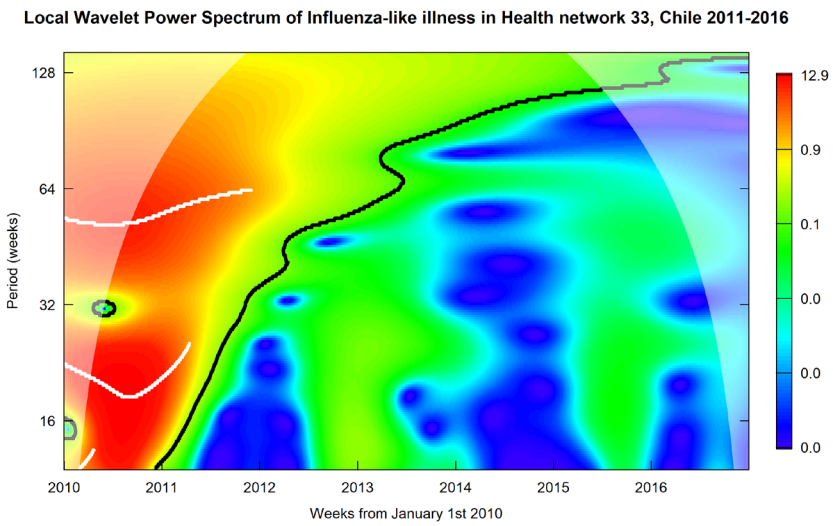
Local Wavelet Power Spectrum of Influenza-like illness in Health network 33, Chile 2011-2016
128
64
32
16
Period (weeks)
2010
2011
2012
2013
2014
2015
2016
Weeks from January 1st 2010
12.9
0.9
0.1
0.0
0.0
0.0

## APPENDIX E: Start and peak of influenza-like illness versus latitude in health networks by year, Chile 2011-2016

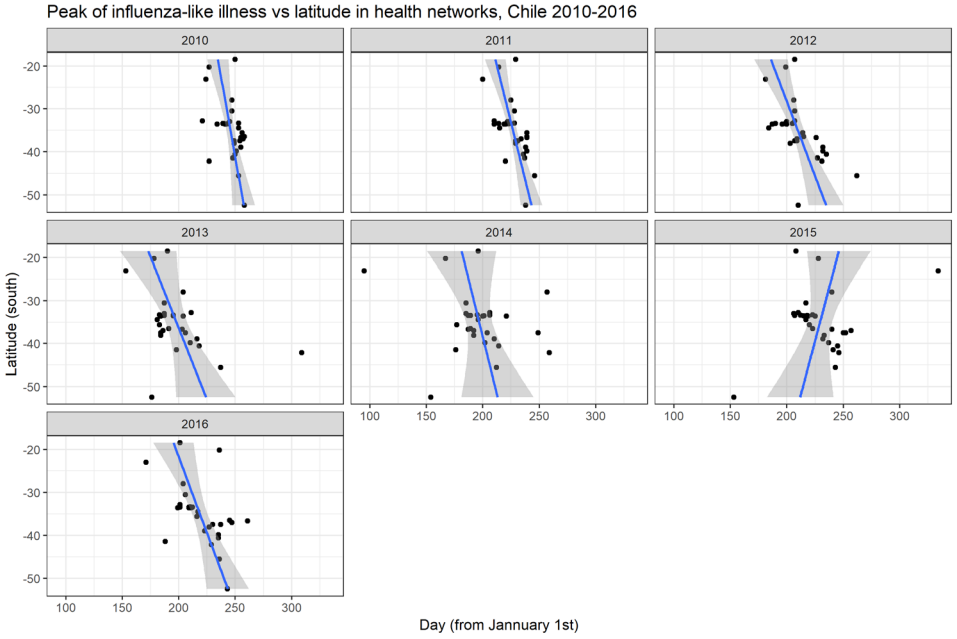


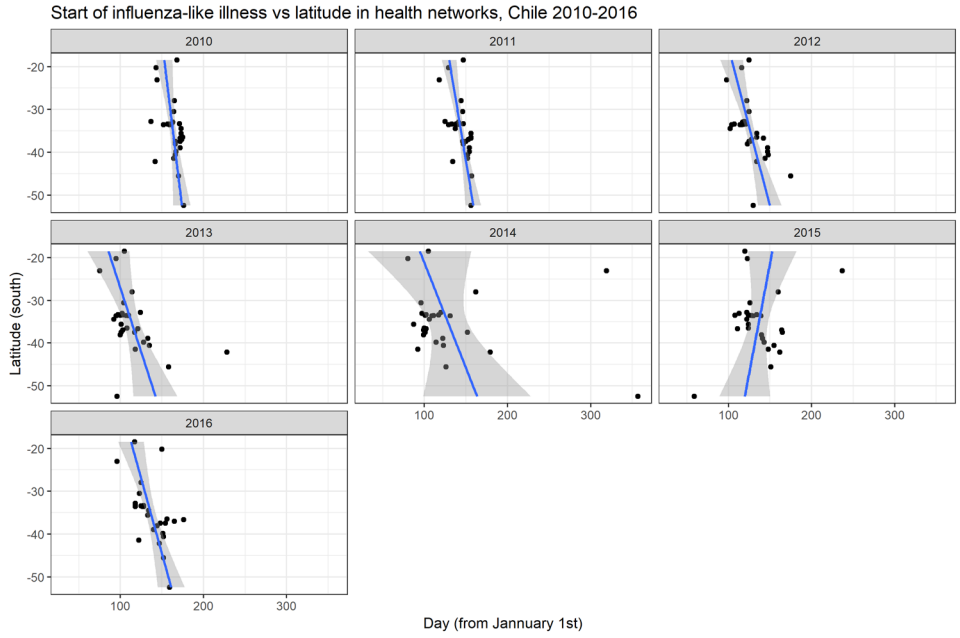

## BIBLIOGRAPHY


1. Lowen AC, Mubareka S, Steel J, Palese P. Influenza virus transmission is dependent on relative humidity and temperature. PLoS pathogens. 2007;3(10):1470-6.
2. Cox NJ, Subbarao K. Influenza. Lancet (London, England). 1999;354(9186):1277-82.
3. World Health Organization [WHO]. Influenza Fact Sheet. 2014.
4. Molinari N-AM, Ortega-Sanchez IR, Messonnier ML, Thompson WW, Wortley PM, Weintraub E, et al. The annual impact of seasonal influenza in the US: measuring disease burden and costs. Vaccine. 2007;25(27):5086-96.
5. Cheng PY, Palekar R, Azziz-Baumgartner E, Iuliano D, Alencar AP, Bresee J, et al. Burden of influenza-associated deaths in the Americas, 2002-2008. Influenza and other respiratory viruses. 2015;9 Suppl 1:13-21.
6. Wong KK, Jain S, Blanton L, Dhara R, Brammer L, Fry AM, et al. Influenza-associated pediatric deaths in the United States, 2004-2012. Pediatrics. 2013;132(5):796-804.
7. Poehling KA, Edwards KM, Weinberg GA, Szilagyi P, Staat MA, Iwane MK, et al. The underrecognized burden of influenza in young children. The New England journal of medicine. 2006;355(1):31-40.
8. Mullooly JP, Bridges CB, Thompson WW, Chen J, Weintraub E, Jackson LA, et al. Influenza- and RSV-associated hospitalizations among adults. Vaccine. 2007;25(5):846-55.
9. Nair H, Brooks WA, Katz M, Roca A, Berkley JA, Madhi SA, et al. Global burden of respiratory infections due to seasonal influenza in young children: a systematic review and meta-analysis. Lancet (London, England). 2011;378(9807):1917-30.
10. Gamblin SJ, Skehel JJ. Influenza hemagglutinin and neuraminidase membrane glycoproteins. The Journal of biological chemistry. 2010;285(37):28403-9.
11. Lofgren E, Fefferman NH, Naumov YN, Gorski J, Naumova EN. Influenza seasonality: underlying causes and modeling theories. Journal of virology. 2007;81(11):5429-36.
12. Potter CW, Oxford JS. Determinants of immunity to influenza infection in man. Br Med Bull. 1979;35(1):69-75.
13. Couch RB, Kasel JA. Immunity to influenza in man. Annual review of microbiology. 1983;37:529-49.
14. Clements ML, Murphy BR. Development and persistence of local and systemic antibody responses in adults given live attenuated or inactivated influenza A virus vaccine. J Clin Microbiol. 1986;23(1):66-72.
15. World Health Organization [WHO]. WHO Public Health Research Agenda For Influenza . Biannual Progress Review and Report 2010-2011. 2013.
16. World Health Organization. Influenza Fact Sheet. 2014.
17. Tamerius J, Nelson MI, Zhou SZ, Viboud C, Miller MA, Alonso WJ. Global influenza seasonality: reconciling patterns across temperate and tropical regions. Environmental health perspectives. 2011;119(4):439-45.

18. Viboud C, Bjornstad ON, Smith DL, Simonsen L, Miller MA, Grenfell BT. Synchrony, waves, and spatial hierarchies in the spread of influenza. Science (New York, NY). 2006;312(5772):447-51.
19. Lipsitch M, Viboud C. Influenza seasonality: lifting the fog. Proceedings of the National Academy of Sciences of the United States of America. 2009;106(10):3645-6.
20. Shaman J, Pitzer VE, Viboud C, Grenfell BT, Lipsitch M. Absolute humidity and the seasonal onset of influenza in the continental United States. PLoS biology. 2010;8(2):e1000316.
21. Shaman J, Kohn M. Absolute humidity modulates influenza survival, transmission, and seasonality. Proceedings of the National Academy of Sciences of the United States of America. 2009;106(9):3243-8.
22. Sagripanti JL, Lytle CD. Inactivation of influenza virus by solar radiation. Photochemistry and photobiology. 2007;83(5):1278-82.
23. Yellon SM, Teasley LA, Fagoaga OR, Nguyen HC, Truong HN, Nehlsen-Cannarella L. Role of photoperiod and the pineal gland in T cell-dependent humoral immune reactivity in the Siberian hamster. Journal of pineal research. 1999;27(4):243-8.
24. von Essen MR, Kongsbak M, Schjerling P, Olgaard K, Odum N, Geisler C. Vitamin D controls T cell antigen receptor signaling and activation of human T cells. Nature immunology. 2010;11(4):344-9.
25. Urashima M, Segawa T, Okazaki M, Kurihara M, Wada Y, Ida H. Randomized trial of vitamin D supplementation to prevent seasonal influenza A in schoolchildren. The American journal of clinical nutrition. 2010;91(5):1255-60.
26. Salah B, Dinh Xuan AT, Fouilladieu JL, Lockhart A, Regnard J. Nasal mucociliary transport in healthy subjects is slower when breathing dry air. Eur Respir J. 1988;1(9):852-5.
27. Mileva M, Bakalova R, Tancheva L, Galabov A, Ribarov S. Effect of vitamin E supplementation on lipid peroxidation in blood and lung of influenza virus infected mice. Comparative immunology, microbiology and infectious diseases. 2002;25(1):1-11.
28. Linde A, Rotzen-Ostlund M, Zweygberg-Wirgart B, Rubinova S, Brytting M. Does viral interference affect spread of influenza? Euro surveillance : bulletin Europeen sur les maladies transmissibles = European communicable disease bulletin. 2009;14(40).
29. Baetjer AM. Effect of ambient temperature and vapor pressure on cilia-mucus clearance rate. Journal of applied physiology. 1967;23(4):498-504.
30. World Bank. World Development Indicators 2019 [Available from: https://databank.worldbank.org/data/reports.aspx?source=2&series=NY.GDP.PCAP.CD.
31. Instituto Nacional de Estadisticas. Compendio Estadistico 2016. Santiago; 2016.
32. Demografia [Internet]. FONASA. 2018. Available from: https://www.fonasa.cl/sites/fonasa/institucional/archivos#documentos-estadisticos-institucionales.
33. Influenza estacional y pandemica (H1N1): Vigilancia epidemiologica, investigacion y control de brotes., B51/20 (2010).
34. Departamento de Epidemiologia. Boletin epidemiologico trimestral. MINSAL; 2018.
35. Instituto de Salud Publica. Informe de Circulación de Virus Respiratorios. 2018 2018.
36. Direccion Nacional de Aeronautica Civel. Direccion meteorologica de Chile 2018 [Available from: www.meteochile.cl
37. Ministerio de Medio Ambiente. Sistema de Informacion Nacional de Calidad del Aire 2018 [Available from: https://sinca.mma.gob.cl/.
38. Research CfCaR. Explorador Climatico [Available from: http://www.cr2.cl/explorador-climatico/.

39. Brauer M, Hoek G, Smit HA, de Jongste JC, Gerritsen J, Postma DS, et al. Air pollution and development of asthma, allergy and infections in a birth cohort. Eur Respir J. 2007;29(5):879-88.
40. Feng C, Li J, Sun W, Zhang Y, Wang Q. Impact of ambient fine particulate matter (PM2.5) exposure on the risk of influenza-like-illness: a time-series analysis in Beijing, China. Environ Health. 2016;15:17-.
41. Kaiser G. A friendly guide to wavelets: Springer Science & Business Media; 2010.
42. Mercado A. De los wavelets a las ondas gravitacionales: las matemáticas detrás de acontecimientos científicos del 2017. El Mostrador. 2017 12/30/2017.
43. Alekseev VI. Wavelet analysis of the El Niño–La Niña phenomenon dynamics and its forecasting. Yugra State University Bulletin. 2018;14(3):75-87.
44. Barish BC. LIGO and Gravitational Waves II: Nobel Lecture, December 8, 2017. Annalen der Physik. 2019:1800357.
45. Rivière A, Lepri S, Colognesi D, Piazza F. Wavelet imaging of transient energy localization in nonlinear systems at thermal equilibrium: The case study of NaI crystals at high temperature. Physical Review B. 2019;99(2):024307.
46. Choisy M, Rohani P. Changing spatial epidemiology of pertussis in continental USA. Proceedings of the Royal Society of London B: Biological Sciences. 2012;279(1747):4574-81.
47. Grenfell B, Bjørnstad O, Kappey J. Travelling waves and spatial hierarchies in measles epidemics. Nature. 2001;414(6865):716.
48. Gubler DJ. Cities spawn epidemic dengue viruses. Nature medicine. 2004;10(2):129.
49. Lima M, Estay SA, Fuentes R, Rubilar P, Broutin H, Chowell-Puente G. Whooping cough dynamics in Chile (1932-2010): disease temporal fluctuations across a north-south gradient. BMC infectious diseases. 2015;15:590-.
50. Magpantay FMG, Rohani P. Dynamics of Pertussis Transmission in the United States. American journal of epidemiology. 2015;181(12):921-31.
51. Teurlai M, Huy R, Cazelles B, Duboz R, Baehr C, Vong S. Can human movements explain heterogeneous propagation of dengue fever in Cambodia? PLoS neglected tropical diseases. 2012;6(12):e1957-e.
52. Thai KT, Cazelles B, Van Nguyen N, Vo LT, Boni MF, Farrar J, et al. Dengue dynamics in Binh Thuan province, southern Vietnam: periodicity, synchronicity and climate variability. PLoS neglected tropical diseases. 2010;4(7):e747.
53. Van Panhuis WG, Choisy M, Xiong X, Chok NS, Akarasewi P, Iamsirithaworn S, et al. Region-wide synchrony and traveling waves of dengue across eight countries in Southeast Asia. Proceedings of the National Academy of Sciences. 2015;112(42):13069-74.
54. Johansson MA, Cummings DA, Glass GE. Multiyear climate variability and dengue—El Nino southern oscillation, weather, and dengue incidence in Puerto Rico, Mexico, and Thailand: a longitudinal data analysis. PLoS medicine. 2009;6(11):e1000168.
55. Thompson WW, Shay DK, Weintraub E, Brammer L, Bridges CB, Cox NJ, et al. Influenza-associated hospitalizations in the United States. Jama. 2004;292(11):1333-40.
56. Thompson WW, Shay DK, Weintraub E, Brammer L, Cox N, Anderson LJ, et al. Mortality associated with influenza and respiratory syncytial virus in the United States. Jama. 2003;289(2):179-86.
57. van Lier A, McDonald SA, Bouwknegt M, Kretzschmar ME, Havelaar AH, Mangen M-JJ, et al. Disease burden of 32 infectious diseases in the Netherlands, 2007-2011. PloS one. 2016;11(4):e0153106.

58. Wong CM, Yang L, Chan KP, Leung GM, Chan KH, Guan Y, et al. Influenza-associated hospitalization in a subtropical city. PLoS medicine. 2006;3(4):e121.
59. Wong C-M, Chan K-P, Hedley AJ, Peiris JM. Influenza-associated mortality in Hong Kong. Clinical Infectious Diseases. 2004;39(11):1611-7.
60. World Health Organization. Pandemic influenza preparedness and response: a WHO guidance document. 2009.
61. Ortiz JR, Sotomayor V, Uez OC, Oliva O, Bettels D, McCarron M, et al. Strategy to enhance influenza surveillance worldwide. Emerging infectious diseases. 2009;15(8):1271.
62. World Health Organization. Global epidemiological surveillance standards for influenza. World Health Organization. 2014.
63. Meerhoff T, Paget W, Aguilera J-F, van der Velden J. Harmonising the virological surveillance of influenza in Europe: results of an 18-country survey. Virus research. 2004;103(1-2):31-3.
64. M'ikanatha NM, Lynfield R, Van Beneden CA, de Valk H. Infectious disease surveillance: John Wiley & Sons; 2008.
65. Shih S-R, Chen G-W, Yang C-C, Yang W-Z, Liu D-P, Lin J-H, et al. Laboratory-based surveillance and molecular epidemiology of influenza virus in Taiwan. Journal of clinical microbiology. 2005;43(4):1651-61.
66. Monto AS, Comanor L, Shay DK, Thompson WW. Epidemiology of pandemic influenza: use of surveillance and modeling for pandemic preparedness. The Journal of infectious diseases. 2006;194(Supplement_2):S92-S7.
67. Call SA, Vollenweider MA, Hornung CA, Simel DL, McKinney WP. Does this patient have influenza? Jama. 2005;293(8):987-97.
68. Monto AS, Gravenstein S, Elliott M, Colopy M, Schweinle J. Clinical signs and symptoms predicting influenza infection. Archives of internal medicine. 2000;160(21):3243-7.
69. Ohmit SE, Monto AS. Symptomatic predictors of influenza virus positivity in children during the influenza season. Clinical infectious diseases. 2006;43(5):564-8.
70. Thursky K, Cordova SP, Smith D, Kelly H. Working towards a simple case definition for influenza surveillance. Journal of Clinical Virology. 2003;27(2):170-9.
71. Navarro-Marí JM, Pérez-Ruiz M, Cantudo-Muñoz P, Petit-Gancedo C, Jiménez-Valera M, Rosa-Fraile M, et al. Influenza-like illness criteria were poorly related to laboratory-confirmed influenza in a sentinel surveillance study. Journal of clinical epidemiology. 2005;58(3):275-9.
72. Zambon M, Stockton J, Clewley J, Fleming D. Contribution of influenza and respiratory syncytial virus to community cases of influenza-like illness: an observational study. The Lancet. 2001;358(9291):1410-6.
73. Ministerio de Salud. Departamento de Estadisticas e Informacion en Salud 2018 [Available from: www.deis.cl.
74. estadisticas Ind. Demograficas y vitales 2018 [Available from: http://www.ine.cl/estadisticas/demograficas-y-vitales.
75. nacionales Mdb. Geoportal de Chile, Catálogo Nacional de Información Geoespacial 2018 [Available from: http://www.geoportal.cl.
76. Sorichetta A, Hornby GM, Stevens FR, Gaughan AE, Linard C, Tatem AJ. High-resolution gridded population datasets for Latin America and the Caribbean in 2010, 2015, and 2020. Scientific data. 2015;2:150045-.
77. Henneman PL, Garb JL, Capraro GA, Li H, Smithline HA, Wait RB. Geography and travel distance impact emergency department visits. The Journal of emergency medicine. 2011;40(3):333-9.

78. Lee DC, Doran KM, Polsky D, Cordova E, Carr BG, editors. Geographic variation in the demand for emergency care: a local population-level analysis. Healthcare; 2016: Elsevier.
79. Sanz-Barbero B, García LO, Hernández TB. The effect of distance on the use of emergency hospital services in a Spanish region with high population dispersion: a multilevel analysis. Medical care. 2012:27-34.
80. Grewal MS. Kalman filtering. International Encyclopedia of Statistical Science: Springer; 2011. p. 705-8.
81. Moritz S, Bartz-Beielstein T. imputeTS: time series missing value imputation in R. The R Journal. 2017;9(1):207-18.
82. Cazelles B, Chavez M, Berteaux D, Ménard F, Vik JO, Jenouvrier S, et al. Wavelet analysis of ecological time series. Oecologia. 2008;156(2):287-304.
83. Torrence C, Compo GP. A practical guide to wavelet analysis. Bulletin of the American Meteorological society. 1998;79(1):61-78.
84. Cazelles B, Chavez M, De Magny GC, Guégan J-F, Hales S. Time-dependent spectral analysis of epidemiological time-series with wavelets. Journal of the Royal Society Interface. 2007;4(15):625-36.
85. Chatfield C. The analysis of time series: an introduction: CRC press; 2016.
86. Rösch A, Schmidbauer H. WaveletComp 1.1: A guided tour through the R package. 2014.
87. Grinsted A, Moore JC, Jevrejeva S. Application of the cross wavelet transform and wavelet coherence to geophysical time series. Nonlinear processes in geophysics. 2004;11(5/6):561-6.
88. Roesch A, Schmidbauer H. WaveletComp: Computational wavelet analysis. R package version. 2014;1.
89. Team RC. R: A Language and Environment for Statistical Computing. Vienna, Austria: R Foundation for Statistical Computing; 2017 2017.
90. Alonso WJ, Viboud C, Simonsen L, Hirano EW, Daufenbach LZ, Miller MA. Seasonality of influenza in Brazil: a traveling wave from the Amazon to the subtropics. Am J Epidemiol. 2007;165(12):1434-42.
91. Bollaerts K, Antoine J, Van Casteren V, Ducoffre G, Hens N, Quoilin S. Contribution of respiratory pathogens to influenza-like illness consultations. Epidemiol Infect. 2013;141(10):2196-204.
92. Kamigaki T, Chaw L, Tan AG, Tamaki R, Alday PP, Javier JB, et al. Seasonality of Influenza and Respiratory Syncytial Viruses and the Effect of Climate Factors in Subtropical-Tropical Asia Using Influenza-Like Illness Surveillance Data, 2010 -2012. PloS one. 2016;11(12):e0167712-e.
93. Omata K, Takahashi Y, editors. Spatiotemporal Analysis of Influenza Epidemics in Japan. Proceedings of the International Conference on Social Modeling and Simulation, plus Econophysics Colloquium 2014; 2015: Springer.
94. Yang L, Wong CM, Lau EHY, Chan KP, Ou CQ, Peiris JSM. Synchrony of clinical and laboratory surveillance for influenza in Hong Kong. PloS one. 2008;3(1):e1399-e.
95. Chowell G, Towers S, Viboud C, Fuentes R, Sotomayor V, Simonsen L, et al. The influence of climatic conditions on the transmission dynamics of the 2009 A/H1N1 influenza pandemic in Chile. BMC Infect Dis. 2012;12:298-.
96. Earn DJ, Dushoff J, Levin SA. Ecology and evolution of the flu. Trends in ecology & evolution. 2002;17(7):334-40.
97. Simonsen L. The global impact of influenza on morbidity and mortality. Vaccine. 1999;17 Suppl 1:S3-10.

98. Chan J, Holmes A, Rabadan R. Network analysis of global influenza spread. PLoS computational biology. 2010;6(11):e1001005-e.
99. He D, Lui R, Wang L, Tse CK, Yang L, Stone L. Global Spatio-temporal Patterns of Influenza in the Post-pandemic Era. Scientific reports. 2015;5:11013-.
100. Yu H, Alonso WJ, Feng L, Tan Y, Shu Y, Yang W, et al. Characterization of regional influenza seasonality patterns in China and implications for vaccination strategies: spatio-temporal modeling of surveillance data. PLoS Med. 2013;10(11):e1001552-e.
101. Chowell G, Viboud C, Munayco CV, Gomez J, Simonsen L, Miller MA, et al. Spatial and temporal characteristics of the 2009 A/H1N1 influenza pandemic in Peru. PloS one. 2011;6(6):e21287.
102. Lee SS, Wong NS. The clustering and transmission dynamics of pandemic influenza A (H1N1) 2009 cases in Hong Kong. J Infect. 2011;63(4):274-80.
103. McDonald SA, van Boven M, Wallinga J. An evidence synthesis approach to estimating the proportion of influenza among influenza-like illness patients. Epidemiology. 2017;28(4):484-91.
104. Ritzwoller DP, Kleinman K, Palen T, Abrams A, Kaferly J, Yih W, et al. Comparison of syndromic surveillance and a sentinel provider system in detecting an influenza outbreak--Denver, Colorado, 2003. MMWR Suppl. 2005;54:151-6.
105. Shah SC, Rumoro DP, Hallock MM, Trenholme GM, Gibbs GS, Silva JC, et al. Clinical predictors for laboratory-confirmed influenza infections: exploring case definitions for influenza-like illness. Infect Control Hosp Epidemiol. 2015;36(3):241-8.
106. Zhang Y, Arab A, Cowling BJ, Stoto MA. Characterizing Influenza surveillance systems performance: application of a Bayesian hierarchical statistical model to Hong Kong surveillance data. BMC Public Health. 2014;14:850-.
107. World Health Organization. A manual for estimating disease burden associated with seasonal influenza: World Health Organization; 2015.
108. Bürger R, Chowell G, Mulet P, Villada LM. Modelling the spatial-temporal progression of the 2009 A/H1N1 influenza pandemic in Chile. Math Biosci Eng. 2016;13(1):43-65.
109. James G, Witten D, Hastie T, Tibshirani R. An introduction to statistical learning: Springer; 2013.
110. Lumley T, Miller A. Leaps: regression subset selection. R package version 2.9. See http://CRAN R-project org/package= leaps. 2009.
111. Vittinghoff E, Glidden DV, Shiboski SC, McCulloch CE. Regression methods in biostatistics: linear, logistic, survival, and repeated measures models: Springer Science & Business Media; 2011.
112. Tamerius JD, Shaman J, Alonso WJ, Bloom-Feshbach K, Uejio CK, Comrie A, et al. Environmental predictors of seasonal influenza epidemics across temperate and tropical climates. PLoS pathogens. 2013;9(3):e1003194-e.
113. Chen PS, Tsai FT, Lin CK, Yang CY, Chan CC, Young CY, et al. Ambient influenza and avian influenza virus during dust storm days and background days. Environmental health perspectives. 2010;118(9):1211-6.
114. Fang L-Q, Wang L-P, de Vlas SJ, Liang S, Tong S-L, Li Y-L, et al. Distribution and risk factors of 2009 pandemic influenza A (H1N1) in mainland China. Am J Epidemiol. 2012;175(9):890-7.
115. Imai C, Hashizume M. Systematic review on methodology: time series regression analysis for environmental factors and infectious diseases. Tropical medicine and health. 2014.

116. Thai PQ, Choisy M, Duong TN, Thiem VD, Yen NT, Hien NT, et al. Seasonality of absolute humidity explains seasonality of influenza-like illness in Vietnam. Epidemics. 2015;13:65-73.
117. Skog L, Linde A, Palmgren H, Hauska H, Elgh F. Spatiotemporal characteristics of pandemic influenza. BMC Infect Dis. 2014;14:378-.
118. Nimbalkar PM, Tripathi NK. Space-time epidemiology and effect of meteorological parameters on influenza-like illness in Phitsanulok, a northern province in Thailand. Geospat Health. 2016;11(3):447-.
119. Shaman J, Goldstein E, Lipsitch M. Absolute humidity and pandemic versus epidemic influenza. American journal of epidemiology. 2010;173(2):127-35.
120. Anderson JO, Thundiyil JG, Stolbach A. Clearing the air: a review of the effects of particulate matter air pollution on human health. Journal of Medical Toxicology. 2012;8(2):166-75.
121. Brunekreef B, Holgate ST. Air pollution and health. The lancet. 2002;360(9341):1233-42.
122. Delfino RJ, Sioutas C, Malik S. Potential role of ultrafine particles in associations between airborne particle mass and cardiovascular health. Environmental health perspectives. 2005;113(8):934-46.
123. Janssen N, Fischer P, Marra M, Ameling C, Cassee F. Short-term effects of PM2. 5, PM10 and PM2. 5–10 on daily mortality in the Netherlands. Science of the Total Environment. 2013;463:20-6.
124. Laden F, Neas LM, Dockery DW, Schwartz J. Association of fine particulate matter from different sources with daily mortality in six US cities. Environmental health perspectives. 2000;108(10):941.
125. Polichetti G, Cocco S, Spinali A, Trimarco V, Nunziata A. Effects of particulate matter (PM10, PM2. 5 and PM1) on the cardiovascular system. Toxicology. 2009;261(1-2):1-8.
126. Schwartz J, Dockery DW, Neas LM. Is daily mortality associated specifically with fine particles? Journal of the Air & Waste Management Association. 1996;46(10):927-39.
127. Dockery DW, Pope CA. Acute respiratory effects of particulate air pollution. Annual review of public health. 1994;15(1):107-32.
128. Wong TW, Lau TS, Yu TS, Neller A, Wong SL, Tam W, et al. Air pollution and hospital admissions for respiratory and cardiovascular diseases in Hong Kong. Occup Environ Med. 1999;56(10):679-83.
129. Chan TL, Lippmann M. Experimental measurements and empirical modelling of the regional deposition of inhaled particles in humans. American Industrial Hygiene Association Journal. 1980;41(6):399-409.
130. Chauhan AJ, Johnston SL. Air pollution and infection in respiratory illness. British medical bulletin. 2003;68(1):95-112.
131. Guaita R, Pichiule M, Maté T, Linares C, Díaz J. Short-term impact of particulate matter (PM2. 5) on respiratory mortality in Madrid. International journal of environmental health research. 2011;21(4):260-74.
132. Maté T, Guaita R, Pichiule M, Linares C, Díaz J. Short-term effect of fine particulate matter (PM2. 5) on daily mortality due to diseases of the circulatory system in Madrid (Spain). Science of the Total Environment. 2010;408(23):5750-7.
133. Qiu H, Yu IT-s, Tian L, Wang X, Tse LA, Tam W, et al. Effects of coarse particulate matter on emergency hospital admissions for respiratory diseases: a time-series analysis in Hong Kong. Environmental health perspectives. 2012;120(4):572.

134. Raaschou-Nielsen O, Andersen ZJ, Beelen R, Samoli E, Stafoggia M, Weinmayr G, et al. Air pollution and lung cancer incidence in 17 European cohorts: prospective analyses from the European Study of Cohorts for Air Pollution Effects (ESCAPE). The lancet oncology. 2013;14(9):813-22.
135. Chen T-M, Kuschner WG, Gokhale J, Shofer S. Outdoor air pollution: nitrogen dioxide, sulfur dioxide, and carbon monoxide health effects. The American journal of the medical sciences. 2007;333(4):249-56.
136. Donaldson K, Tran CL. Inflammation caused by particles and fibers. Inhalation toxicology. 2002;14(1):5-27.
137. Kim CS, Kang TC. Comparative measurement of lung deposition of inhaled fine particles in normal subjects and patients with obstructive airway disease. American journal of respiratory and critical care medicine. 1997;155(3):899-905.
138. Lee GI, Saravia J, You D, Shrestha B, Jaligama S, Hebert VY, et al. Exposure to combustion generated environmentally persistent free radicals enhances severity of influenza virus infection. Particle and fibre toxicology. 2014;11:57.
139. Li XY, Gilmour PS, Donaldson K, MacNee W. Free radical activity and pro-inflammatory effects of particulate air pollution (PM10) in vivo and in vitro. Thorax. 1996;51(12):1216-22.
140. Liang Y, Fang L, Pan H, Zhang K, Kan H, Brook JR, et al. PM2.5 in Beijing - temporal pattern and its association with influenza. Environ Health. 2014;13:102.
141. De Leon AP, Anderson HR, Bland JM, Strachan DP, Bower J. Effects of air pollution on daily hospital admissions for respiratory disease in London between 1987-88 and 1991-92. Journal of Epidemiology & Community Health. 1996;50(Suppl 1):s63-s70.
142. Pönkä A, Virtanen M. Asthma and ambient air pollution in Helsinki. Journal of Epidemiology & Community Health. 1996;50(Suppl 1):s59-s62.
143. Yorifuji T, Suzuki E, Kashima S. Hourly differences in air pollution and risk of respiratory disease in the elderly: a time-stratified case-crossover study. Environ Health. 2014;13:67-.
144. Bertoglia M. Modelo de asociacion de brotes de influenza y variables ambientales basado en consultas en servicios de urgencia. Region Metropolitana 2011-2013.: Universidad Catolica de Chile; 2015.
145. Agresti A. An introduction to categorical data analysis: Wiley; 2018.
146. Cox DR. Some remarks on overdispersion. Biometrika. 1983;70(1):269-74.
147. Johnson NL, Kemp AW, Kotz S. Univariate discrete distributions: John Wiley & Sons; 2005.
148. Diez-Roux AV. Multilevel analysis in public health research. Annual review of public health. 2000;21(1):171-92.
149. Diggle P, Liang K, Zeger S. Analysis of Longitudinal Data: Oxford Statistical Science Series. 1994.
150. Brooks MEK, Kasper; van Benthem, Koen; Magnusson, Arni; Casper, Berg; Nielsen, Anders; Skaug, Hans; Maechler, Martin; Bolker, Benjamin. glmmTMB Balances Speed and Flexibility Among Packages for Zero-inflated Generalized Linear Mixed Modeling. The R Journal. 2017;9(2):378--400.
151. Brooks ME, Kristensen K, van Benthem KJ, Magnusson A, Berg CW, Nielsen A, et al. Modeling Zero-Inflated Count Data With glmmTMB. bioRxiv. 2017:132753.
152. Chowell G, Echevarría-Zuno S, Viboud C, Simonsen L, Tamerius J, Miller MA, et al. Characterizing the epidemiology of the 2009 influenza A/H1N1 pandemic in Mexico. PLoS medicine. 2011;8(5):e1000436.

153. Novikov I, Kalter-Leibovici, O., Chetrit, A. et al. . Weather conditions and visits to the medical wing of emergency rooms in a metropolitan area during the warm season in Israel: a predictive model. Int J Biometeorol. 2012;56(121).